博士論文

Comparison of sand behavior under repeated liquefaction in triaxial and shaking table tests

（三軸試験と振動台実験における砂の複数回液状化挙動の比較)

By

Teparaksa Jirat

(テパラクサ ジラット)

A thesis submitted in partial fulfillment
of the requirements for the degree of

Doctor of Philosophy

Department of Civil Engineering
University of Tokyo
Tokyo, Japan

September 2017

Abstract

Liquefaction is a phenomenon wherein soil loses its strength due to cyclic loading; for example, earthquake, and flows in a liquid manner which usually occurs in saturated cohesionless soils. Liquefaction phenomenon was first recognized in the event of Niigata earthquake in Japan in 1964, which vastly caused damage to many civil engineering structures. Since then, the topic of liquefaction interested many geotechnical researchers and practicing engineers.

However, in the past few decades, there have been many reports in many countries such as Japan, New Zealand and Greece that liquefaction took place again at sites where liquefaction had already occurred. This phenomenon is so called multiple liquefaction, reliquefaction or repeated liquefaction. It is not necessary that repeated liquefaction occurs during the same event of earthquake but also within a long period of time where dissipation of previously generated excess pore water pressure and soil reconsolidation has already done. This can be implied that although sand becomes denser after liquefaction and reconsolidation, soil liquefaction might still likely to occur. Therefore, recently, this issue has been being studied intensively by using both element test and model test; for instance, shaking table test, triaxial test, simple shear test and torsional shear test.

Regarding to repeated liquefaction studies, most of the pioneer works has been focused on using single apparatus and each with different conditions and materials. Thus, results from two major types of test; element test and model test, are difficult to compare. For comparison purpose, although, it cannot be completely concluded that which apparatus is more capable of predicting soil behavior in the field, it is still better to be able to predict soil behavior in model test by having only data of element testing or vice versa. There have been several researchers tried to compare repeated liquefaction behavior between element test and shaking table test. However, the comparison was made by using simplified conventional estimation of stress ratio which depends on the peak amplitude of ground response. Besides, the numbers of liquefaction stage were also limited. For comparative point of view, this thesis is aimed to investigate and compare soil behavior in terms of repeated liquefaction with triaxial and shaking table test for the same sand using the method of energy approach and cumulative damage concept in comparison. However, in this study, Silica sand with number seven grading which is artificial

sand produced from crushed rock was employed instead of Toyoura sand, a Japanese standard sand, due to its availability and high cost as their grain size distributions are similar.
In triaxial testing, three series of test were conducted in order to study three major aspects which are the effect of cyclic stress, the effect of strain history and the effect of small strain history or so-called pre-shearing. For the first series, the specimens were isotropically consolidated to the desired confining pressure before subjecting to repeated liquefaction test with various cyclic stress ratios but constant strain amplitude history ($\varepsilon_{a(DA)} = 5\%$). It was found out that at higher cyclic stress ratio, liquefaction was prone to occur and liquefaction resistance, in terms of number of cycle to cause certain double amplitude strain, increased with liquefaction stages.

For the effect of strain history study, similar to the first test series, but after consolidation, specimens were subjected to cyclic loading with constant cyclic stress ratio but various strain amplitude histories ($\varepsilon_{a(DA)}$ = 1%, 2%, 5%, 7% and 10%). The results showed that repeated liquefaction resistance was greatly affected more by strain history than by relative density. The specimens which were cyclic loaded with lower strain amplitude showed higher liquefaction resistance although an increase in relative density due to reconsolidation was smaller. On the other hand, the specimens with higher strain amplitude history showed lower liquefaction resistance. Nonetheless, the lowest strain amplitude applied to the specimens in this test series was only 1%. Thus, another series of test was conducted to cover the effect of small strain history. In this case, specimens were subjected to small strain amplitude at the first stage of liquefaction (e.g. $\varepsilon_{a(DA)}$ = 0.1%, 0.2% and 0.5%) with constant cyclic stress ratio as the second test series. This small strain history is sometimes called as pre-shearing as the effective stress still does not equal to zero yet; i.e. liquefaction still does not occur. The specimens were then subjected to 2% of strain amplitude in the following stages. Second stage liquefaction resistances of specimens with small pre-shearing history were even larger than that of specimens in second test series. This was another strong evidence that reliquefaction resistance does not correspond well with relative density but strain history. More interestingly, among various small strain histories, the specimen with 0.1% strain history did not show the highest liquefaction resistance as can be expected based on previous finding in the second test series. This behavior can be explained by using energy approach.

In shaking table testing, repeated liquefaction tests were carried out also on the Silica sand which was prepared as an air-pluviated flat ground model consisted of five 10-cm-thick layers.

Input motion of 20 sinusoidal cycles with various starting accelerations were applied to the ground model; e.g. 200 gal, 300gal and 400 gal. The input acceleration of the next stage was determined based on the previous liquefaction behavior. If the soil model showed liquefaction, the same acceleration amplitude was repeated in the next liquefaction stage; however, if the soil model did not liquefy, acceleration was raised by 100 gal for the next shaking stage. Ground response was monitored by means of acceleration, pore water pressure and settlement. By employing Newton law of motion and double integration, shear stress and shear strain can be computed. In this manner, similar to triaxial analysis, liquefaction resistance in shaking table can also be calculated in terms of number of cycle to cause certain double amplitude strain.

The result of each shaking table test can be divided into repeated liquefaction series under the same input acceleration. The first repeated liquefaction series was during the ground model repeatedly liquefied at starting input acceleration without any increase. When liquefaction stopped to occur at starting acceleration, input acceleration was raised until ground model started to liquefy again. The second series was during the second time that ground model continuously liquefy under constant input acceleration. In the each series, it was found that soil liquefaction resistance in the first shake event was always higher than that in the second shake event. However, different in input acceleration also affected liquefaction resistance and number of liquefaction stages. At maximum starting input acceleration of 400 gal, ground model started to liquefy at low number of cycle and continued for 8 stages while only 2 liquefaction stages were observed for the lowest starting input acceleration at 200 gal with higher number of cycle needed to cause liquefaction.

In order to investigate reliquefaction behavior, maximum strain amplitude was calculated for each stage. It was found that future liquefaction can be briefly predicted under the same or lower input acceleration during two stages of liquefaction. It was noticed that lower future liquefaction resistance can be expected in the case where the current liquefaction stage showed higher strain amplitude than the previous one. On the other hand, the liquefaction resistance of the next stage can be expected to be higher when the strain amplitude of current stage is found to be lower than the previous one. It is important to note that, unlike triaxial or other element tests, cyclic stress amplitude and strain history cannot be controlled in shaking table test. Thus, in each liquefaction stage, the model was subjected to various uncontrolled strain history. Even more, the cyclic stress ratio during shaking was not uniform. Thus, it was challenge to compare the result of both tests.

Due to irregular loading response in shaking table test, uniform equivalent stress ratio shall be evaluated in order to compare the both results. Many researchers have tried with conventional method which has some limitations as only the peak stress ratio was taken into the account. It is not only considered too simplified but also, in many cases, liquefaction occurred far earlier before reaching the peak. Some researchers used input acceleration to compute stress ratio which is uniform. However, the ground response during liquefaction is no longer uniform. Thus, using input acceleration may be under or over estimated. This thesis used another method so called cumulative damage concept. This method evaluate fatigue in materials. it assumes that each half pulse of stress ratio gives certain damage to the ground model. When the value of cumulative damage equal to or larger than unity, the failure occurs. Thus, this method allows every stress ratio amplitude before the soil failure or liquefaction to be taken into the account in evaluating uniform equivalent stress ratio. By this manner, relationship between cyclic stress ratio and number of cycle to trigger liquefaction; i.e. liquefaction curve, of shaking table can be drawn. It was found that liquefaction curve of shaking table lies above that of triaxial which can be implied that higher liquefaction resistance was observe in shaking table. Possible reasons such as saturation condition, pore water pressure dissipation and testing conditions were discussed in this thesis.

Further investigation was carried out using energy approach. In geotechnical engineering, during shearing, there is dissipated energy due to sliding mechanism which can be computed based on hysteresis loop of stress-strain relationship. Pioneer works found a virtual boundary which distinguish the amount of dissipated energy to cause positive impact and negative impact resulting in an increase and a decrease in liquefaction resistance of the next stage respectively. Positive impact is defined as amount of dissipated energy during shearing before the stress path crossing phase transformation line (PTL). After the PTL, amount of dissipated energy shall be negative impact. However, for comparison purpose, because of difference in confining pressure between both tests, modified energy dissipation or normalized dissipated energy by confining pressure was used. In such a case, modified dissipated energy was calculated based on a hysteresis loop of stress ratio (q/p' or τ/p') and strain relationship. It was found that relationship between positive and negative impact together with the next liquefaction properties was well defined for each test apparatus results. However, inconsistence results between shaking table and triaxial was found which might be due to in appropriate virtual boundary.

Acknowledgement

I would like to express my deepest and sincere gratitude to my advisor, Prof. Junichi Koseki for his enlightening guidance, support and assistance. His office door was always open whenever I faced trouble and had questions regarding research. Prof. Koseki has been patiently answered all of my questions and gave me advises, comments, encouragements and positive inspirations numerous times. Not only the research aspect, but he also shared tips of everyday life during my stay in Japan. Under his supervision, I have learnt the method of doing research, the way of thinking and even the way of living during my doctoral study.

I also would like to express the deepest appreciation to thesis committee members, Prof. Reiko Kuwano, Assoc. Prof. Tato Uchimura, Prof. Tsutomu Namikawa and Assoc. Prof. Takashi Kitoya for suggestions and advice during discussions and lab seminars. With their comments, the thesis was much fulfilled. I cannot adequately express how thankful I am to Mr. Takeshi Sato for designing, creating, advices and fixing the apparatuses I used during my study. His expertise made the most difficult jobs seemed to be easy. Without him, I am sure that there would be much delay in testing. In addition, I would like to send special thanks to Ms Miyashita Yukika who gave me advices in doing triaxial testing and also computer coding for the experiment. I also deeply appreciated the help to Assoc. Prof. Hiroyuki Kyokawa, Dr. Takaki Matsumaru, Mr. Nunokawa, Mr. Nakade and Mr. Eisaku Takayama in operating the shaking table and also suggestion for my study.

I would like to also super thank Mr. Zhao Zhung who entered to the Geotechnical lab at the same interval for always being a good colleague and a good friend. Many thanks to all the shaking table members; Mr. Shahid Iqbal, Mr. Zamsyar Giendhra Fad, Ms. Catherine W. Kariuki, Mr. Nakamura Junichiro. Without them, the work of preparing ground model in shaking table test would be so much difficult. My special thanks goes to my tutors who made my struggles during living in japan so much easier; Mr. Ryuichiro Hoshino, Mr. Koji Tanaka and additionally, Mr. Nakamura Junichiro who can always made me smile. Also, my appreciations goes to all the Geotechnical lab members, , Mr Yudai Aoyagi, Mr. Wuwei Mao, Mr. Jayload Tan Tian, Mr. Zian Maqsood, Mr. Hayato Hamaguchi, Mr. Ahmed Tripolian, Mr. Sajjad M. Babar, Ms. Wage Thanuja, Mr. Kapila R. Withanage, Ms. Yuki Okabe, Shangning

Tao, Mr. Hemekanth, Ms. Wenli Lin, Mr. Jiren Xie, Mr. Tokio Morimoto. All of them have made my study and research full of smile and enjoyments.
I would like to express my deepest gratitude to Japanese Ministry of Education, Culture, Sports, Science and Technology for generous funding during my three years study in Phd. Also, thanks to Civil Engineering office members who always help with my general documents and problems that I have made.

Last but not least, I would like to thank all my family members, parents, brother and sister in Thailand. They always send their support even they stay thousands miles apart from me. It meant everything to me.

Table of Contents

List of Tables

List of Figures

1. Introduction

Contents

Chapter 1 Introduction

1.1 Background

1.1.1 Background of repeated liquefaction case history

The objectives of this thesis is to investigate and compare repeated liquefaction behavior of Silica sand with number seven grading in triaxial and shaking table tests. Liquefaction is a phenomenon wherein soil loses strength due to cyclic loading; for example; earthquake, and flows in a liquid manner which usually occurs in saturated cohesionless soils. Liquefaction was first recognized in the event of Niigata Earthquake in Japan in 1964, which vastly cased damage to civil engineering structures (Ishihara and Koga, 1981). Since then, the topic of liquefaction interested many geotechnical researchers and practicing engineers. In addition, following 1964 Niigata earthquake, there were many reports of liquefaction triggered by earthquake around the world such as 1964 Alaska Earthquake (McCulloch and Bonilla, 1970), 1975 Haicheng and 1976 Tangshan Earthquake (Shengcong and Tatsuoka, 1984), 1999 Chi Chi Earthquake (Yuan et al., 2004) and the recent 2016 Kumamoto Earthquake (Kiyota et al., 2017).

During seismic loading in the saturated sandy soil ground, excess pore water pressure rapidly builds up and causes a decrease in effective stress. Once, the generated excess pore water pressure equals to the initial effective stress, there is no contact force between each soil particle. Thus, the soil no more behaves in solid manner but liquid. Olson et al. (2001) suggested that the process of liquefaction consists of three phases; (1) destruction of pre-earthquake soil structure and aging effects during liquefaction; (2) postliquefaction consolidation and densification; and (3) postliquefction aging. There are many factors attributes to liquefaction occurrence; for instance, shape of material (Poulos et al., 1985), initial static shear stress due to consolidation (Seed 1979), effective overburden pressure and fine content (Pathak et al.). However, in general, liquefaction does not harm people but give damage to the structures by means of settlement or uplifting.

Since the Niigata earthquake, what the researchers and engineers found was that liquefaction can still occur repeatedly over time in the same site where the excess pore water pressure previously generated in the past earthquake was already fully dissipated and reconsolidation

together with soil aging was taken place or, in some cases, aftershock. The pioneer investigation on repeated liquefaction was reported by Kuribayashi and Tatsuoka (1975). Approximately 44 earthquakes occurred during century were investigated and it was found that several zones, in Japan, liquefaction occurred repeatedly. Those zones were Hokuriku Region, Nobi (Mino-Owari) Region and Kanto Region. The investigation discovered that old river courses and reclaimed lands along seas or lakes were more susceptible to liquefaction. Another example of pioneer work was published by Yasuda, Tohno (1988) where repeated liquefaction was observed during 1983 Nihonkai-Chubu main earthquake and aftershock about one month later. Almost 10 repeated liquefaction areas were reported including previous liquefaction sites which were induced by 1964 Niigata Earthquake and 1968 Tokachi-oki earthquake in almost 20 years period. The recent study was carried out due to 2011 great East Japan earthquake with magnitude of 9.0. Wakamatsu (2011) surveyed within 500-km long zone from Iwate to Kanagawa and identified 62 sites of liquefaction reoccurrence during 2011 earthquake and 1987 Chibaken Toho-oki. Wakamatsu (2012) extended the survey to 650-km long zone from Aomori to Kanagawa and found out 23 sites apart from previous report. The most importance of the survey was that the second liquefaction at every site induced by 9.0 magnitude earthquake was severe than the one that occurred during 1987 earthquake (magnitude of 6.7).

Repeated liquefaction is not only found in Japan, but also the rest of the world. Youd and Hoose (1978) summarized many types of soil failure in Northern California induced by earthquake. There were several sites in which sand boiling, ground crack associated with lateral spread and settlement occurred repeatedly. Youd and Wieczorek (1982) showed liquefaction sites occurred during 1940 and 1979 Imperial Valley Earthquake. However, in this case, the effect due to the second earthquake was less than the first one which was contradicted to the research in Japan. Papathanassiou, Pavlides et al. (2005) confirmed repeated liquefaction occurrence from approximately 308 cases which were triggered by 88 earthquakes in the Aegean region including Greece, Turkey, Bulgaria, Albania and Montenegro during the period of 1509 to 2003. The most recent report seems to be in 2010-2011 Christchurch earthquakes reported by Cubrinovski, Henderson et al. (2012). The report showed that there was an area near to the sea where liquefaction occurred induced from three major earthquakes in September 2010 (M 7.1), February 2011 (M 6.2) and June 2011 (M 5.3 and M 6.0). Repeated liquefaction occurred in New Zealand caused severe damage to civil engineering structure such as bridges, residential houses (Kiyota, Yamada et al. 2012).

Since all the evidences have yielded that liquefaction can be occurred over time at the same spot and even can cause more damage than the previous one. It was somehow mysterious that when liquefaction takes place, ground becomes denser due to the process of excess pore water pressure dissipation and reconsolidation. Logically, this phenomenon should promote higher liquefaction resistance in the next event due to soil densification but it is not the case from the reports. Therefore, researchers and geotechnical engineers started to study on the topic of repeated liquefaction. Most of the pioneer works tried to simulate first liquefaction by applied stress and strain history so called "pre-shearing" and followed by the second liquefaction test.

1.1.2 Effect of strain history on soil liquefaction behavior

As previously discussed, there were many evidences on repeated liquefaction reoccurrence which is contradicted to the thought that liquefaction is unlikely to occur after soil densification and reconsolidation. Finn et al. (1970) was the first researcher to point out the effect of strain history to liquefaction resistance in simple shear test. Their first liquefaction test was carried out until reaching target strain amplitudes. After reconsolidation, the second liquefaction test was conducted. It was reported that large shear strain amplitude during the first liquefaction reduced the liquefaction resistance in the second liquefaction test. However, small shear strain or partial liquefaction would lead to an increase in the next cyclic resistance. Seed et al. (1977) later supported the previous finding by using shaking table test. With low magnitude of shake during the first stage of test, when the specimen did not develop liquefaction; i.e. limited excess pore water pressure developed, the cyclic resistance in the next stage was found to be increase with limited change in density. These two researches indicated that relative density alone is unreliable as a measure for liquefaction potential.

Ishihara and Okada (1978) also discovered the effect of small pre-shearing specimen on liquefaction resistance and pore water pressure buildup in a triaxial apparatus. It was suggested that the hardening effect following small pre-shearing is attributed to plastic yielding. For the large pre-shearing, Ishihara and Okada (1982) performed liquefaction test on large pre-sheared specimens. Ishihara and Okada (1982) found that re-liquefaction behavior not only depend on pre-shearing strain amplitude but also anisotropy as well as Yamada (et al. 2010) and Towhata and Ishihara (1985). Apart from these frontier works, there were many researchers conducted repeated liquefaction test regarding this topic; for instance, Suzuki and Toki (1984), Oda et al. (2001), Wichtmann et al. (2005) and Ha et al. (2011). However, all of the researches described

above only determined two stages of liquefaction. Recently, the studies conducted by Wahyudi et al. (2015) and Wahyudi et al. (2013) using stack-ring shear apparatus support demonstrated more than 5 liquefaction stages. They supported the effect of strain history on liquefaction resistance. In the model test, El-Sekelly et al. (2016) conducted centrifuge test in investigate the effect of preshaking with many shaking histories using in total 60 low intensity shakes and 6 relatively stronger shakes. It was concluded that the strong shake event tends to decrease liquefaction resistance. Nonetheless, with a few following small shake, liquefaction resistance can be recovered to the initial resistance.

This thesis conducted repeated liquefactions test using both triaxial and shaking table to observe the sand behavior in terms of strain history or liquefaction history effects.

1.1.3 Energy approach in liquefaction investigation

As pioneer researchers successfully investigated repeated liquefaction behavior using energy approach (Wahyudi and Koseki, 2015), (Aoyagi et al., 2016). This study also tries using the method of energy approach to compare repeated liquefaction test result from element test and physical model test. The method of energy approach was first used in liquefaction topic by Nemat-Nasser and Shokooh (1979). For the constant stress test in both element and model test, it was proposed that there is a relationship between density change and dissipated energy. The amount of energy is expended by rearrangement of soil particles. In the case of drained test, an increase of energy normally occurs when void ratio is decreasing or contractive behavior while a decrease happens during dilative behavior. This theory can be applied to the case of undrained test as well. Similar method was also purposed to evaluate liquefaction potential (Berrill and Davis 1985).

Since then, there were many studies used dissipated energy in liquefaction analysis. The frontier work was to point out unique relationship between excess pore water pressure build-up during liquefaction test and dissipated energy (Towhata and Ishihara, 1985). This relationship was also investigated by Okada and Nemat-Nasser (1994), Kazama et al. (2000), Jafarian et al. (2012), Kokusho (2013), Azeiteiro et al. (2017) among others. Those researchers suggested that the dissipated energy depends on the type of sand, density, consolidation history.

The use of dissipated energy to evaluate liquefaction behavior was studied by Figueroa et al. (1994), Kazama et al. (2003). It was pointed out that the dissipated energy is higher at the initial number of cycles compared to that at high number of cycle. Kokusho (2013) and Kokusho and Mimori (2015) compared between the method of energy-based and stress-based in liquefaction potential evaluation. It was found that both method gave different result if the ground motion is too large or too small. This thesis employed the method of dissipated energy to investigate repeated liquefaction behavior in both triaxial where stress is uniform and shaking table where the stress is non-uniform.

1.1.4 Comparison of element and model testing of liquefaction behavior

There were several researchers tried to compare the result of liquefaction test using element tests and models test. It is known that it is quite difficult work to compare element and model test in terms of liquefaction since the stress and strain in element tests generally can be control while it is irregular response of stress in model test. Ohara (1972) made a comparison between shaking box and triaxial test at the same relative density of specimen. The comparison was made in terms of relationship between cyclic stress ratio (CSR) and number of cycle to cause liquefaction as shown in *Figure 1-1*. It can be seen that the curve of shaking box lied above that of triaxial results indicating stronger behavior. Even though relative density of specimens in shaking box and simple shear were not equal. The specimen in shaking box had lower relative density but higher cyclic resistance. However, the author did not describe on how cyclic stress ratio was calculated. It is believed that either the simplified method or input stress was used.

Pathak et al. (2010) conducted liquefaction test at various relative density of specimens on shaking table apparatus and compared the results with element tests from literatures. The data supported the finding of Ohara (1972). Liquefaction resistance of specimen in shaking table test was higher than that in triaxial test, simple shear test and torsional test (see *Figure 1-2*, *Figure 1-3*). In this case, the simplified method purposed by Seed and Idriss (1971) was used to evaluate cyclic stress ratio. This method only based on the maximum peak stress regardless of number of cycle, the other peak stress, duration and so on. Thus, the determined cyclic stress ratio may not be accurate.

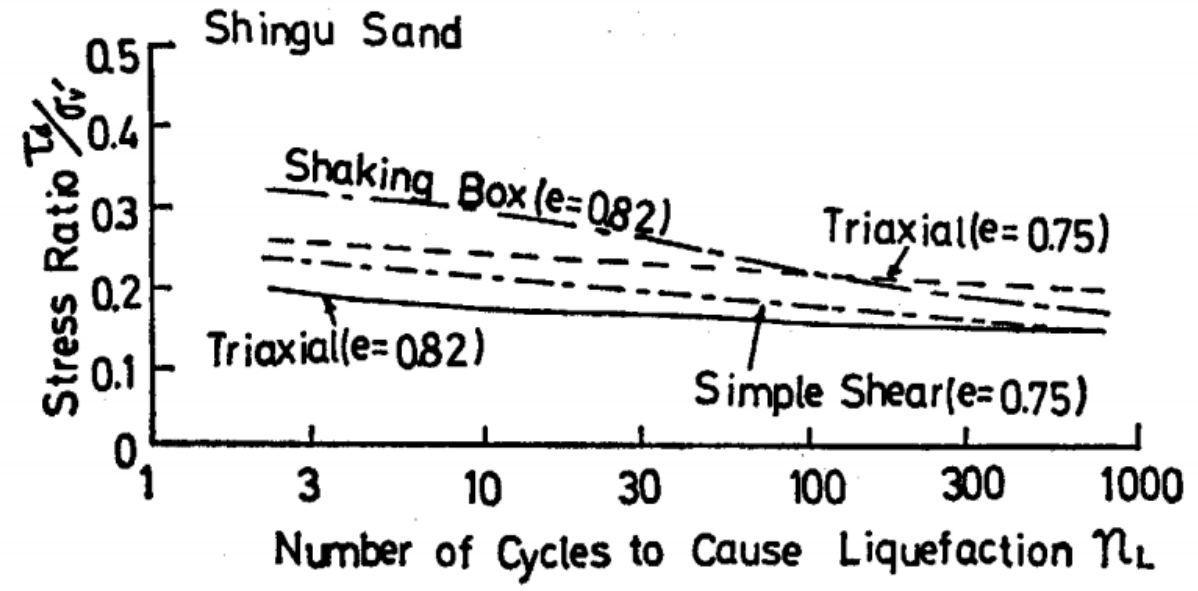

Figure 1-1. Comparison of stress ratio required to cause liquefaction in three different test (Ohara, 1972)

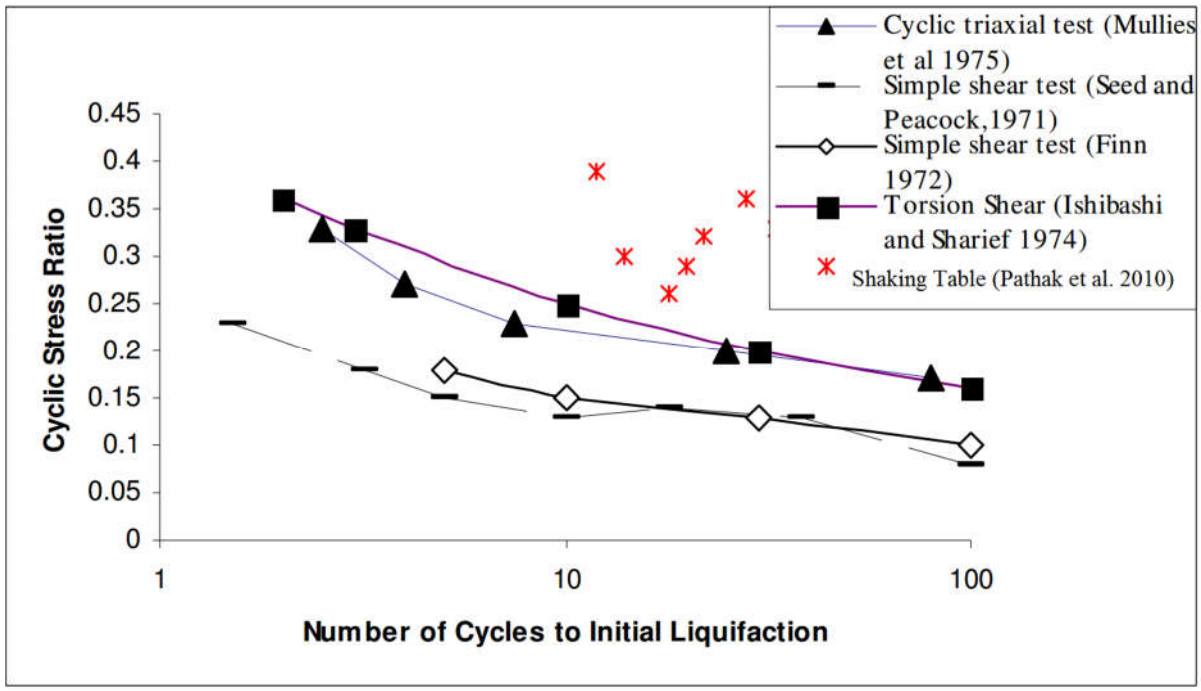

Figure 1-2. Comparison of liquefaction resistance in shaking table and others element tests (Pathak et al., 2010)

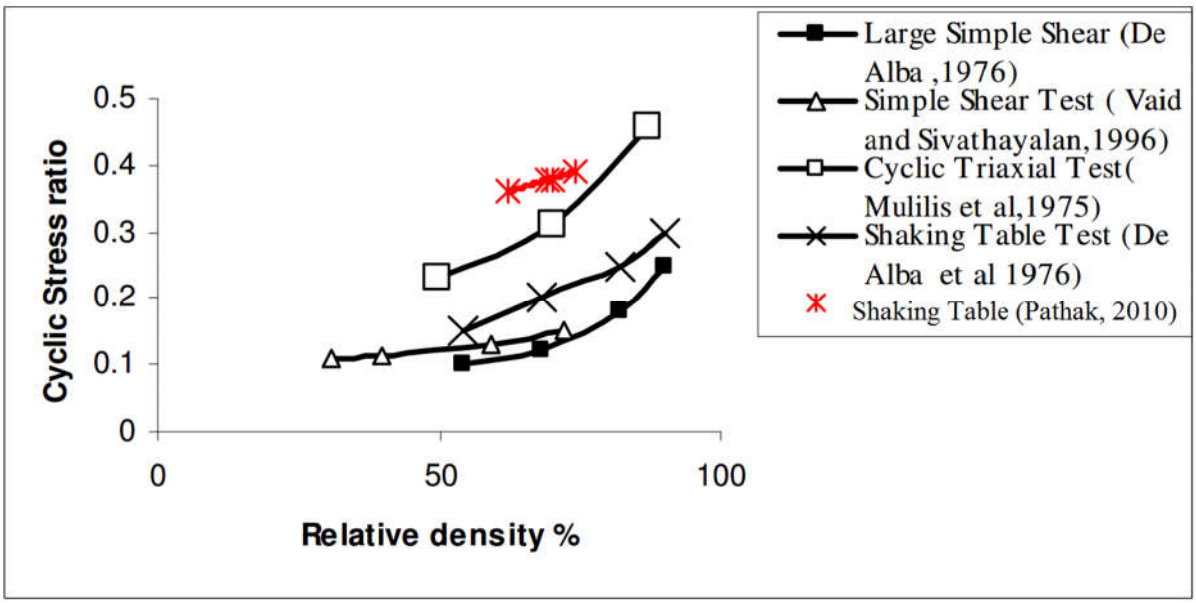

Figure 1-3. Relationship between cyclic stress ratio and relative density of shaking table test and other element tests (Pathak et al., 2010)

1.2 Research objective

The main objective of this research is to investigate repeated liquefaction behavior of the Silica sand using triaxial and shaking table apparatus and their comparison. The objective in detail can be describe as follow;

1. Investigate Silica sand behavior under repeated liquefaction in shaking table test.

   In reality, especially in Japan, the ground suffered from numerous earthquakes and reliquefaction. However, most of the works focused only for several stages. In this study, the shaking tables were carried out more than 20 stages. It was attempted to find trend of liquefaction resistance over repeated liquefaction phenomenon.

2. Investigate Silica sand behavior under repeated liquefaction in triaxial test

   In general, researchers used various types of sand depending on their country's standard, availability or objective. This different sand gives difficulty in comparison purpose between element and model test.

3. Investigate soil behavior under repeated liquefaction using energy based approach

   There has been attempts to use dissipated energy on repeated liquefaction tests in element tests where uniform cyclic loading was applied. In this thesis not only the method was employed for triaxial tests but also shaking table tests where the ground model response during liquefaction is rather non-uniform.

4. Compare sand repeated liquefaction behavior between triaxial and shaking table tests by combining energy approach and cumulative damage concept

   Normally, it is challenge to compare the result between element test and model test since the soil response in the model test usually comes in irregular manner while it is uniform in element test. Some method has been developed to convert irregular loading into uniform loading pattern. However, the conventional type only based on the peak response regardless of number of cycle, duration and so on.

1.3 Organization of the thesis

Chapter 1	**Introduction** This chapter introduces the background of liquefaction and repeated liquefaction history, the literature review of this study, study objective and thesis organization
Chapter 2	**Apparatus and Methodology** This chapter describes tested material, apparatus and testing methodology. As two types of test were employed in this thesis, this chapter is divided into several parts as follow; - Tested Material - Shaking Table Apparatus - Shaking table methodology - Method of calculation for shaking table test - Detail of triaxial apparatus - Triaxial testing procedure
Chapter 3	**Triaxial Test Result** This chapter reports the test result of triaxial repeated liquefaction test in terms of - Effect of cyclic stress ratio - Effect of strain amplitude history - Effect of small strain amplitude history
Chapter 4	**Shaking Table Test Result** This chapter presents the test result of shaking table repeated liquefaction test
Chapter 5	**Investigation of Repeated Liquefaction Behavior Based on Energy Approach** This chapter shows the characteristic of sand under repeated liquefaction using energy approach
Chapter 6	**Comparison of Sand Behavior under Repeated Liquefaction** This chapter introduces the comparison of triaxial and shaking table test in terms of repeated liquefaction using energy approach and cumulative damage concept
Chapter 7	**Conclusions** This chapter summarizes the findings from the results of both triaxial and shaking table tests and suggestion for further researches

1.4 References

Aoyagi, Y., WAHYUDI, S., KOSEKI, J., SATA, T. and MIYASHITA, Y., 2016 Behavior of Multiple-Liquefaction under Small to Large Strain Levels and Its Analysis Based on Dissipated Energy. JSCE Journal of Earthquake Engineering, 72(4), pp.I_167-I_176

AZEITEIRO, R.J., COELHO, P.A., TABORDA, D.M. and GRAZINA, J.C., 2017. Energy-based evaluation of liquefaction potential under non-uniform cyclic loading. *Soil Dynamics and Earthquake Engineering,* **92**, pp. 650-665.

BERRILL, J. and DAVIS, R., 1985. Energy dissipation and seismic liquefaction of sands: revised model. *Soils and Foundations,* **25**(2), pp. 106-118.

CUBRINOVSKI, M., HENDERSON, D. and BRADLEY, B., 2012. Liquefaction impacts in residential areas in the 2010-2011 Christchurch earthquakes.

FIGUEROA, J.L., SAADA, A.S., LIANG, L. and DAHISARIA, N.M., 1994. Evaluation of soil liquefaction by energy principles. *Journal of Geotechnical Engineering,* **120**(9), pp. 1554-1569.

FINN, W., BRANSBY, P.L. and PICKERING, D.J., 1970. Effect of strain history on liquefaction of sand. *Journal of Soil Mechanics & Foundations Div,* **96**(SM6),.

HA, I., OLSON, S.M., SEO, M. and KIM, M., 2011. Evaluation of reliquefaction resistance using shaking table tests. *Soil Dynamics and Earthquake Engineering,* **31**(4), pp. 682-691.

ISHIHARA, K. and KOGA, Y., 1981. Case studies of liquefaction in the 1964 Niigata earthquake. *Soils and foundations,* **21**(3), pp. 35-52.

ISHIHARA, K. and OKADA, S., 1982. Effects of large preshearing on cyclic behavior of sand. *Soils and Foundations,* **22**(3), pp. 109-125.

ISHIHARA, K. and OKADA, S., 1978. Effects of stress history on cyclic behavior of sand. *Soils and Foundations,* **18**(4), pp. 31-45.

JAFARIAN, Y., TOWHATA, I., BAZIAR, M., NOORZAD, A. and BAHMANPOUR, A., 2012. Strain energy based evaluation of liquefaction and residual pore water pressure in sands using cyclic torsional shear experiments. *Soil Dynamics and Earthquake Engineering,* **35**, pp. 13-28.

KAZAMA, M., SENTO, N., OMURA, H., TOYOTA, H. and MASAKI, K., 2003. Liquefaction and settlement of reclaimed ground with gravelly decomposed granite soil. *Soils and Foundations,* **43**(3), pp. 57-72.

KAZAMA, M., YAMAGUCHI, A. and YANAGISAWA, E., 2000. Liquefaction resistance from a ductility viewpoint. *Soils and Foundations,* **40**(6), pp. 47-60.

KIYOTA, T., IKEDA, T., KONAGAI, K. and SHIGA, M., 2017. Geotechnical Damage Caused by the 2016 Kumamoto Earthquake, Japan. *International Journal of Geoengineering Case Histories,* **4**(2),.

KIYOTA, T., YAMADA, S. and HOSONO, Y., 2012. Repeated liquefaction observed during the 2010-2011 Canterbury earthquakes. *Bulletin of Earthquake Resistant Structure Research Center, Institute of Industrial Science, University of Tokyo,* (45),.

KOKUSHO, T. and MIMORI, Y., 2015. Liquefaction potential evaluations by energy-based method and stress-based method for various ground motions. *Soil Dynamics and Earthquake Engineering,* **75**, pp. 130-146.

KOKUSHO, T., 2013. Liquefaction potential evaluations: energy-based method versus stress-based method. *Canadian Geotechnical Journal,* **50**(10), pp. 1088-1099.

KURIBAYASHI, E. and TATSUOKA, F., 1975. Brief review of liquefaction during earthquakes in Japan. *Soils and Foundations,* **15**(4), pp. 81-92.

MCCULLOCH, D.S. and BONILLA, M.G., 1970. *Effects of the earthquake of March 27, 1964, on the Alaska Railroad.* US Government Printing Office.

NEMAT-NASSER, S. and SHOKOOH, A., 1979. A unified approach to densification and liquefaction of cohesionless sand in cyclic shearing. *Canadian Geotechnical Journal,* **16**(4), pp. 659-678.

ODA, M., KAWAMOTO, K., SUZUKI, K., FUJIMORI, H. and SATO, M., 2001. Microstructural interpretation on reliquefaction of saturated granular soils under cyclic loading. *Journal of Geotechnical and Geoenvironmental Engineering,* **127**(5), pp. 416-423.

OKADA, N. and NEMAT-NASSER, S., 1994. Energy dissipation in inelastic flow of saturated cohesionless granular media. *Geotechnique,* **44**(1), pp. 1-19.

OLSON, S.M., OBERMEIER, S.F. and STARK, T.D., 2001. Interpretation of penetration resistance for back-analysis at sites of previous liquefaction. *Seismological Research Letters,* **72**(1), pp. 46-59.

PAPATHANASSIOU, G., PAVLIDES, S., CHRISTARAS, B. and PITILAKIS, K., 2005. Liquefaction case histories and empirical relations of earthquake magnitude versus distance from the broader Aegean region. *Journal of Geodynamics,* **40**(2), pp. 257-278.

PATHAK, S., DALVI, R. and KATDARE, A., 2010. Earthquake Induced Liquefaction using Shake Table Test.

PATHAK, S., JOSHI, M. and KSHIRSAGAR, M., EFFECT OF FINES ON LIQUEFACTION USING SHAKE TABLE TEST.

POULOS, S.J., CASTRO, G. and FRANCE, J.W., 1985. Liquefaction evaluation procedure. *Journal of Geotechnical Engineering,* **111**(6), pp. 772-792.

SEED, B., 1979. SOIL LIQUEFACTION AND CYCLIC MOBILITY EVALUTION FOR LEVEL GROUND DURING EARTHQUAKES. *Journal of Geotechnical and Geoenvironmental Engineering,* **105**(ASCE 14380),.

SEED, H.B., MORI, K. and CHAN, C., 1977. Influence of seismic history on liquefaction of sands. *Journal of Geotechnical and Geoenvironmental Engineering,* **103**(Proc. Paper 11318 Proceeding),.

SEED, H.B. and IDRISS, I.M., 1971. Simplified procedure for evaluating soil liquefaction potential. *Journal of Soil Mechanics & Foundations Div,* .

SHENGCONG, F. and TATSUOKA, F., 1984. Soil liquefaction during Haicheng and Tangshan earthquake in China; a review. *Soils and foundations,* **24**(4), pp. 11-29.

SUZUKI, T. and TOKI, S., 1984. Effects of preshearing on liquefaction characteristics of saturated sand subjected to cyclic loading. *Soils and foundations,* **24**(2), pp. 16-28.

TOWHATA, I. and ISHIHARA, K., 1985. Shear work and pore water pressure in undrained shear. *Soils and foundations,* **25**(3), pp. 73-84.

TOWHATA, I. and ISHIHARA, K., 1985. Undrained strength of sand undergoing cyclic rotation of principal stress axes. *Soils and Foundations,* **25**(2), pp. 135-147.

WAHYUDI, S. and KOSEKI, J., ANALYSIS OF RE-LIQUEFACTION PROPERTIES BASED ON ENERGY APPROACH.

WAHYUDI, S., KOSEKI, J., SATO, T. and CHIARO, G., 2015. Multiple-Liquefaction Behavior of Sand in Cyclic Simple Stacked-Ring Shear Tests. *International Journal of Geomechanics,* **16**(5), pp. C4015001.

WAHYUDI, S., KOSEKI, J., SATO, T. and MIYASHITA, Y., EFFECTS OF PRE-SHEARING HISTORY ON REPEATED LIQUEFACTION BEHAVIOR OF SAND USING STACKED-RING SHEAR APPARATUS.

WAKAMATSU, K., 2011. Recurrent liquefaction induced by the 2011 Great East Japan earthquake compared with the 1987 earthquake, *Proceedings of the international symposium on engineering lessons learned from the* 2011.

WAKAMATSU, K., 2012. Recurrent liquefaction induced by the 2011 great east Japan earthquake. *Journal of Japan Association for Earthquake Engineering,* **12**(5), pp. 69-88.

WICHTMANN, T., NIEMUNIS, A., TRIANTAFYLLIDIS, T. and POBLETE, M., 2005. Correlation of cyclic preloading with the liquefaction resistance. *Soil Dynamics and Earthquake Engineering,* **25**(12), pp. 923-932.

YAMADA, S., TAKAMORI, T. and SATO, K., 2010. Effects on reliquefaction resistance produced by changes in anisotropy during liquefaction. *Soils and Foundations,* **50**(1), pp. 9-25.

YASUDA, S. and TOHNO, I., 1988. Sites of reliquefaction caused by the 1983 Nihonkai-Chubu earthquake. *Soils and Foundations,* **28**(2), pp. 61-72.

YOUD, T.L. and HOOSE, S.N., 1978. *Historic ground failures in northern California triggered by earthquakes.* US Govt. Print. Off.

YOUD, T.L. and WIECZOREK, G.F., 1982. Liquefaction and secondary ground failure. *The Imperial Valley, California, Earthquake of October,* **15**(1979), pp. 223-246.

YUAN, H., YANG, S.H., ANDRUS, R.D. and JUANG, C.H., 2004. Liquefaction-induced ground failure: a study of the Chi-Chi earthquake cases. *Engineering Geology,* **71**(1), pp. 141-155.

2. Tested Material, Apparatus and Methodology

Contents

Chapter 2 Tested Material, Apparatus and Methodology

2.1 Introduction

In this chapter, the details of tested materials, cyclic undrained triaxial apparatus, shaking table apparatus, monitoring instruments and experiment procedure will be described. Triaxial and shaking table repeated liquefaction tests were conducted at the Geotechnical Laboratory, the University of Tokyo using Silica sand with number seven grading.

For the shaking table tests, the model was built as uniform flat ground which consisted of five 10cm-thick layers by air-pluviation method using sand hopper. Accelerometers, pore water pressure transducers and laser sensors were used for monitoring soil response and liquefaction behavior of ground model. After each shaking, time was allowed for excess pore water pressure dissipation. The ground behavior was initially checked for possible strain accumulation before commencing the next shaking; i.e. next liquefaction test.

On the other hand, for cyclic undrained triaixial tests, in order to compare the result, specimens were also prepared by air-pluviation method. Specimens were isotropically consolidated before subjecting to liquefaction test. After each liquefaction test, excess pore water pressure was dissipated by opening drainage valve allowing specimen to reconsolidate. The specimens was left for consolidation time before conducting the next liquefaction test. External displacement transducer, load cell and Low Capacity Differential Pressure Transducer were employed to monitor the specimen behavior.

2.1 Tested Material

a. Silica sand with number seven grading

In Japan, as a Japanese standard, Toyoura sand is widely used among researchers and geotechnical practicing engineers. However, in shaking table test, Silica sand with number seven grading was used instead as a substitute for Toyoura sand which is highly demanded

and expensive. The silica sand is generally artificial sand produced from crashed rock. It is uniformly distributed sand and its grain size distribution is similar to Toyoura sand. The properties and cumulative grain size distribution are shown in *Table 2-1* and *Figure 2-1*, respectively together with the Toyoura sand. However, in case of shaking table test, the tested sand was reused by oven dry instead of an intact one as the amount of sand used for one test was relatively much higher (approximately 700 kg). For the triaxial testing, in order to compare the results in terms of repeated liquefaction, the silica sand was also used. Due to the fact that triaxial specimen was much smaller than ground model in shaking table test, the sand used for the triaxial tests was intact.

Figure 2-2 and *Figure 2-3* show laser scaning photo of silica sand with number seven grading and Toyoura sand. The Silica sand seems to be more angular. Comparing both sands in terms of shape, it is known that the more narrowly graded and the more rounded grained are susceptible to liquefaction (Poulos et al., 1985). Thus, it can be implied that the Silica sand might be stronger than Toyoura sand by means of liquefaction resistance.

Table 2-1. Properties of silica sand with number seven grading and Toyoura sand

Properties	**Silica Sand with number seven grading**	**Toyoura Sand**
Specific gravity	2.640	2.656
Maximum Void Ratio	1.243	0.992
Minimum Void Ratio	0.743	0.632
Mean Particle Diameter, D_{50} (mm)	0.206	0.190

b. Black colored sand

The ground model in shaking table test was prepared layer by layer (10 cm). In order to observe ground model behavior through transparent wall of soil container, black-colored silica sand with number seven grading was used to make horizontal lines indicating layers (see *Figure 2-4*). The black-colored sand is only place adjacent to the transparent wall with small amount. It was made by mixing with color agent in the ratio of 25kg of sand, 20grams of color agent and 500 ml ethanol (see *Figure 2-5*). It is noted that before using colored sand, at least 24 hours should be left after mixing allowing the sand to fully dry.

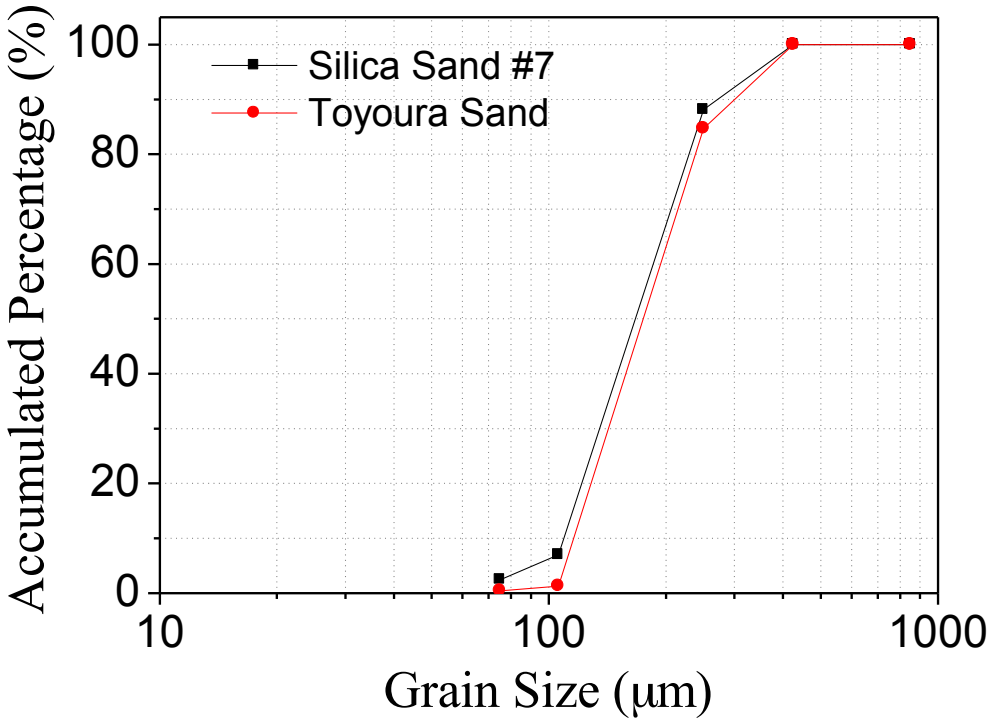

Figure 2-1 Grain size distribution of Toyoura sand and Silica sand with number seven grading

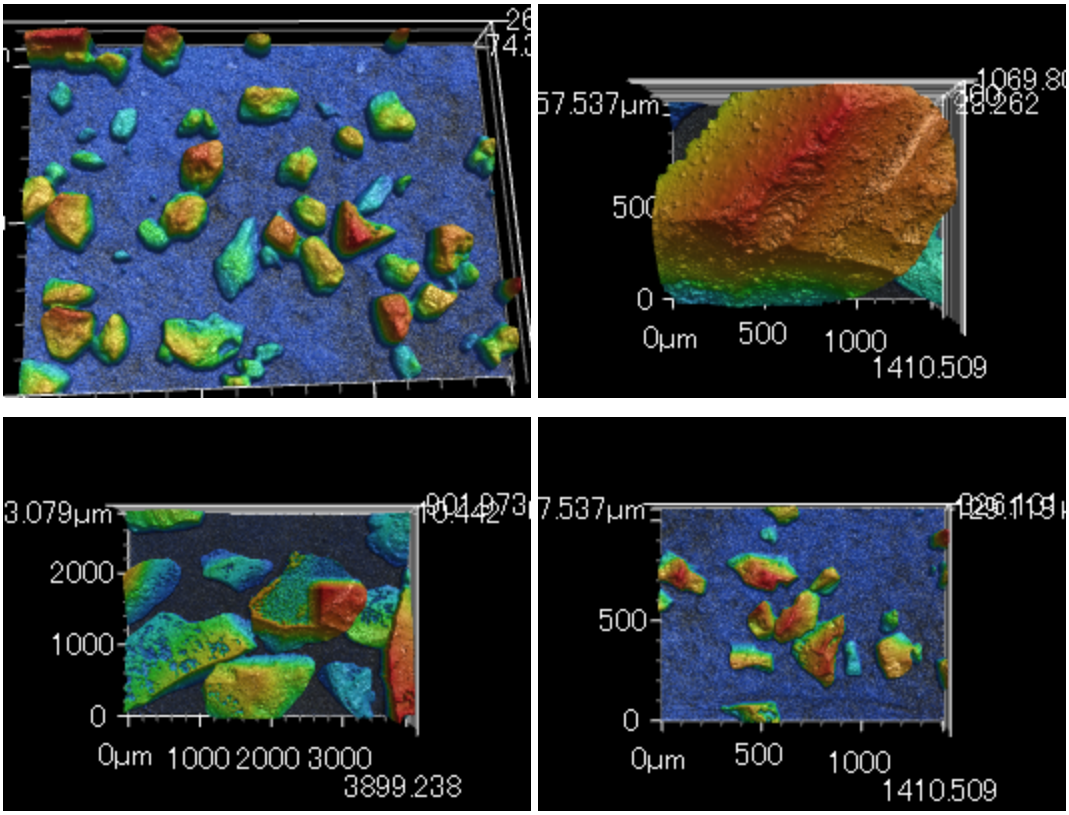

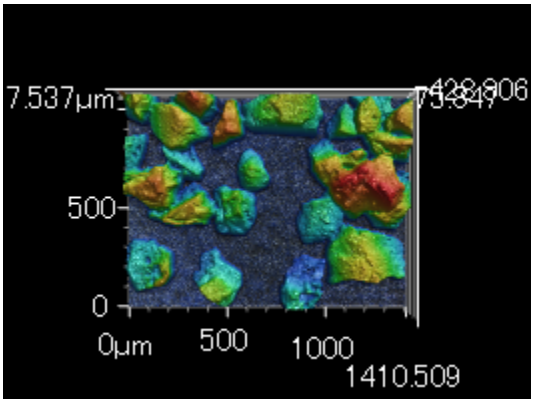

Figure 2-2. Microscopic photos of Silica sand with number seven grading

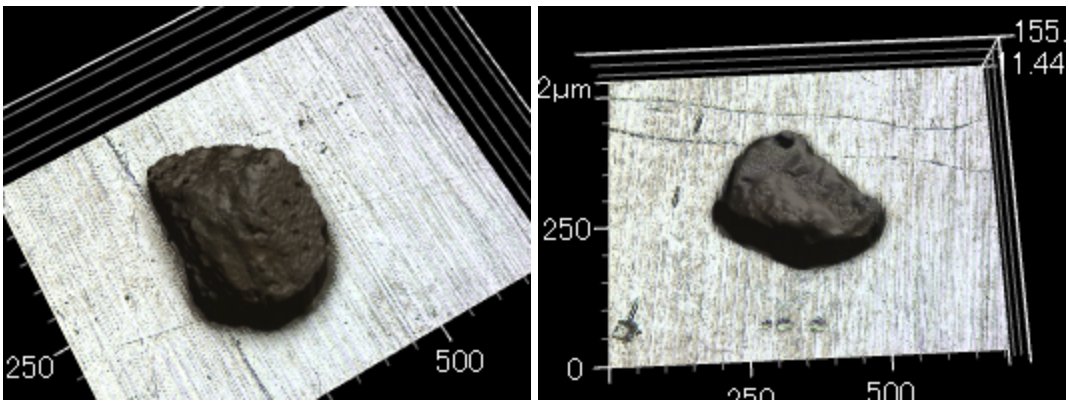

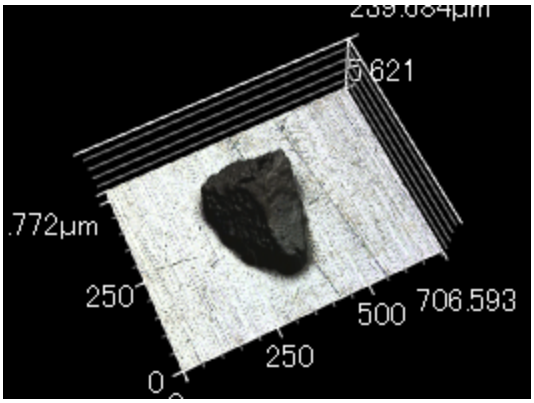

Figure 2-3. Microscopic photos of Toyoura Sand

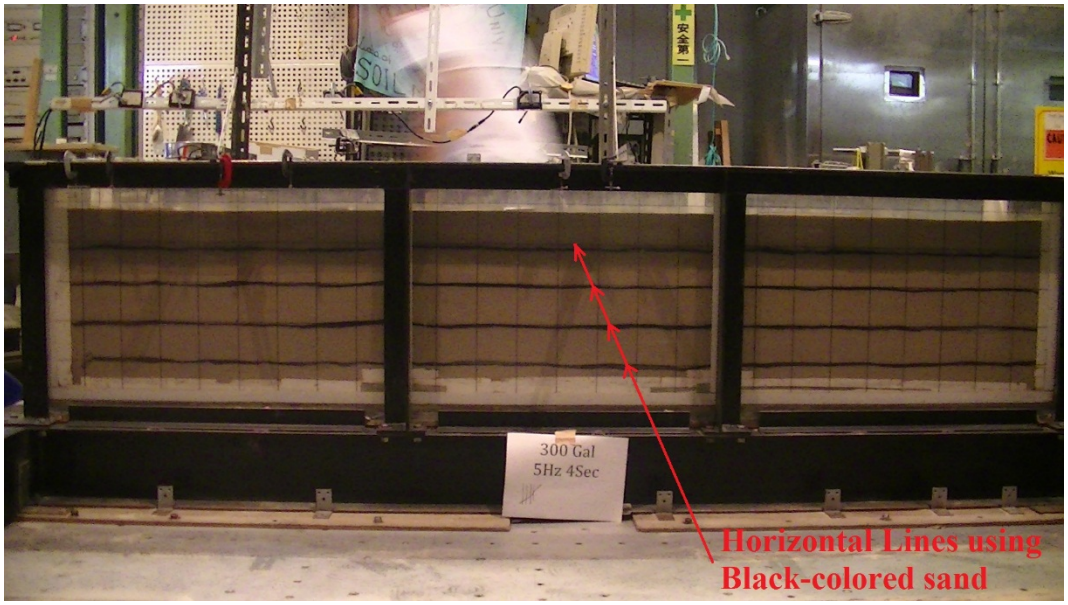

Figure 2-4. Horizontal lines indicating layers of 10 cm thick in soil model in shaking table tests

Figure 2-5. Color agent and ethanol for black colored sand

2.2 Shaking Table Apparatus and Monitoring Instruments

2.2.1 Shaking Table Apparatus

The shaking table is 3m in length and 2m in width capable of 2-dimensional in x and y direction (horizontal) shaking. *Figure 2-6* presents the top view of shaking table and soil container installed on the top. The properties of shaking table are show in *Table 2-2*. The wave form can be generated using computer program in which direction, acceleration, duration, frequency and timing can be set. It is advised that time gap of about 5 seconds should be used from execution in computer program to the start of shaking. If some mistakes occurred, the test can still be stopped before the shake.

Table 2-2. Shaking table properties

Dimension	3m x 2m
Shaking direction	X and Y axis (Horizontal)
Loading Capacity	7 tons
Frequency range	2-30 Hz
Maximum displacement	+/- 200 mm
Maximum Velocity	27 cm/s
Maximum acceleration	1000 Gal

2.2.2 Data Logger

There were six data loggers but only four loggers were used for data acquisition in this test. Each data logger provides 10 channels. The specification of data logger is presented in *Table 2-3*. It is capable of measuring both strain and voltage. Data sampling of these data loggers is 1000Hz at maximum. In this research, due to limited number of data recording of 49152, the data sampling rate of 500Hz was used providing approximately 98 seconds of data record. These four data loggers were connected to each other and to the computer. In general, there was no time or phase difference occurred between the data loggers. However, to avoid any error in time or phase difference, it is suggested that the sensors in the same group of data computation should be connected to only one single logger. *Figure 2-7* shows data loggers used in this study.

Table 2-3. Data logger properties

Model	DRC-101C
Number of channel	10
Measuring object	Strain and voltage
Measuring Range	50000 x 10-6 strain
Frequency range	DC 2.5kHz
Weight	9 kg
Dimension	430 (W) x 148 (H) x 330 (D) mm
Power supply	AC90-250V 50/60Hz 120VA Max

2.2.3 Soil Container

Soil Container for shaking table test used in this research is shown in *Figure 2-8*. It was made from steel frame structure and transparent acrylic glass wall. Grid of 10cm x 10cm was drawn on the glass wall for the simplicity during model preparation. The bottom was mounted to the shaking table with wooden plate in between. Nine water pipes were attached at every 30cm under the container allowing water to rise uniformly and constantly. These pipes were connected through the bottom where mesh was placed to protect sand particle going inside the pipe promoting clogging problem. At the inner base of soil container, plastic plate with meashed-holes was placed following with geotextile sheet. *Figure 2-9* shows the bottom of the soil container where inlet and outlet pipes were installed. However, during preparation, water should be raised at low discharge to avoid any soil disturbance by water flow. The dimension of soil container was 0.60m in height, 0.40m in width and 2.60 in length. As the shaking direction in this study was in the longitudinal side, on the width side of container, damping material was placed to reduce the impact of rigid boundary effect (see *Figure 2-10*).

2.2.4 Piezometer

Four piezometers were installed with the soil container at the back side to measure water table inside ground model. It was assembled using plastic tube and connected to the soil container. The piezometers are cleared by using high air pressure before ground model preparation. At the connection, the water valve is installed which is closed during model preparation and liquefaction test. During model preparation where air-pluviation method is used, there might be sand particles and dust clogging at the connection between soil container and piezometer. After finishing the model and rising water table, the valve is open to check

water table. The valve was again closed during liquefaction test as excess pore water pressure can also be dissipated through the piezometer.
Figure 2-11 shows a picture of piezometers.

2.2.5 Accelerometer

Accelerometers were used to observe acceleration response in the ground model during performing model shaking by embedded them in the ground. *Figure 2-12* shows a photo of accelerometer used in this research. This accelerometer is designed to measure absolute acceleration which applied to it in one direction only. This means that if the sensor is placed vertically, it only senses the gravity acceleration which is 1g. Thus, during the model preparation process, the accelerometer must be placed carefully to measure the desired direction. In addition, the direction of positive and negative should also be ensured to avoid phase different. For this reason, a plastic cup is attached to the bottom of the sensor by super glue to prevent the sensor from tilting, rotating and moving from the desired position after installation. In this research the accelerometer measured acceleration level in the shaking direction. Besides, it was not only used for soil acceleration monitoring but also the base input motion. There was one accelerometer attached to the soil box for measuring base acceleration. Accelerometers were calibrated with gravity and the calibration is given in Appendix A.

2.2.6 Pore Water Pressure Transducer

Pore water pressure transducers were used to monitor static pore water pressure and excess pore water pressure, during liquefaction test, at specific location. It should be noted that the transducer must be placed in the perpendicular to shaking direction in order to avoid dynamic water pressure induced by shaking. Moreover, any air trapped inside the sensor should be removed or else the sensor not only senses pore water pressure but also air pressure. Before placing the sensor into the ground model, the sensor should be saturated. This can be done by opening the cap of sensor under the water and ensuring of air removal. Then, the cap was closed before placing at the desired position. Another important issue to be noted is that the location of the sensor must be fixed and refrained from moving downward or upward. During soil liquefaction where there is no effective stress, the sensor would sink down and observe

wrong value of pore water pressure. *Figure 2-13* shows a picture of pore water pressure transducer.

Prior to the test, the pore water pressure transducers were calibrated by measuring reading voltage at different known-water level. As the relationship between pore water pressure and voltage are linear, the relationship was established to obtain calibration factor as shown in Appendix A.

2.2.7 Laser Sensor

Laser sensor model IL-300 made by KEYENCE was employed to monitor ground settlement by measuring the change of height from prior to the liquefaction test to the end of the test. The laser sensor system consisted of a laser sensor itself IL-300, an amplifier IL-1000 and power unit KZ-U3 as shown in *Figure 2-14*.

The sensor was placed with the steel bar on the top of soil container using double tape and clamps. The setup of laser sensor is presented in *Figure 2-15*. The laser light is pointed to the target placed on the top of ground model using nails to keep the target in place. The laser light is reflected back to the sensor; thus, the target of laser should be in white color to avoid possible errors. In addition, the target should also be somewhat water-resistant as there might be water accumulating on the top surface and damages the target. In the case of this study, a cardboard with white paper on top was used. The surface of ground model should be flatten avoiding vertical movement of the target. The settlement value measured by the laser sensor was then used to calculate soil relative density change in the container as a whole.

Figure 2-6. Top view of shaking table and soil container installed on the top.

Figure 2-7. Data loggers

Figure 2-8. Soil container

Figure 2-9. Holes for water inlet and outlet at the base of soil container

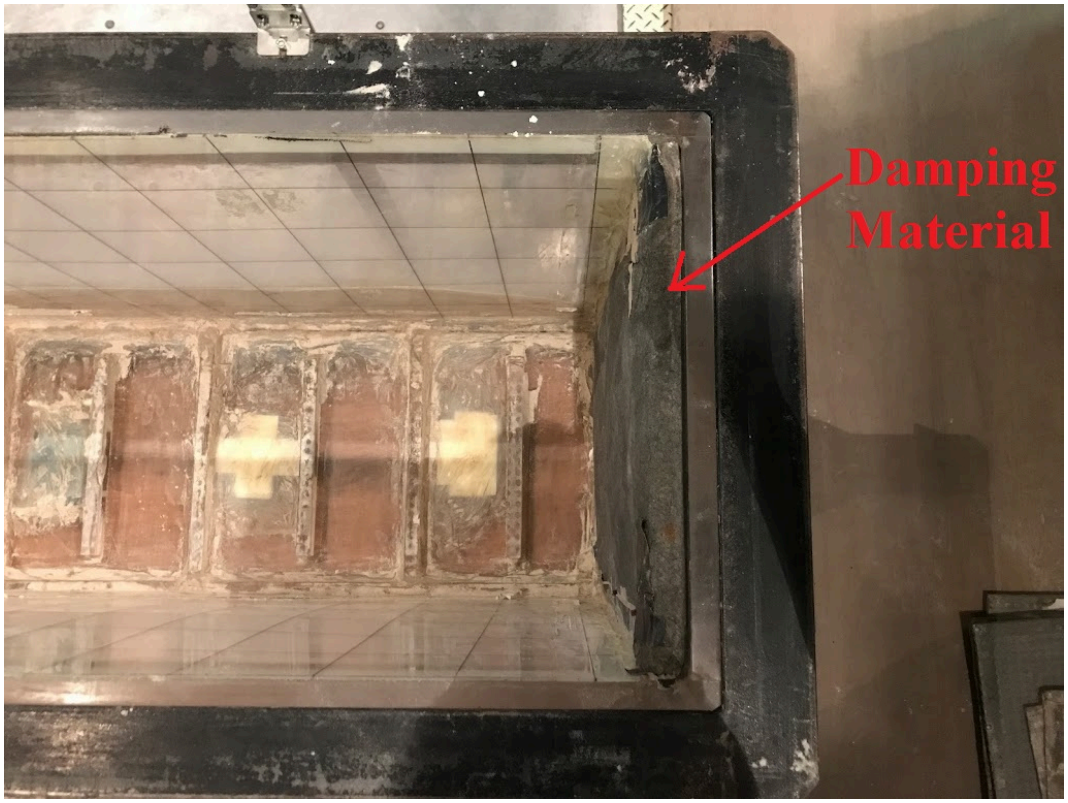

Figure 2-10. Damping material on the side wall to reduce impact of rigid boundary effect

Figure 2-11. Piezometer installed to the soil container

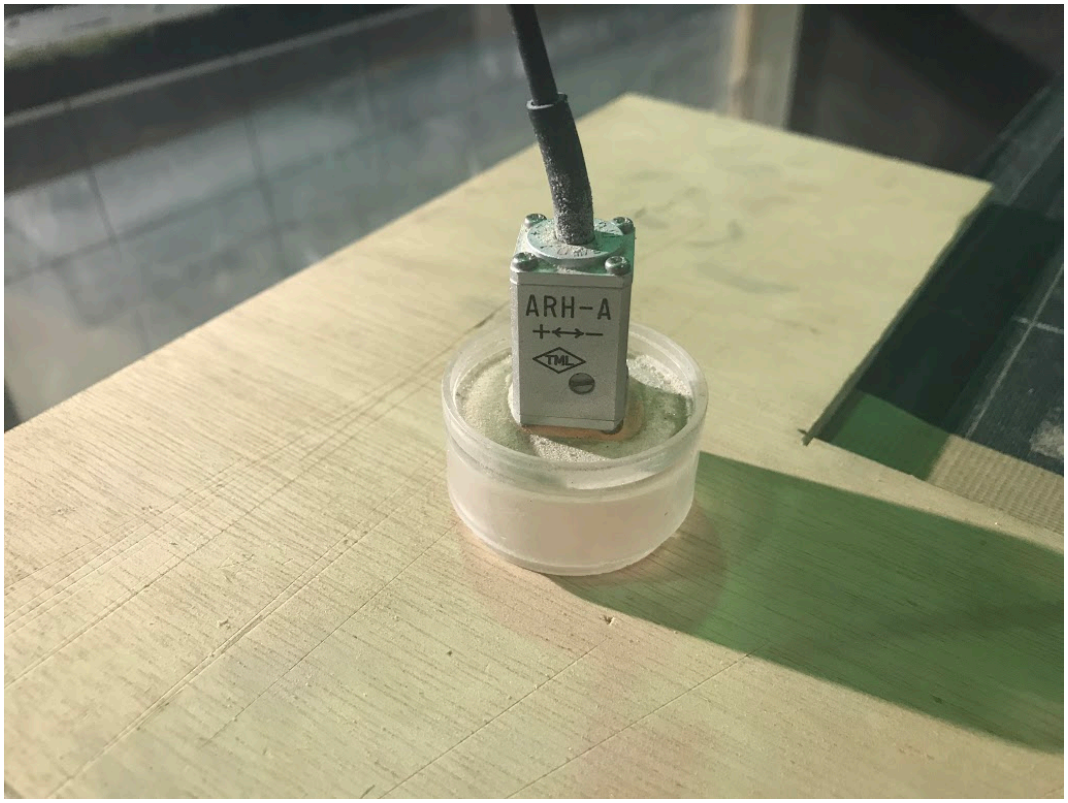

Figure 2-12. Accelerometer

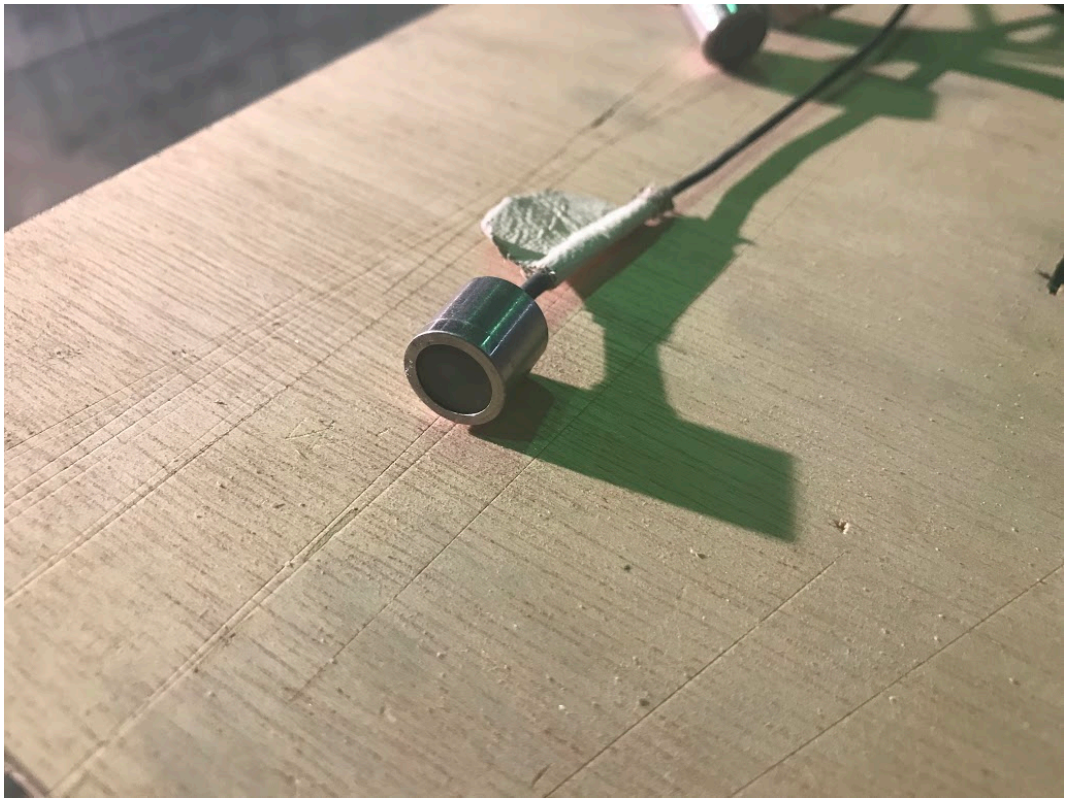

Figure 2-13. Pore water pressure transducer

Figure 2-14. Laser Sensor Instrument

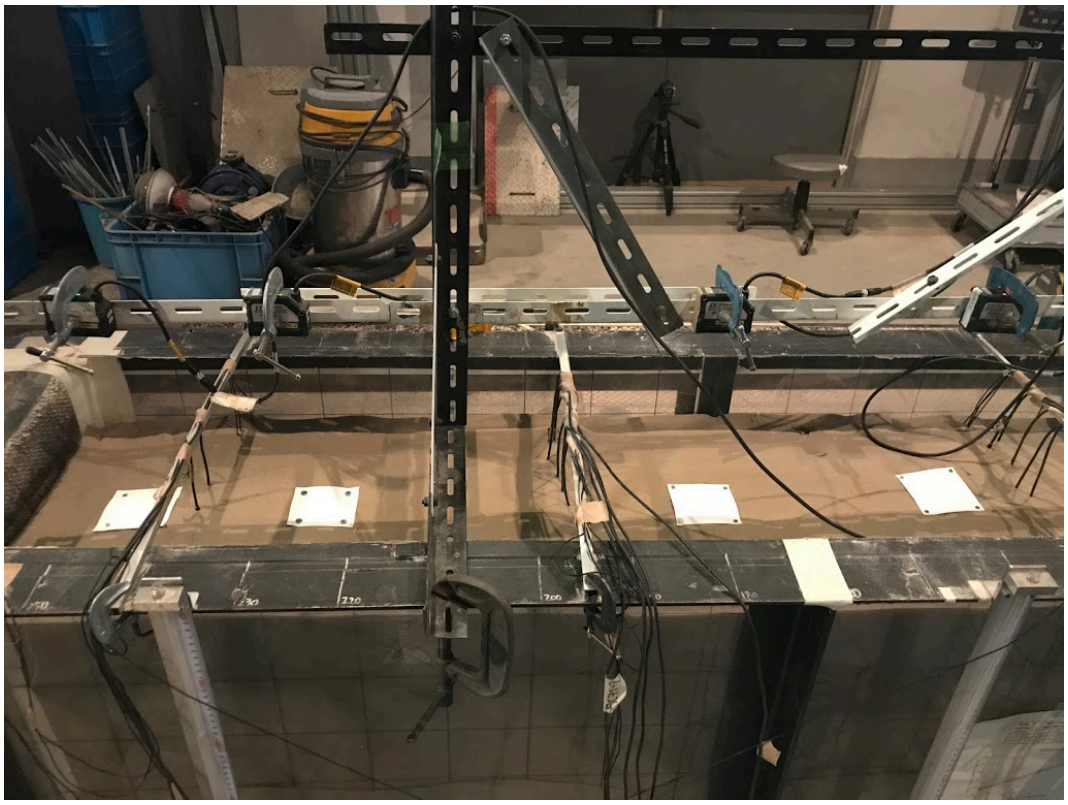

Figure 2-15. Set up of laser sensor above ground model

2.3 Methodology of Shaking Table Test

2.3.1 Ground Model Preparation

Air-pluviation method was employed to prepare uniform ground model. In order to achieve target relative density of about 50-55%, sand hopper was developed as shown in *Figure 2-16*. The falling height was 900 mm to the inner bottom of soil container. At the bottom of the bucket, there were holes of which the opening can be adjusted. Also, three layers of mesh were installed after the opening to ensure that the falling material are uniformly distributed.

However, in this case, the falling height cannot be adjusted since the moving bucket is fixed and is refrained from moving vertically. Unlike air-pluviation method used in element test, flowing rate of sand was controlled instead of falling height by adjusting the size of the opening. The larger amount of material flow is, the lower density is. However, the falling height was not constant throughout the process as the soil layer keep accumulating from bottom to the top, the opening of the sand hopper changed layer by layer from larger for the bottom layers to smaller for the top layers. It is noted that before starting air-pluviation process, the wooden plate was placed on the top of soil container to detain falling material that spill out of the container. The detained material was then scaled and used to compute initial relative density of soil model (see *Figure 2-17*). The ground model was made in 5 layers with 10cm thick as shown schematically in *Figure 2-18*.

2.3.2 Sensor Installation

Sensor plan is shown schematically in *Figure 2-18.* Sand liquefaction behavior in the soil container is different depending on the location due to rigidity of soil container side wall promoting boundary effect. Therefore, the primary column of sensors was installed at the middle of the soil container; as this location would the most simulate sand behavior closed to reality. Another column at the quarter of soil container is used as a secondary set of data in case where sensors in the primary column accidentally did not work. The data for this column can be also used to study the effect of regid side wall in comparison with the data for the primary column Sensors in two columns at the edge of the container were installed to observe boundary effect of this container, which will be discussed in detail later.

During ground preparation, accelerometers and pore water pressure transducers were placed after finishing the soil preparation at target level. When the sand liquefies, where the effective stress is equal to zero, sensors would sink down to the bottom because of their higher density compared to the surrounding sand. Thus, the sensors were then hung with the steel bar on the top of soil container to keep sensor in original position and height during liquefaction (see *Figure 2-19*). The plastic cup attached to the bottom of accelerometer also helped to prevent possible rotation (see *Figure 2-12*). After finishing ground model, the wooden plate and sand hopper were removed and the steel frame was instead attached to the top of the container by using clamps. The laser sensor was then installed with that steel frame.

2.3.3 Input and output of water

Water was input to the container through pipes at the bottom (see *Figure 2-20*). The discharge should be kept small so that there is limited soil disturbance especially at the bottom of ground model. As the ground model takes about two days to prepare, the water should be filled after finishing the work of each day. This is to keep the installed pore water pressure transducers inside ground model saturated avoiding air trapped inside transducers. However, with time, there would be suction of top unsaturated soil and water evaporation, the water should be filled up to above the highest pore water pressure transducers so that after evaporation and suction taking place, the water level is still higher than the transducers. Plastic sheet is suggested to cover the top of soil container to prevent evaporation.

After finishing all the layers of ground model, the water was filled in up to desired level, in this case, at 40cm from the bottom. The water level was confirmed by piezometers before executing liquefaction test. After each test, the water level was monitored and was adjusted to be always at 40cm before the test.

2.3.4 Experiment Program of Shaking Table Test

In this section, experimental program will be described briefly where the detailed program will be discuss later in the shaking table test section. In every test, the ground model was subjected to 20 sinusoidal loading cycles with frequency of 5 Hz and duration of 4 seconds. The tests started from low acceleration level (200 gal, 300 gal and 400 gal).If the ground

model did not liquefy, the acceleration is increased by 100 gal. Tests were terminated when the acceleration level of 1000 gal was reached which is the capacity of shaking table at Geotechnical Laboratory, the University of Tokyo. Generally, during liquefaction excess pore water pressure builds up to be equal to the vertical effective stress. The acceleration also shows amplification. The examples of acceleration and pore water pressure time history data in the case where the ground model liquefies and does not liquefy are shown in *Figure 2-21*. It is also noted that between each liquefaction test, time was allowed for excess pore water pressure generated in previous liquefaction test to be fully dissipated.

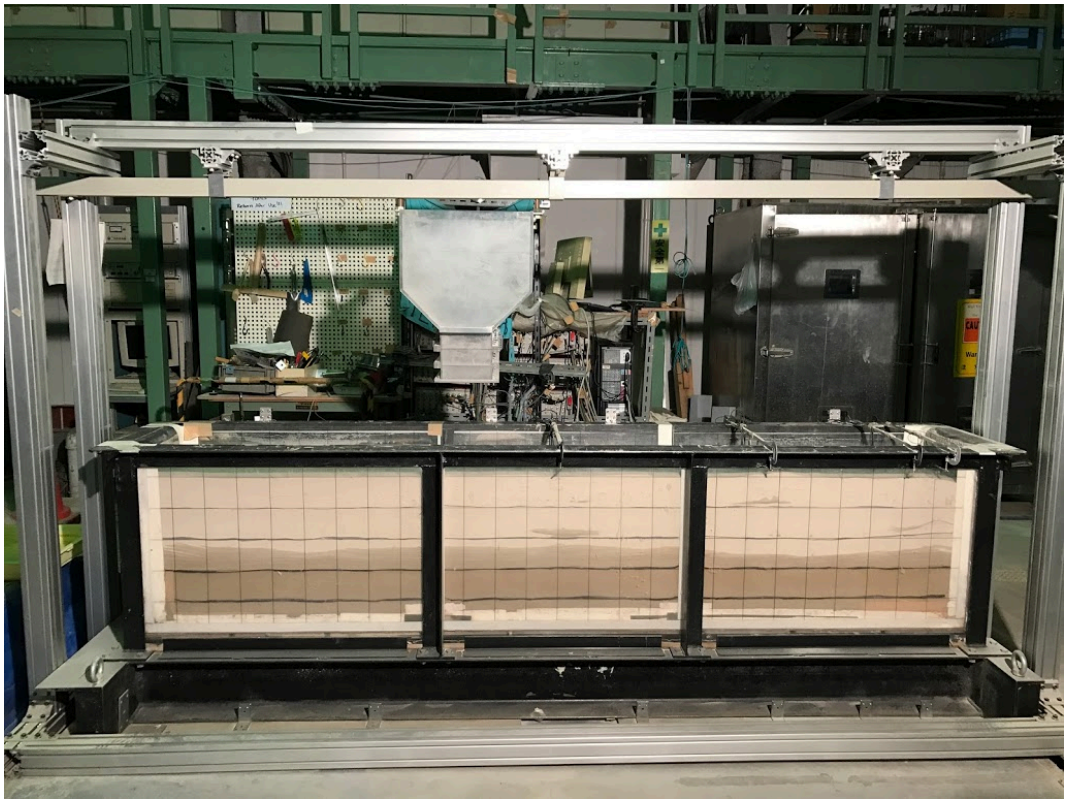

Figure 2-16. Sand hopper for air-pluviation

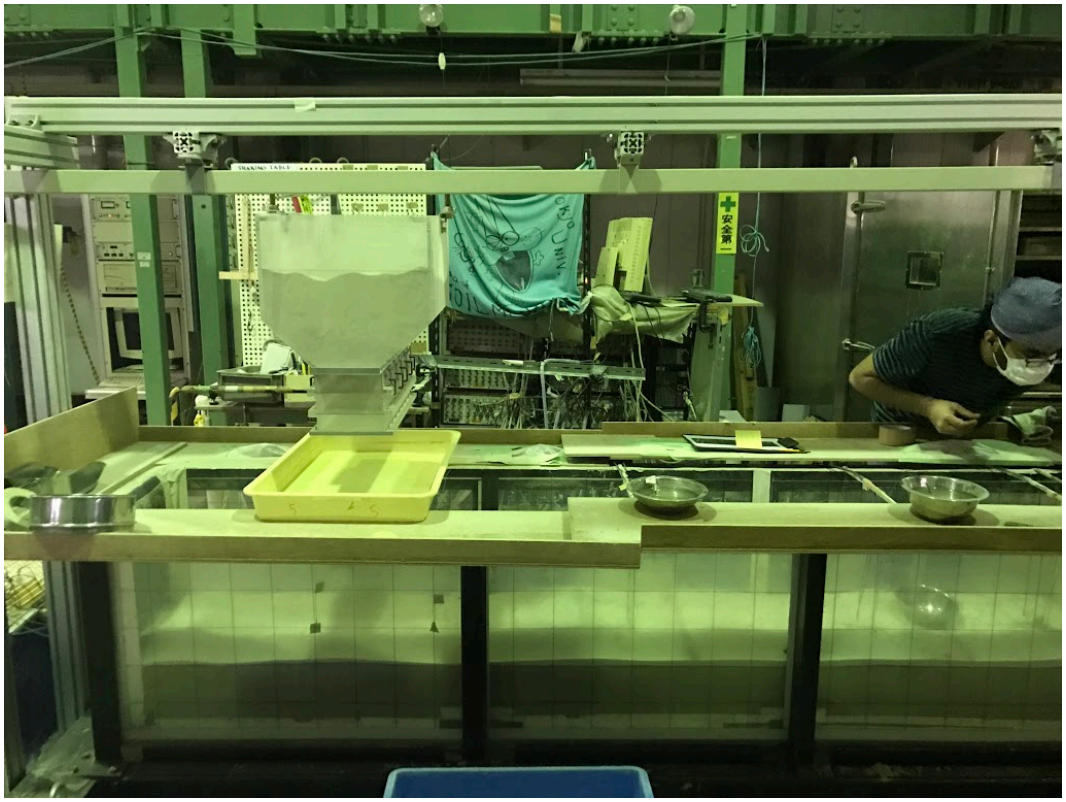

Figure 2-17. Wooden plate on the top of soil container

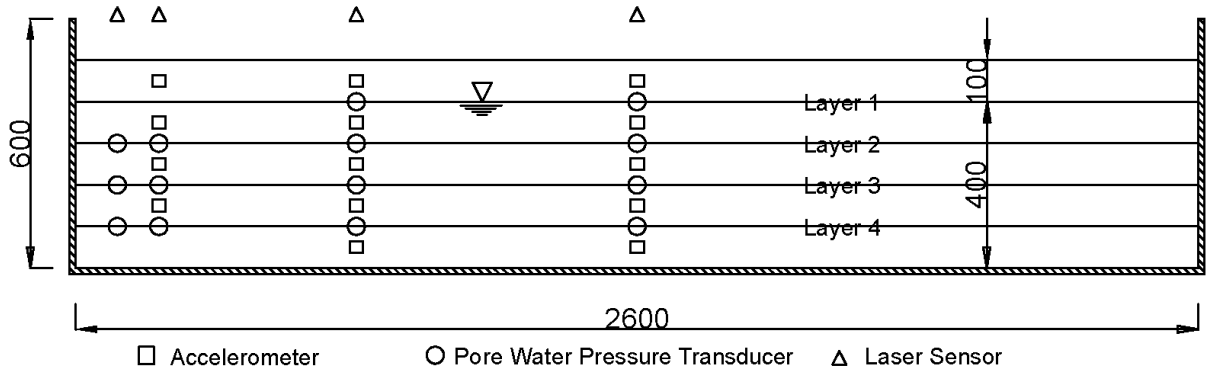

Figure 2-18. Instrumentation arrangement of shaking table

Figure 2-19. Sensors hanging with the steel bars on the top of soil container

Figure 2-20. Pipes installed at bottom of soil container for water input and output

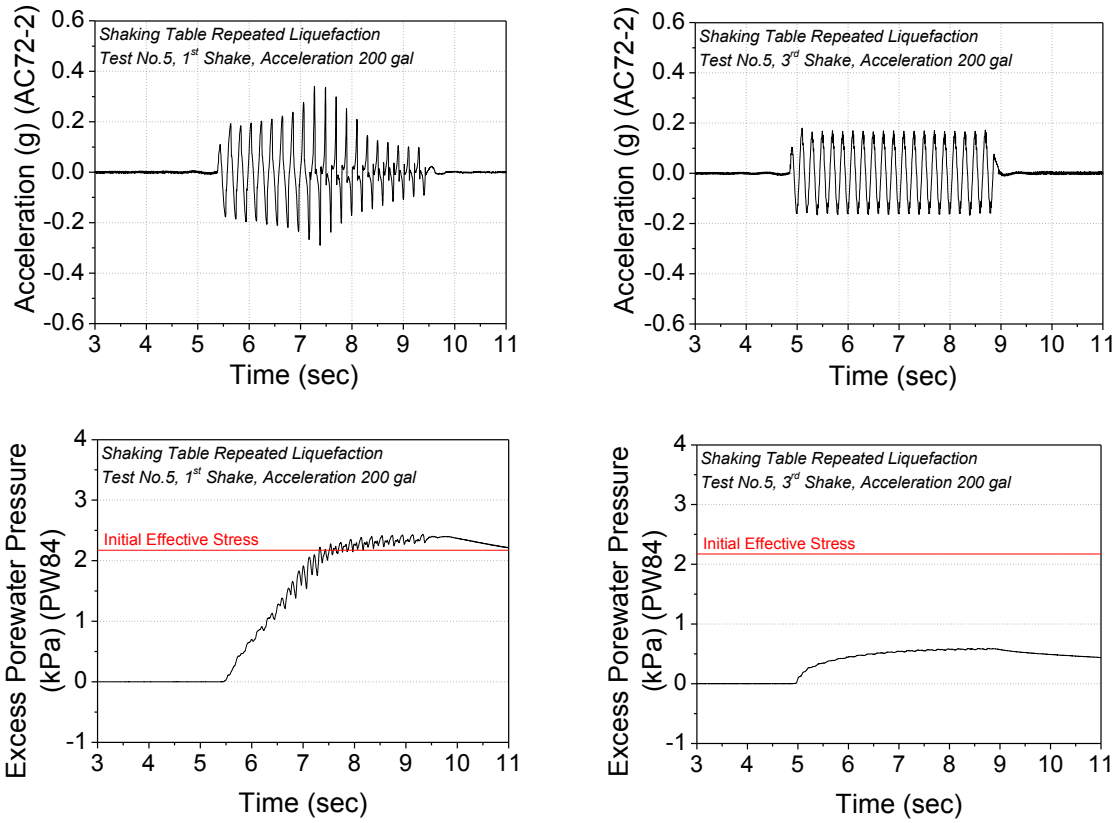

Figure 2-21. Acceleration and excess pore water pressure time history when ground model liquefies (a, b) and when ground model does not liquefy (c, d)

2.5 Method of Calculation

In this section, the method of calculation used in this research will be introduced. There are in total three types of raw data as follow; acceleration, pore water pressure and ground model settlement. All of the data were used for calculation.

2.5.1 Shear strain

Generally, shear strain can be measured directly using strain gauge. However, it is also possible to calculate horizontal shear strain from the differential displacement between two accelerometers using equation

$$\gamma = \frac{\Delta d}{\Delta h}$$

where ∆d is differential displacement between two accelerometers and ∆h is the vertical distance between those two accelerometers (see *Figure 2-22*). It is noted that the displacement of the accelerometer can be computed by double integration of acceleration data. Unexpectedly these data contain some errors; for instance, noise, drift and offset, due to

numerical calculation and data recording. In order to avoid these errors, the raw acceleration data was high-pass filtered and offset adjusted before the first and second integration as well as after the second integration procedure.

2.5.2 Shear stress

The shear force during liquefaction can also be computed from acceleration data by following the first Newton's laws of motion given in equation

$$F = \sum ma$$

where F is force, m is mass and a is acceleration. Moreover, the shear stress can be computed using force given in the equation divided by cross section area. *Figure 2-22* illustrates soil column for shear stress and shear strain calculation. In shaking table case, the shear stress was computed as a summation of multiplied results of mass and acceleration. In the case of soil mass column where the cross section area is 1x1, thus the cross section area is equal to unity given the shear stress equation as

$$\tau = \sum ma$$

where τ is shear stress, m is mass and a is acceleration.

2.5.3 Vertical effective stress

The effective stress can be calculated followed equation

$$\sigma'_v = \sigma_v - u$$

where σ'_v is vertical effective stress, σ_v is vertical total stress and u is pore water pressure. The vertical total stress and pore water pressure can be computed by the equation

$$\sigma_v = H_{soil}\gamma_{soil}$$

$$u = H_{water}\gamma_{water}$$

where H is height and γ is unit weight.

During liquefaction, excess pore water pressure is generated promoting a decrease in effective stress. With the excess pore water pressure data from the pore water pressure transducers, vertical effective stress time history during shaking can be computed by the equation

$$\sigma'_v = \sigma_v - u - \Delta u_e$$

Where $\triangle u_e$ is excess pore water pressure. In addition, with the computed shear stress discussed before, the effective stress path during liquefaction can be drawn.

In the case of mean effective stress (p') calculation for shaking table test, the coefficient of earth pressure at rest (k_0) was assumed to be 0.5. Thus, s_h equal to $0.5\sigma_v$ and p' can be computed using equation

$$p' = \frac{\sigma_v + 2\sigma_h}{3}$$

$$p' = \frac{2\sigma_v}{3}$$

2.5.4 Number of cycle

Liquefaction resistance normally evaluated in terms of number of cycle to reach the certain double amplitude shear strain which can be computed using the equation shown below.

$$N\gamma = \left(\frac{(\gamma_{DA} - \gamma_{DA(Ni)})}{(\gamma_{DA(ni+0.5)} - \gamma_{DA(Ni)})} \times 0.5\right) + Ni$$

Where N_γ is number of cycle to liquefaction, γ_{DA} is the target double amplitude shear strain, $\gamma_{DA(Ni)}$ and $\gamma_{DA(Ni+0.5)}$ are the double amplitude shear strain at the loading cycle before and half cycle after the target double amplitude shear strain, and Ni is the number of cycle at which target double amplitude shear strain is reached (see *Figure 2-23*).

In some cases of triaxial testing, the tests were terminated immediately after reaching target desired double amplitude strain. Thus, the double amplitude shear strain at half cycle after the target double amplitude shear strain could not be determined. In such a case, the number of cycle required to trigger liquefaction was calculated based stress instead of strain using following equation;

$$N\gamma = \left(\frac{q_f}{q}\right) + Ni$$

Where N_γ is number of cycle to liquefaction, q_f is deviator stress at test termination, q is maximum deviator stress used in the test which depends on CSR value and Ni is the number of cycle at which target double amplitude axial strain is reached (see *Figure 2-24*).

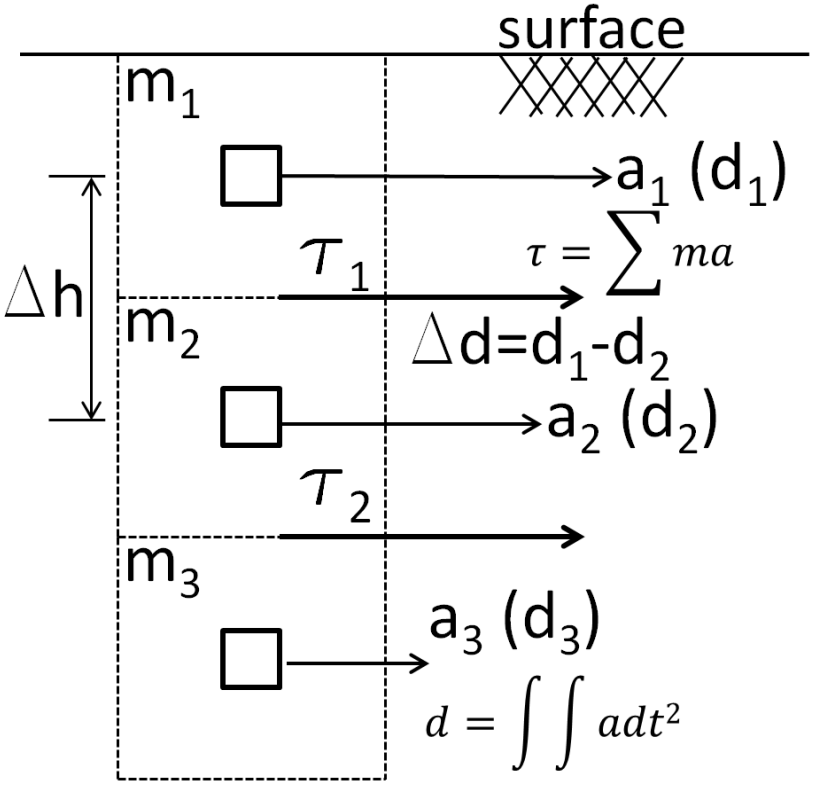

Figure 2-22. Computation of shear stress and shear strain

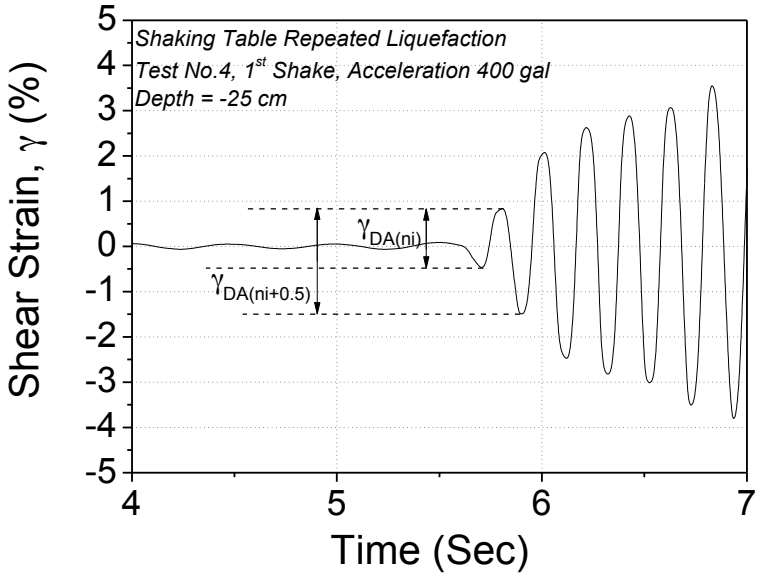

Figure 2-23. Definition of of parameters in number of cycle calculation based on strain

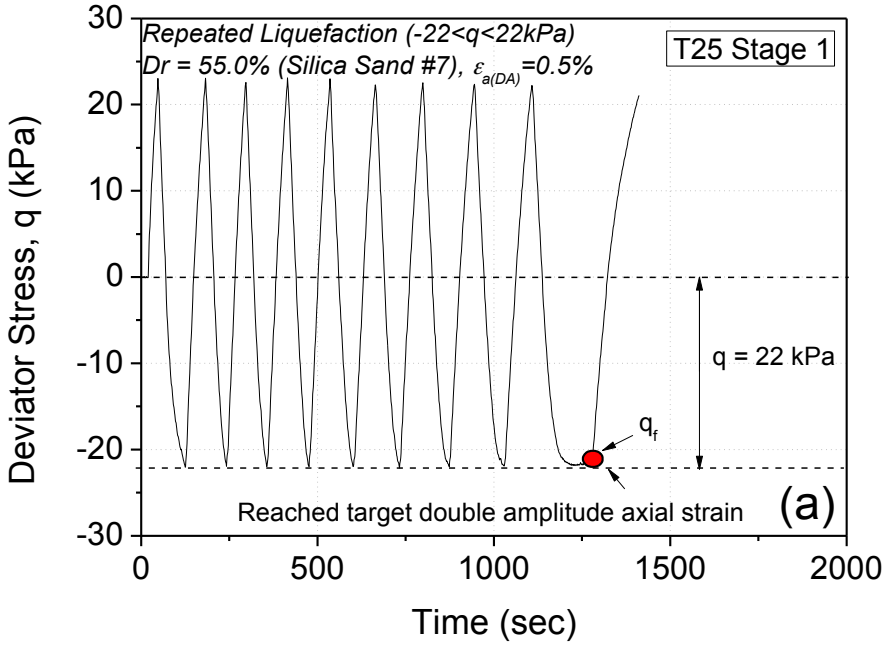

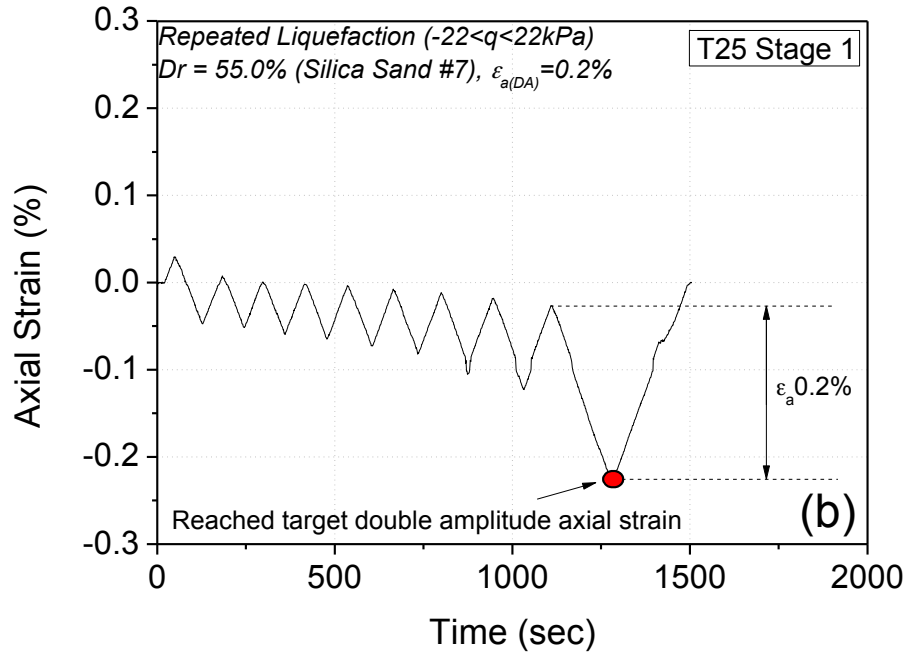

Figure 2-24. Definition of parameters in number of cycle calculation based on stress in (a) deviator stress time history and (b) axial strain time history

2.6 Triaxial Apparatus and Monitoring Instruments

2.6.1 Triaxial Apparatus

The triaxial apparatus used in this research was developed by Geotechnical Laboratory, the University of Tokyo as shown in *Figure 2-25*. It is capable of cyclic loading liquefaction test using stress control which means that uniform stress can be applied and the test can be terminated automatically when the target strain value is reached. The load is generated by electric driven gear controlled by a computer. The pressure cell was made of transparent glass with a capacity of approximately 1 MPa. Monitoring instruments such as load cell and displacement transducer are described below.

2.6.2 Inner Load Cell

The axial load during the test was monitored using a strain-gauge-typed load cell with capacity of 5 kN as shown in *Figure 2-26*. It was installed inside the cell at the tip of the loading piston with the top cap screwed below. In this way, the effect of loading piston friction can be eliminated (Tatsuoka, 1988). It was calibrated by loading and unloading with known weights with some increments. The calibration chart is given in Appendix A.

2.6.3 External Displacement Transducer (EDT)

The specimen axial displacement during the test was measured by a conventional type of transducer called "external displacement transducer (EDT)". It was installed vertically and measured the vertical displacement at the clamp which was attached to the loading piston. The maximum capacity of EDT is 20 mm so the initial position of EDT should be set at around the middle as during cyclic loading specimen was subjected to both compression and extension. In this study, EDT was used to monitoring specimen's vertical displacement which was further calculated to axial strain during consolidation and testing process. It was calibrated by measuring the height of a known standard blocks in voltage value as the relation between the displacement and output voltage is linear. The photo of EDT is presented in *Figure 2-27*. The calibration chart is given in *Appendix A*.

2.6.4 Low Capacity Differential Pressure Transducer (LCDPT)

In order to monitor the specimen global volumetric strain by measuring the volume of water drained out of specimen, the low capacity differential pressure transducer was used. In the liquefaction test, volume change in specimens occurs during consolidation process and reconsolidation in case of repeated liquefaction test. The drained water was then accumulated in the burette. The photo of LCDPT is shown in *Figure 2-28*.

2.6.5 Pore water pressure and cell pressure transducer

The pore water pressure and cell pressure transducer was used to measure the back pressure and cell pressure during the consolidation and liquefaction test. This value was then calculated for effective confining pressure and also mean effective stress. The *Figure 2-29* shows the photo of the transducers. On the top, there was opening which can be close by screws. This opening is used for saturation of all the tube to avoid an error in measurement. It was calibrated with a known pressure using pressure gauge and the calibration chart is given in Appendix A.

Figure 2-25. Triaxial Apparatus

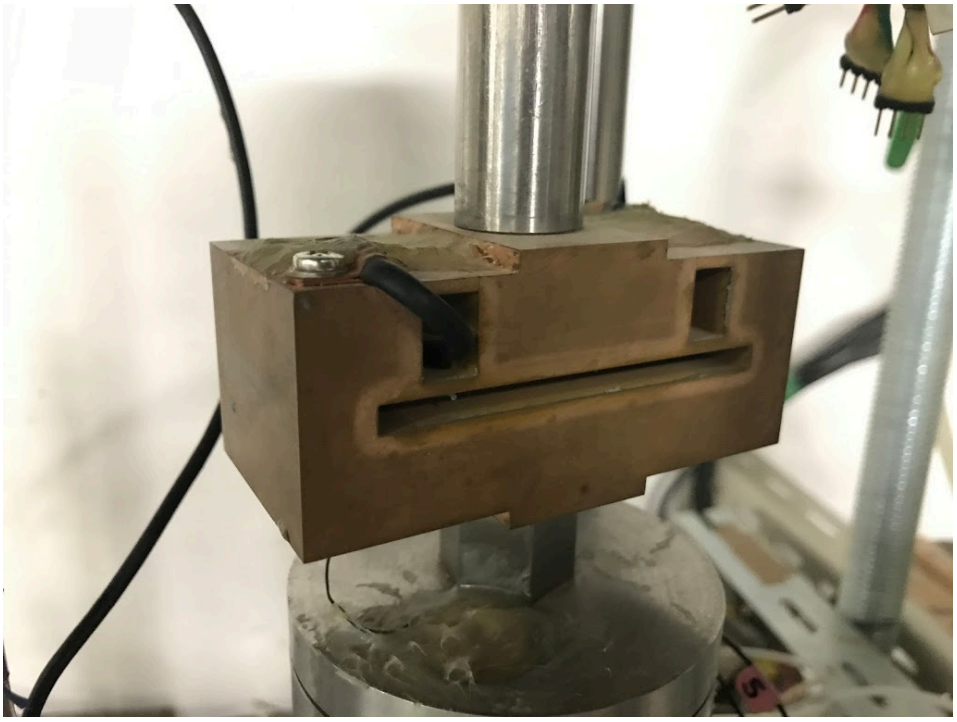

Figure 2-26. Inner Load Cell

Figure 2-27. External Displacement Transducer (EDT)

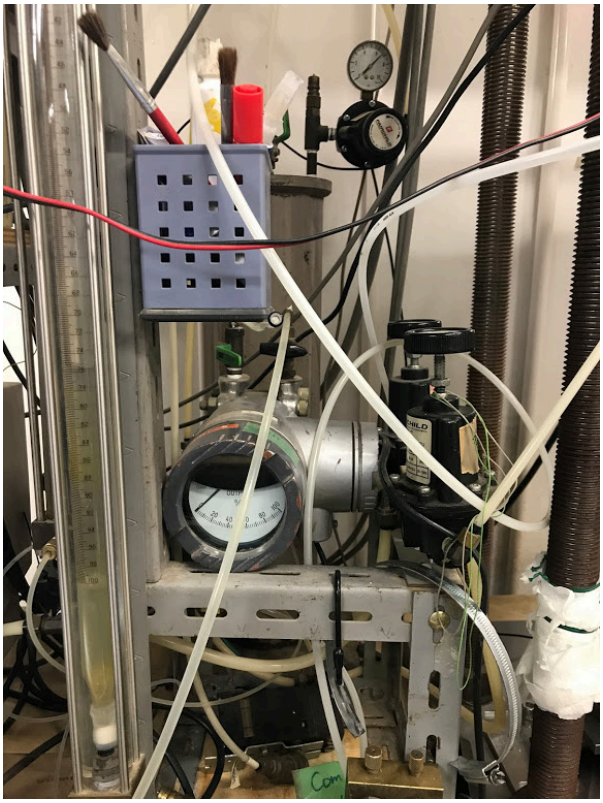

Figure 2-28. Low Capacity Differential Pressure Transducer (LCDPT)

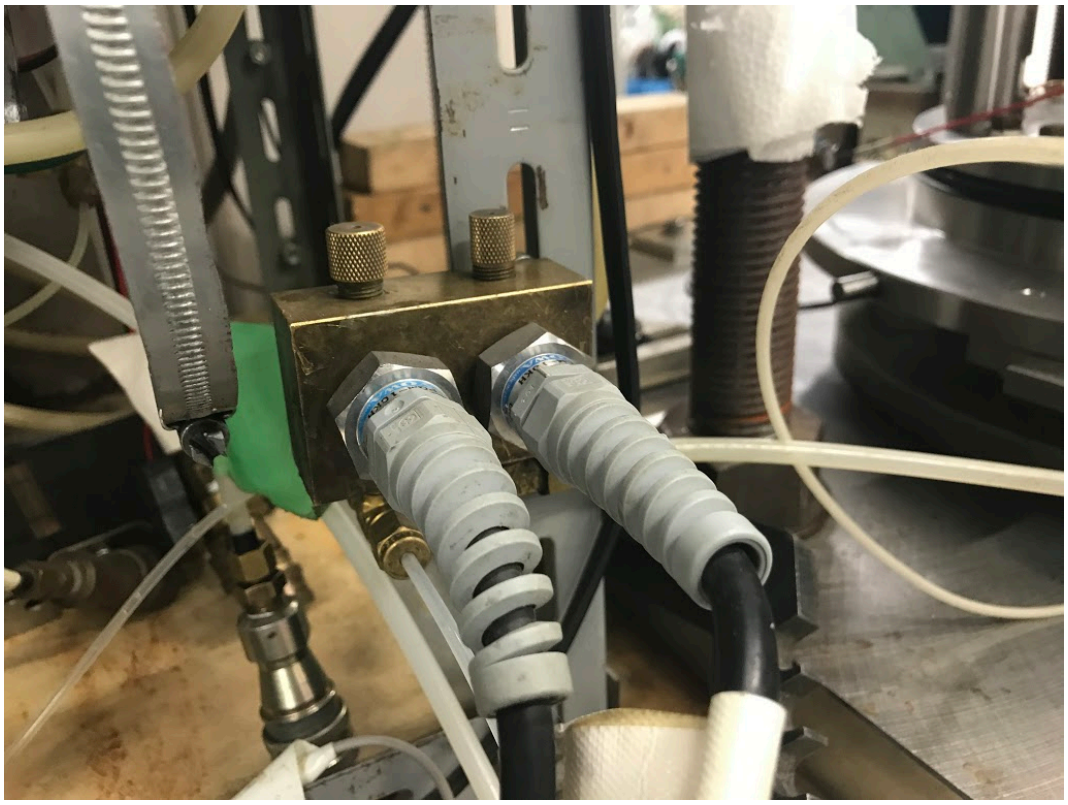

Figure 2-29. Pore water pressure and cell pressure transducer

2.7 Methodology of Triaxial Test

2.7.1 Specimen Preparation

Air-pluviation method was used to prepare specimen by free-falling the material from a nozzle to a mold of 150mm height and 75mm diameter. This nozzle allows constant flow rate of material accumulating from the bottom of the mold to the top. Unlike ground model preparation in shaking table apparatus, uniform target relative density (Dr) can be achieved by adjusting drop-height instead of opening. To ensure that the falling height is maintained constant throughout the air-pluviation process, a thin rope is attached at the tip of the nozzle to define the height. *Figure 2-30* illustrates air-pluviation method used in this research. The process continued until material overfills a mold. It is noted that before starting air-pluviation, a plastic sheet was attached at the top of the mold to detain the material that might fall out of the mold. The detained material was then scaled for accurate calculation of material used in specimen preparation for initial relative density computation. The top specimen surface was then leveled by scraping with a thin plate so that the material inside of a mold remains undisturbed. Two porous stones were placed at the top and the bottom of specimen. It must be noted that these porous stone was reusable. Thus, in order to prevent clogging, the porous stones were washed by water and air clean to clear the sand particles before oven dried. It was ensured that the stones were fully dried before used to avoid suction which raise difficulty in saturation process. The membrane used in this study was rubber membrane with 0.3 mm thickness. After preparation, specimen height and diameter was measured.

A Confining pressure of 30 kPa was then applied in order to keep the specimen in cylindrical shape. Specimen saturation was performed by double vacuum method (Ampadu and Tatsuoka, 1993). Before starting water flow, specimen was left vacuuming for at least 1.5 hour to ensure that air bubble is enlarged and is sucked out. Consequently, Skempton B-value was checked to be over 0.95, which is assumed that specimen is saturated.

It must be noted that counter weight balance of loading piston was employed to avoid specimen disturbance during specimen preparation as shown in *Figure 2-31*. Before placing loading piston on the specimen, some weights were put on the balance. After balancing, with

zero reading value in deviator stress, the piston was gently brought down to touch the top of specimen. Then, the rubber membrane was secured to the top cap. During increasing or decreasing vacuum pressure, there might also be a change in balance weight due to changing pressure acting on the specimen. Thus, the axial stress should be checked in every increments of vacuum pressure increase and adjust for the appropriate balance weight.

2.7.2 Consolidation

The testing procedure for repeated liquefaction test is schematically illustrated in *Figure 2-32*. After ensuring degree of saturation by confirming the B-value over 0.95, the specimen was then isotropically consolidated from a confining pressure of 30 kPa to 100 kPa as presented as stage A to Stage B in the Figure a. It is noted that an increasing rate of confining pressure should be kept small so that deviatoric stress can be maintained at 0 kPa by controlling simultaneously the axial loading system. Thus, the consolidation process took approximately 14 minutes. Consequently, specimen was left for consolidation time of 15 minutes before execution of liquefaction test.

2.7.3 Liquefaction Test

Following the equation,

$$CSR = \frac{q}{2\sigma'_c}$$

where CSR is cyclic stress ratio, q is deviatoric stress and σ'_c is confining effective stress, the target single amplitude of cyclic deviatoric stress, q, for a specified CSR can be computed. In this study, an initial confining pressure of 100 kPa was always used. By performing cyclic loading under undrained condition, excess pore water pressure is gradually generated together with axial strain accumulation. In general, liquefaction occurs at the point where effective stress is zero; i.e. excess pore water pressure becomes equal to initial effective confining pressure. However, the liquefaction stage in this study was defined based on the double amplitude axial strain percentage of the initial specimen height. When a specified amount of double amplitude axial strain was reached, the cyclic loading stopped and the left over axial strain was adjusted back to the initial value; i.e. 0%, as shown in *Figure 2-32* from stage C to stage C'. After that, excess pore water pressure was released out by slowly opening the specimen drainage valve allowing dissipation and reconsolidation as shown from stage C' to

Stage D. It must be noted that in order to maintain isotropic condition, the drainage valve should be opened slowly so that the deviatoric stress can be controlled at zero. Reconsolidation time of five minutes was allowed before the next liquefaction test. In addition, it is ensured that cyclic loading was terminated on the extension side; i.e. negative axial strain to unify possible effects if induced anisotropy. The repeated liquefaction test was done by repeating the described procedure as shown in *Figure 2-32* from stage D to stage E.

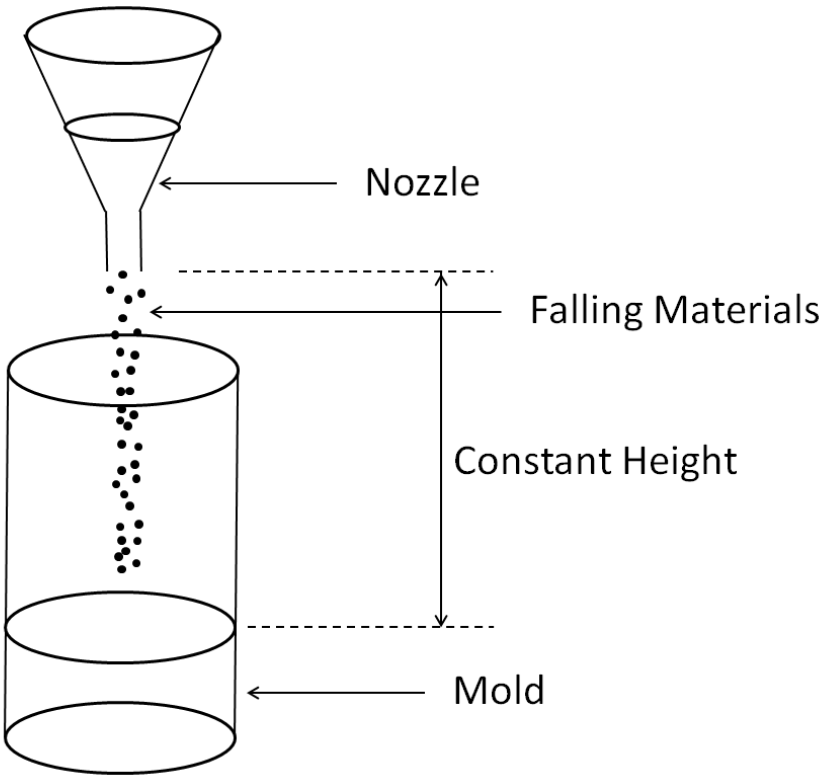

Figure 2-30. Schematic illustration of air-pluviation method in specimen preparation for triaxial liquefaction test

Figure 2-31. Counter weight balance for loading piston

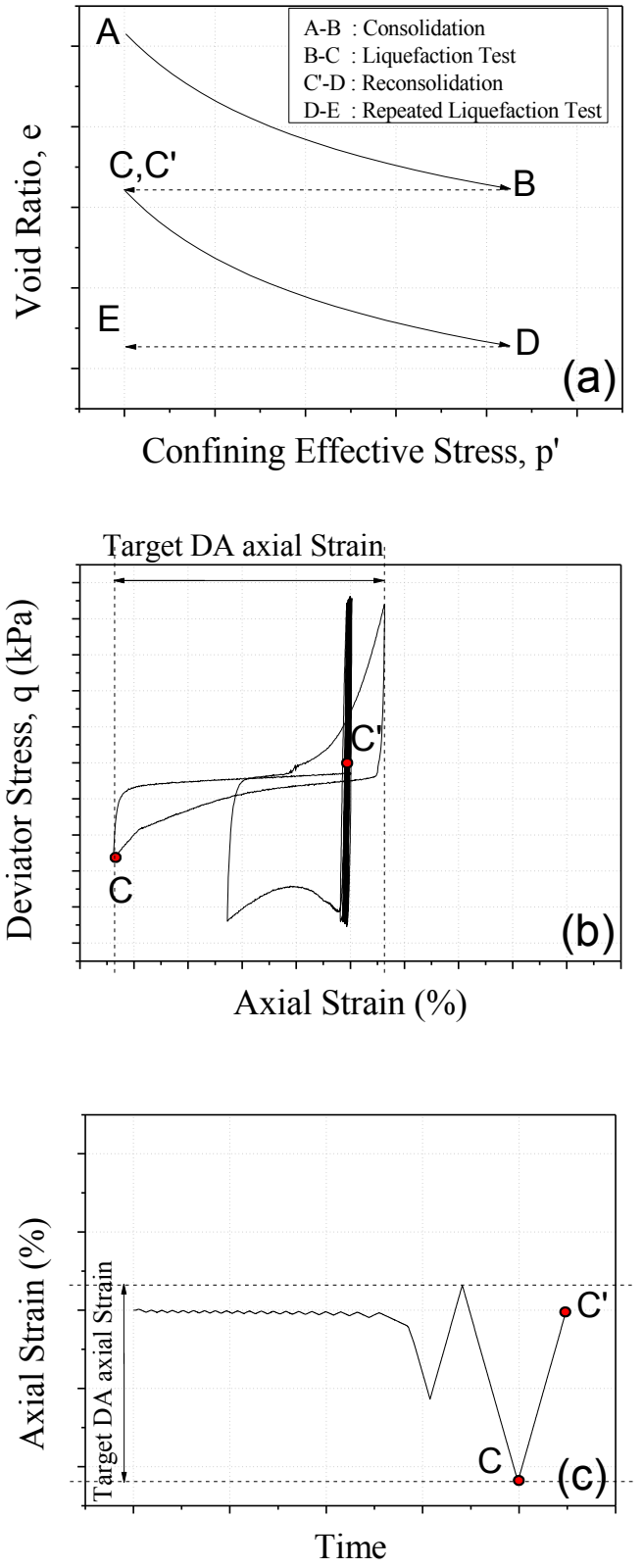

Figure 2-32. Liquefaction test stage (a) schemetic change in void ratio; (b) stress-strain relationship; (c) axial strain time history

2.8 References

AMPADU, S. and TATSUOKA, F., 1993. Effect of setting method on the behaviour of clays in triaxial compression from saturation to undrained shear. *Soils and Foundations,* **33**(2), pp. 14-34.

POULOS, S.J., CASTRO, G. and FRANCE, J.W., 1985. Liquefaction evaluation procedure. *Journal of Geotechnical Engineering,* **111**(6), pp. 772-792.

TATSUOKA, F., 1988. State-of-the-Art Paper: Some Recent Developments in Triaxial Testing Systems for Cohesionless Soils. *Advanced triaxial testing of soil and rock.* ASTM International, .

3. Repeated Liquefaction Behavior of Silica Sand in Triaxial Apparatus

Contents

Chapter 3 Repeated Liquefaction Behavior of Silica Sand in Triaxial Apparatus

3.1 Introduction

Undrained cyclic loading triaxial tests were conducted to investigate repeated liquefaction behavior. As already described in Chapter 1, there are many major parameters that influence liquefaction resistance of soil; for instance, relative density, strain amplitude history, anisotropy and liquefaction history. This chapter focuses on the effect of cyclic stress and mainly on the effect of strain amplitude history and effect of small strain during repeated liquefaction in cyclic triaxial test.

The frontier works on the effect of strain history to the next liquefaction resistance were Finn et al. (1970) and Seed et al. (1977). Unlike the logical thought that liquefaction resistance should increase with liquefaction history due to densification of soil, it was found that stress and strain history also plays an important role apart from density alone. Finn et al. (1970) was the first to point out the effect of previous strain amplitude (or pre-shearing) history on the reliquefaction resistance in a simple shear apparatus. The low strain amplitude of the first liquefaction test (±0.5%) promoted significant advantageous effect on the second liquefaction resistance; however, it was found that larger strain amplitude (±2%) drastically reduce the liquefaction resistance compared to the specimen subjected to lower strain amplitude. Using shaking table test, Seed et al. (1977) discovered that the same effect of strain amplitude. Further investigation on this issue was carried out by Ishihara and Okada (1978) and Ishihara and Okada (1982). The boundary which divides higher and lower of the next liquefaction was purposed. If the stress path crossed phase transformation line in the first liquefaction, it was suggested that the specimen should showed lower liquefaction resistance in the next stage. With smaller strain history where stress path did not cross the phase transformation line, the specimen should present higher reliquefaciton resistance. This boundary was also used to investigate repeated liquefaction behavior by several researchers (Wahyudi and Koseki, 2015) (Aoyagi et al. 2016).

.

Following the pioneer works, there have been many studies regarding this topic in both element test and model test. Since most of the works focused on the two stage of liquefaction, this thesis tried to investigate repeated liquefaction behavior. However, the number of liquefaction stage was limited in triaxial due to the fact that there were membrane wrinkles at about 3^{rd}-4^{th} stage. The experiment was divided into three series which is described further in the next section.

3.2 Experimental program

In order to study the repeated liquefaction properties of silica sand with number seven grading, three types of experimental programs were decided. In all cases, the initial relative density of specimen was attempted to be in the range of 50-55% using air-pluviation method. Repeated liquefaction tests were carried out by slowly opening the drainage valve allowing excess pore water pressure generated during the previous liquefaction test to dissipate and also reconsolidate. In triaxial test, due to the wrinkles in membrane at high liquefaction stages, the test was limited up to 4 stages (see *Figure 3-1*). In this section, the detail of each program will be discussed as follow:

3.2.1 The effect of cyclic stress

A series of repeated liquefaction tests were carried out to investigate the effect of cyclic stress by varying the cyclic stress ratio (CSR). There were 6 repeated liquefaction tests in total. Each test, the specimen was subjected to different CSR ranging from 0.09 to 0.20 which was kept constant throughout the test. Initial relative density was about 50-55%. However, due to isotropic consolidation to the initial effective confining pressure of 100 kPa before the first stage of liquefaction test, relative density after consolidation and prior to the liquefaction test was approximately 55-60%. After each stage of liquefaction test, the excess pore water pressure was drained by slowly opening drainage valve allowing dissipation and reconsolidation before starting the next liquefaction stage. In this case, the liquefaction was defined as 5% double amplitude axial strain. Once the specimen was subjected to the target strain, the cyclic loading stopped and the left over strain was adjusted back to 0%. In this series of test, the repeated liquefaction was carried out up to 4 liquefaction stages.

3.2.2 The effect of strain amplitude history

In this test series, the repeated liquefaction tests were done at the constant CSR value but specimens were subjected to constant various double amplitude axial strain history; e.g. 1%, 2%, 5%, 7% and 10% to study the effect of strain amplitude. The CSR value was fixed at 0.11. In the following stages, the test was terminated at the same double amplitude axial strain as in the previous stage. Therefore, the only difference between each test; or each specimen, was double amplitude axial strain history. The liquefaction tests were conducted in the same manner as the effect of cyclic stress study mentioned in the section 2.2.1. However, due to the difference in target strain amplitude of each specimen, the liquefaction resistance was computed as the number of cycle to reach 1% double amplitude axial strain, in order to be able to calculate the resistance for all specimens.

3.2.3 The effect of small strain history

The objective of this test series was to investigate the effect of small strain history or so-called pre-shearing on liquefaction resistance. The undrained cyclic tests were conducted in the same manner as in the second series. In the first liquefaction stage, each double amplitude small axial strain histories of 0.1%, 0.2% and 0.5% was applied to the specimen followed by 2% double amplitude strain history in the following stages (up to four stages). Thus, in this test series, the difference in strain amplitude only presented in the first liquefaction stage. The three following stage, regardless of pre-shearing history, the all specimens were then subjected to 2% strain amplitude. In addition, for comparison purpose, the test with constant strain amplitude of 2% in the second series was also employed for this test series result discussion. Due to the fact that the strain amplitudes employed in the first liquefaction test were very small, the liquefaction resistance in the first stage was calculated at maximum strain amplitude that applied to that specific specimen. For the rest of stages, liquefaction resistance was calculated when the strain amplitude reach 1% double amplitude axial strain.

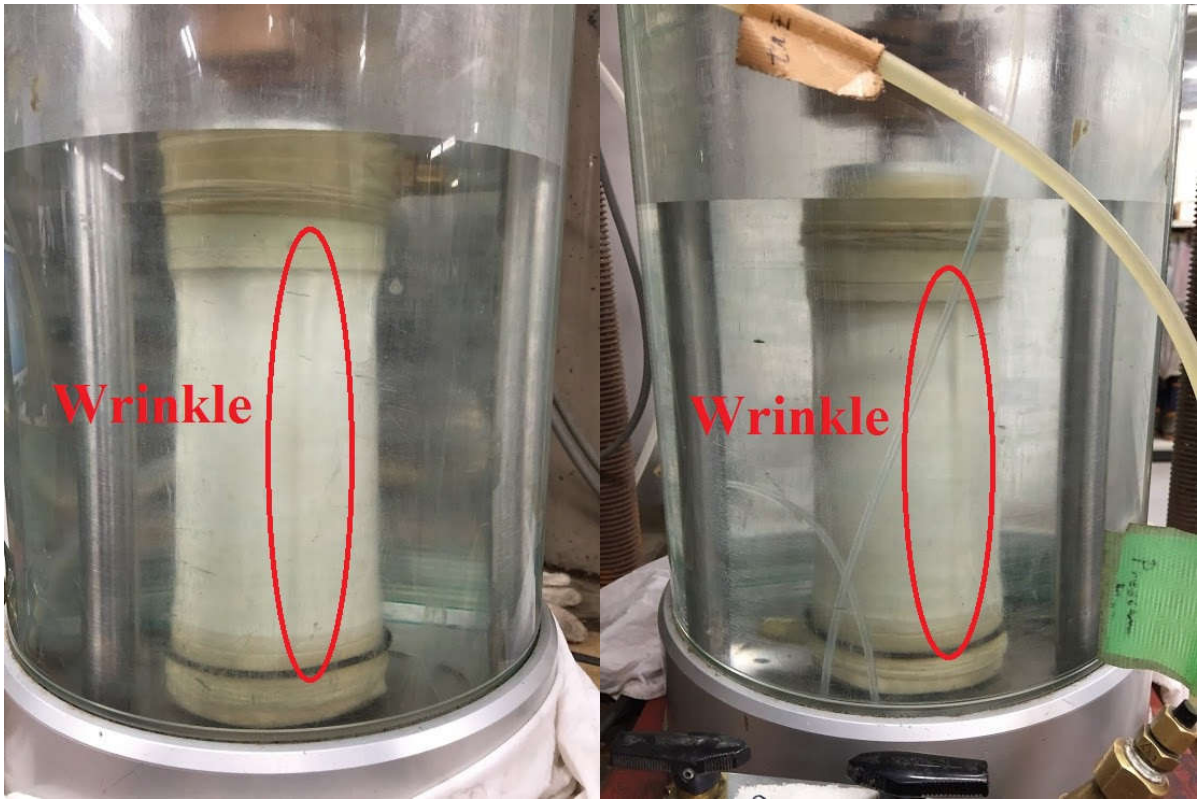

Figure 3-1. Wrinkle in membrane at 4th liquefaction stage

3.3 Results and discussions

Three types of experimental program have been conducted in cyclic undrained triaxial apparatus to investigate repeated liquefaction behavior of the silica sand in terms of cyclic stress effect, strain amplitude effect and small strain amplitude effect (pre-shearing). The finding results and detailed discussion of each aspect is described in this section.

3.3.1 The effect of cyclic stress study

In this study the tests were carried out under different CSR with constant double amplitude axial strain history at 5%. In order to confirm repeatability of the specimens, relationship between volumetric strain and axial strain during consolidation was plotted as *Figure 3-2*. Due to the fact that before consolidation, specimen was intact; thus, the relationship showed similar trend. However, in Test T9 (CSR = 0.09), there might be slippage of displacement transducer resulting in little increase in axial strain while constant value of volumetric strain of about 0.07%. For the reconsolidation process after subjecting to the first liquefaction test,

the behavior cannot be compared anymore since specimens were subjected to different history.

For the liquefaction test, typical deviator stress – axial strain relationships of different repeated liquefaction stages ranging from stage 1 to stage 4 of 0.10 CSR test are shown in *Figure 3-3* while the corresponding effective stress paths are presented in *Figure 3-4*. In the first stage of liquefaction, it can be seen that there was a sudden decrease in mean effective stress (p') which was corresponding with large axial strain accumulation. The p' reduction became gradually less in the following stages. It can be said that, in the initial stage, specimen with low relative density did not develop cyclic mobility while in the later stages, cyclic mobility developed. The excess pore water pressure ratio in each liquefaction stage are given in *Figure 3-5* together with a mark when double amplitude axial strain equaled to 5%. In the first stage of liquefaction, excess pore water pressure did not reach 1.0 yet before the test termination at 5% double amplitude axial strain. However, after 2nd liquefaction stage, excess pore water pressure became unity before reaching 5% double amplitude axial strain. In all of the cases, excess pore water pressure built up rapidly at the very beginning of the test and followed by steady increase. It started to raise quickly again when the ratio was closed to zero.

As each specimen were subjected to different cyclic stress amplitude, the effective stress path comparison of the first liquefaction stage is shown in *Figure 3-6*. It can be seen that when the CSR was larger than 1, specimens exhibited strain softening corresponding with rapid reduction in mean effective stress toward zero during the first cycle. This reduction occurred at much lower mean effective stress approximately 40 kPa and 30 kPa for specimen subjected to 0.1 and 0.09 CSR, respectively. For the following stages, cyclic strength seemed to be developed observably in specimen subjected to CSR 0.125 (see *Figure 3-7*).

The relative density change during repeated liquefaction is presented in *Figure 3-8*. The trend of relative density increase of each repeated liquefaction tests seems to be similar to each other. Since strain amplitude was the same for all specimens, it can be implied that the CSR did not affect the relative density change.

The soil resistance to liquefaction in terms of number of cyclic to liquefy which, in this test series, was defined and calculated at 5% double amplitude axial strain, of each liquefaction

stage is shown in *Figure 3-9*. Soil liquefaction resistance increased with the liquefaction stages in all cases. However, the cyclic resistance depends on the applied CSR. In addition, it can be observed that the smaller of the CSR was, the larger of soil liquefaction resistance was. In the case of small CSR value at 0.09 at the third stage, the specimen did not show any liquefaction potential even at very high number of cycles because of low cyclic stress amplitude and high relative density. Data of this test series is summarized in the *Table 3-1*. Furthermore, liquefaction curve in terms of CSR and number of cycle to liquefy was drawn in *Figure 3-10*. Similar trend of liquefaction resistance of each stage can be observed. With lower CSR, the specimen showed higher liquefaction resistance and vice versa. From this test series, it can be implied that although the relative density of specimens was similar, the liquefaction resistance of the specimens with lower CSR history are higher than the soils with higher CSR history indicating the effect of CSR (see *Figure 3-11*). In addition, repeated liquefaction resistance was increased with liquefaction stage under the same strain amplitude and same CSR.

Table 3-1. Summary of repeated liquefaction test with constant strain amplitude

Test Number	CSR	Relative Density (%)					Number of Cycle required to trigger 5% double amplitude strain			
		Initial	Stage 1	Stage 2	Stage 3	Stage 4	Stage 1	Stage 2	Stage 3	Stage 4
T4	0.2	49.7	41.5	61.4	67.7	73.3	0.60	0.97	1.86	3.76
T5	0.15	52.6	55.0	65.3	72.7	79.3	0.64	0.98	1.73	4.19
T6	0.1	54.1	57.7	66.7	74.0	80.5	8.88	15.0	55.86	96.80
T8	0.135	56.7	58.3	66.1	72.6	78.1	0.87	1.77	4.38	13.77
T9	0.09	54.2	56.4	65.6	74.0	-	34.96	149.7	-	-
T10	0.125	52.4	54.5	64.4	71.2	77.1	0.69	3.88	7.34	34.81

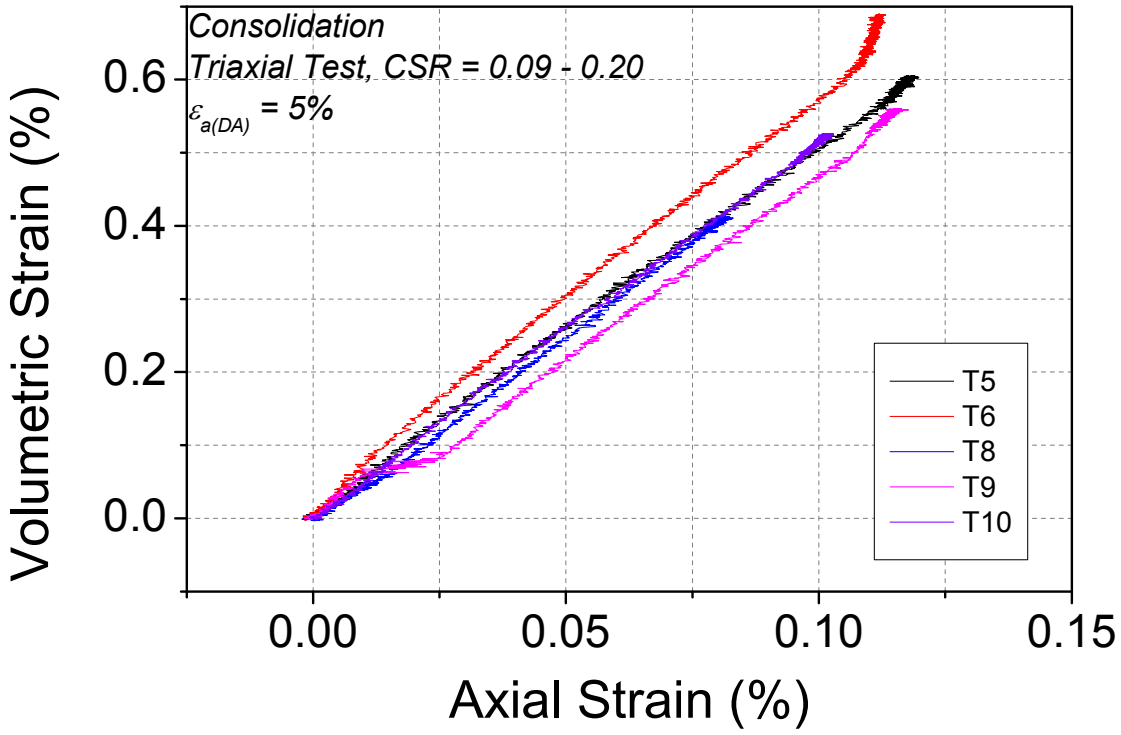

Figure 3-2. Relationship between volumetric strain and axial strain during consolidation

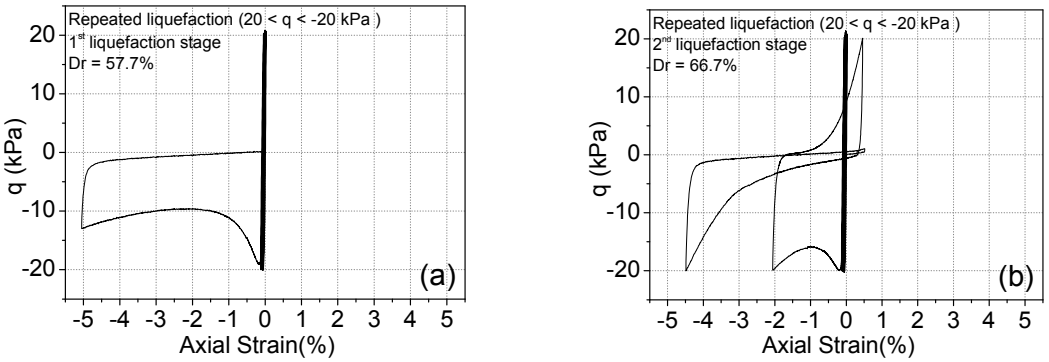

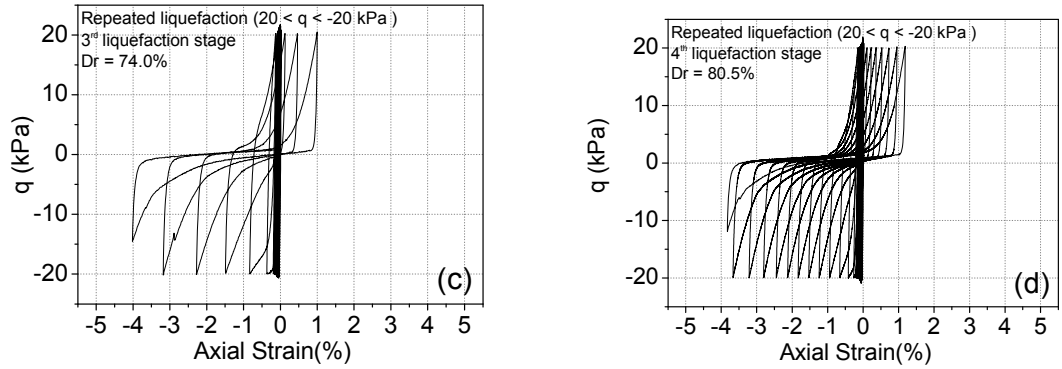

Figure 3-3. Typical deviator stress – axial strain relationships of the repeated liquefaction test stage 1 (a), stage 2 (b), stage 3 (d) and stage 4 (d) (T6 Test) (CSR = 0.1, $\varepsilon_{a(DA)}$ = 5%)

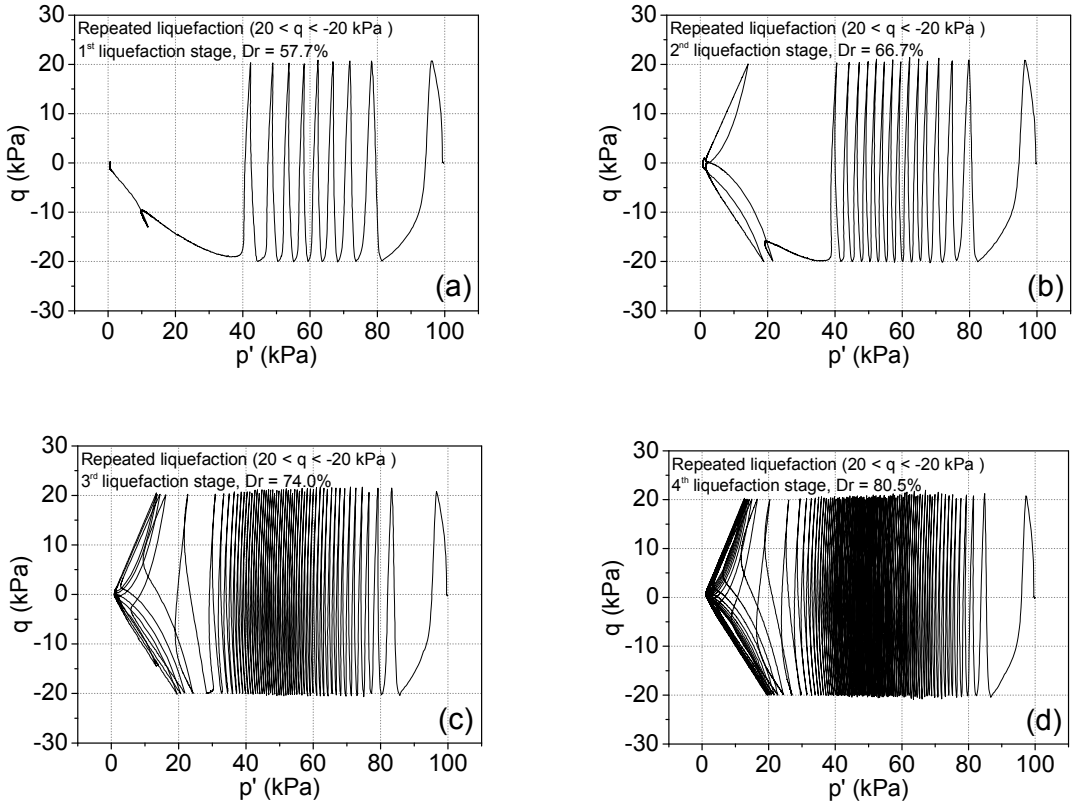

Figure 3-4. Typical deviator stress – mean effective stress relationships of the repeated liquefaction test stage 1 (a), stage 2 (b), stage 3 (d) and stage 4 (d) (T6 Test) (CSR = 0.1, $\varepsilon_{a(DA)}$ = 5%)

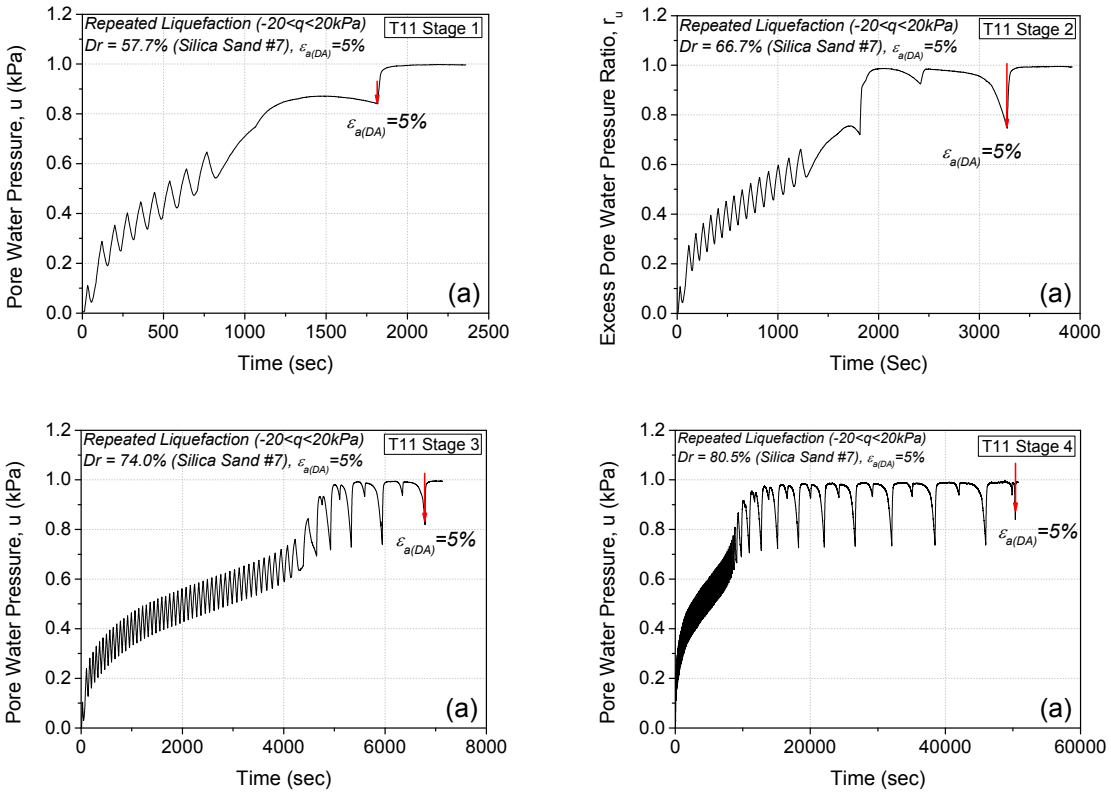

Figure 3-5. Excess pore water pressure ratio (ru) of the repeated liquefaction test (a) stage 1, (b) stage 2, (c) stage 3 and (d) stage 4

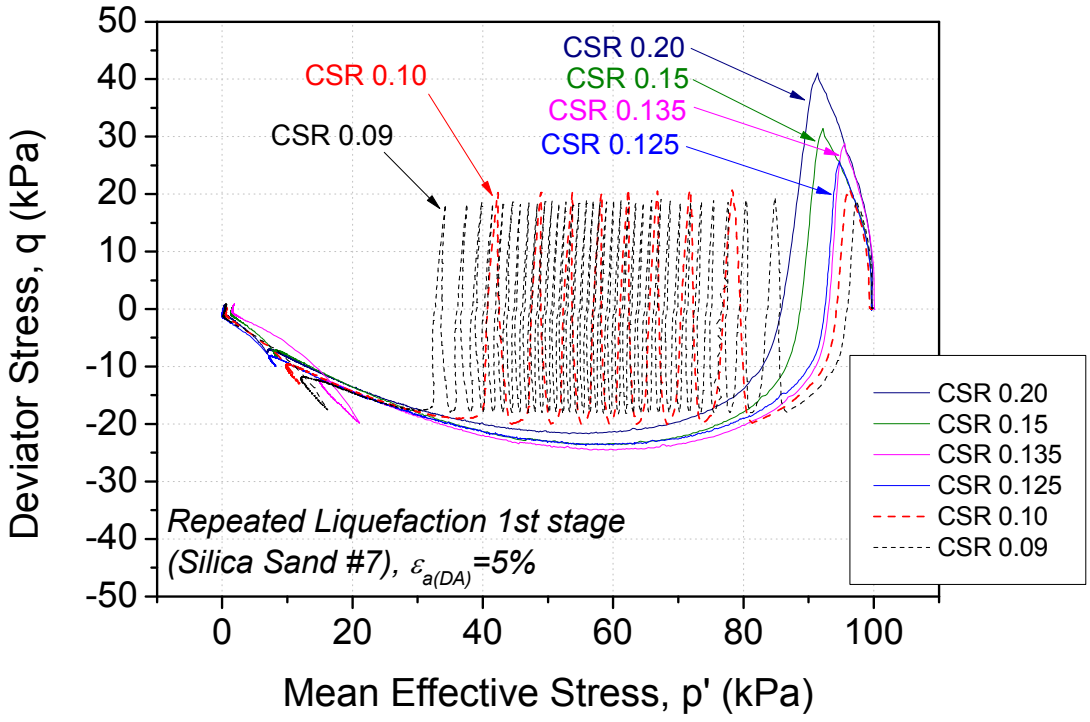

Figure 3-6. Effective stress path comparison of specimens with different CSR during the first liquefaction stage

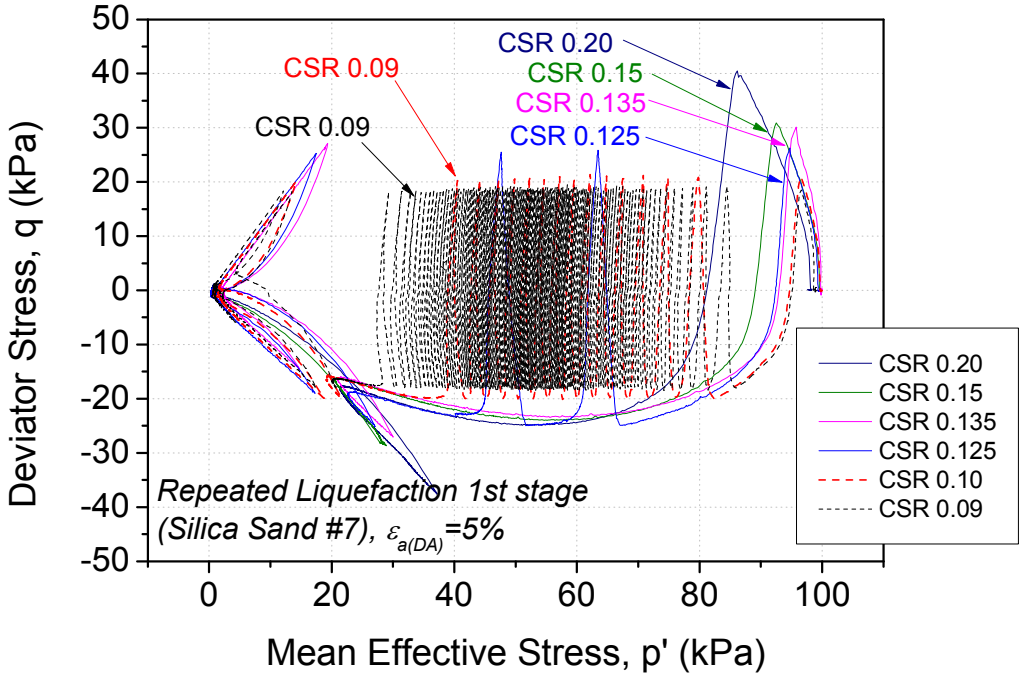

Figure 3-7. Effective stress path comparison of specimens with different CSR during the second liquefaction stage

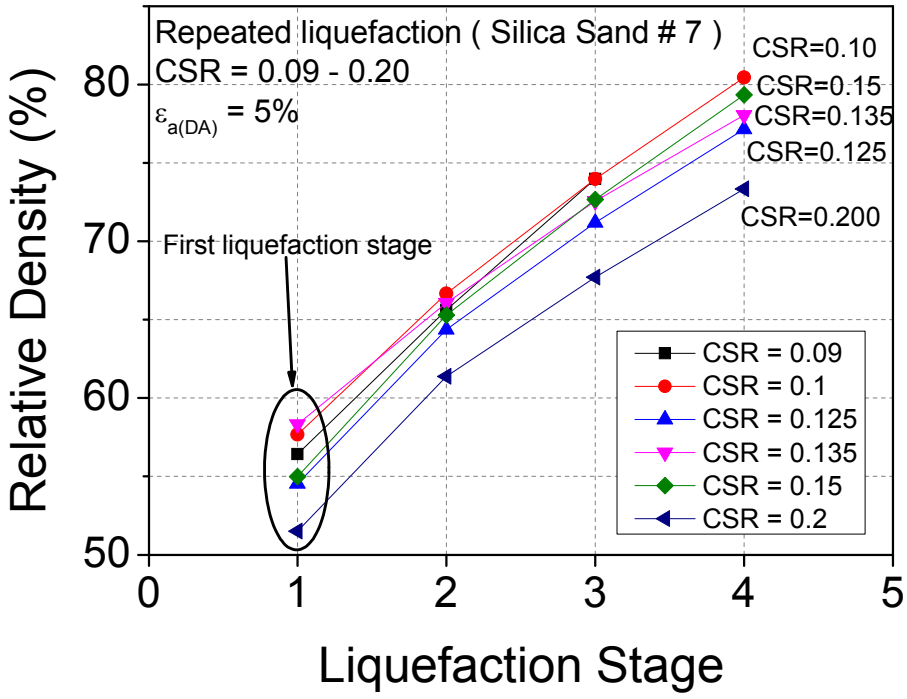

Figure 3-8. Relative density change of silica sand with number seven grading in repeated liquefaction tests with CSR ranging from 0.09-0.20 and constant 5% double amplitude axial strain

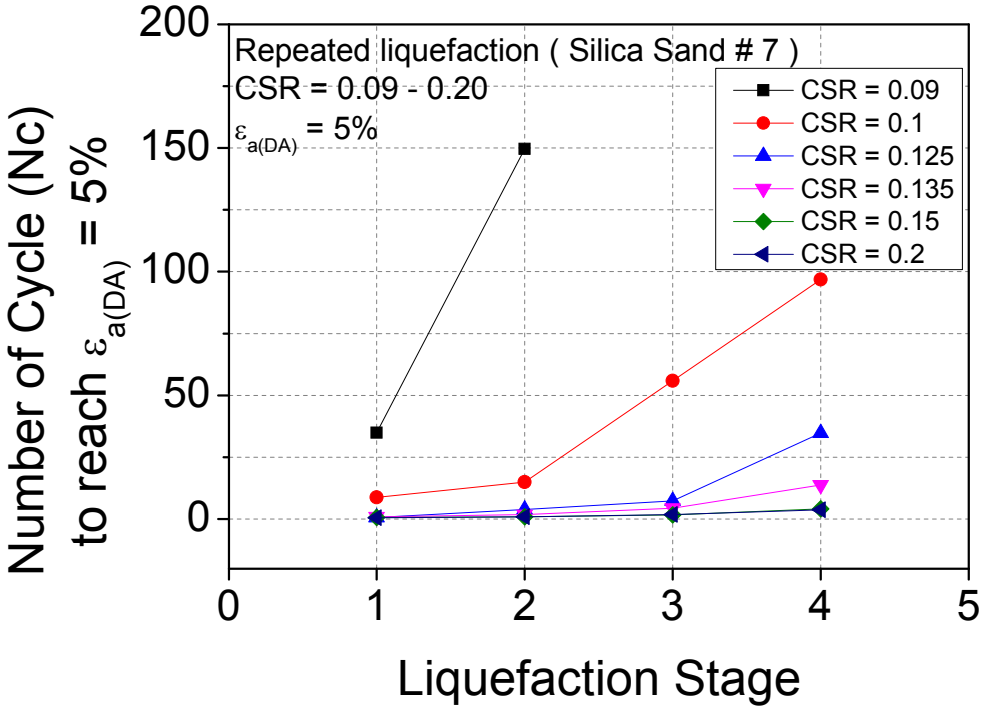

Figure 3-9. Liquefaction resistance of silica sand with number seven grading in repeated liquefaction tests

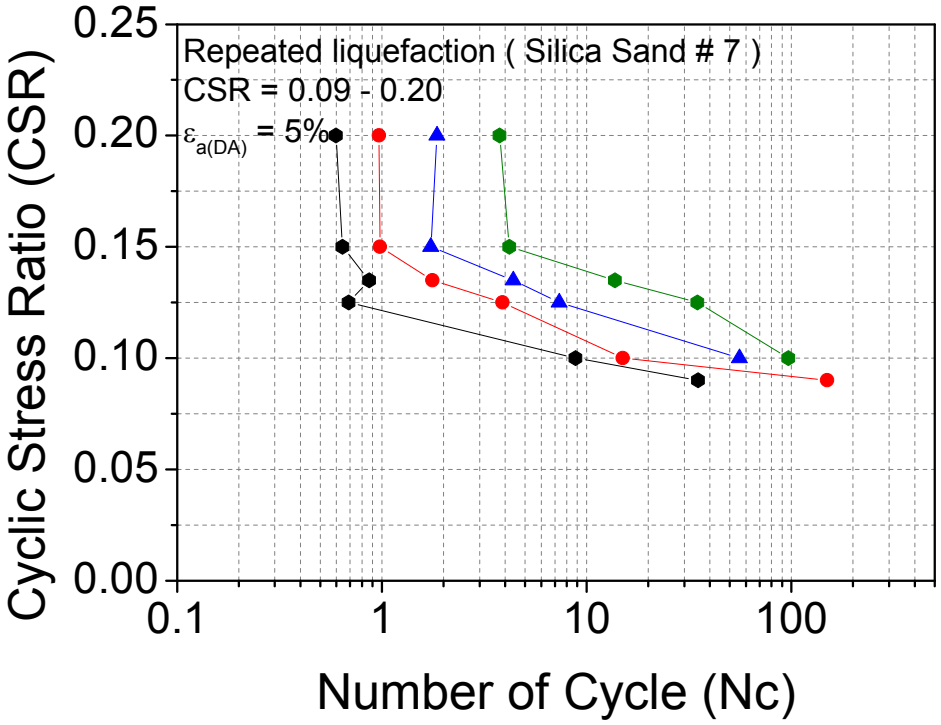

Figure 3-10. Liquefaction curve of silica sand with number seven grading in repeated liquefaction tests

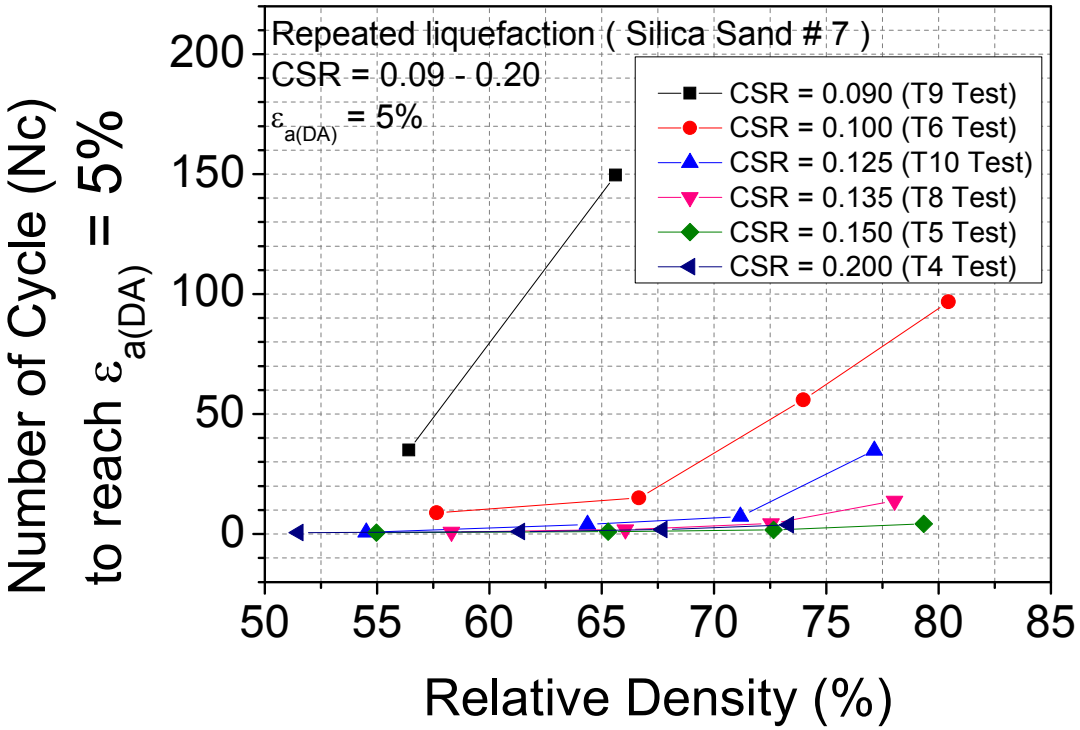

Figure 3-11. Liquefaction resistance of silica sand with number seven grading with relative density change in repeated liquefaction tests

3.3.2 The effect of strain amplitude history

In this study the tests were carried out under the condition where CSR is constant at 0.11 with various double amplitude axial strain history at 1%, 2%, 5%, 7% and 10%. Each specimen was subjected to constant CSR and constant strain amplitudes throughout the repeated liquefaction test. Due to the difference in double amplitude axial strain, it must be noted that in this study, the cyclic resistance was computed at the minimum double amplitude axial strain; e.g. 1%. Repeated liquefaction tests were done up to 4 stages. However, in order to avoid possible anisotropy, the tests which reached target double amplitude strain on compression side; i.e. terminated on while compression, were omitted. In the same manner as discussed in the first series of test, the relationships between volumetric strain and axial strain during the first consolidation of specimens were drawn as given in *Figure 3-12*. All the specimen showed similar relationship indicating repeatability. It should be noted that there might be a problem with external displacement transducer in some ranges (slippage) resulting in steep increase in axial strain over a short time.

The change in relative density of each liquefaction stage is shown in *Figure 3-16*. It is obvious that relative density increased with liquefaction stages and depended on the double amplitude axial strain history since CSR was constant for every test. As there was a variation in initial relative density in preparation process ranging from 54.9% to 56.4%, the effect of strain amplitude history is more clearly seen in terms of increment as presented in *Figure 3-17*. To be more specific, the larger of double amplitude axial strain history was, the higher increase in relative density during excess pore water pressure dissipation and reconsolidation was and vice versa.

Liquefaction resistance was calculated in terms of number of cycle to reach 1% double amplitude axial strain as mentioned previously and the resistance of each liquefaction stage is reported in *Figure 3-18* with the closer view at second liquefaction stage is given in *Figure 3-19*. *Table 3-2* showed summary of test result in this series. From the figure, it seems to be no trend as relative density of specimens in both the second and third stage were significantly different and also due to the difference in strain history. In order to take relative density into the account, relationship between liquefaction resistance and relative density was drawn and reported in *Figure 3-20*. Interestingly, it can be clearly seen that in the case of 1% and 2% double amplitude axial strain history specimens showed sharp increase in liquefaction resistance although the increase in relative density is much lower compared to the others. This behavior of specimens when subjected to small amplitude strain was corresponding with previous research works (Ishihara and Okada, 1978) (Wahyudi et al., 2015). It was suggested that the behavior under small pre-shearing may be attributed by microscopic fabric change (Suzuki and Toki, 1984). However, the specimens with double amplitude axial strain history of more than 5% was in somewhat random trend with an increase in reliquefaction resistance in all specimens. This was contradicted to the past researchers where it was presented that with large pre-shearing strain, reliquefaction resistance decreased. This thesis failed to recognize the reasons. One possible reason may be that during specimen preparation, specimen disturbance or some special structure was developed. Anyhow, it is still clear that at low strain amplitude history, the influence of relative density became minor and it is more governed by the strain history. In addition, during the first two liquefaction stages, it is quite also clear that the increment between liquefaction resistance to relative density change of the specimen with lower strain amplitude history was higher than that of specimen with higher

strain amplitude history. This suggests that with lower strain amplitude, specimen tends to exhibit higher cyclic resistance with lower increase in relative density.

It is noted that at axial strain reached 1%, the ratio of excess pore water pressure to the initial confining pressure was not 1.0 yet. *Figure 3-21* showed the excess pore water pressure time history of the repeated liquefaction test with 2% double amplitude history from stage 1 to stage 4 with a mark where axial strain reached 1%. From the figures of the specimen subjected to 2% strain amplitude history, it can be seen that r_u did not reach 1.0 for all stages at 1% double amplitude strain. At 2% strain amplitude where the test was terminated, there were only stage 3 and stage 4 where r_u was nearly 1.0.

Table 3-2. Summary of repeated liquefaction test with constant CSR / various strain amplitude

Test Number	Strain Amplitude (εa(DA))	Relative Density (%)					Number of Cycle required to trigger 1% double amplitude strain			
		Initial	Stage 1	Stage 2	Stage 3	Stage 4	Stage 1	Stage 2	Stage 3	Stage 4
T13	1%	54.0	56.4	59.8	62.3	64.6	4.75	25.94	110.9	-
T14	5%	53.7	55.7	65.1	72.1	78.2	7.79	19.89	39.78	-
T15	2%	53.6	55.6	61.3	65.4	69.27	4.74	17.96	34.68	115.9
T16	1%	53.4	55.8	59.1	61.7	63.9	6.8	26.96	157.3	-
T17	7%	52.9	54.9	67.2	78.3	84.1	4.76	14.88	176.4	
T19	10%	54.1	55.8	72.6	83.7	-	7.79	19.97		
T20	6.55%	53.9	55.3	65.9	75.0	83.6	5.81	8.85	49.82	565.0

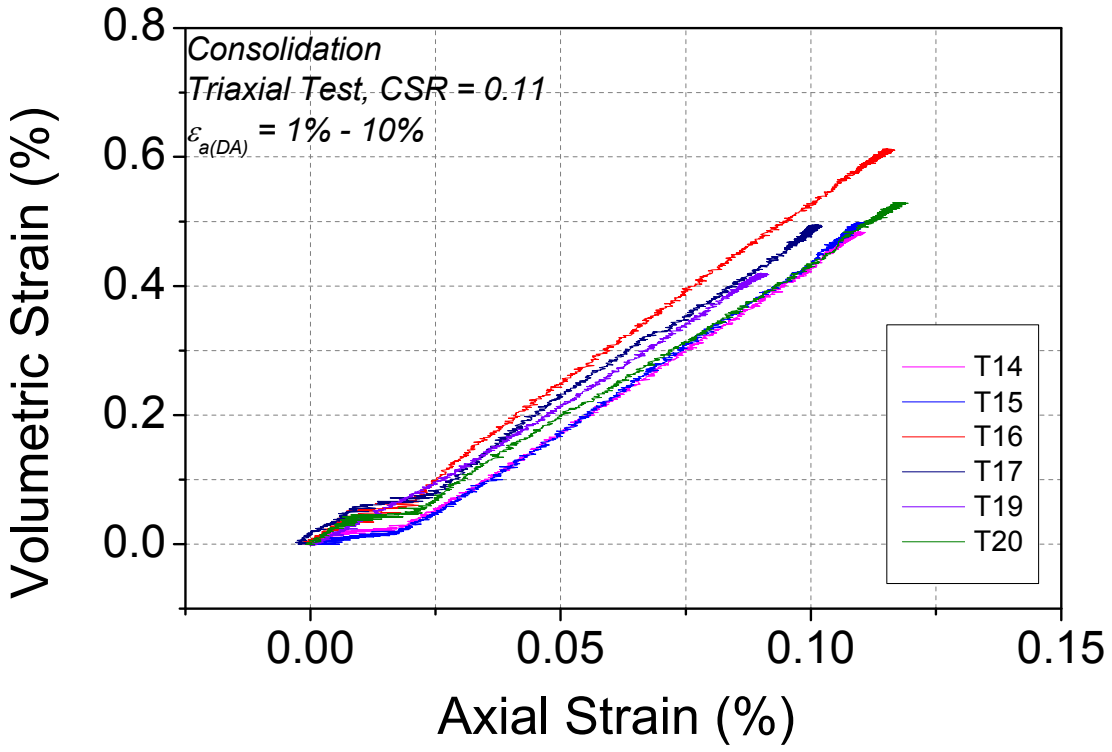

Figure 3-12. Relationship between volumetric strain and axial strain during consolidation

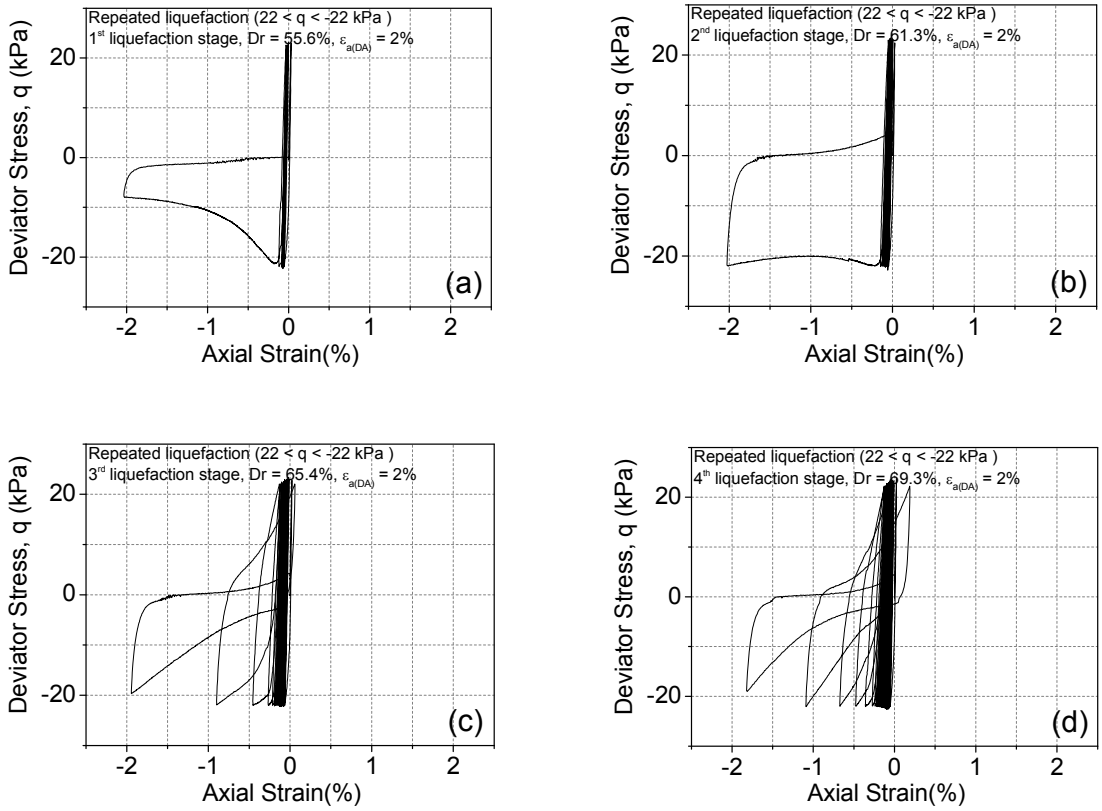

Figure 3-13. Typical deviator stress – axial strain relationships of the repeated liquefaction test stage 1 (a), stage 2 (b), stage 3 (d) and stage 4 (d) (T15 Test) (CSR = 0.11, $\varepsilon_{a(DA)}$ = 2%)

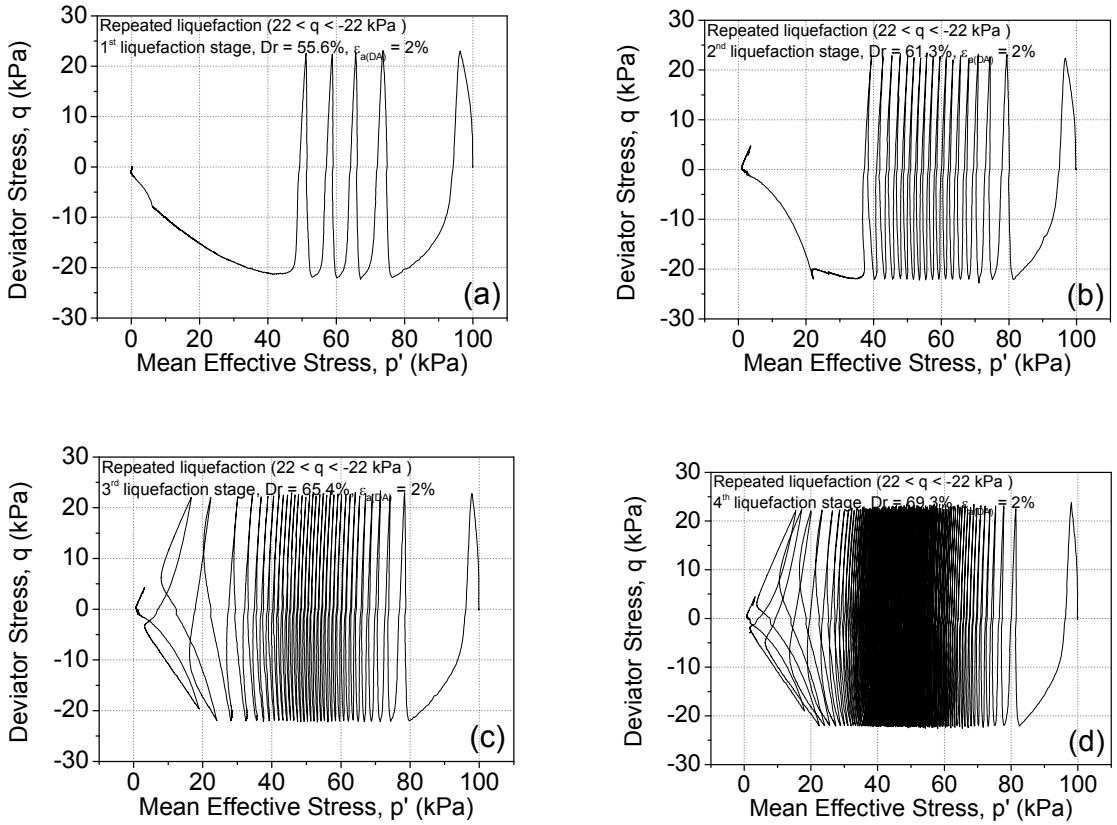

Figure 3-14. Typical deviator stress – mean effective stress relationships of the repeated liquefaction test stage 1 (a), stage 2 (b), stage 3 (d) and stage 4 (d) (T15 Test) (CSR = 0.11, $\varepsilon_{a(DA)}$ = 2%)

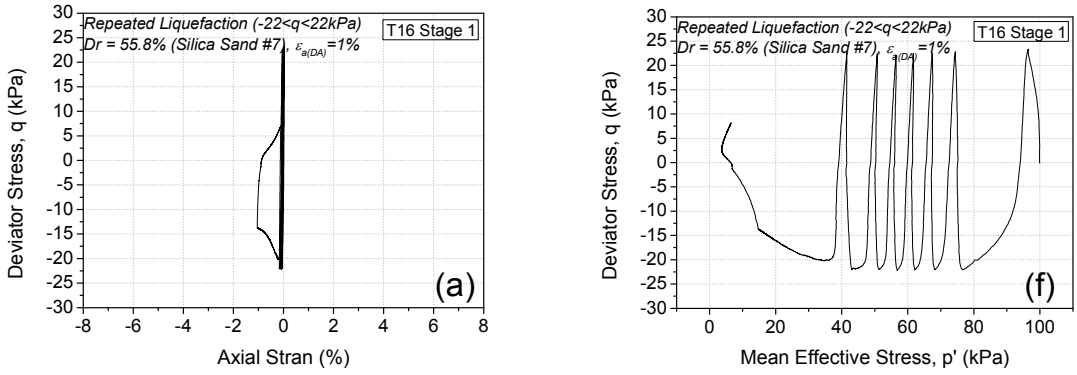

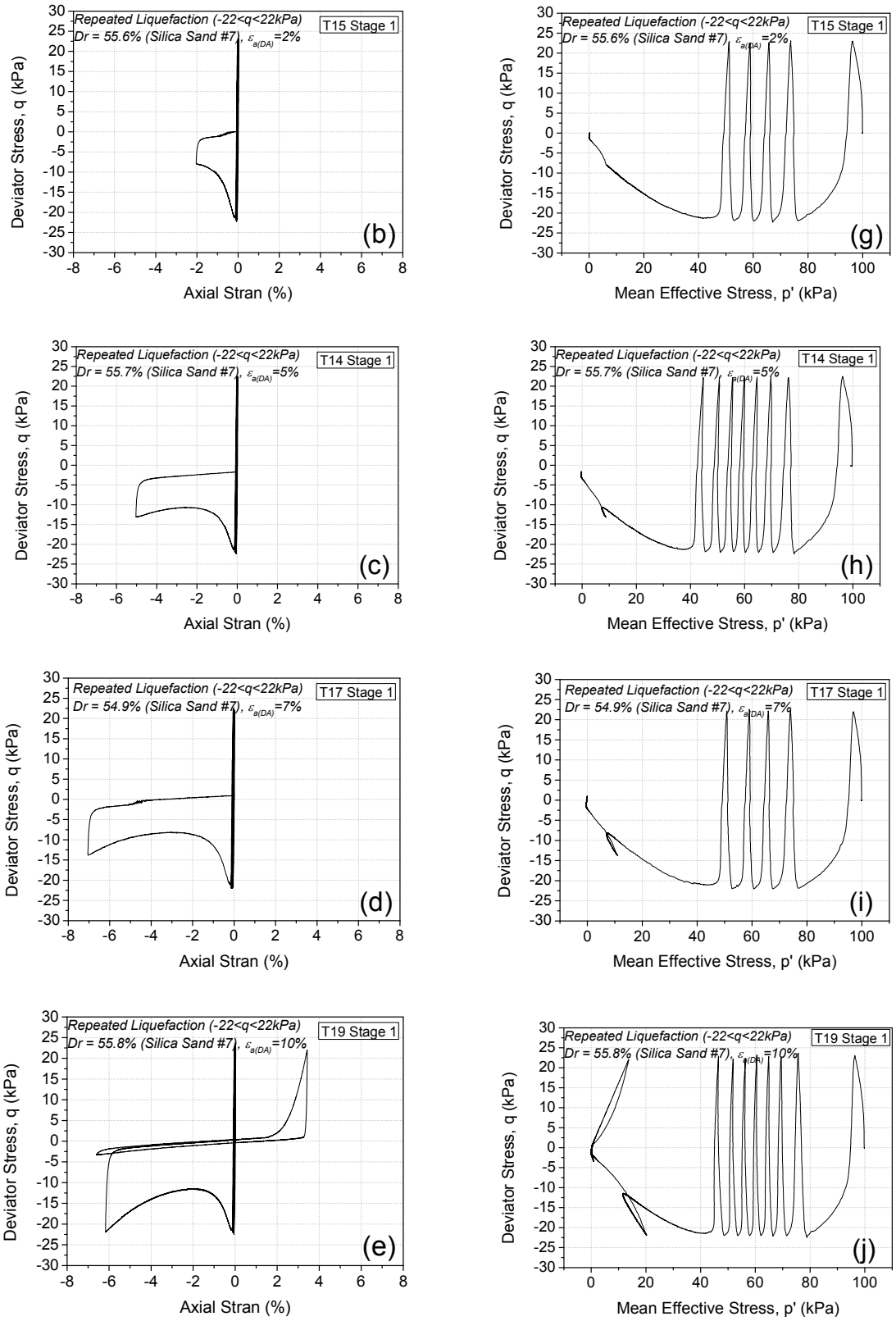

Figure 3-15. (a-e) Relationship between deviator stress and axial strain of test at strain amplitude of (a) 1%, (b) 2%, (c) 5%, (d) 7%, (e) 10% and (f-j) Effective stress path of test at strain amplitude of (f) 1%, (g) 2%, (h) 5%, (i) 7%, (j) 10%

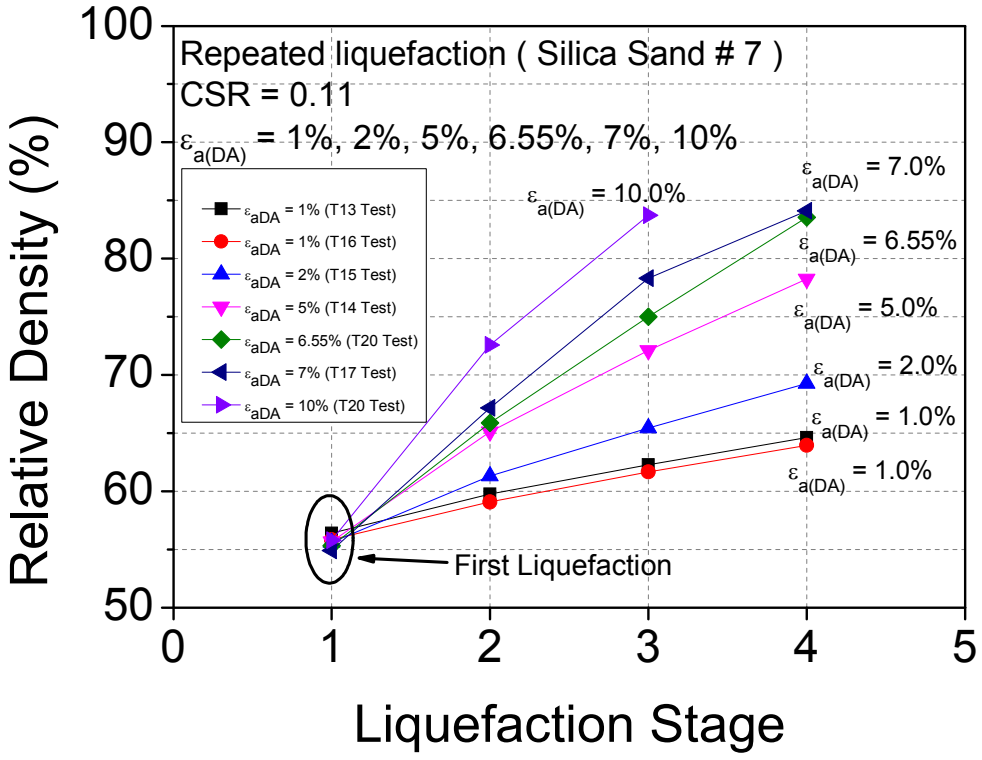

Figure 3-16. Relative density change of silica sand with number seven grading in repeated liquefaction tests with constant CSR at 0.11 and various double amplitude axial strain history

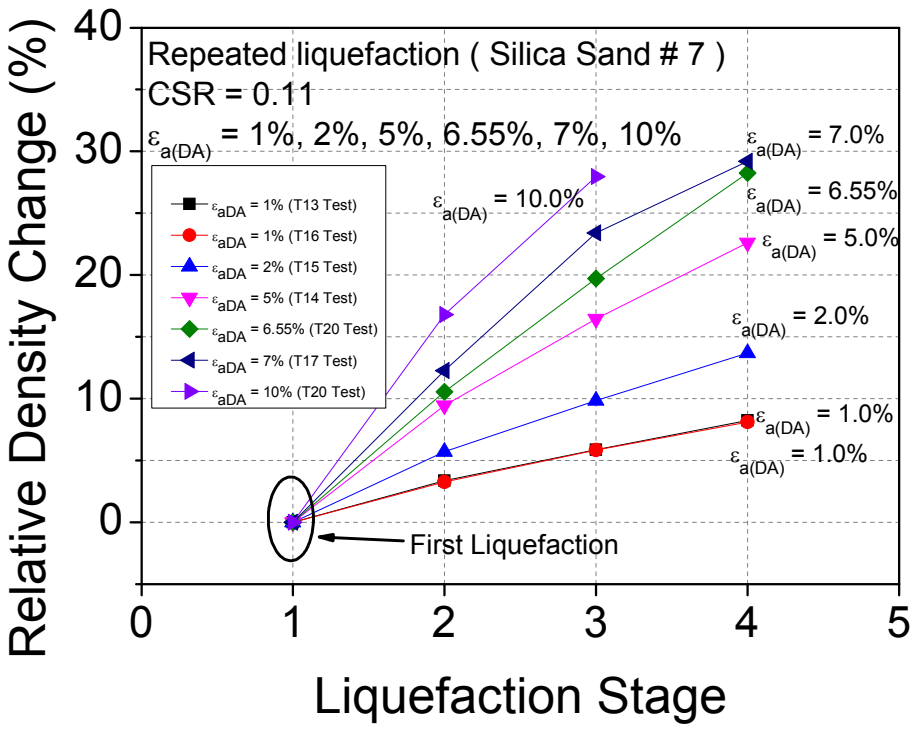

Figure 3-17. Relative density change increment of silica sand with number seven grading in repeated liquefaction tests with constant CSR at 0.11 and various double amplitude axial strain history

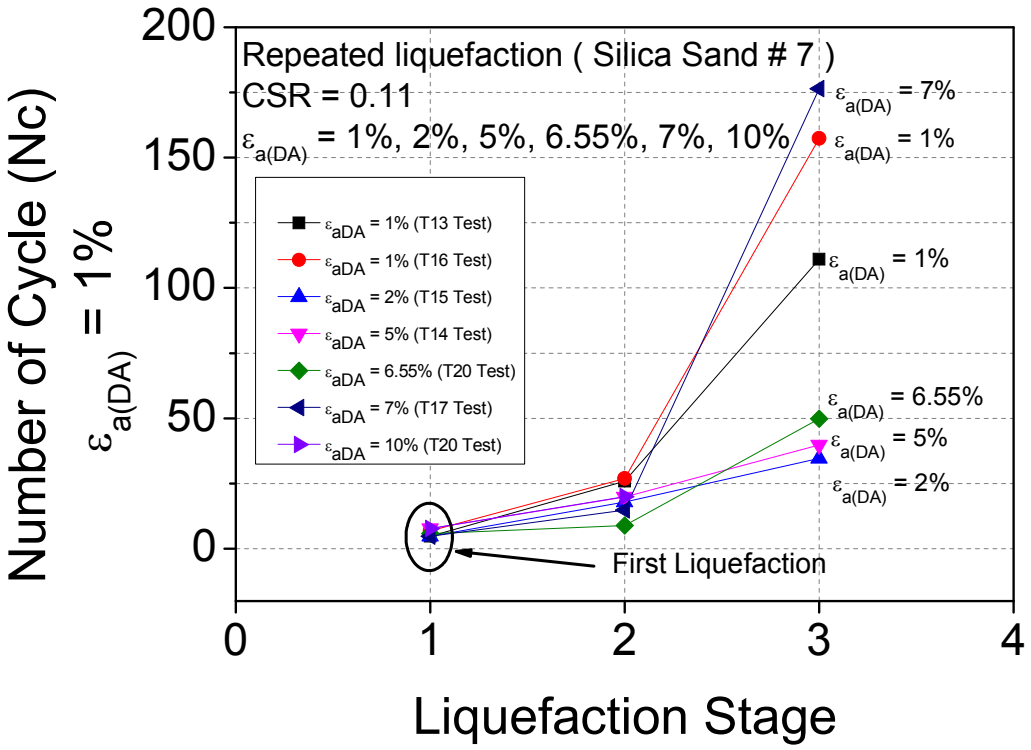

Figure 3-18. Liquefaction resistance of silica sand with number seven grading in repeated liquefaction tests

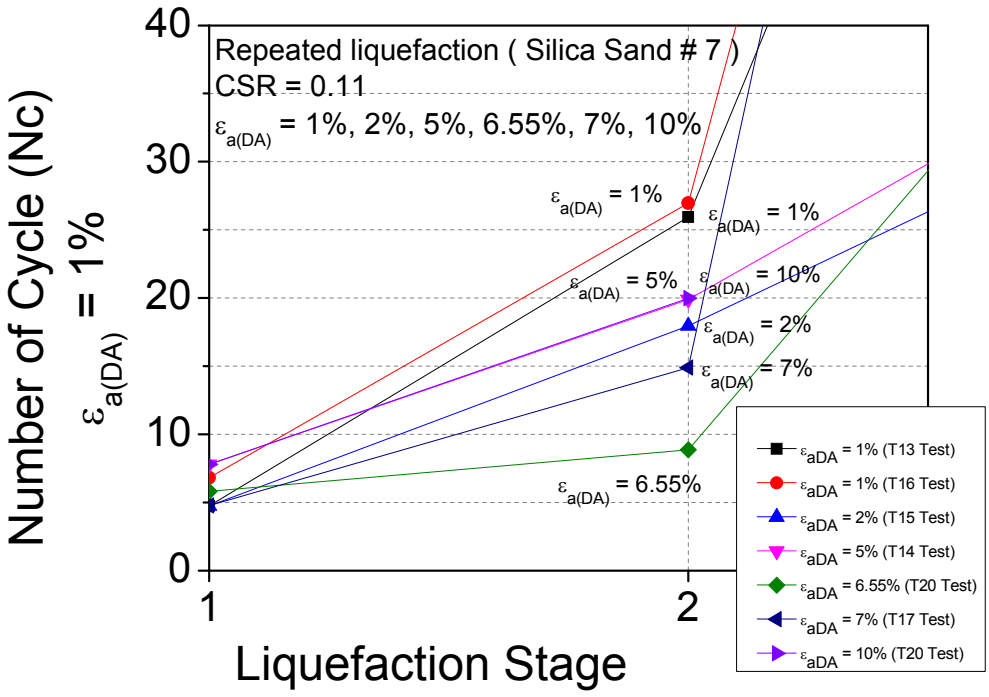

Figure 3-19. Liquefaction resistance of silica sand with number seven grading in repeated liquefaction tests

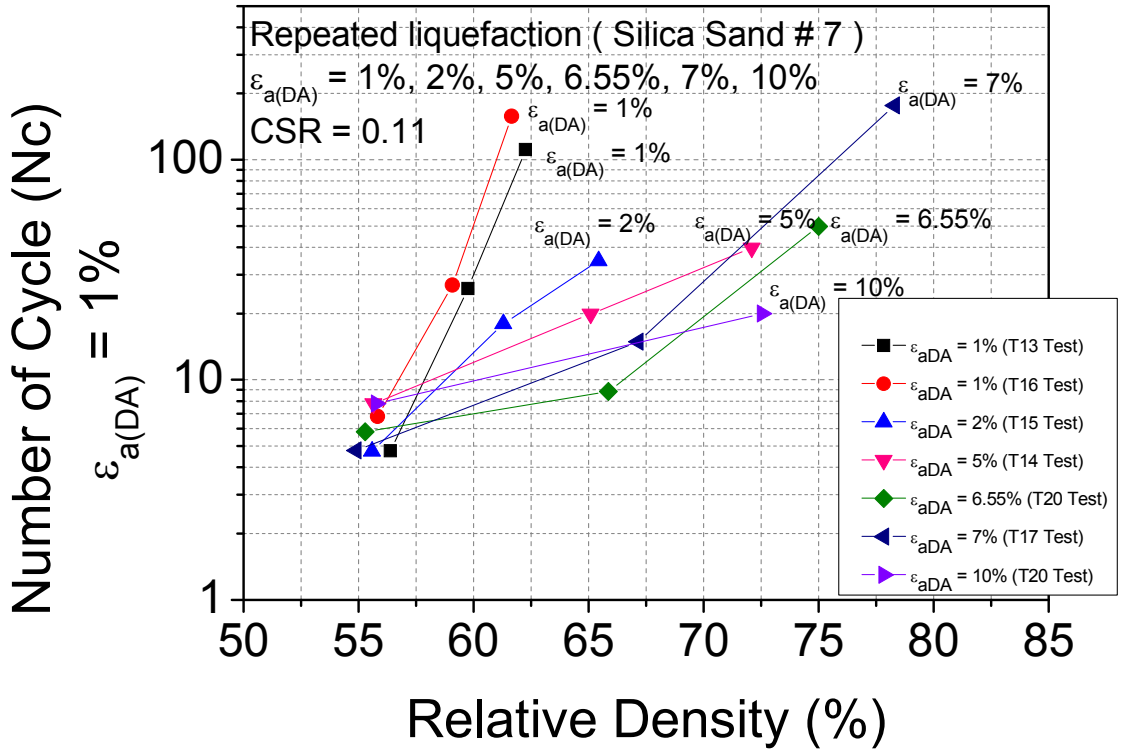

Figure 3-20. Relationship between liquefaction resistance of silica sand with number seven grading and relative density in repeated liquefaction tests

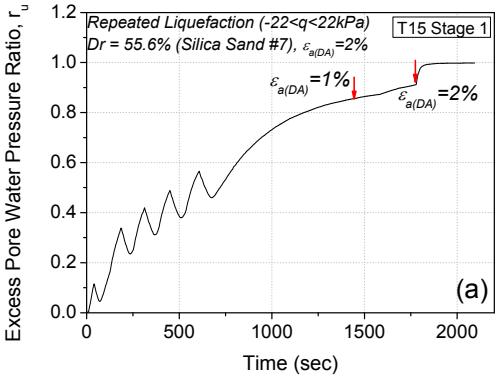

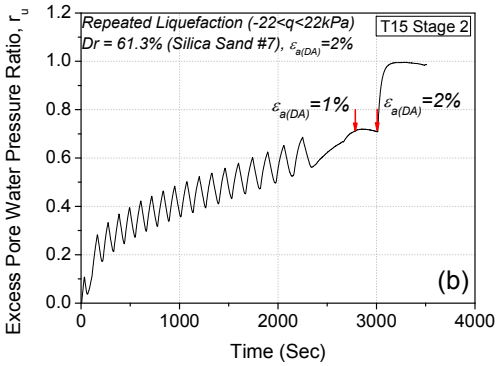

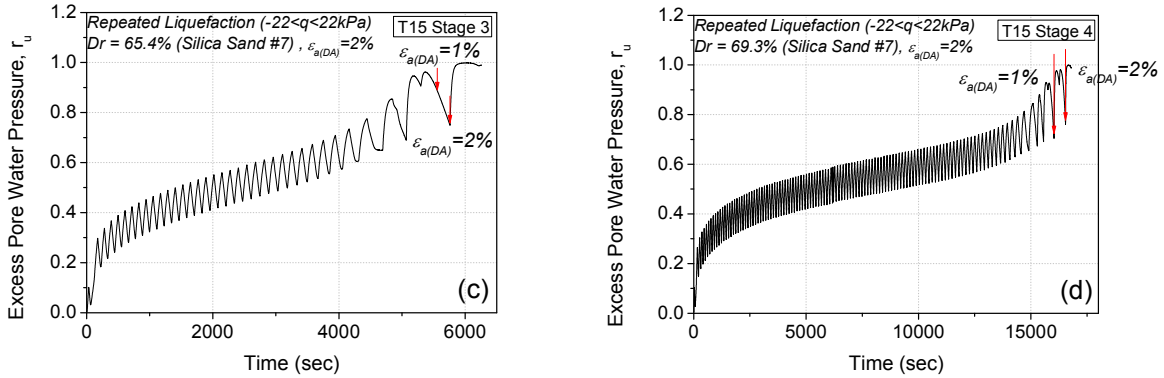

Figure 3-21. Excess pore water pressure ratio (r_u) time history of liquefaction test (a) stage 1, (b) stage 2, (c) stage 3 and (d) stage 4 (T15 Test) (CSR = 0.11, $\varepsilon_{a(DA)}$ = 2%)

3.3.3 The effect of small strain amplitude history

In this study the tests were carried out under constant CSR condition at again 0.11 with various small double amplitude axial strain histories at 0.1%, 0.2% and 0.5% only in the first liquefaction stage. In the following stages, the specimens were subjected to double amplitude axial strain of 2%. To confirm repeatability, all specimens showed rather similar trend of relationship between volumetric strain and axial strain during the first consolidation. For liquefaction test, typical relationships between deviatoric stress and axial strain during the first liquefaction stage together with effective stress path are presented in *Figure 3-23*. In addition, corresponding excess pore water pressure ratio time history is given in *Figure 3-24*. It can be seen that when the test was terminated at 0.1% double amplitude axial strain, the mean effective stress was still relatively high approximately 50 kPa. The terminated mean effective stress became lower with the larger with the order of axial strain. Consequently, excess pore water pressure at 0.1%, 0.2% and 0.5% were about 0.4, 0.55 and 0.73 in order. For the stress path, with the range of 0.1% double amplitude axial strain, the specimen behaved in elastic manner. For the specimen which subjected to 0.2% strain amplitude, it started to show non-elastic behavior when the strain amplitude approximately over 0.11%.

Because of the fact that only limited small strains (0.1%, 0.2% and 0.5%) were applied, all specimens did not reach the point where effective stress equals to zero in the first liquefaction stage which sometimes defined as initial liquefaction. Thus, since liquefaction did not take place, limited increase relative density can be expected. The relative density change during after the first liquefaction and reconsolidation is shown in *Figure 3-25*. As mentioned in

previous section, even with small strain cases, relative density increased proportionally to the strain history.

After subjecting to small strain at the first liquefaction stage, the specimens were further applied with 2% double amplitude axial strain in the following stages up to four stages. Typical deviator stress and axial strain relationships and corresponding effective stress paths of the four liquefaction stages are shown in *Figure 3-26*. It can be seen that after subjected to small strain amplitude of 0.2%, there was still no cyclic mobility in the second liquefaction stage; however, the number of cycle during elastic behavior was relatively extremely high. In the third and final stages, cyclic mobility of specimen was observed. *Figure 3-27* shows the corresponding excess pore water pressure ratio (r_u) time history with a mark where double amplitude axial strain equal to 1% and 2%. In the first stage, due to low strain amplitude, excess pore water pressure ratio of only about 0.55 was developed. In the second stage, although the test was terminated at 2% strain amplitude, r_u was still not unity. For the following stages, r_u was almost 1.0 when double amplitude axial strain reached 2.0%.

The relative density change from the first stage to the fourth stage is reported in *Figure 3-28* together with the history of specimen which was subjected to 2% since the first liquefaction stage. It is observed that even though specimens were subjected to small strain in the first liquefaction stage, the increase of relative density after that was still increase linearly at the same proportion to the 2% double amplitude axial strain history line. This can be implied that the increase in relative density due to reconsolidation after subjected to liquefaction is not influenced by the strain history. As there was a variation in initial relative density (54.9%-56.1%), it can be seen clearer in terms of change in relative density increment as presented in *Figure 3-29*.

It should be noted that in the case of small double amplitude axial strain (lower than 1%), the number of cycle to liquefy was computed based on the applied maximum strain. For the following liquefaction stages which was terminated at 2% strain amplitude, the cyclic resistance was computed at 1% double amplitude axial strain. *Table 3-3* summarizes the test results. Repeated liquefaction resistance is shown in *Figure 3-30*. It can be seen in the second liquefaction stage that the liquefaction resistance of specimens with small strain history exhibited relatively higher than the one with 2% double amplitude axial strain history. However, the liquefaction resistance dropped in the third liquefaction stage. *Figure 3-31*

presents relationship of repeated liquefaction and relative density. It is more obvious that although second stage's liquefaction resistance of 0.1% double amplitude axial strain history was lower than that of 0.2% history, the increment of increase with relative density (slope) was higher. This means the lower of strain history was, the larger of increase increment with relative density was. Another evidence is that the increment of 0.5% double amplitude axial strain history was smaller than that of 0.1% and 0.2% strain history, respectively. In short, the liquefaction resistance of the second stage was highest when the specimen subjected to 0.2% strain pre-shearing. For the specimens with 0.1% and 0.5% pre-shearing, the next stage liquefaction resistance were rather similar. Suzuki and Toki (1984) and Wahyudi and Koseki (2015) also reported this behavior. It was suggested by Suzuki and Toki (1984) that when the specimen was pre-sheared in the range of zero percent to threshold strain, the reliquefaction strength kept increasing and reached peak resistance at threshold pre-shearing strain. If the specimen was pre-sheared over this threshold strain amplitude, the reliquefaction started to decrease. This threshold value is somehow not constant depending on the loading conditions. In the case of this study, it can be said that the threshold pre-shearing strain value was 0.2%. In addition, this behavior can be explained using energy approach which will be discussed later on in this thesis.

In the third liquefaction stage, after subjected to 2% double amplitude axial strain, the liquefaction resistance dropped and again increased in the fourth stage. This increase during the third and fourth stage tended to join the 2% strain normal history line. Therefore, it is quite clear that the liquefaction resistance not only depends on the strain history but may only influenced by the previous strain history.

One assumption for this behavior in terms of soil structure is that when the specimen subjected to small strain amplitude; i.e. no liquefaction, the specimen becomes denser and might develop some structure. Thus in the second liquefaction stage, specimen showed high cyclic resistance. However, after subjected to liquefaction, soil structure was destroyed resulting in lower resistance in the third stage.

Table 3-3. Summary of repeated liquefaction test with constant CSR / various small strain amplitude

Test Number	Small Strain Amplitude	Relative Density (%)					Number of Cycle required to trigger 1% double amplitude strain			
		Initial	Stage 1	Stage 2	Stage 3	Stage 4	Stage 1	Stage 2	Stage 3	Stage 4
T24	0.5%	53.0	55.0	57.2	61.9	66.0	2.87	31.87	16.66	56.77
T25	0.2%	54.3	56.1	57.3	61.8	65.6	8.97	81.91	21.69	75.98
T27	0.2%	52.8	54.9	56.1	61.0	65.0	7.95	72.87	21.67	74.89
T28	0.1%	52.8	54.9	55.7	60.8	65.5	3.99	30.78	13.54	69.65

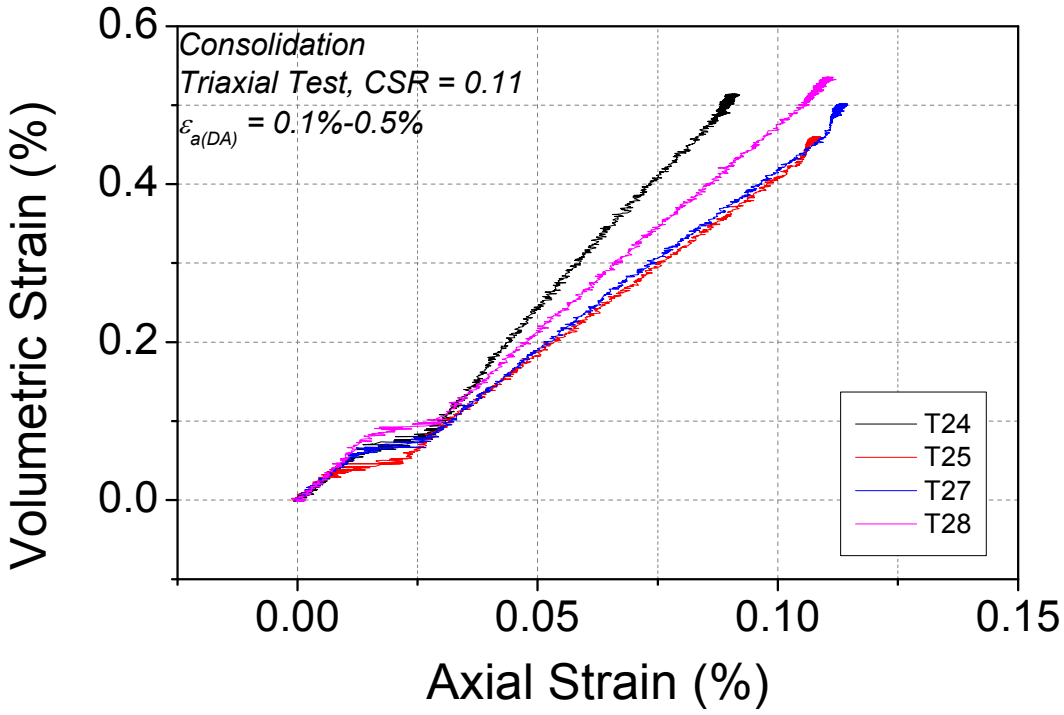

Figure 3-22. Relationship between volumetric strain and axial strain during the first liquefaction

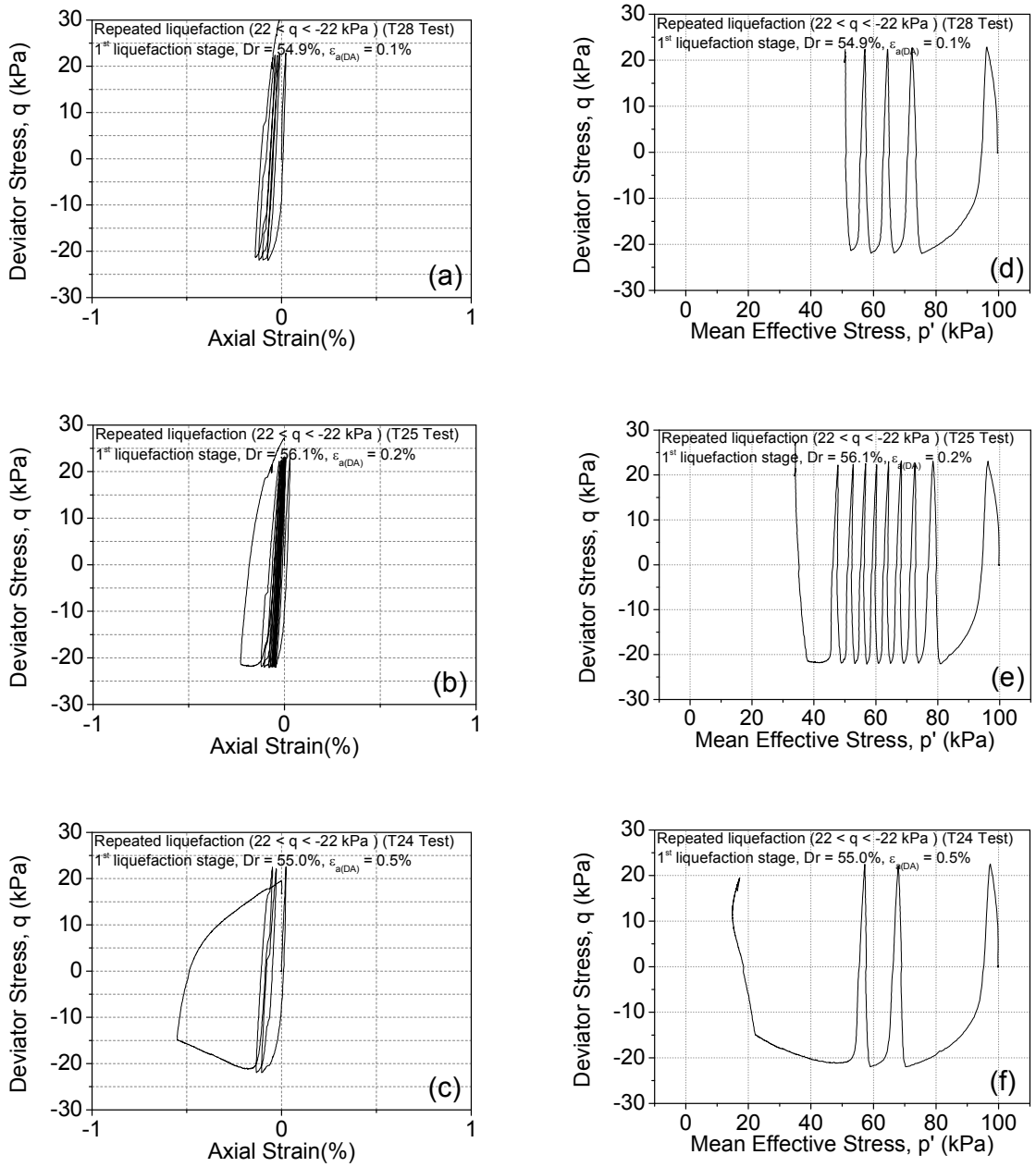

Figure 3-23. Typical deviator stress – axial strain relationships of the first liquefaction stage at 0.1% (a) (T28 Test), 0.2% (b) (T25 Test) and 0.3% (c) (T24 Test) and Typical deviator stress – mean effective stress relationships of the first liquefaction stage at 0.1% (d) (T28 Test), 0.2% (e) (T25 Test) and 0.3% (f) (T24 Test) at CSR 0

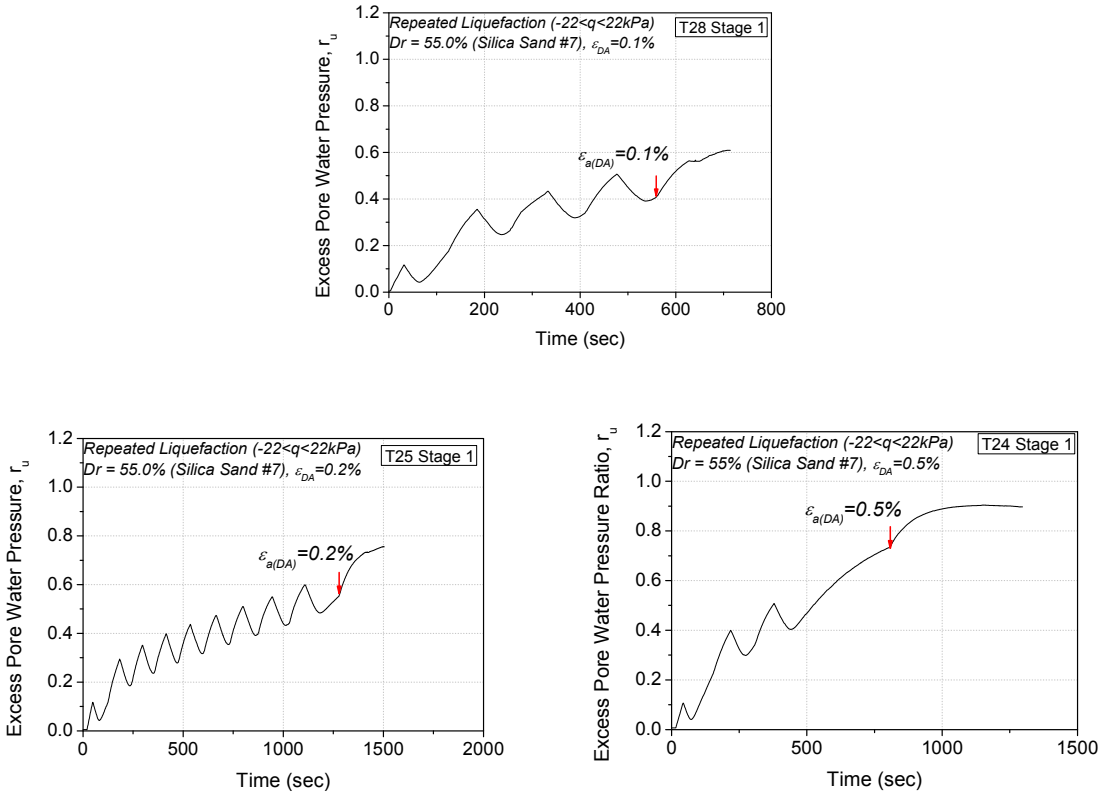

Figure 3-24. Excess pore water pressure ratio (ru) time history of the first liquefaction stage of specimen with (a) 0.1%, (b) 0.2% and (c) 0.5% double amplitude axial strain history

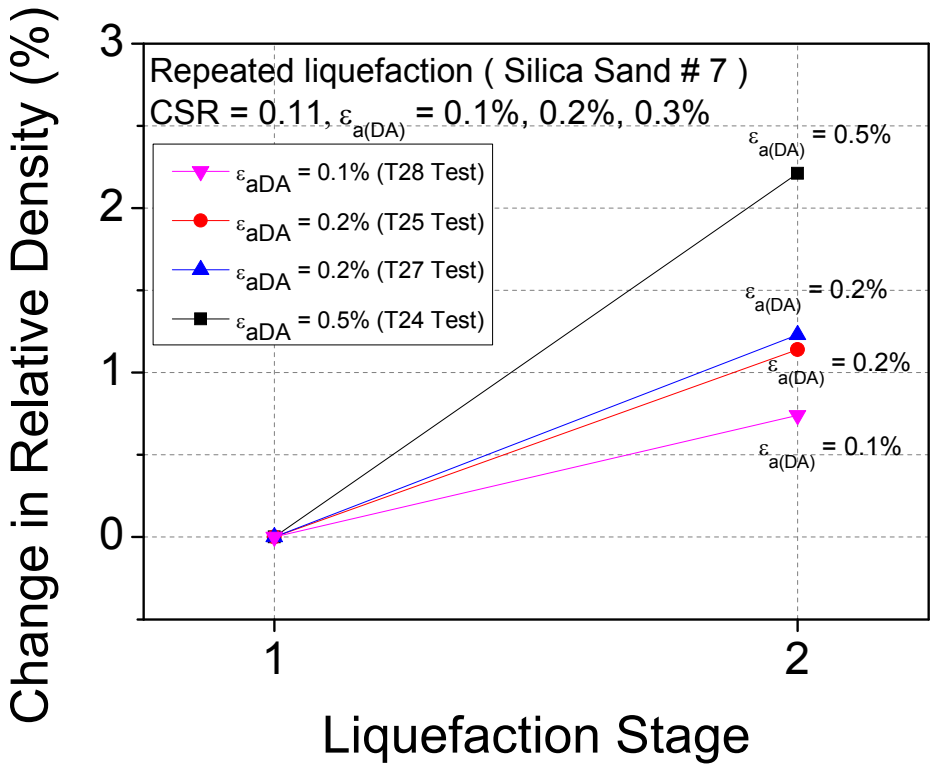

Figure 3-25. Change in relative density increment after the first liquefaction stage with small strain double amplitude axial strain and reconsolidation

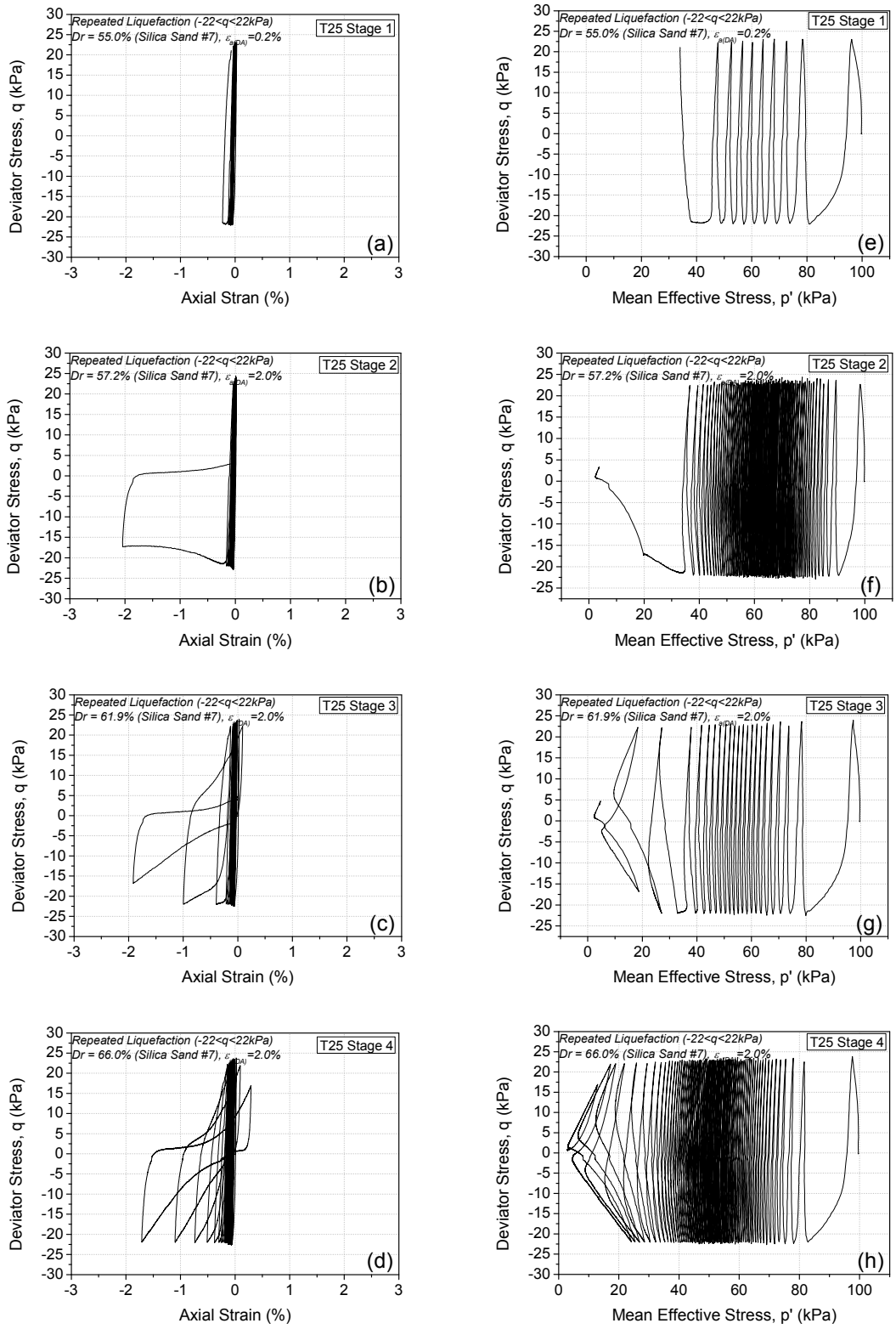

Figure 3-26. (a-d) Relationship of deviator stress and axial strain (a) 1st stage (b) 2nd stage (c) 3rd stage (d) 4th stage, (e-h) effective stress path (e) 1st stage (f) 2nd stage (g) 3rd stage (h) 4th stage (T25)

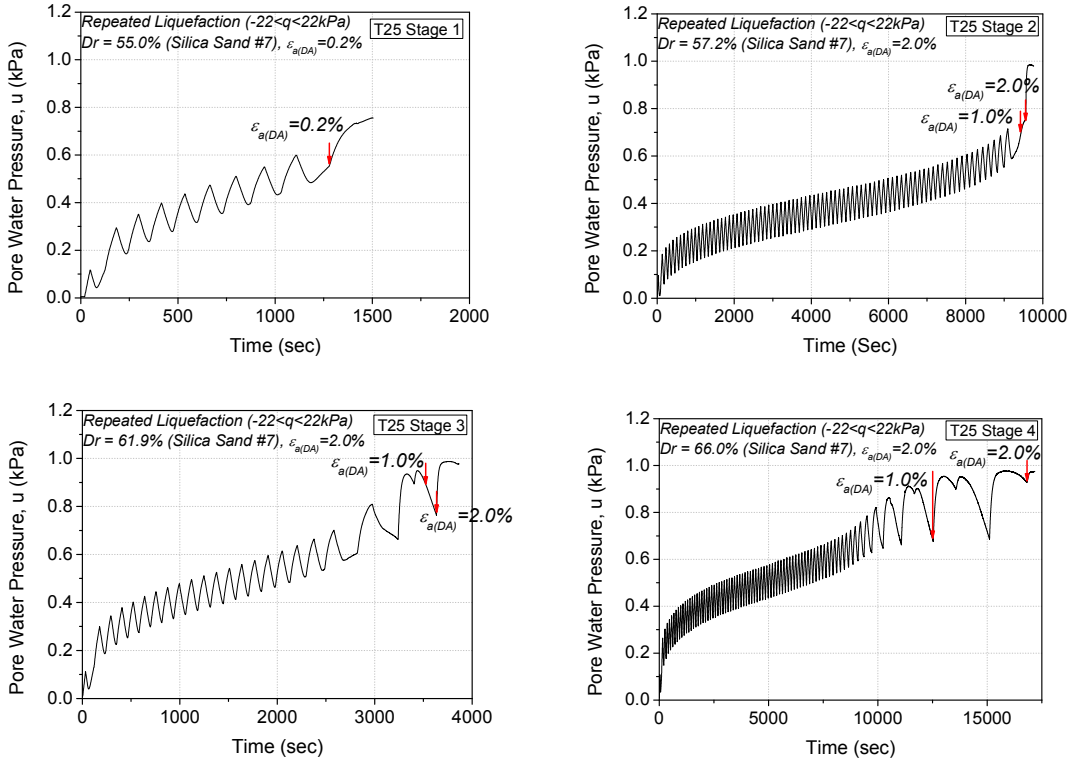

Figure 3-27. Excess pore water pressure ratio (ru) time history of liquefaction (a) stage 1 (0.2%), (b) stage 2 (2%), (c) stage 3 (2%) and (d) stage 4 (2%) (T25)

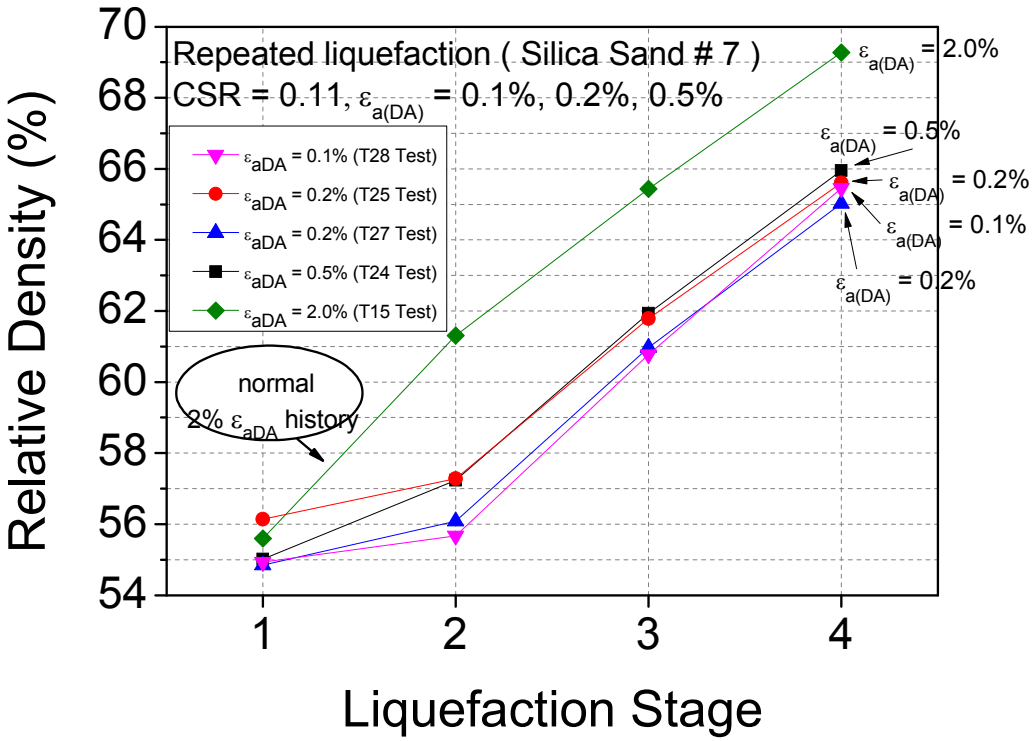

Figure 3-28. Relative density change of silica sand with number seven grading in repeated liquefaction tests with constant CSR at 0.11 and various small double amplitude axial strain history

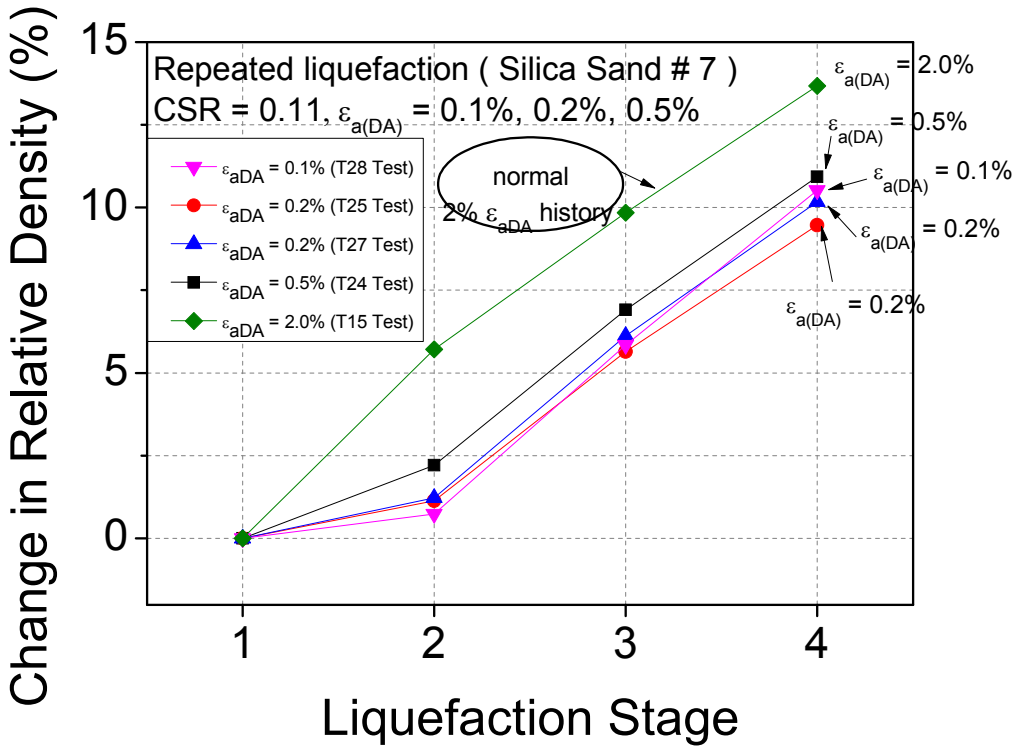

Figure 3-29. Relative density change increment of silica sand with number seven grading in repeated liquefaction tests with constant CSR at 0.11 and various small double amplitude axial strain history

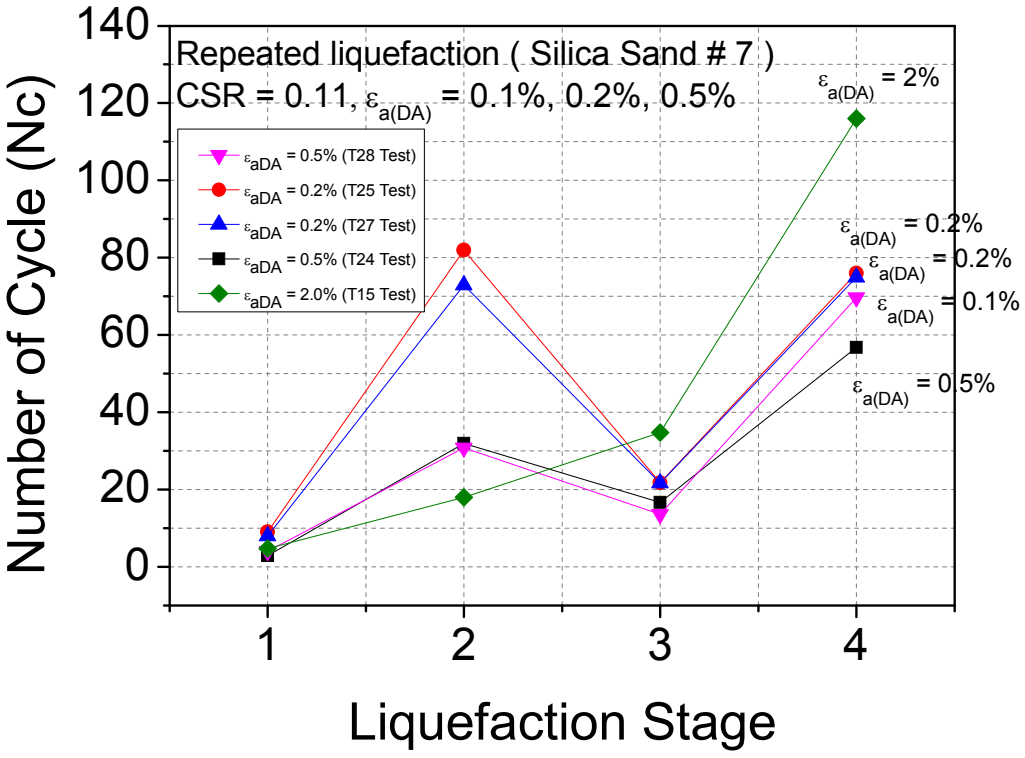

Figure 3-30. Liquefaction resistance of silica sand with number seven grading in repeated liquefaction tests

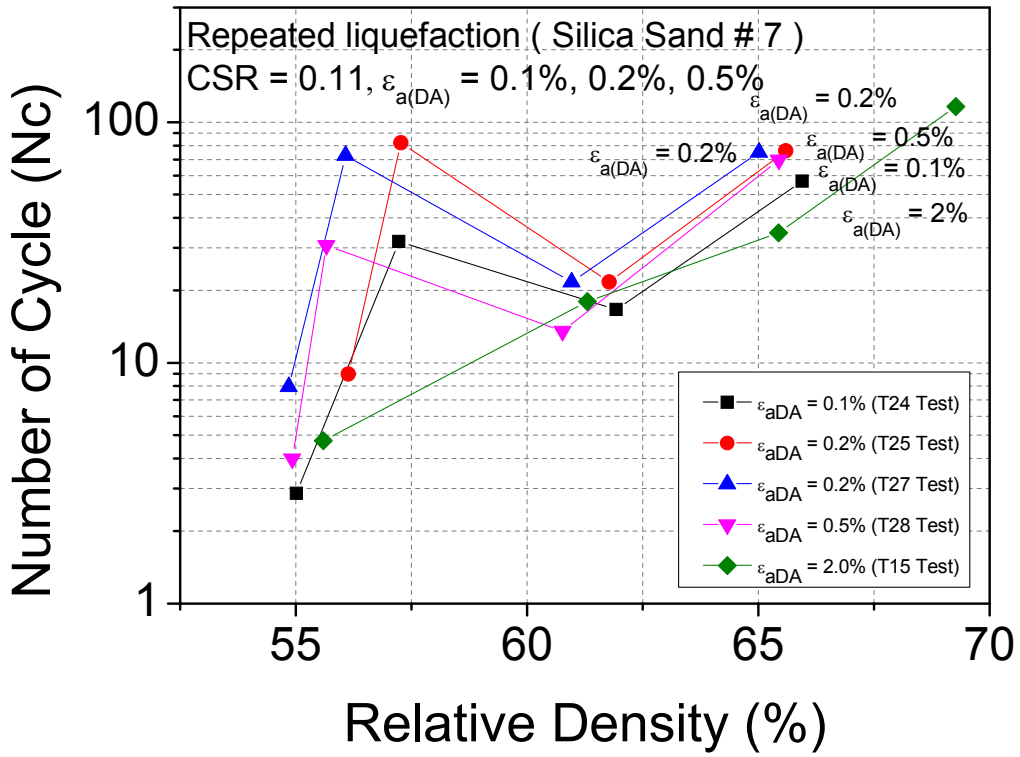

Figure 3-31. Relationship between liquefaction resistance of silica sand with number seven grading and relative density in repeated liquefaction tests

3.4 Summary

Series of cyclic undrained triaxial test were performed in order to investigate repeated liquefaction behavior of silica sand with number seven grading in three aspects; e.g. the effect of cyclic stress, the effect of strain history and the effect of small strain history. From the investigation following conclusions can be drawn:

1. In the first series, the cyclic tests were conducted under various CSR with constant DA strain at 5%. Strain softening corresponding with sharp decrease in mean effective stress was found in the initial stage which gradually bcome less in the following stages.
2. Results of the first series also showed that soil resistance against repeated liquefaction increases with number of liquefaction stage. Similar trend of relationship between CSR and number of cycle to liquefation can be found among different stages.
3. In the second test series (effect of strain history), the specimens were subjected to undrained cyclic loading at constant CSR but various DA strain histories. It was found

that the increase in relative density was affected by the degree of axial strain amplitude. With the result of the first series, it can be said that relative density change is not affected by CSR but strain amplitude. Results also showed that specimen which subjected to low DA strain (1% and 2%) gained relatively higher liquefaction resistance than the other even though their relative density slightly increased. This can be implied the change in relative density due to reconsolidation process did not much affect liquefaction resistance. It was much more influenced by strain history. However, under higher than 5% of DA strain, a random trend was found.

4. In the final series (effect of small strain history), specimens were first undrained cyclic loaded at various very small DA strain levels followed by 2% DA strain in the following liquefaction tests. Liquefaction resistance was observed to be sharply increased in the second stage after subjected to small strain histories in the previous stage which supports conclusion number 3.
5. Again in the third series, soil resistance dropped in the third stage of liquefaction altought they showed relatively high resistance in previous stage due to pre-shearing history. This can be concluded that liquefaction resistance depends on previous DA strain. The threshold pre-shearing strain which leads to the peak liquefaction resistance in the next stage was found to be 0.2%.
6. Because of reconsolidation process, there is a change in specimen density and volume which also promotes a change in specimen shape. This non-cylindrical shape results in non-uniform confining stress to the specimen. Not only non-uniform confining stress, but also more impotantly, the wrinkle might promote local drainage of excess pore water pressure and relocates excess pore water pressure to another location. As a result, liquefaction resistance of the test where wrinkle exists is believed to be overestimated. Thus, repeated liquefaction test in a triaxial apparatus is limited to 3-4 stages. Besides, it also depends on DA strain since the larger of DA strain is, the larger decrease in specimen volume and causes membrane wrinkle.

3.5 References

FINN, W., BRANSBY, P.L. and PICKERING, D.J., 1970. Effect of strain history on liquefaction of sand. *Journal of Soil Mechanics & Foundations Div,* **96**(SM6),.

ISHIHARA, K. and OKADA, S., 1982. Effects of large preshearing on cyclic behavior of sand. *Soils and Foundations,* **22**(3), pp. 109-125.

ISHIHARA, K. and OKADA, S., 1978. Effects of stress history on cyclic behavior of sand. *Soils and Foundations,* **18**(4), pp. 31-45.

SEED, H.B., MORI, K. and CHAN, C., 1977. Influence of seismic history on liquefaction of sands. *Journal of Geotechnical and Geoenvironmental Engineering,* **103**(Proc. Paper 11318 Proceeding),.

SUZUKI, T. and TOKI, S., 1984. Effects of preshearing on liquefaction characteristics of saturated sand subjected to cyclic loading. *Soils and foundations,* **24**(2), pp. 16-28.

WAHYUDI, S. and KOSEKI, J., ANALYSIS OF RE-LIQUEFACTION PROPERTIES BASED ON ENERGY APPROACH.

WAHYUDI, S., KOSEKI, J., SATO, T. and CHIARO, G., 2015. Multiple-Liquefaction Behavior of Sand in Cyclic Simple Stacked-Ring Shear Tests. *International Journal of Geomechanics,* **16**(5), pp. C4015001.

AOYAGI, Y., WAHYUDI, S., KOSEKI, J., SATO, T. and MIYASHITA, Y., 2016. Behavior of Multiple-Liuqefaction Under Small to Large Strain Levels and Its Analysis Based on Dissipated Energy. *Structural Engineering and Earthquake Engineering Journal*, **72**(4), pp. I_167-I_176.

4. Repeated Liquefaction Behavior of Silica Sand in Shaking Table Apparatus

Contents

Chapter 4 Repeated Liquefaction Behavior of Silica Sand in Shaking Table Apparatus

4.1 Introduction

Shaking table apparatus has been used to attempt understanding sand behavior under liquefaction by many researchers. Not only ground model but, in many occasions, the structure with the ground model was also adopted. For liquefaction study purpose, there are many variable parameters in shaking table test that affects the liquefaction behavior; for example, input acceleration, water table, shaking direction, shaking duration, density of model, and frequency. There have been works done on investigation single liquefaction. However, with repeated liquefaction, most of the researches were carried out by element tests or numerical simulation. Study on repeated liquefaction using shaking table seem to be very limited.

Repeated liquefaction with two stages in large scale model test was firstly conducted by Seed et al. (1977). Low magnitude of shake was first applied following by second liquefaction test. Comparing with the virgin soil model, it was reported that the cyclic resistance of test with pre-shearing was higher than the intact one although their relative density were similar. Ye et al. (2006) showed that reliquefaction was possible even soil get denser due to liquefaction and reconsolidation. Cyclic mobility also developed with liquefaction stages. Ha et al. (2011) used shaking table to conduct repeated liquefaction up to 5 stages. It was confirmed that when applying high acceleration in the first stage, cyclic resistance in the second stage dropped. The cyclic resistance started to develop from the third stage. It was suggested that not only relative density and strain amplitude affects reliquefaction resistance but also post-liquefaction consolidation (Ecemis et al., 2014), (Ecemis et al., 2015). It can be said that, most of the pioneer works on repeated liquefaction in shaking table test focused on initial stages. This study conducted large number of liquefaction stage with various input acceleration. The detail of the test program, result and discussion are described in this chapter.

4.2 Experimental program

In order to study the repeated liquefaction properties of silica sand with number seven grading, various of experimental programs were decided. In all cases the initial relative density was attempted to be in the range of 50-55%. The input motion of 20 sinusoidal cycles was applied in each shake for duration of 4 second with frequency of 5 Hz. Acceleration started at various level; e.g. 200, 300 and 400 gal and ended at 1000 gal which is capacity of shaking table. The number of cycle is mostly influenced by the earthquake magnitude (Liu et al., 2001). However, it seems that relation between earthquake magnitude and number of cycle depends on the method to evaluate equivalent number of cycle. Green and Terri (2005) concluded that the number of equivalent stress cycle is also affected by distance to the source and depth in soil profile apart from earthquake magnitude alone. For simplicity, Idriss amd Boulanger (2008) purposes simple relationship between number of cycle and earthquake magnitude. The number of cycle of 20 used in this test would equal to approximately earthquake magnitude of 7.8. For comparison with triaxial purpose, liquefaction here in this shaking table test was defined as 1.5% double amplitude shear strain which is equal to 1% double amplitude axial strain in triaxial test. However, liquefaction resistance calculated using pore water pressure ratio was also carried out to compare with the one using 1.5% double amplitude strain. In general, there were two types of shaking table test. When the ground model liquefies, the next step's input acceleration stay the same as the previous shake in the first type where the next step's input acceleration decreased by 100 gal in the second type. If the ground model does not liquefy, the next step's input acceleration for both types increased by 100 gal until reached 1000 gal. In this section, the detail of each program will be discussed.

4.2.1 Test with increase of acceleration

In this test series, the input acceleration in the next shaking step increased by 100 gal when the ground model did not reach 1.5% double amplitude shear strain and stayed at the same level when the ground model did. For instance, the test starts at 200 gal and shows more than 1.5% shear strain amplitude. In the next shaking step, the input acceleration would be again 200 gal. However, if, at 200 gal, shear strain was not exceed 1.5%, the next step input acceleration would be 300 gal. There were, in total, three tests conducted under this condition started with 200 gal, 300 gal and 400 gal. Following condition described, all three tests were terminated at

1000 gal which is capacity of shaking table. Frequency and duration of shaking were 5 Hz and 4 seconds giving 20 cycles in each shake. Example of flow chart of this test series is given in *Figure 4-1*. The arrangement of monitoring instruments of each test with 200 gal, 300 gal and 400 gal input acceleration are shown in *Figure 4-2*, *Figure 4-3* and *Figure 4-4*. The order of the test done was T4 (400 gal), T5 (200 gal) and T7 (300 gal) respectively. After the test T4 (400 gal), it was found out that there was time lag between data logger due to possible heat up of data logger. Thus, For Test T5 (200 gal) and after, the sensors which are used in the same data calculation were put in the same data logger. For Test T7 (300 gal), there was a trial for primary wave measurement so that the sensors were moved to the other side of soil container to install the primary wave instrument. As, the data computation used raw data from the sensors at the middle, it is believed that there was no effect of the changing the position of sensors. The data of primary wave trial is given in *Appendix B*.

4.2.3 Test with decrease of acceleration

Due to the fact that, the first test series, liquefaction continuously occurred at the same input acceleration level for many steps. Thus, the soil might also repeatedly liquefy even at the lower input acceleration level once it already liquefied at high acceleration level. In this test series, the input acceleration in the next step decreased when shear strain amplitude of ground model exceeded 1.5% and increased when there was limited shear strain developed (less than 1.5%). For example, if the ground model liquefied at 500 gal, the input acceleration in the next step would be 400 gal instead of 500 in previous test series. On the other hand, if the shear strain amplitude was lower than 1.5% at 500 gal, the input acceleration in the next step would be 600 gal. Because of complexity in data analysis and interpretation, there was only one test in this series. The test started at 200 gal following the condition described above and ended at 1000 gal. Frequency and duration of shaking were the same as the first test series which were 5 Hz and 4 seconds giving 20 cycles in each shake. For better understanding, *Figure 4-5* summarizes flow chart of testing program for this test series. It should be noted that the lowest input acceleration used in this test series was 200 gal and 300 gal was skipped. That means although shear strain did not exceed 1.5% at 200 gal, the next input acceleration would be still at 200 gal. Additionally, in the initial shaking steps, in order to confirm that repeated liquefaction started to occur, the input acceleration shall be repeated for approximately 3 steps before

starting decrease in put acceleration. *Figure 4-6* shows monitoring instruments plan in the ground model.

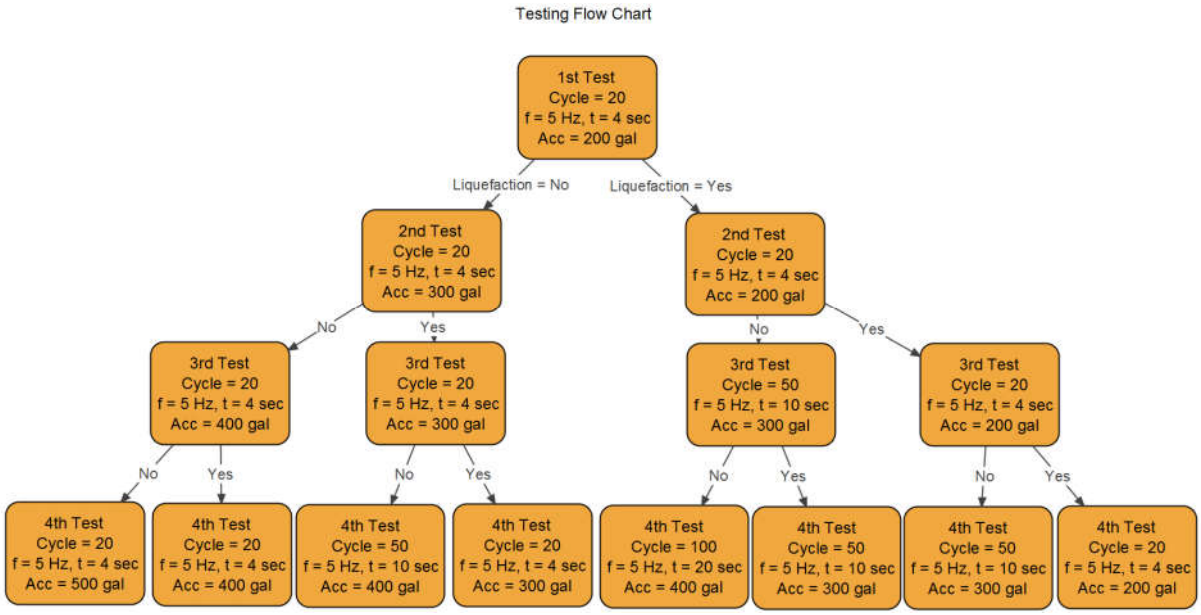

Figure 4-1. Testing flow chart for the first test series (with increase in input acceleration)

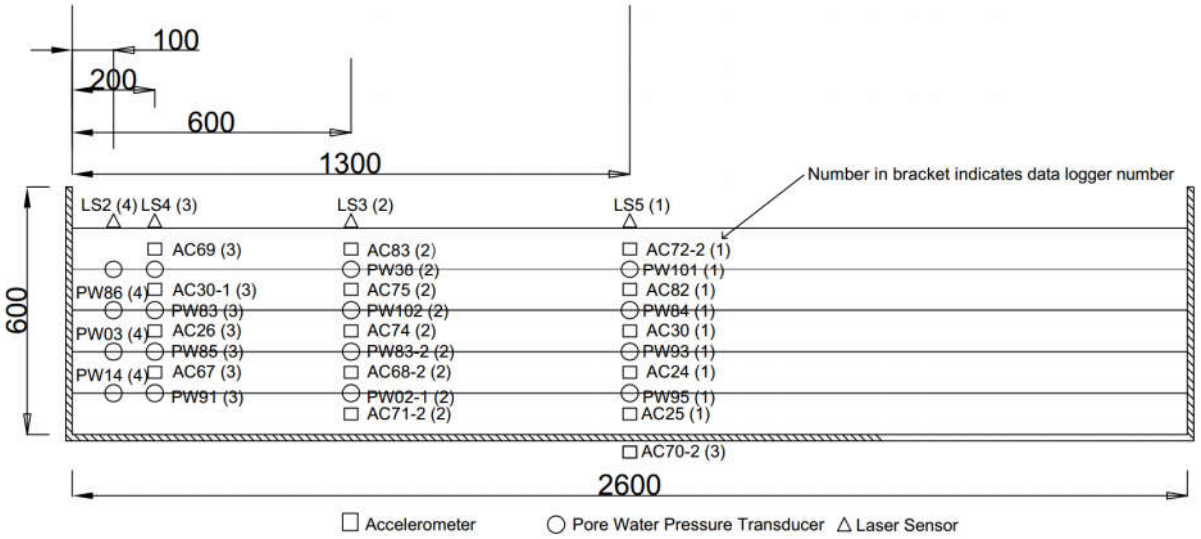

Figure 4-2. Monitoring Instruments arrangement of the test with 200 gal input acceleration (T5 Test) (unit in mm)

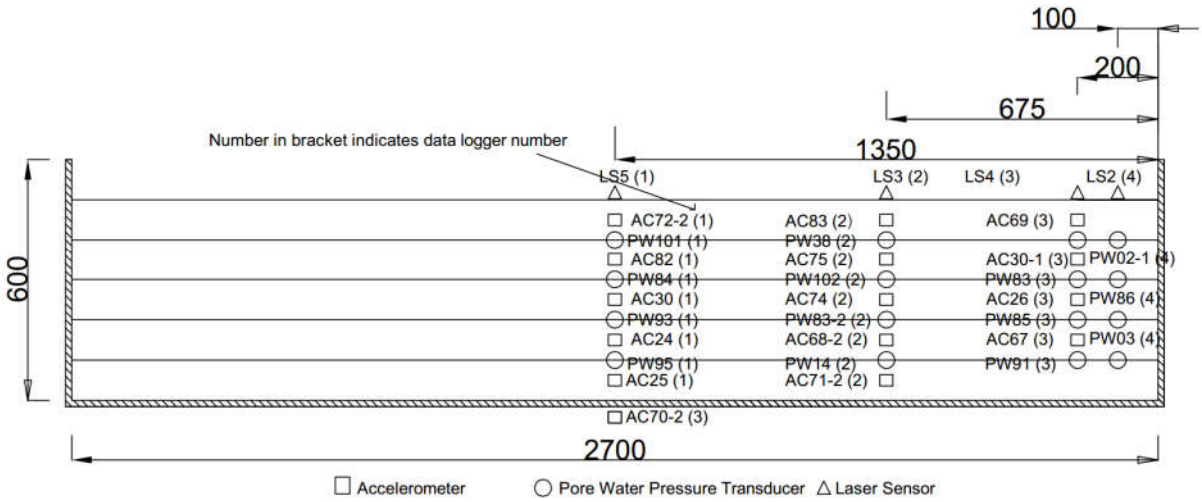

Figure 4-3. Monitoring Instruments arrangement of the test with 300 gal input acceleration (T7 Test) (unit in mm)

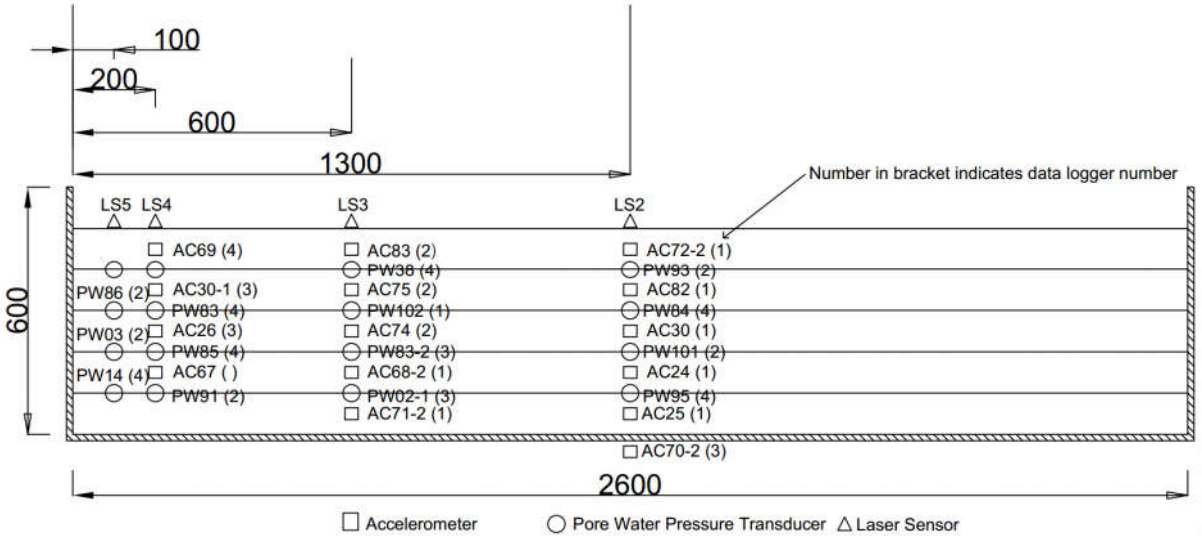

Figure 4-4. Monitoring Instruments arrangement of the test with 400 gal input acceleration (T4 Test) (unit in mm)

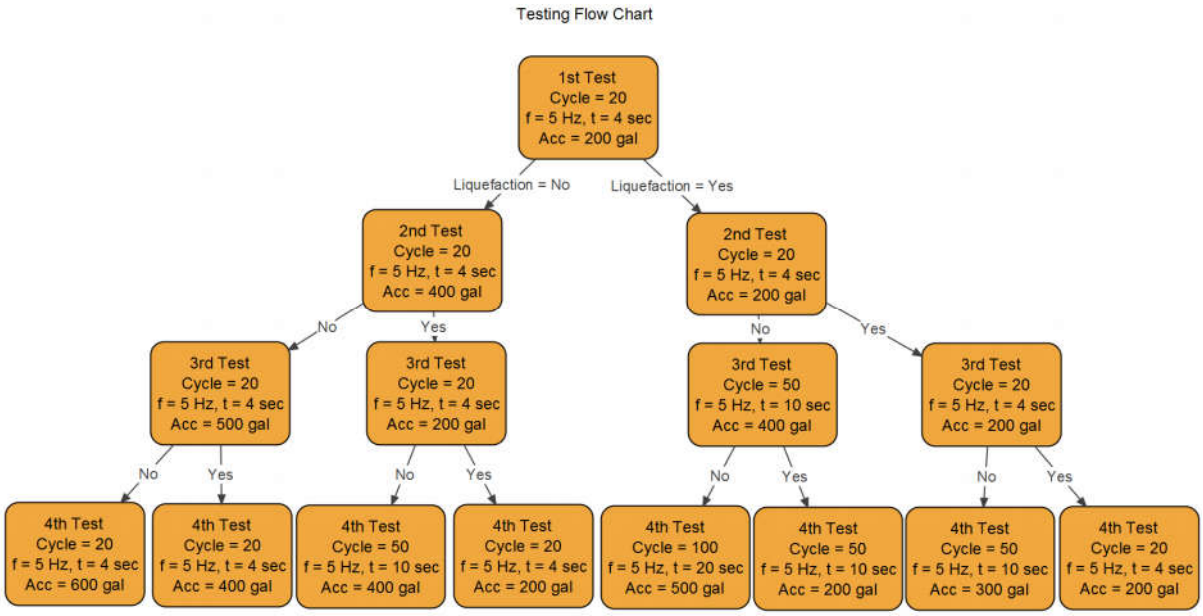

Figure 4-5. Testing flow chart for the second test series (with decrease in input acceleration)

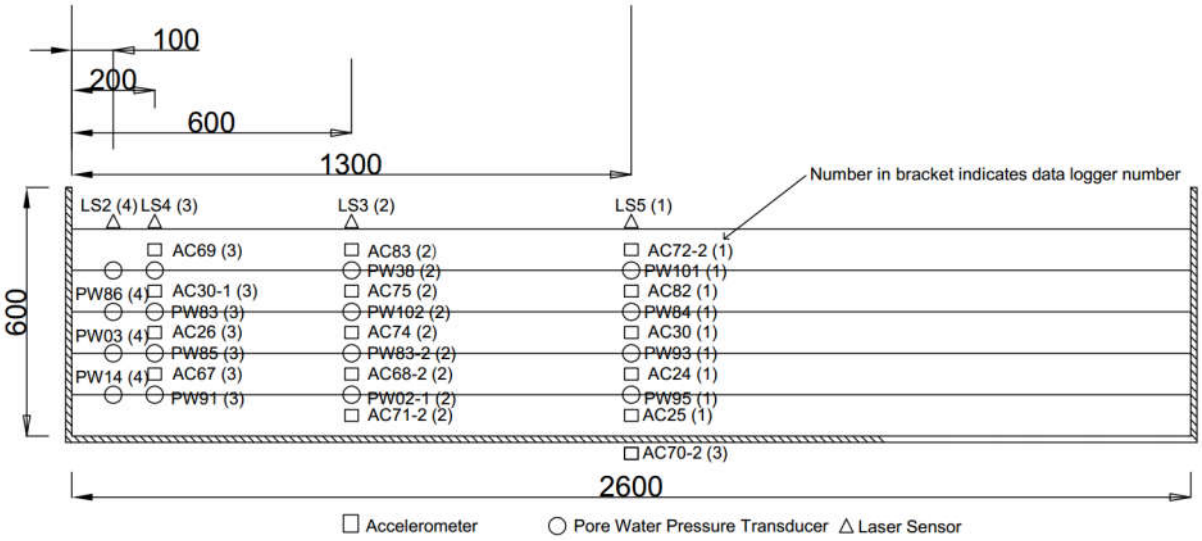

Figure 4-6. Monitoring Instruments arrangement of the test with 200 gal input acceleration (T6 Test) (unit in mm)

4.3 Results and discussions

Various types of experimental program have been conducted in shaking table apparatus to investigate repeated liquefaction behavior of the silica sand. The monitoring was made in terms of acceleration, pore water pressure and ground settlement. Using all this raw data, ground response was investigated. The finding results and discussion of each aspect are described in this section.

4.3.1 Ground response

4.3.1.1 Acceleration response

During shaking, acceleration was measured at various locations by using accelerometers as previously shown. Typical ground response in terms of acceleration at different depth during the first shaking stage at the input acceleration of 300 gal are presented in *Figure 4-7*. These examples of acceleration record were at the middle of soil container. Acceleration responses were different from place to place as they measured local ground behavior. It can be clearly seen that the acceleration responses near the surface at -5 and -15 cm showed amplification after the third cycle with amplification ratio around 2.1-2.7. For the depth at -25 cm, the acceleration response started to amplify after the seventh cycle with lower amplification ratio of about 2.0. At the depth of -35 cm and -45 cm, amplifications were limited and the response was similar to the input acceleration indicating no liquefaction taken place. Only the response at -5 cm showed attenuation of acceleration amplitude after amplification started around the eighth cycle. This attenuation can be used for liquefaction justification during testing as time was limited for strain calculation. In general, when the soil liquefied, acceleration response amplifies or attenuates. However, at lower depth, there was limited amplification of acceleration as the soil hardly liquefy due to higher effective stress; i.e. overburden pressure.

Acceleration time histories were then double integrated for displacement histories. Before doing so, the acceleration time histories were high pass filtered and offset adjusted to eliminate possible data noise and offset. The offset sometimes occurred due to little tilting when placing accelerometer in the ground model or during zero value adjustment. The corresponding displacement time histories computed from acceleration during the first shake at 300 gal input acceleration is given in *Figure 4-8*. Generally, displacement time history is corresponding to acceleration time history. Where amplification is observed, normally, associated with large

displacement and vice versa. The displacement was then used to calculate shear strain as already explained in Chapter 2.

This shear strain was calculated at the middle between two adjacent accelerometers. In other words, shear strain, which was calculated using horizontal displacement at -5 cm and -15 cm, is assumed to be at the location of -10 cm from the surface, which is at the middle of two adjacent accelerometers used in calculation. This location will be then called "Layer 1". By using this method, the location of layer 2, 3 and 4 can also be defined at -20 cm, -30 cm and -40 cm from the ground model surface respectively, as shown in *Figure 4-9*. This definition of Layer 1 to Layer 4 will be used in shaking table analysis from now on. The computed shear strain time histories at different layers are presented in *Figure 4-10*. It can be seen that shear strain responds were different depending on the depth. Generally, at lower depth, liquefaction hardly occurs compared to layers near to surface due to higher effective stress; for instance, layer 4 in this case. For the layers closed to ground surface, liquefaction takes place relatively easier; therefore, there was high shear strain respond in those layers. For the layer 1, as the top layer was unsaturated or partly saturated due to suction, thus liquefaction also hardly occurred.

In addition, acceleration was not only used for shear strain computation but also shear stress calculation by employing Newton's law of motion as already described in Chapter 2. For analysis purpose, shear stress was also calculated at the same depth as shear strain at -10 cm (layer 1), -20 cm (layer 2), -30 cm (layer 3) and -40 cm (layer 4) using summary of mass and acceleration. *Figure 4-11* shows time histories of computed shear stress at different layers. In general, largest shear stress can be expected at the bottom layer since it is computed by accumulation of multiplied production of mass and acceleration from the top layers.

By combining shear stress and shear strain time histories, relationship between shear strain and shear strain can be drawn. *Figure 4-12* presents typical shear stress and shear strain relationship at different layers. This calculation method was used by several researcher such as Koga and Matsuo (1990), Zeghal and Elgamal (1994) and El-Sekelly et al. (2016). The objective of using this method was to compare repeated liquefaction in the same manner as used in triaxial analysis.

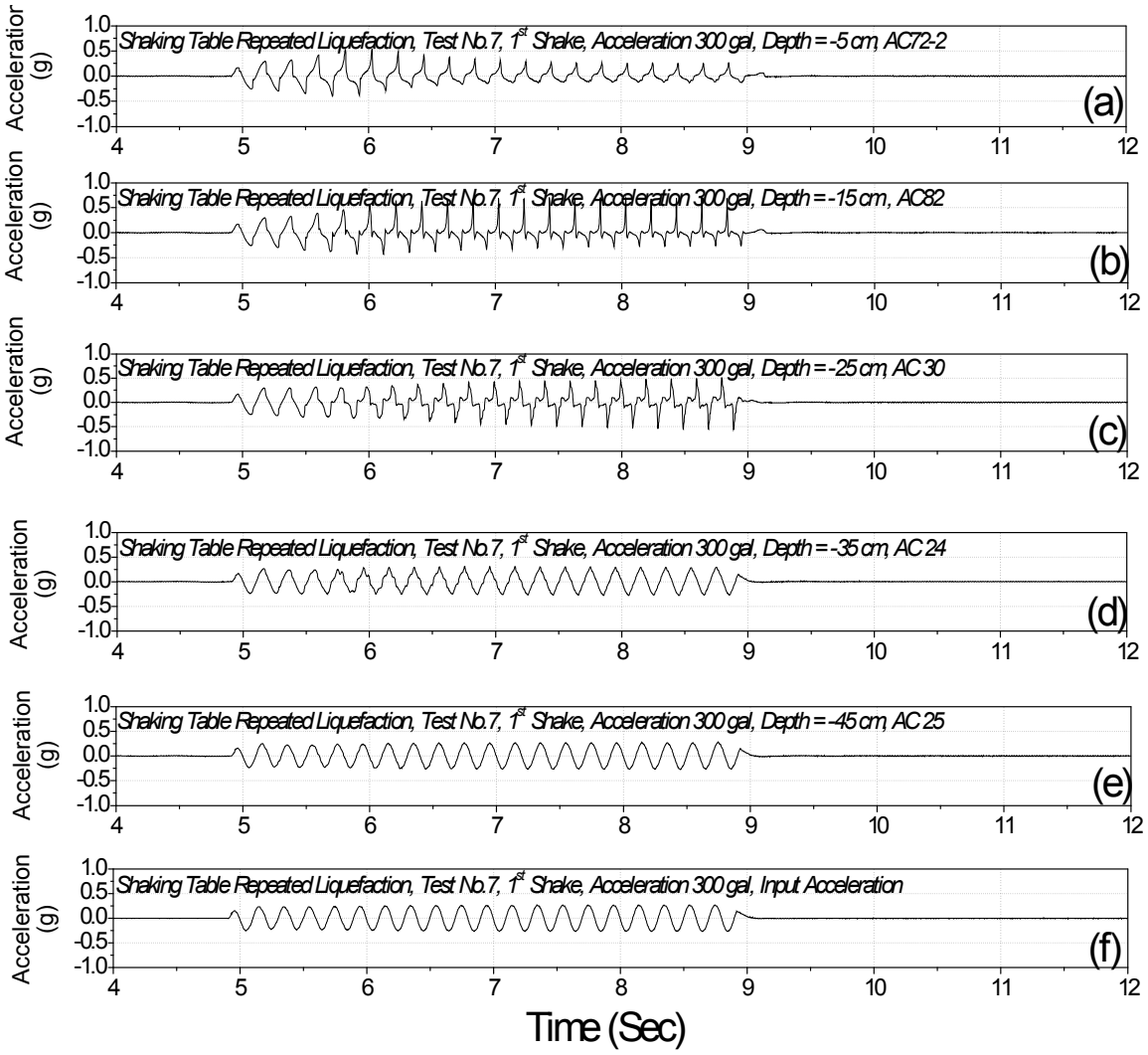

Figure 4-7. Acceleration time history of accelerometer at (a) -5cm, (b) -15cm, (c) -25cm, (d) -35cm, (e) -45cm and (f) input acceleration measured at soil container (T7, 1st shake, 300 gal)

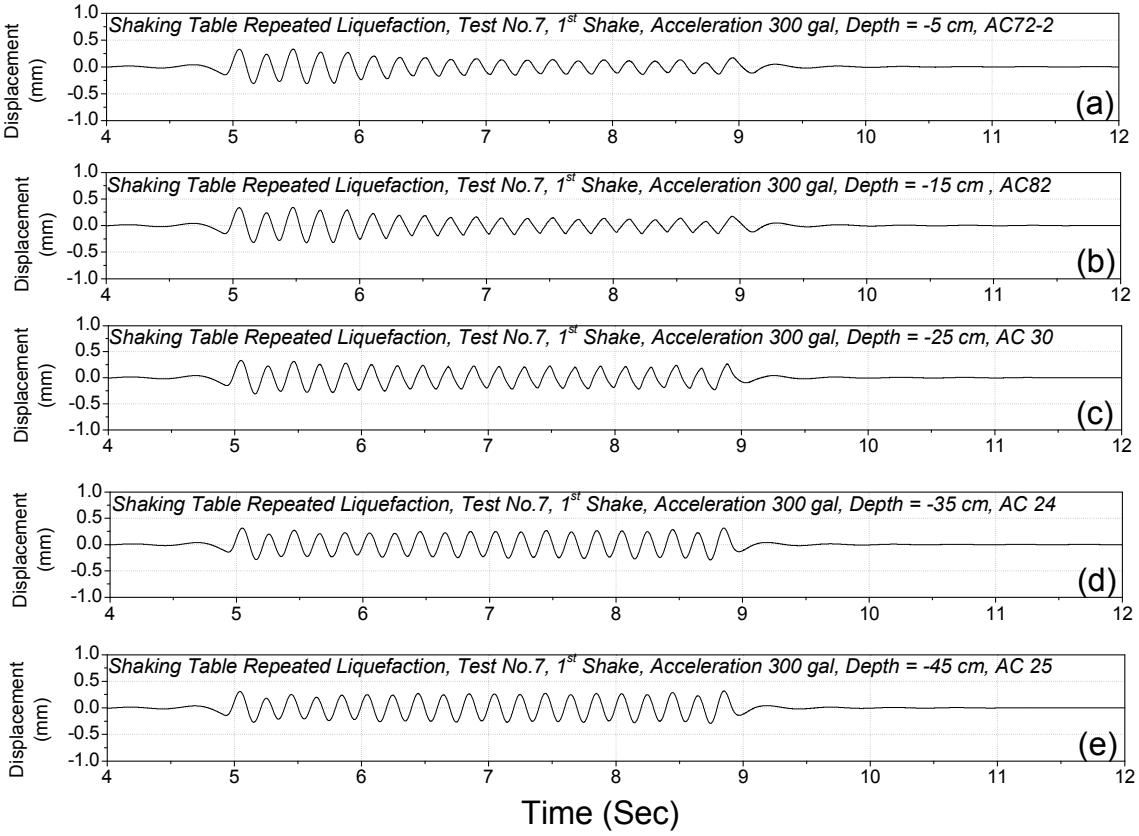

Figure 4-8. Displacement time history of accelerometer at (a) -5cm, (b) -15cm, (c) -25cm, (d) -35cm, (e) -45cm and (f) input acceleration measured at soil container (T7, 1st shake, 300 gal)

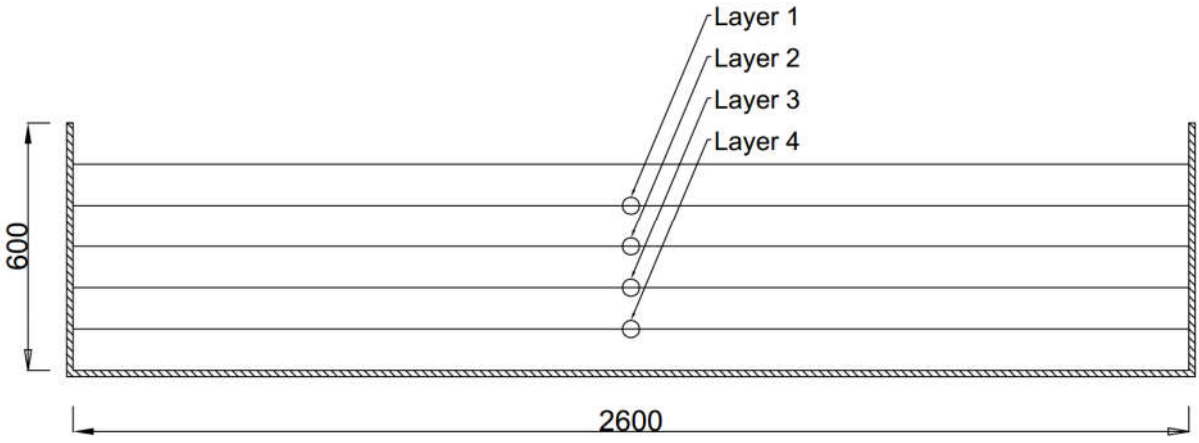

Figure 4-9. Location definition

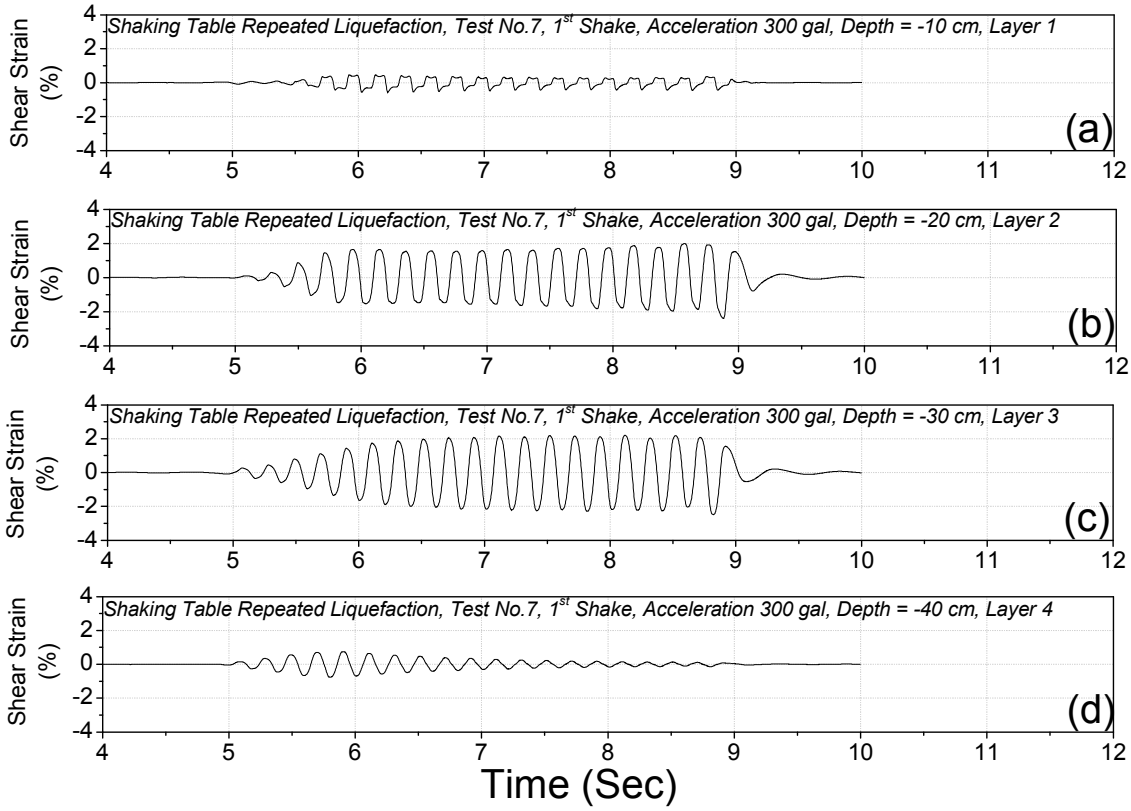

Figure 4-10. Shear strain time history computed from acceleration at (a) -5cm, (b) -10cm, (c) -20cm, (d) -30cm and (e) -40cm (T7, 1st shake, 300 gal)

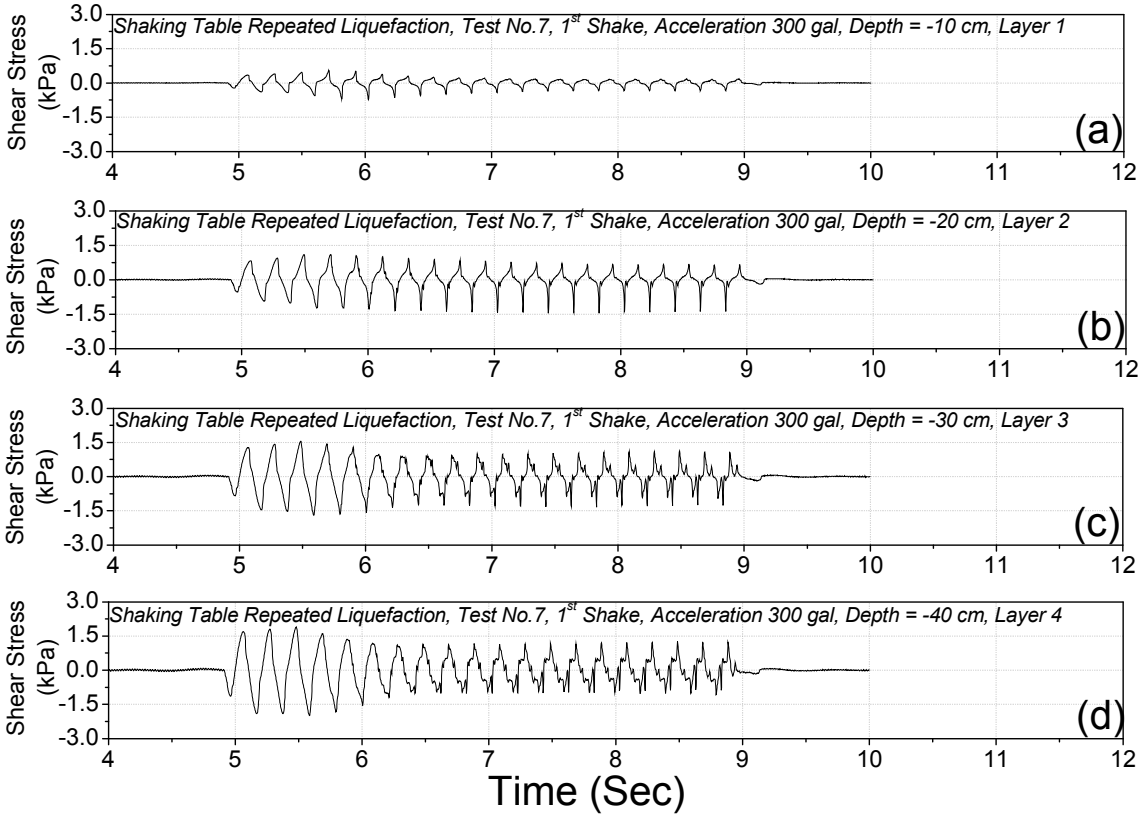

Figure 4-11. Shear stress time history computed from acceleration at (a) -5cm, (b) -10cm, (c) -20cm, (d) -30cm and (e) -40cm (T7, 1st shake, 300 gal)

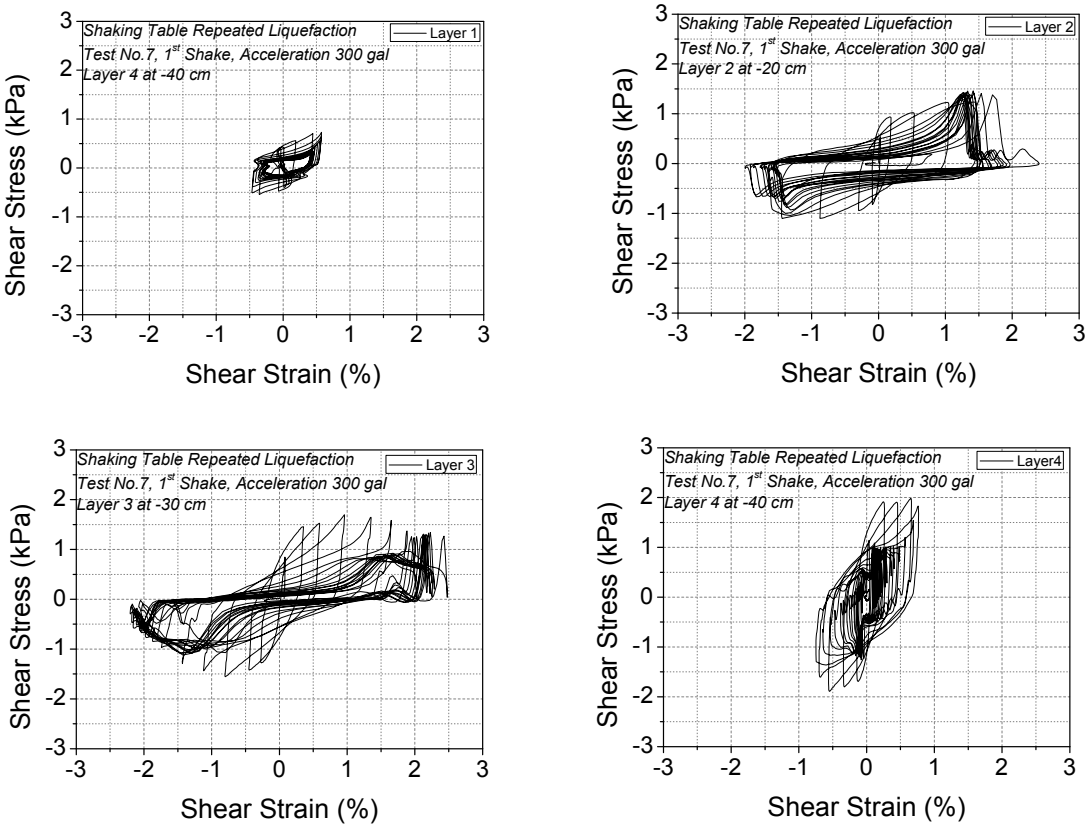

Figure 4-12. Relationship of shear stress and shear strain computed from acceleration at (a) -5cm, (b) -10cm, (c) -20cm, (d) -30cm and (e) -40cm (T7, 1st shake, 300 gal)

4.3.1.2 Pore water pressure response

Pore water pressure was monitored during liquefaction test in ground model at various depth and location using pore water pressure transducers generally at Layer 1 (-10 cm), Layer 2 (-20 cm), Layer 3 (-30 cm) and Layer 4 (-40 cm). By neglecting initial static water pressure, excess pore water pressure can be computed. Typical excess pore water pressure responses at different depths are presented in *Figure 4-13*. This excess pore water pressure data was corresponding with acceleration data shown in previous section. In all layers, excess pore water pressure generated rapidly. It was suggested that the displacement during liquefaction was imposed by excess pore water pressure generation (Sasaki et al., 1992). It also can be seen that at the layer 2 (-20cm) and layer 3 (-30cm), excess pore water pressure ratio was approximately equal to 1.0 indicating liquefaction. However, in this thesis, liquefaction was defined by double amplitude shear strain. Additionally, the excess pore water pressure data was used for analysis with energy approach which is discussed later on in the next Chapter. It must be noted that pore water transducers were installed inside the soil model with their wires hanging from the metal

bar to keep them at the same depth during liquefaction and also it was installed perpendicular to the direction of shake. Nevertheless, little rotation or little settlement of transducer was still possible during ground liquefaction. If rotation occurred, it would result in measuring dynamic water response as effect of shaking direction. Possible settlement during liquefaction would promote higher measured pore water pressure.

By combining shear stress which can be computed from acceleration data and excess pore water pressure data, the effective stress path can be plotted at each Layer as shown in *Figure 4-14*. Since shear stress was calculated as a summation from the top layer, the bottom layer showed highest value of shear stress and also attenuation although the pore water pressure ratio did not reach unity resulting from liquefaction at top layers. It can also be seen that the effective stress of Layer 2 and Layer 3 was negative which might due to possible settlement of transducer.

Note that in triaxial test, liquefaction resistance was calculated based on double amplitude axial strain of 1%. In order to compare the result between shaking table tests and triaxial tests, the cyclic resistance in shaking table tests was also computed in terms of shear strain of 1.5% which equals to 1% axial strain based on assumption that the earth pressure coefficient at rest is 0.5. For the example given, there was liquefaction observed at Layer 2 and Layer 3. It is worth to mention when did shear strain of 1.5% occurred. *Figure 4-15* presents excess pore water pressure ratio during shaking with arrows mark indicating the time when double amplitude shear strain reached 1.5%. It can be observed that when the shear strain amplitude reached 1.5%, the excess pore water pressure was yet unity with the value of 0.6 and 0.9 for Layer 2 and Layer 3 respectively. However, the size of the shaking table might also influence the induced strain during shaking. Pathak and Patki (2013) conducted small shaking table test and observed much lower shear strain when the excess pore water pressure reached peak value.

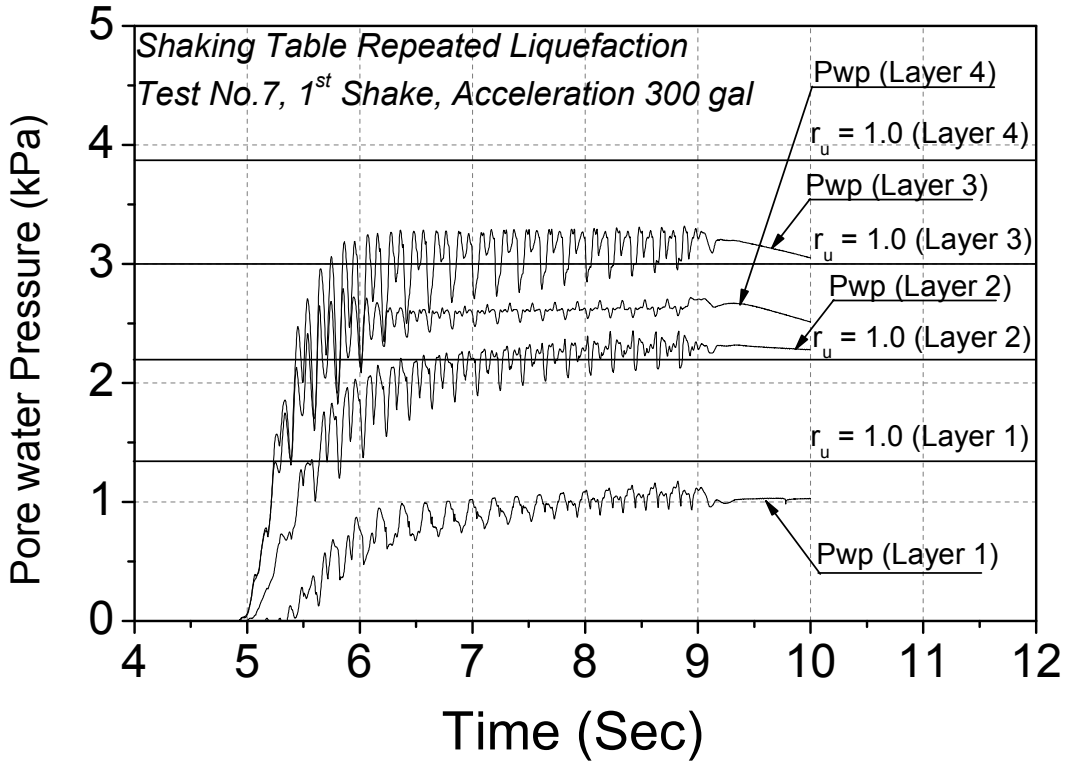

Figure 4-13. Excess pore water pressure time history at -10cm, -20cm, -30cm and -40cm (T7, 1st shake, 300 gal)

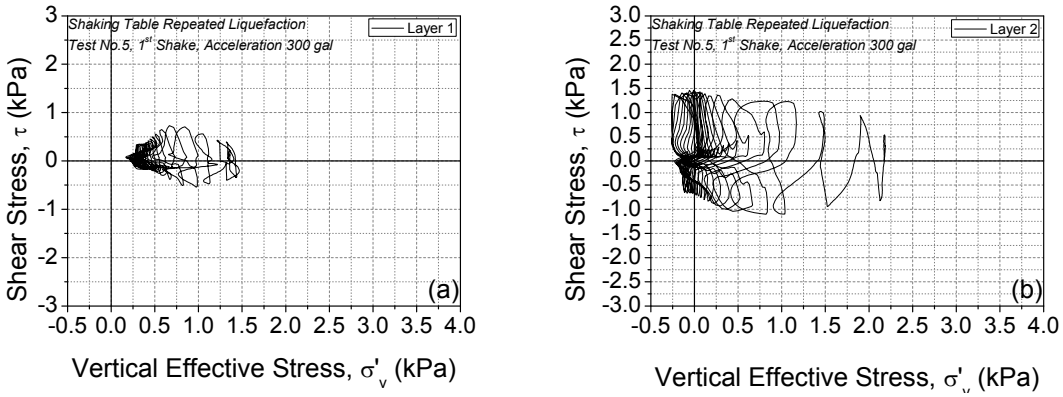

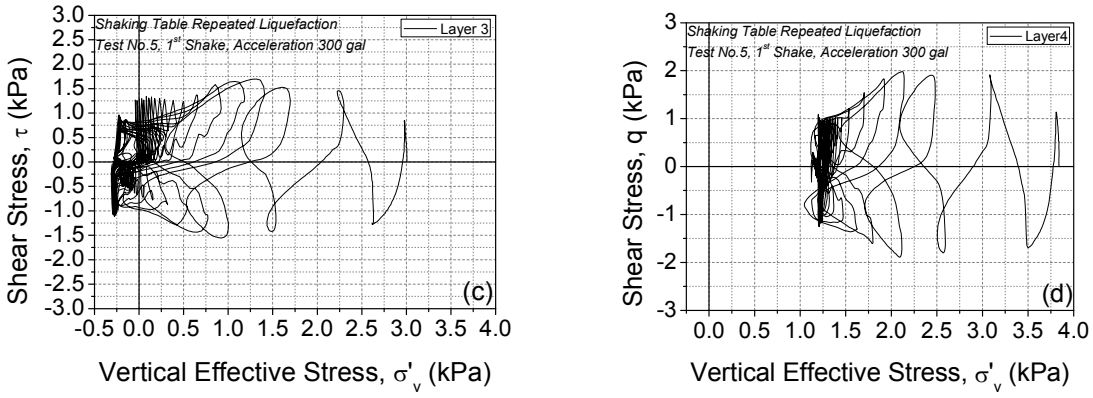

Figure 4-14. Effective stress path at (a) -10cm, (b) -20cm, (c) -30cm and (d) -40cm (T7, 1st shake, 300 gal)

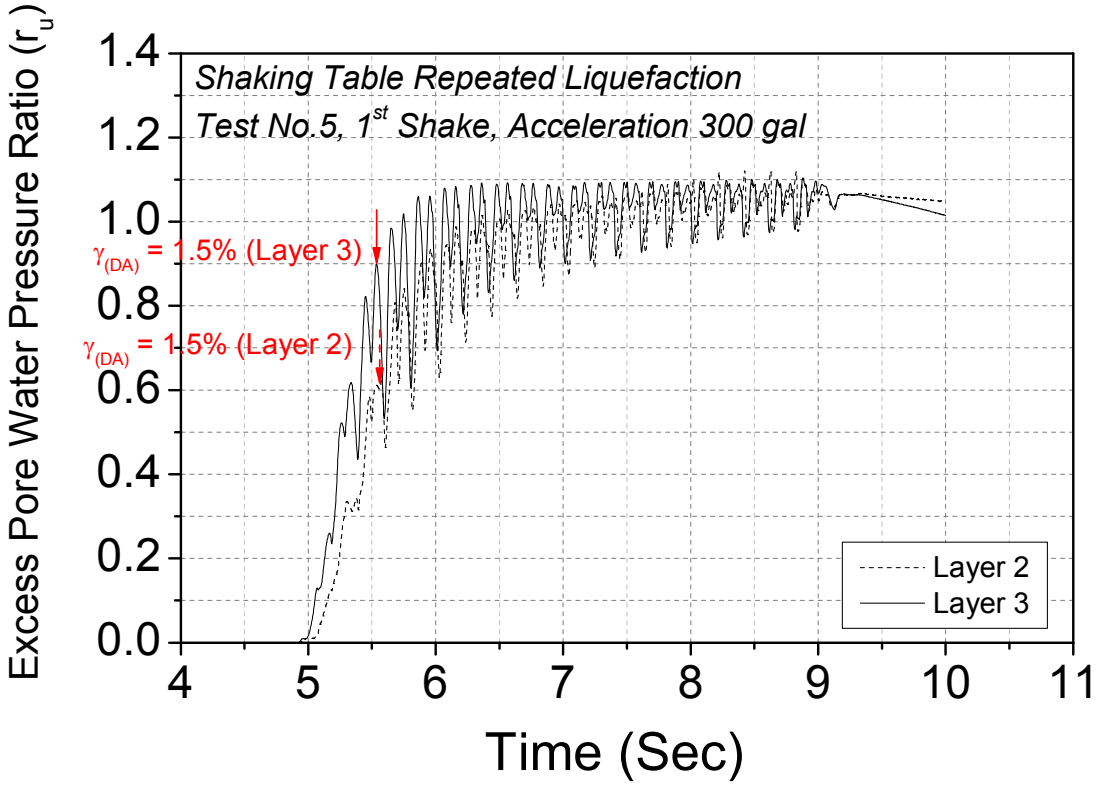

Figure 4-15. Excess pore water pressure ratio (ru) during shaking for Layer 2 and Layer 3 (T7, 1st shake, 300 gal)

4.3.1.3 Ground settlement response

There were four laser sensors used in this research. Each sensor was installed above soil container to measure global settlement (vertical displacement) at different locations as shown in *Figure 4-3*. In general, the sensors provided settlement value around the instrument column (accelerometers and pore water pressure transducers). Typical settlement time histories recorded by those sensors are presented in *Figure 4-16*. Settlement increased not only during liquefaction but also during reconsolidation where excess pore water pressure was being dissipated. Final value of settlement results were then used for relative density calculation. As settlement monitoring was made only on the ground model surface, relative density, thus, can be only calculated as a whole. Typical relative density change during the test was computed and shown in *Figure 4-17*. It is noted that the relative density was calculated before each shaking event. Ground relative density changed significantly when the ground model liquefied at initial stages. The increase became lower at later stages of liquefaction. In the shaking stage where the ground model did not liquefy, relative density change was limited. This behavior was also reported earlier by Ueng et al. (2010).

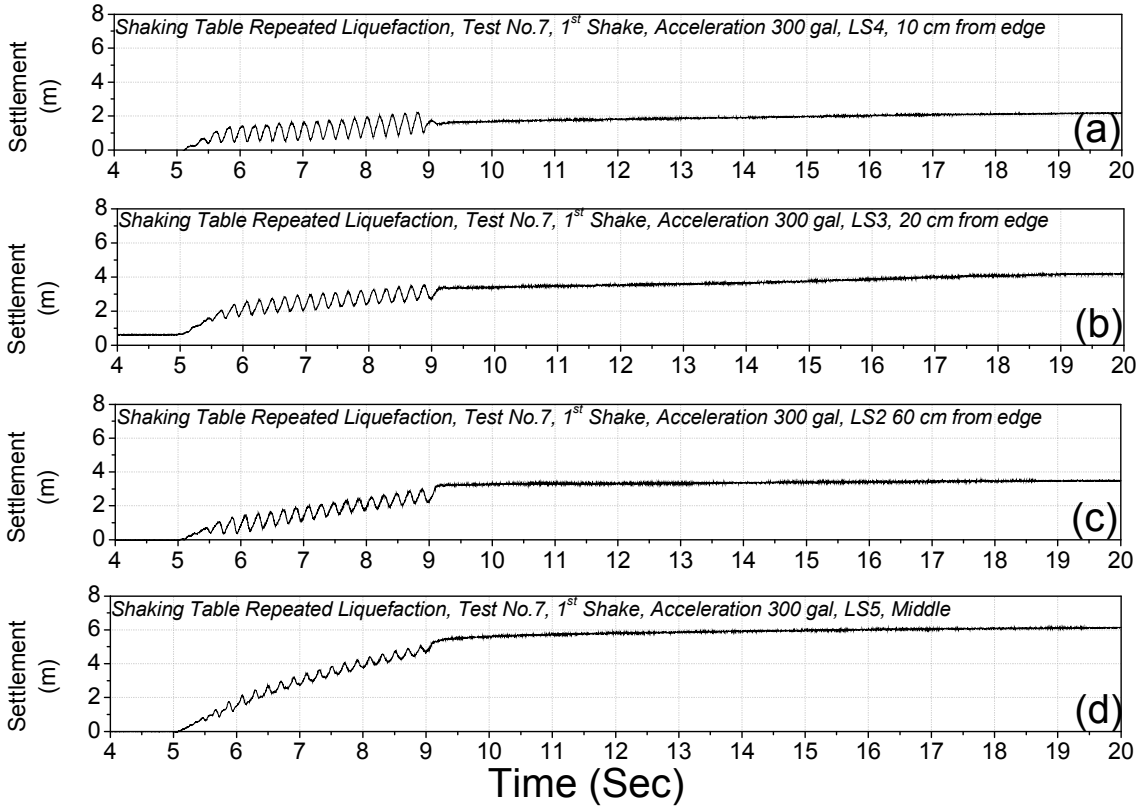

Figure 4-16. Settlement time history of laser sensor at different locations (a) 10 cm, (b) at 20 cm, (c) at 60 cm from the edge and (d) at the middle of soil container

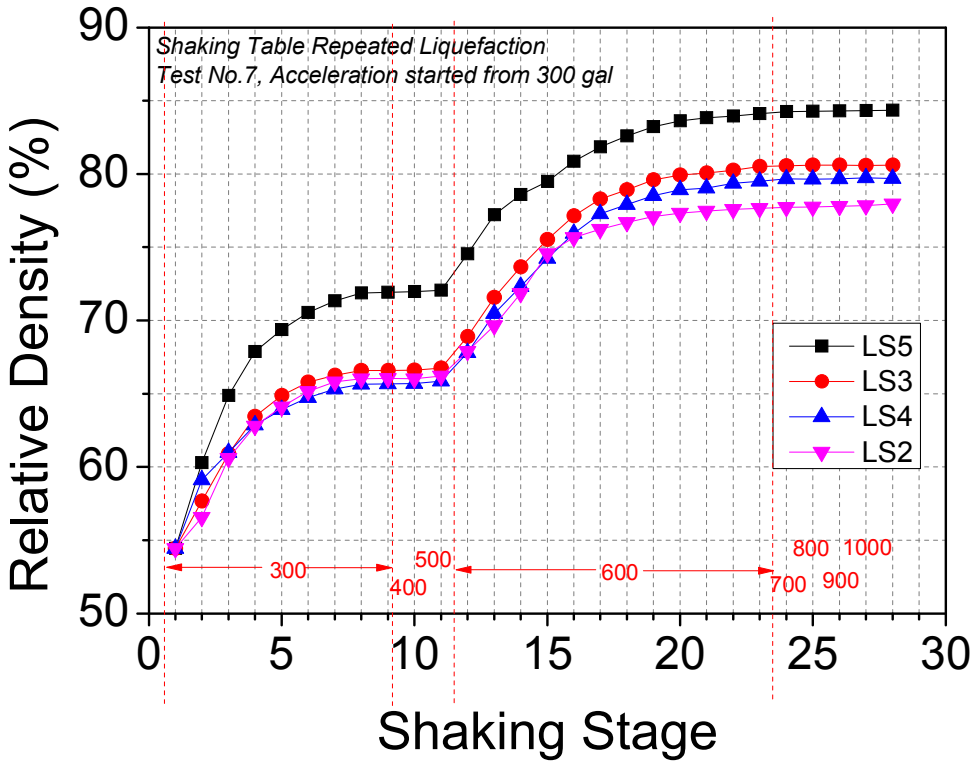

Figure 4-17. Relative density change during repeated liquefaction test measured by laser sensor at different locations

4.3.2 Boundary effect

The soil container used in this experiment was made of steel frame with transparent glass. Thus, the boundary was rigid. In this section the effect of boundary is discussed using test T5 at the first liquefaction stage. The instrument plan is given in *Figure 4-2*. *Figure 4-18* shows excess pore water pressure response at the same depth but different location; i.e. at the middle of soil container and at 10 cm from the edge. It can be seen that excess pore water pressures built up at the edge of soil container was limited compared to that at centerline.

The difference behavior at the center and edge of soil container was not only observed for pore water pressure response but also acceleration response as presented in *Figure 4-19*. When ground model did not liquefy; for example, at depth -25cm and -35cm, the acceleration responses are quite similar. However, when liquefaction occur, the sand behaves like liquid resulting in large deformation and large acceleration response. Due to the rigid boundary at one side, the acceleration response observed at -20 cm, from the edge of soil container were not realistic. The difference can be seen clearly at the depth -5cm where acceleration record at the

edge showed unsymmetric response. Therefore, for further analysis, only data acquired at the center of soil container was used.

As can be observed in *Figure 4-17*, the settlement of LS5 which was measure at the middle of soil container was higher than the others. This also indicates boundary effect on settlement as well. It seems that rigid boundary affected the result of settlement largely during the initial shake up to about 5-6 stages. At the input acceleration of 600 gal, there was less boundary effect observed

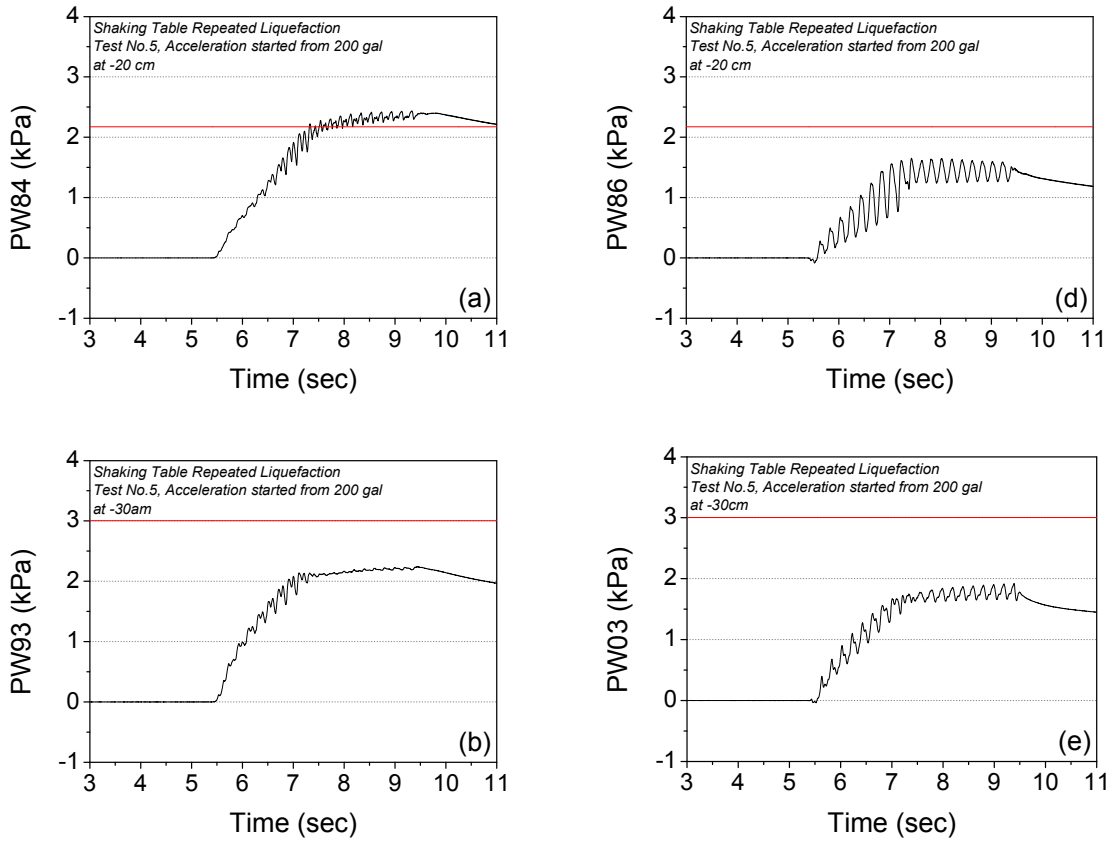

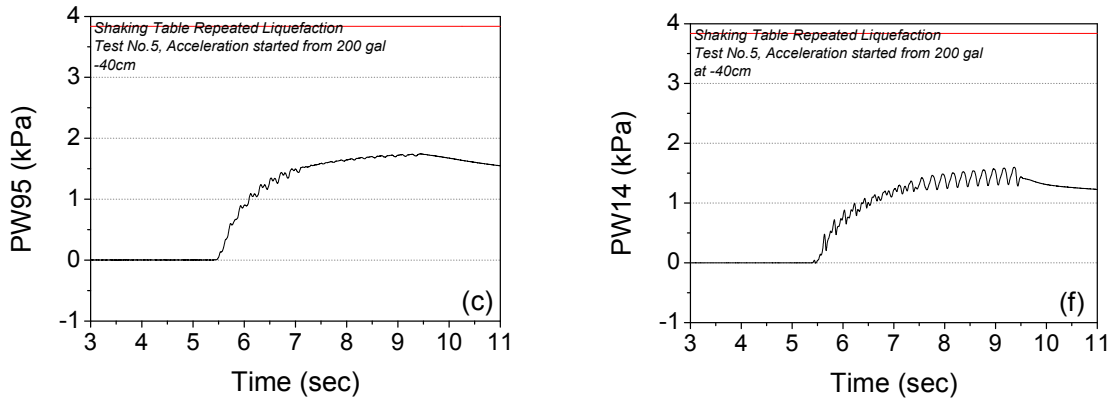

Figure 4-18. Excess pore water pressure response monitored during liquefaction test (a-c) at centerline (d-f) at 10cm from the edge of soil container and (a, d) at depth -20cm (b, e) at depth -30cm and (c, f) at -40cm

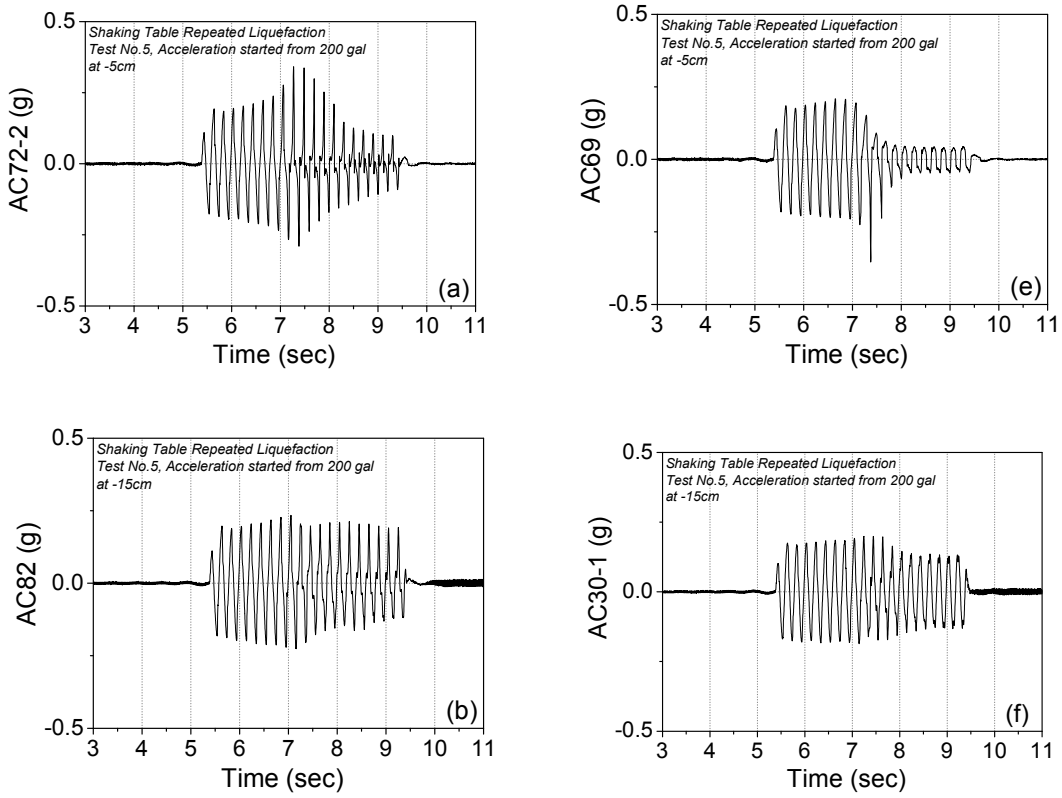

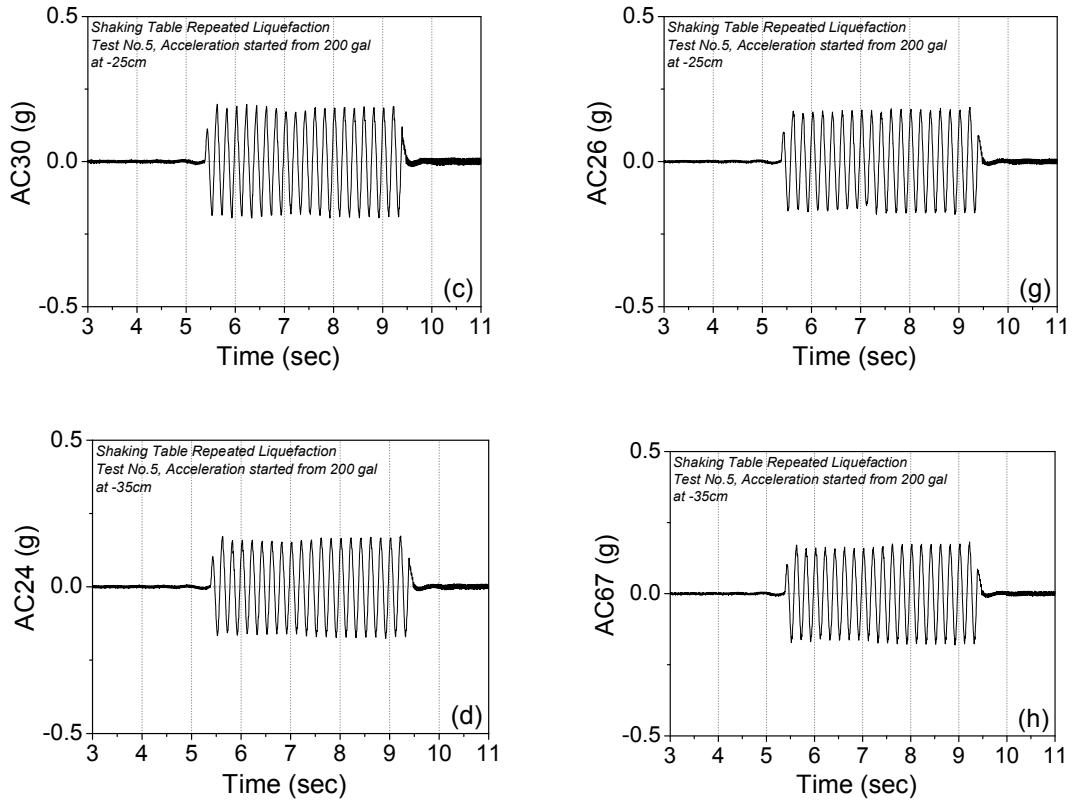

Figure 4-19. Acceleration response monitored during liquefaction test (a-d) at centerline (e-h) at 10cm from the edge of soil container and (a, e) at depth -5cm (b, f) at depth -15cm, (c, g) at depth -25cm and (d, h) at -35cm

4.3.3 Repeated liquefaction behavior

4.3.3.1 Repeated liquefaction behavior in the tests with increase in input acceleration

As mentioned, the tests were started with low various acceleration levels at 200, 300 and 400 gal. When any layer showed shear strain amplitude of more than 1.5%, the same input acceleration level was repeated for the next shaking stage. If observed shear strain amplitude was less than 1.5%, the acceleration was raised by 100 gal. This testing condition was repeated until the final acceleration at 1000 gal. The shake acceleration histories of each shake are summarized in *Table 4-1*. Due to difference in acceleration history, the number of shaking stage was vary between each test. It seems that higher input acceleration resulted in lower number of shaking stage.

Table 4-1 Input acceleration history of shaking table tests (T4, T5 and T7)

	T5		T7		T4	
Shake No.	Acceleration Level (gal)	Shear Strain > 1.5%	Acceleration Level (gal)	Shear Strain > 1.5%	Acceleration Level (gal)	Shear Strain > 1.5%
1	200	Yes	300	Yes	400	Yes
2	200	Yes	300	Yes	400	Yes
3	200	No	300	Yes	400	Yes
4	300	Yes	300	Yes	400	Yes
5	300	Yes	300	Yes	400	Yes
6	300	Yes	300	Yes	400	Yes
7	300	Yes	300	Yes	400	Yes
8	300	No	300	No	400	Yes
9	400	No	400	No	400	No
10	500	Yes	500	No	500	No
11	500	Yes	600	Yes	600	Yes
12	500	Yes	600	Yes	600	Yes
13	500	Yes	600	Yes	600	Yes
14	500	Yes	600	Yes	600	Yes
15	500	Yes	600	Yes	600	Yes
16	500	Yes	600	Yes	600	Yes
17	500	Yes	600	Yes	600	Yes
18	500	Yes	600	Yes	600	Yes
19	500	Yes	600	Yes	600	Yes
20	500	No	600	Yes	600	Yes
21	600	No	600	No	600	No
22	700	No	600	No	700	No
23	800	Yes	600	No	800	No
24	800	Yes	700	No	900	No
25	800	Yes	800	No	1000	No
26	800	Yes	900	No	-	-
27	800	Yes	1000	No	-	-
28	800	Yes	-	-	-	-
29	800	Yes	-	-	-	-
30	800	Yes	-	-	-	-
31	800	Yes	-	-	-	-
32	800	Yes	-	-	-	-
33	800	Yes	-	-	-	-
34	800	Yes	-	-	-	-

35	900	Yes	-	-	-	-
36	1000	Yes	-	-	-	-

In each shake, relationship between shear stress and shear strain was computed as described in Chapter 4.3.1 and only for the data acquired at the middle of soil container due to boundary effect. By using obtained relationships, liquefaction resistance can be computed in the same manner as in triaxial case. In shaking table, liquefaction was defined as 1.5% double amplitude shear strain which equals to 1.0% double amplitude axial strain in triaxial testing assuming that the coefficient of earth pressure at rest is 0.5. The number of cycle was computed for every shake and in every layer. The results are presented in *Figure 4-20, Figure 4-21* and *Figure 4-22* for the test started at 200, 300 and 400 gal respectively together with maximum shear strain amplitude of each shake. However, as can be observed in *Figure 4-12*, it should be noted that the maximum shear strain amplitude level and shear stress level in shaking table cannot be controlled. Nonetheless, in the case where liquefaction did not occur; in other words, double amplitude shear strain did not exceed 1.5%, the results were omitted. Thus, another set of graph, *Figure 4-23, Figure 4-24* and *Figure 4-25*, summarizes maximum double amplitude shear strain in each shaking event. Besides, relative density history measured before each shaking by laser sensor on the top of ground model is given in *Figure 4-26*. Noted that relative density was calculated after each shaking allowing dissipation of excess pore water pressure and reconsolidation.

From these results, some observations can be made as follow;

1. The liquefaction resistance of the first shaking event was affected by acceleration level. The higher input acceleration caused ground model to liquefy much faster; i.e. lower number of cycle or lower liquefaction resistance. It can be seen that by applying input acceleration of 400 gal, the shear strain exceeded 1.5% during the first two cycles while the test which started with input acceleration of 200 gal, ground model started to liquefy at about 7-10th cycles. The test with 300gal input acceleration showed liquefaction resistance in between those two results. Similar observation was also reported by Varghese and Latha (2014). Initial result of three tests started at different input acceleration is plotted and presented in *Figure 4-27*. It was not only the first shaking but also the following stages. Repeated liquefaction resistance of the ground model

subjected to higher input acceleration level was lower than that of subjected to lower acceleration.

2. The liquefaction resistance of the first shaking event was relatively higher than the second shaking event. This reduction can be observed at any depth. Similar behavior was also reported by Ha et al. (2011). They suggested that aged soil fabric was destroyed over the first shaking event resulting in sand reconsolidation as a young, normally consolidated sand. Further investigation in this research also found that this reduction in liquefaction resistance between first and second shaking event depended on input acceleration level. At high input acceleration; for example, 400gal, the reduction of liquefaction resistance is relatively low compared to the test at 200 gal input acceleration.

   After liquefaction stopped at the initial input acceleration, input acceleration was raised by 100gal until the ground model liquefy again. The similar behavior was again observed at high acceleration. The first liquefaction resistance during higher input acceleration was relatively much higher compared to the second liquefaction resistance (see *Figure 4-20, Figure 4-21* and *Figure 4-22*). For example, in T5 where acceleration started at 200 gal, ground model started to liquefy again at 300 gal in the 4^{th} shake event at approximately 6-12^{th} cycle. In the 5^{th} shake event, liquefaction resistance dropped sharply. Also, in T7 where input acceleration was 300 gal, the test started to liquefy again at 600 gal input acceleration at 11^{th} shake event. Liquefaction resistance at 12^{th} shake event dropped significantly compared to the 11^{th} cycle. This behavior continued until 1000 gal input acceleration.

   High liquefaction resistance in the first shake event at higher acceleration; second repeated liquefaction series, might due to the effect of pre-shearing as describe in Chapter 3 in the case of Triaxial testing. Because in the previous shake; for example, 3^{rd} shake of T5 and 10^{th} shake, there was no liquefaction observed in every layer. This promoted very small shear strain amplitude to the ground model.

3. It is quite obvious that the top layer; i.e. Layer 1 (-10.0 cm from surface), was the most prone to repeated liquefaction. In very high stages, only the first layer was considered

liquefied. For instance, for input acceleration of 300 and 400 gal, after the 5th and 6th stage, only the top layer showed shear strain higher than 1.5%.

4. *Figure 4-27* also demonstrates that high input acceleration caused ground model to repeatedly liquefy for larger number of stage. At input acceleration of 200 gal, liquefaction was observed in only 2 stages while the input acceleration of 300 gal and 400 gal promoted repeated liquefaction up to 7 and 8 stages, respectively.

5. In order to investigate relative density, Figure 4-28 illustrates initial relative density and density change during the first repeated liquefaction at input acceleration. Initial relative density prior to the test was targeted around 50-55%. Due to dissipation of excess pore water pressure generated during each shaking, settlement occurred resulting in an increase in relative density. It can be seen from the *Figure 4-28* that higher input acceleration caused much larger increase in relative density.

6. To evaluate the effect of relative density, further plot between liquefaction resistance and relative density was drawn as shown in *Figure 4-29*. As discussed, in the first stage, relative density of each test were similar. However, in the second stage, the ground model which was subjected to 400 gal showed higher relative density but lower liquefaction resistance. This behavior might due to both input acceleration and strain amplitude as described in triaxial analysis or different in input acceleration. Anyhow, it can be said that relative density alone cannot be the indicator of liquefaction resistance.

7. Another observation can be made using *Figure 4-20*, *Figure 4-21* and *Figure 4-22*. Under the same input acceleration level, future liquefaction resistance can be roughly predicted by using current and previous maximum double amplitude shear strain. In most of the cases, when current maximum double amplitude shear strain is higher than the previous one, future liquefaction resistance can be expected to be lower. On the other hand, if current maximum double amplitude shear strain is lower than the previous one, future liquefaction can be predicted to be larger.

   For better understanding, the example of T5 Layer 3 is used to describe (*Figure 4-20*). At the 11th shake, the maximum shear strain was 10.9% which was larger than the previous maximum shear strain of 8.6% in 10th shake event. In the 12th shake,

liquefaction resistance can be expected to be lower as maximum shear strain amplitude of 11th shake was larger than 10th shake. On the other hand, the maximum shear strain in 13th shake event (5.5%) was lower than that in 12th shake event (7.8%); therefore, liquefaction resistance in the next shake event (14th) can be predicted to be higher. However, this observation is based on the same input acceleration.

8. Liquefaction resistance calculated using pore water pressure ratio was also carried out for test T5 which started at 200 gal input acceleration. The number of cycle to promote unity pore water pressure ratio was computed and compare with the one calculated at 1.5% double amplitude shear strain. Time history example of pore water pressure generation was already shown in *Figure 4-15*. When the shear strain amplitude reached 1.5%, the pore water pressure ratio have not reached unity yet. The comparison is presented in *Figure 4-30*. It can be seen that the number of cycle calculated at unity excess pore water pressure ratio were higher than that calculated based on 1.5% strain amplitude.

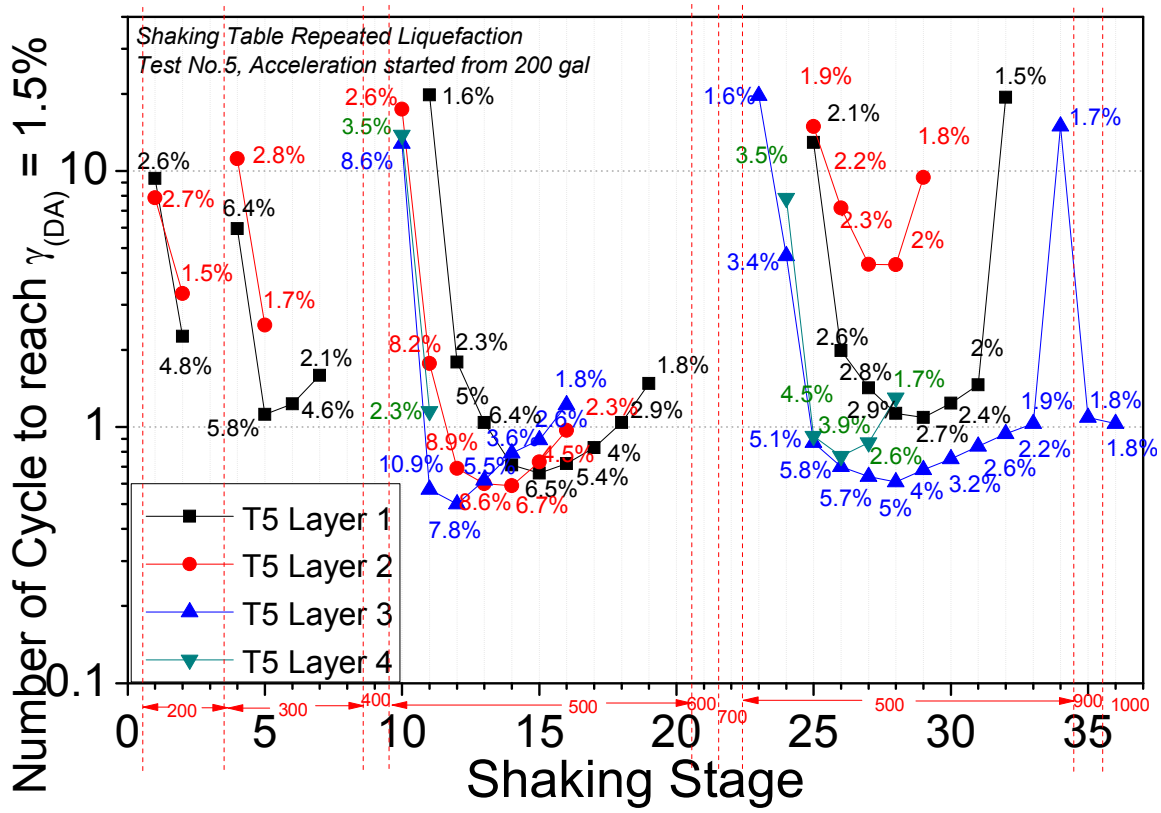

Figure 4-20. Relationship of number of cycle to cause 1.5 double amplitude shear strain and shaking stage of T5 (started at 200 gal)

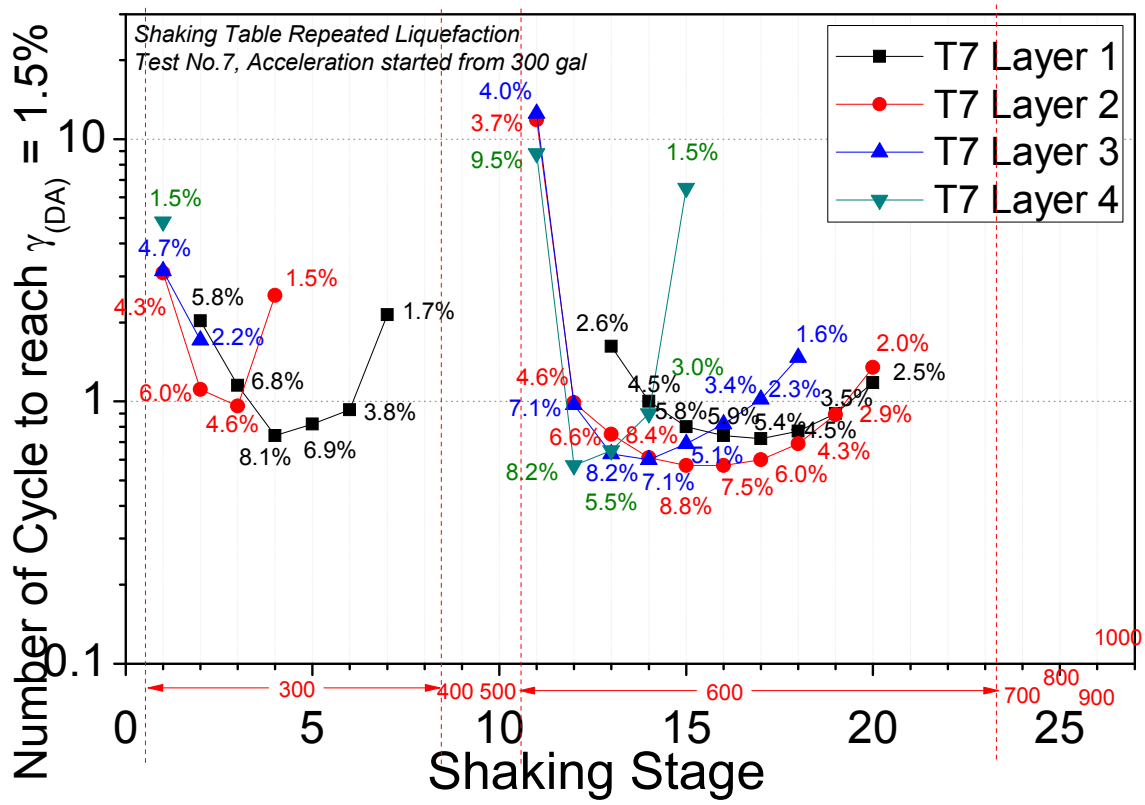

Figure 4-21. Relationship of number of cycle to cause 1.5 double amplitude shear strain and shaking stage of T7 (started at 300 gal)

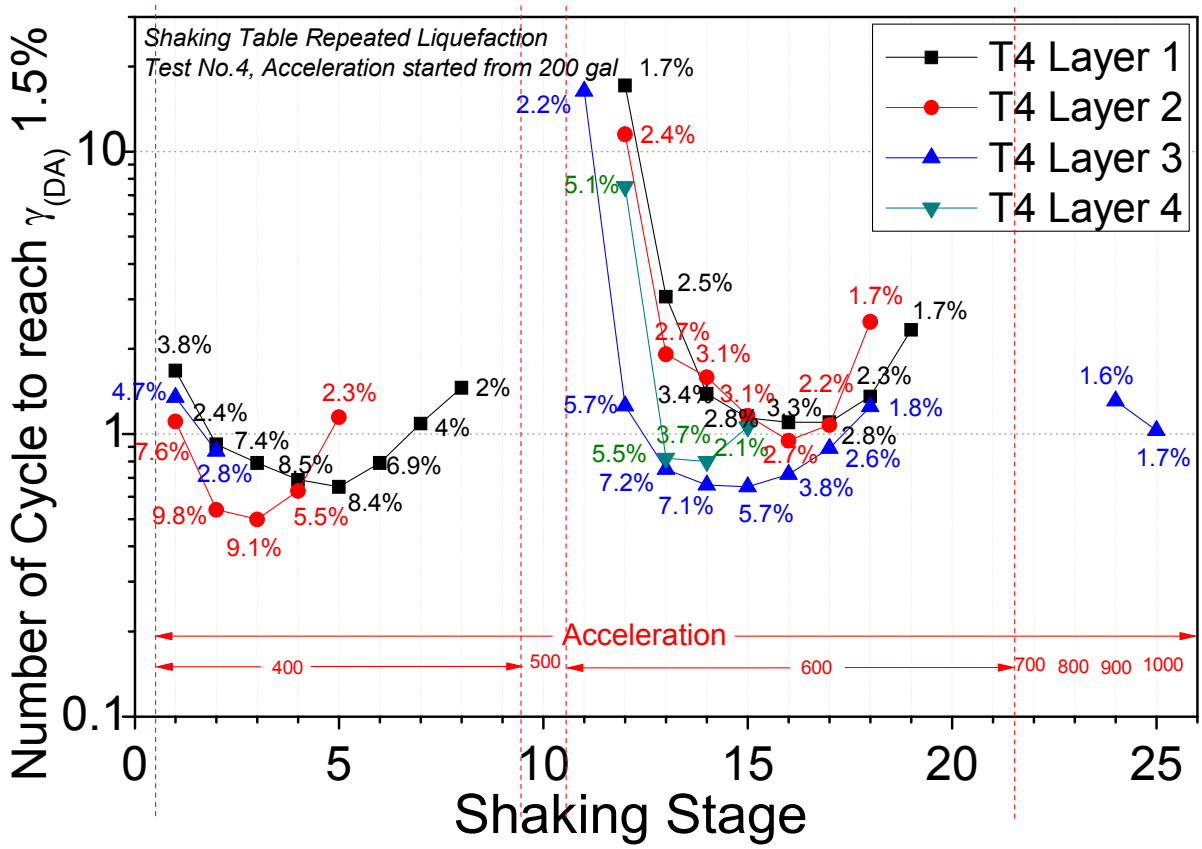

Figure 4-22. Relationship of number of cycle to cause 1.5 double amplitude shear strain and shaking stage of T4 (started at 400 gal)

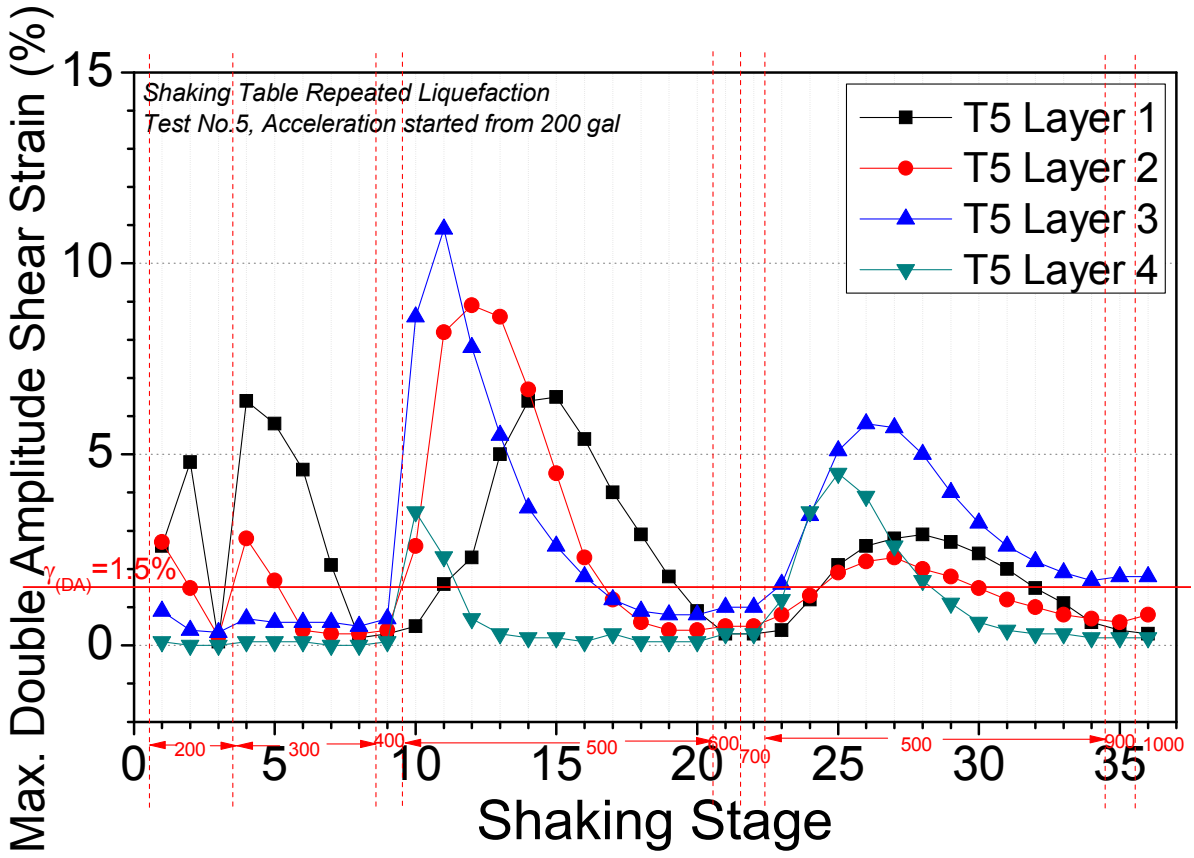

Figure 4-23. Maximum strain amplitude in each shaking stage of test T5 started from 200 gal

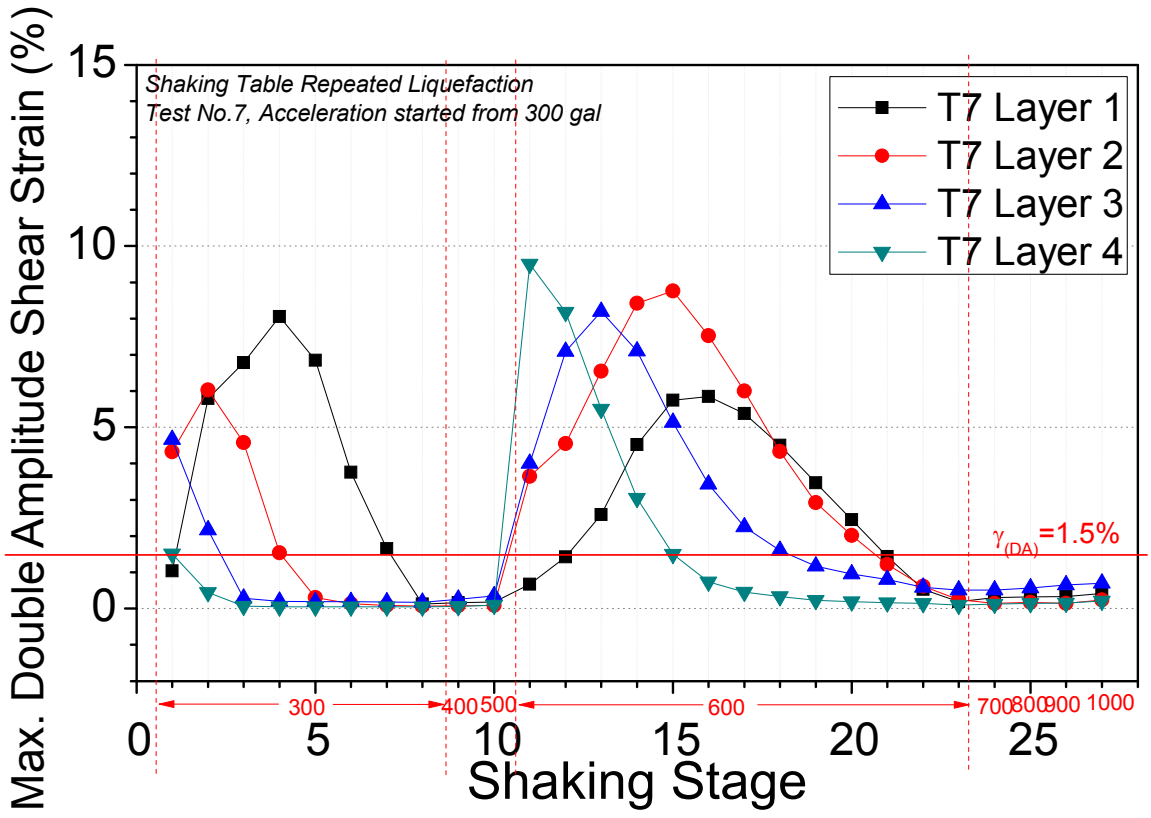

Figure 4-24. Maximum strain amplitude in each shaking stage of test T7 started from 300 gal

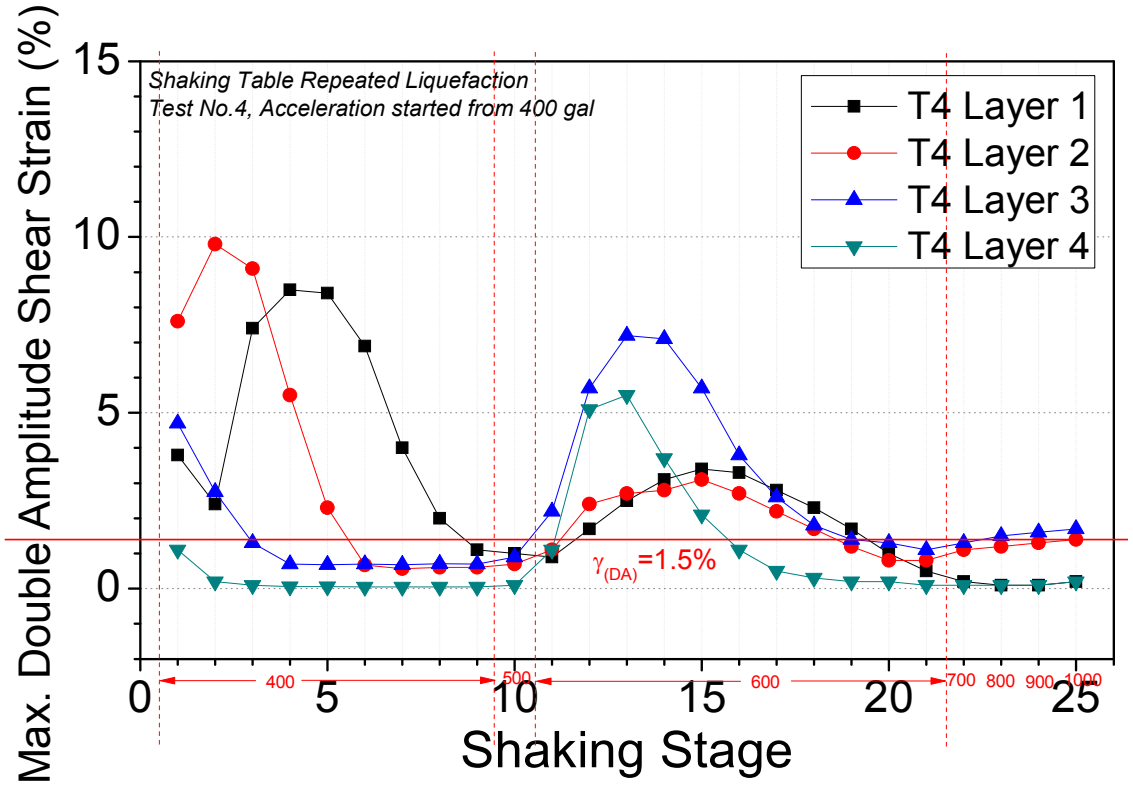

Figure 4-25. Maximum strain amplitude in each shaking stage of test T4 started from 400 gal

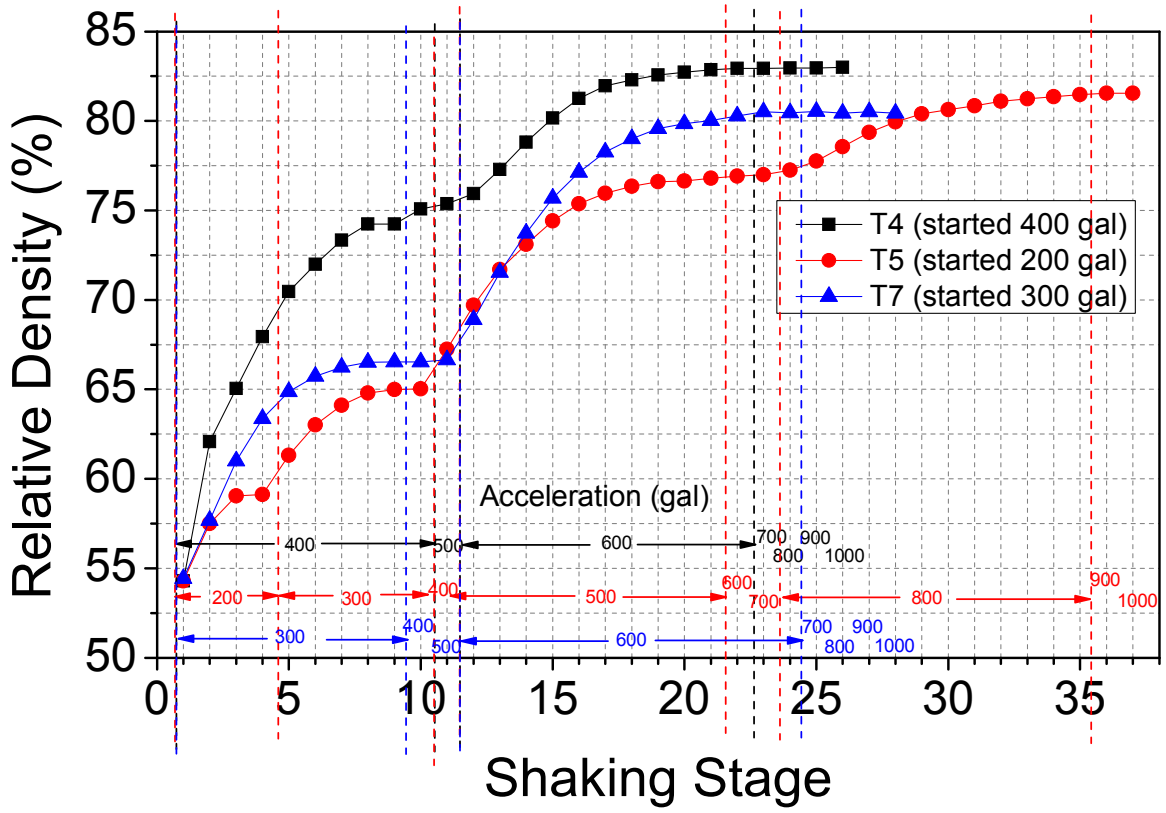

Figure 4-26. Relative density history of shaking table tests (T4, T5 and T7)

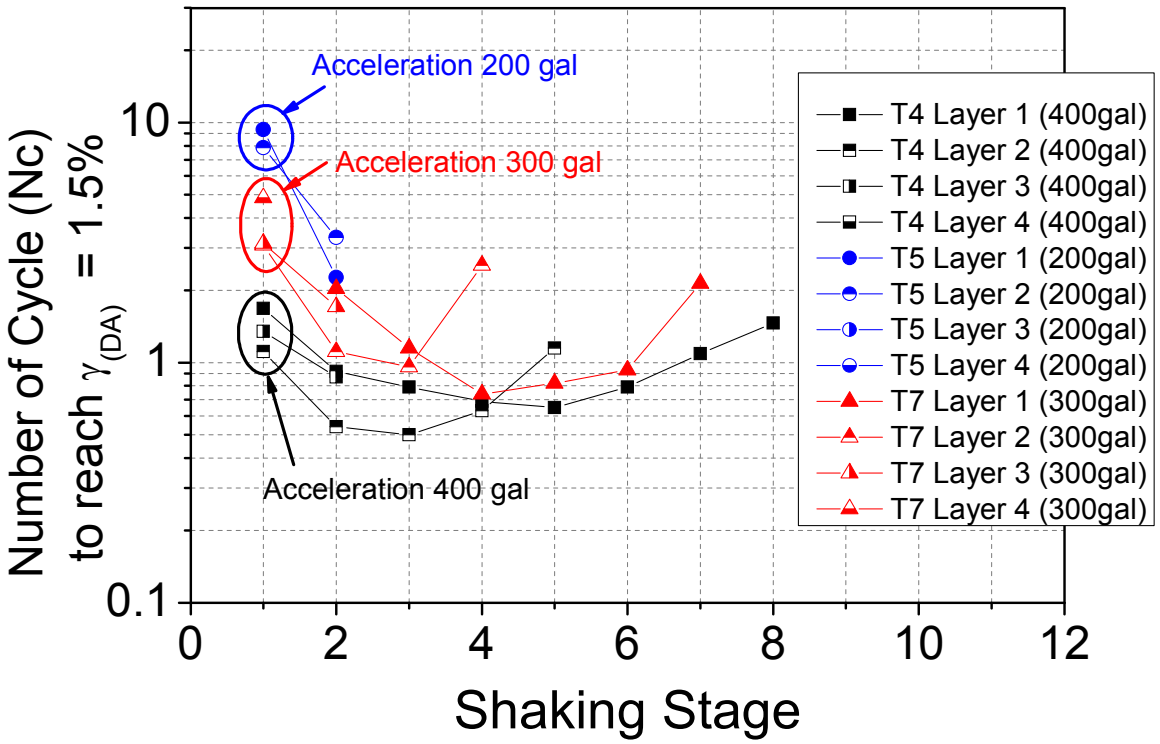

Figure 4-27. Comparison of cyclic resistance at early stages of tests started at 200 gal, 300 gal and 400 gal (T4, T5 and T7)

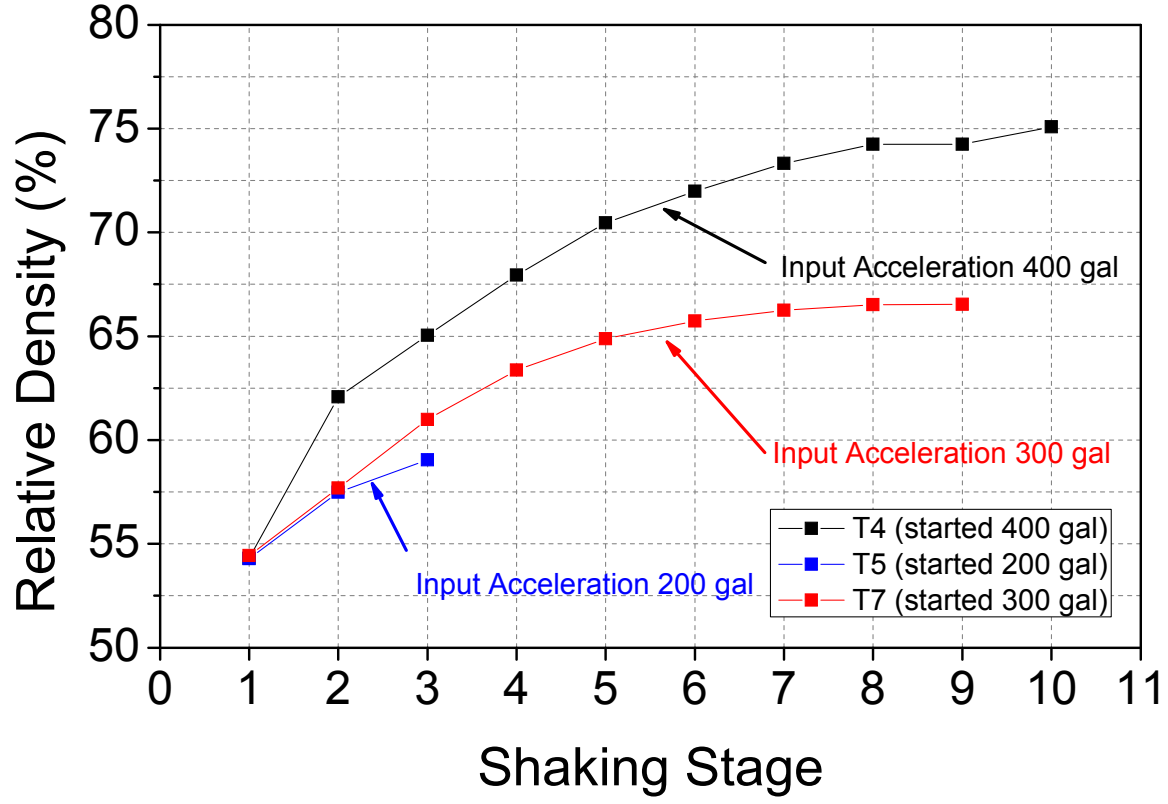

Figure 4-28 Relative density history at early stages of tests started at 200 gal, 300 gal and 400 gal (T4, T5 and T7)

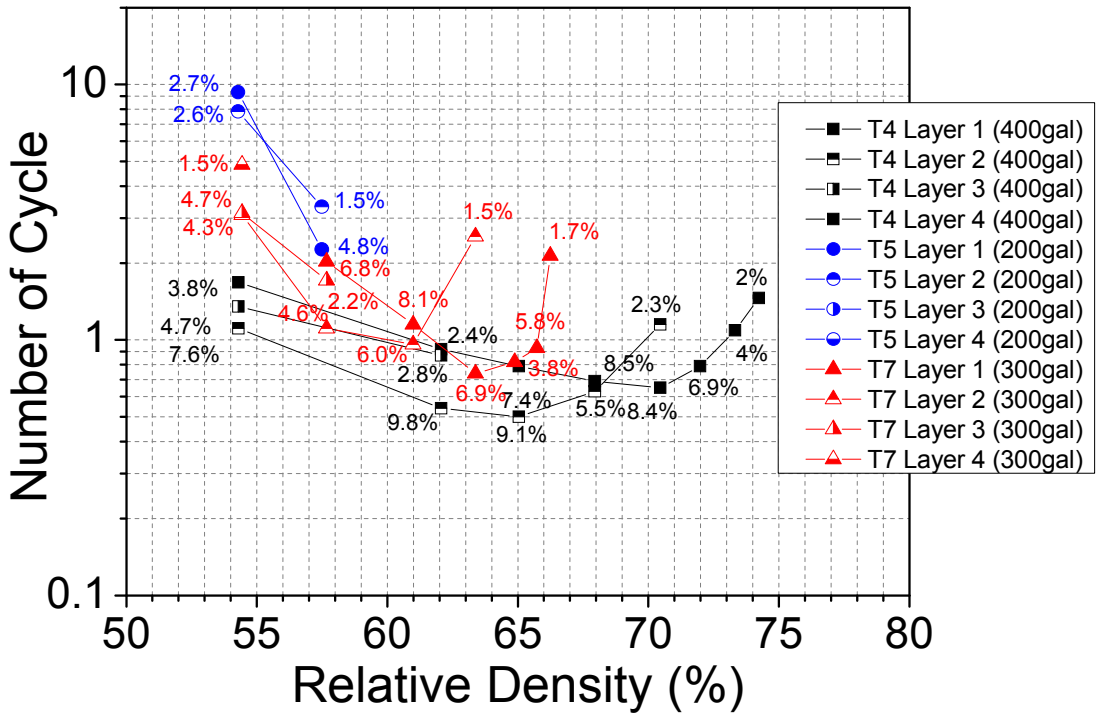

Figure 4-29. Relationship between liquefaction resistance and relative density (T4, T5 and T7)

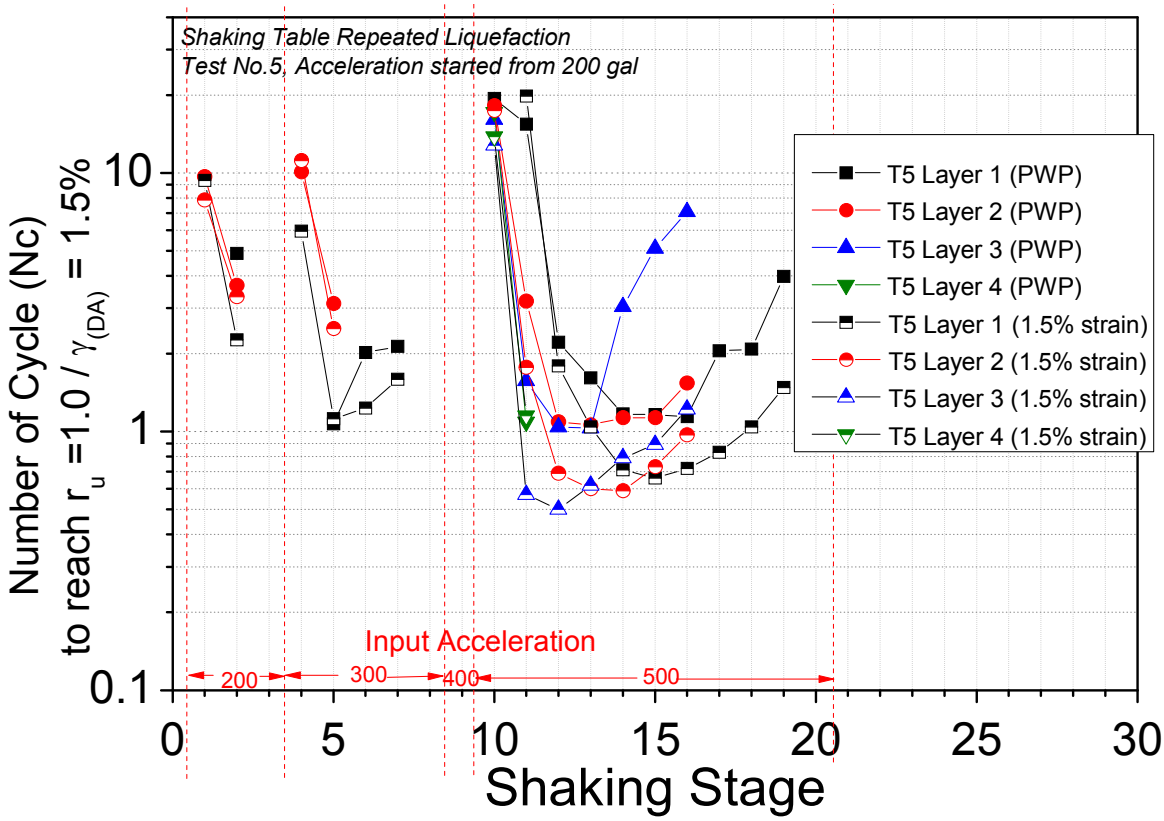

Figure 4-30. Comparison of liquefaction resistance in terms of number of cycle to reach unity excess pore water pressure ratio and to reach 1.5% double amplitude shear strain

4.3.3.2 Repeated liquefaction behavior in the tests with decrease in input acceleration

Since liquefaction was observed to be repeated for several stage under the same in put acceleration in the previous test series, the special test which included reduction in acceleration level where the liquefaction was found in previous stage was carried out (named T6, started at 200 gal input acceleration). The summary of acceleration history is given in *Table 4-2*. It is noted that due to time limit to avoid time effect during each shaking stage, shear strain was not computed during time interval. Thus, in some stages, liquefaction occurrence was misjudged; for example, shaking stage 14 and 16. In the 13th stage, shear strain did not exceed 1.5%. Acceleration should have increased to 700 gal instead of 500 gal in the 14th shake event. In the 15th stage where none of the layers showed shear strain over than 1.5%, acceleration should have increase to 500 gal instead of lowering to 200 gal in the 16th shake. Interesting point to be stated during the 13th stage where shear strain was limited; i.e. lower than 1.5%, liquefaction was observed at 14th stage where acceleration level was lower. In the late stages, from 21st stage at 800 gal, with a decreasing acceleration, the ground model continuously showed shear strain higher than 1.5% until 26th stage suggesting there was a large decrease in cyclic resistance.

Figure 4-31 presents liquefaction resistance with shaking stage together with maximum strain amplitude while *Figure 4-32* and *Figure 4-33* shows maximum strain amplitude and relative density change in each shaking stage. Several points discussed in previous series of test were also observed in this series though after the first liquefaction, acceleration was lowered.

1. In terms of number of cycle to trigger 1.5% double amplitude shear strain, it was observed that liquefaction resistance which occurred after the shake where no liquefaction was observed; i.e., 21st stage Layer 3 and Layer 4, was found to be relatively high. In the 22nd stage even though the input acceleration was lowered from 800 gal in the previous stage to 700 gal, cyclic resistance dropped significantly.

2. The method of future liquefaction resistance prediction using strain amplitude of current and previous stage can also be applied in this series (see *Figure 4-31*). For example, in Layer 3, at 22nd shaking stage, maximum shear strain was 6.3% which was higher than 4.0% in the 21st shaking stage. Liquefaction resistance in the 23rd stage was

expected to be lower. On the other hand, shear strain in 24th shake event (3.6%) was lower than that in 23rd event (5.9%); therefore, in the 25th shaking stage, liquefaction resistance can be predicted to be higher.

All the result of 4 tests were summarized in *Figure 4-34* in terms of differential of the current and previous shear strain with the differential of the next and current liquefaction resistance. If the result corresponding with the described prediction method on the increasing trend, the data should lie on the positive differential liquefaction resistance and negative differential shear strain marked as green shadow. On the other hand, for the decreasing trend, the data should lie on the negative differential liquefaction resistance and positive differential shear strain marked as red shadow. There were in total 164 data in this analysis. Of those, there were 9 data which were not corresponding with the method giving approximately 94.5% good prediction.

The author tried to apply the assumption for the real earthquakes occurred during 2010-2011 in Christchurch, New Zealand. There were three large earthquake occurred in September 2010, February 2011 and June 2011. Acceleration data at two sites (Ashburton and Walkari) (www.geonet.org.nz) was used to calculate double amplitude maximum displacement and number of cycle to cause double amplitude displacement of 5 mm as shown in *Figure 4-35*. It is noted that the acceleration was measured at single depth making shear strain calculation impossible. In this case study, it was, therefore, expressed in terms of displacement instead of shear strain. For these three earthquakes, it was monitored that the acceleration was lower in the second and third earthquakes whose condition is the same as in this test series where the input acceleration is decrease when the double amplitude shear strain is over than 1.5%. It can be seen from the figure that the brief method of liquefaction resistance prediction can be applied to real situation as well. All of the cases, maximum displacement observed during the earthquake event of Feb 2011 was higher than that during Sep 2010. Thus, liquefaction resistance in all cases increased in the third stage.

3. It can be still said that change in relative density was only significant when the ground model liquefy.

However, several differences between the test with and without acceleration lowering were observed.

1. However, due to lowered input acceleration, repeated liquefaction was observed to be less continuous. This might because lower input acceleration tends to promote lower strain amplitude. It was found in the triaxial test in this thesis and also in the literature that when the soil subjected to low strain amplitude, the future liquefaction resistance tends to increase. Thus, due to lower acceleration which would correspond with lower strain amplitude, cyclic resistance in this test series developed much faster during repeated liquefaction.

2. Relative density change was compared with the previous test series and illustrated in *Figure 4-36*. Due to limited space in the figure, input acceleration is not given and it should be noted that all of the shaking table tests (T4, T5, T6 and T7) which started at different input acceleration and testing program, all the tests were terminated when reaching 1000 gal. From the figure, although strain amplitude applied differently during repeated liquefaction test, the final relative densities among the tests were ranging from approximately 78-83%. It can be implied that strain amplitude affects repeated liquefaction behavior but after certain density, in the case of the silica sand, it was found that there is no more liquefaction even at high acceleration and different strain history.

Table 4-2 Summary of input acceleration of repeated liquefaction test (T6)

Shaking Stage	Acceleration (gal)	Shear Strain > 1.5%
1	200	No
2	400	Yes
3	400	Yes
4	400	Yes
5	200	Yes
6	200	Yes
7	200	No
8	400	Yes
9	200	No
10	200	No

Shaking Stage	Acceleration (gal)	Shear Strain > 1.5%
18	500	No
19	600	No
20	700	No
21	800	Yes
22	700	Yes
23	600	Yes
24	500	Yes
25	400	Yes
26	200	Yes
27	200	No

11	400	No
12	500	No
13	600	No
14	500	Yes
15	400	No
16	200	No
17	400	No

28	400	No
29	500	No
30	600	No
31	700	No
32	800	No
33	900	No
34	1000	No

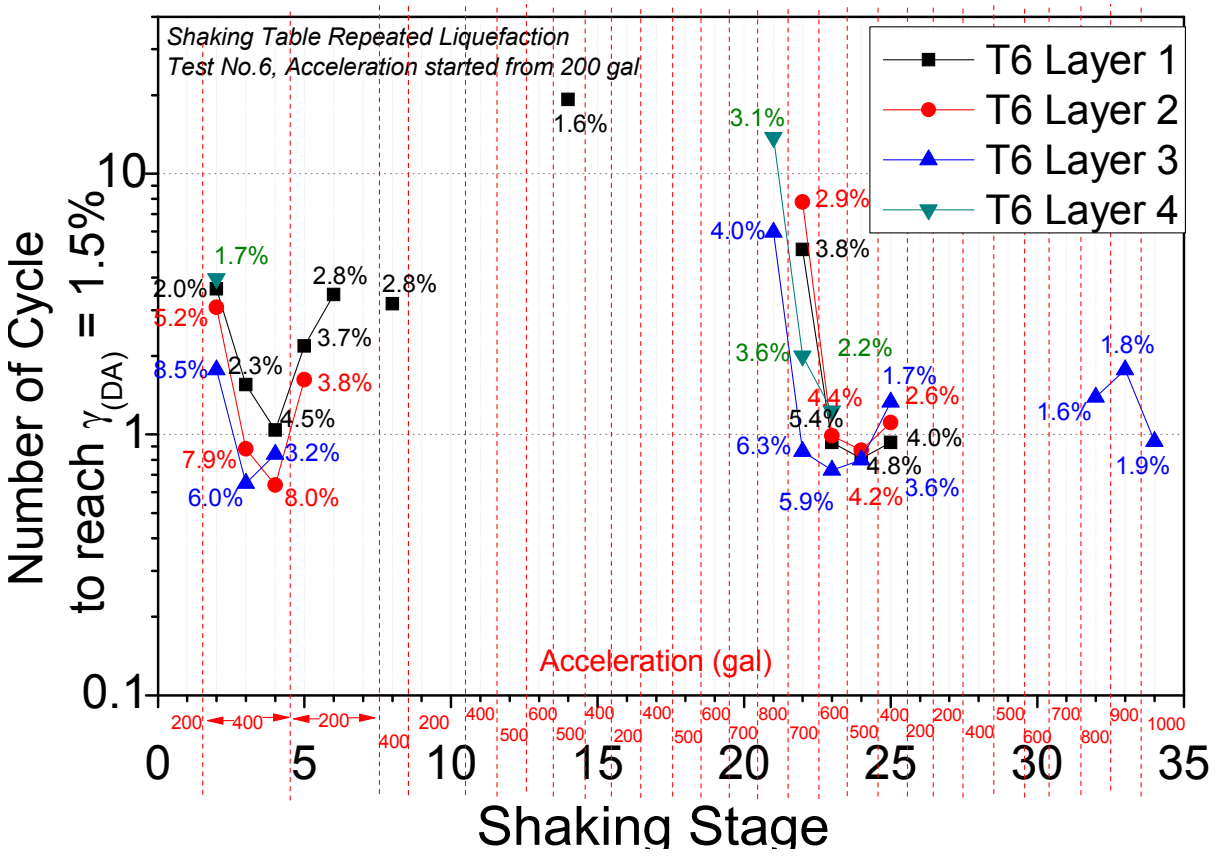

Figure 4-31. Repeated liquefaction resistance of shaking table test (T6)

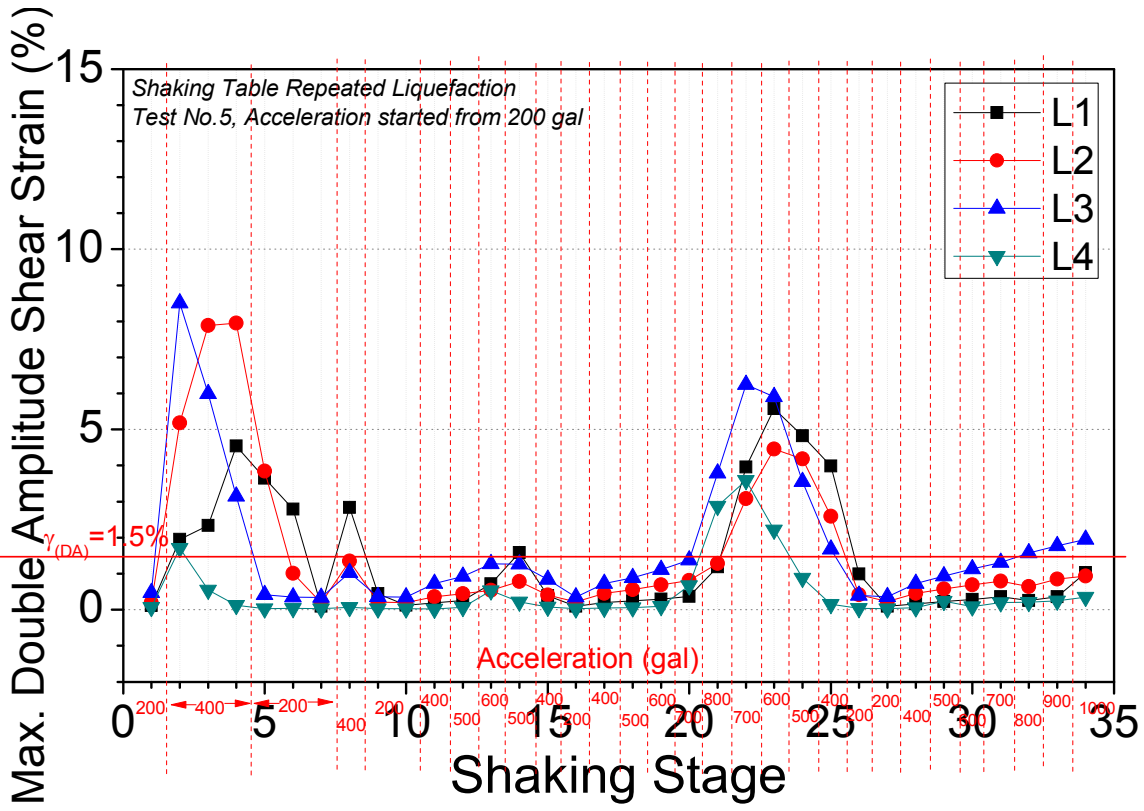

Figure 4-32. Maximum shear strain amplitude of shaking table test (T6)

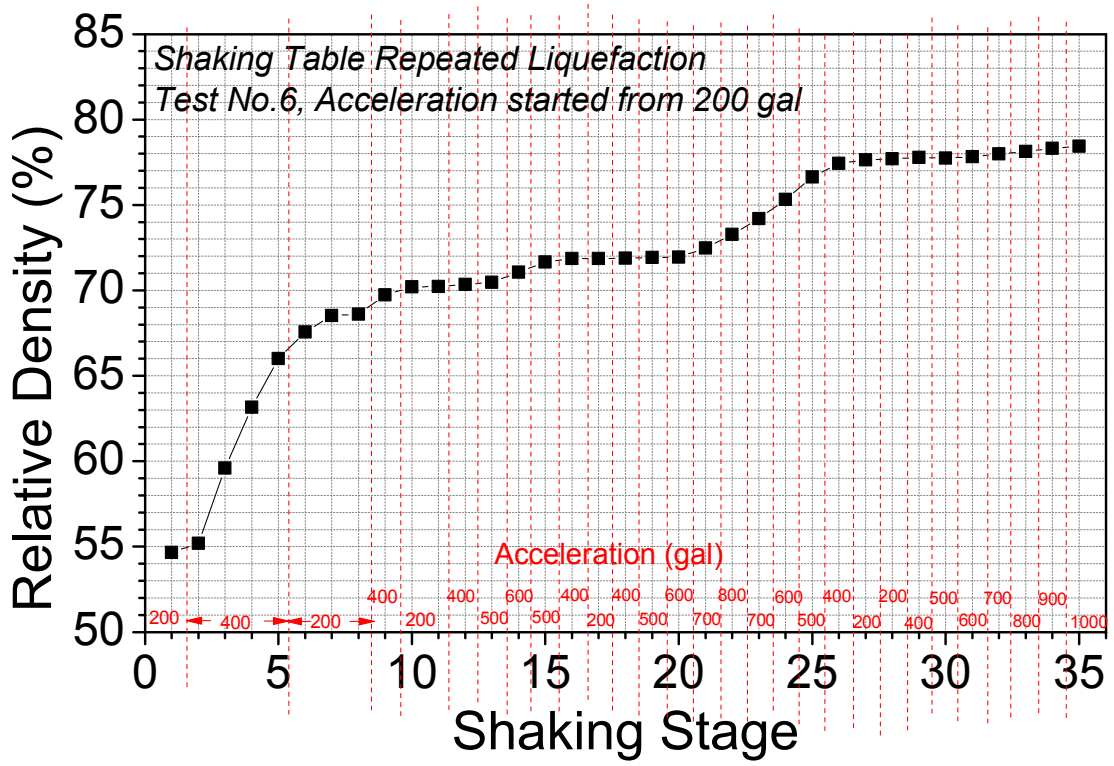

Figure 4-33. Relative Density change of shaking table test (T6)

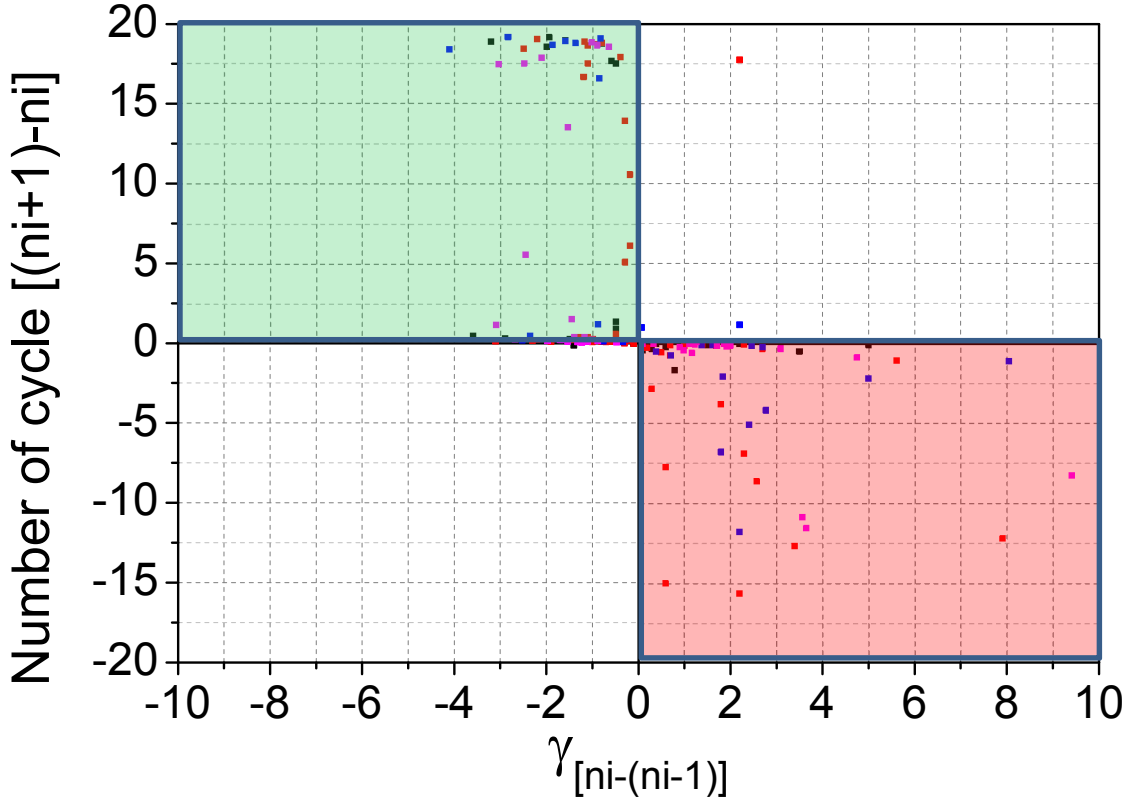

Figure 4-34. Relationship between differential of the current and previous shear strain and differential of the next and current liquefaction resistance in terms of number of cycle

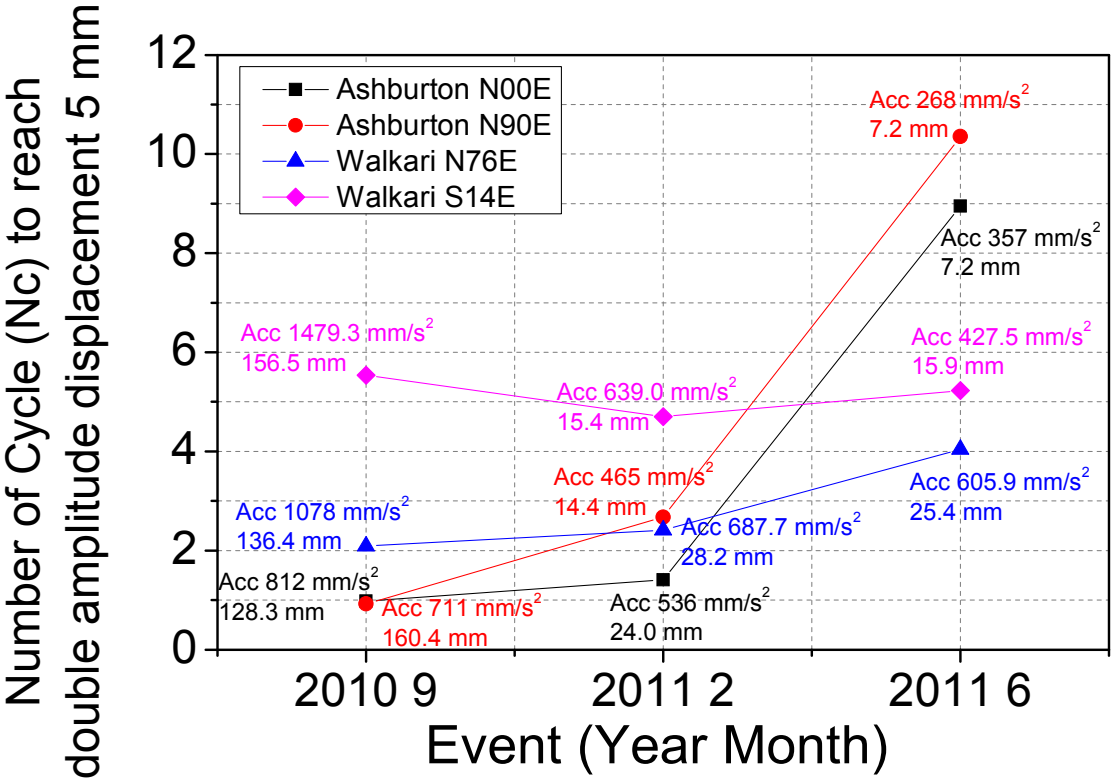

Figure 4-35. Liquefaction resistance computed from the 2010-2011 Christchurch Earthquakes, Newzealand (computed from the data provided at www.geonet.org.nz)

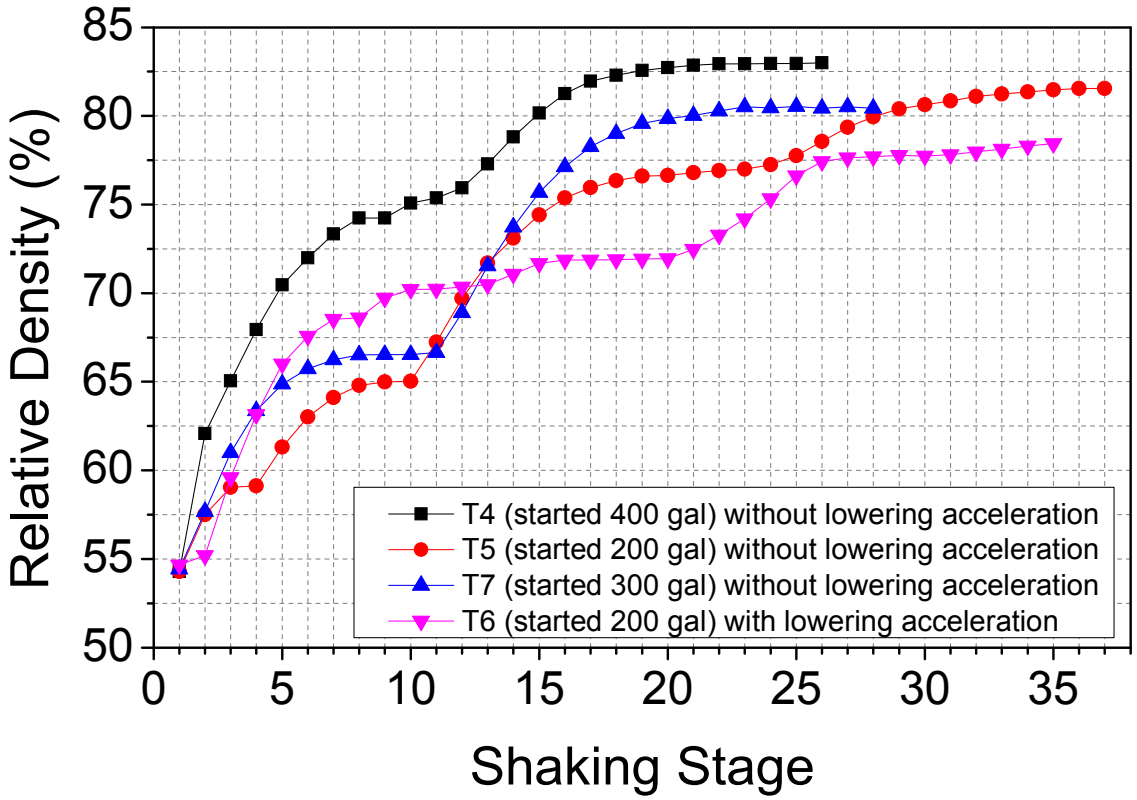

Figure 4-36. Relative Density change of shaking table tests (T4, T5, T6 and T7)

4.4 Cumulative Damage Concept

As can be seen in the *Figure 4-7* that the ground acceleration response during soil liquefaction was in irregular manner. While using ground acceleration response in shear stress calculation, the computed shear stress was also in irregular response which give difficulty in stress ratio estimation. As discussed in the introduction, there are methods to convert irregular response into equivalent uniform response proposed by many researchers. In this thesis, the method of cumulative damage concept was selected.

Cumulative damage concept was firstly introduced for evaluate fatigue damage for metal structure not only civil engineering structure but also the others such as aircraft due to stress changes or stress cycles. In geotechnical engineering, several researcher have applied this method to evaluate irregular loading stress to equivalent uniform loading stress or liquefaction potential (Donovan, 1972), (Annakai and Lee, 1976), (Annaki and Lee, 1977) and (Tatsuoka et al., 1986).

In this concept, cyclic shear stress time histories were decomposed into half pulses. In each half pulses, maximum cyclic shear stress was calculated which usually located in the middle between two adjacent zero value of shear stress. The absolute value of maximum cyclic shear stress in each half pulses was then marked as SRi where i is the order number where in this test series (20 cycle) SR is ranging from SR_1 to SR_{40}. Damage given to the ground model from each half pulse can be calculated by

$$Damage\ due\ to\ each\ half\ pulse = \frac{1}{2N_i}$$

where Ni is cyclic resistance in terms of number of cycle to cause 1% double amplitude axial strain for given liquefaction strength curve. The concept is lustrated in *Figure 4-37*. In this thesis, in order to compute Ni, strength curve of triaxial test given in *Figure 4-38* were used. Damage due to each half cycle was calculated based on corresponding Ni with given value of SRi in shaking table test. Then the total accumulated damage for given time history of cyclic shear stress is calculated by

$$DM = \sum_{i=1}^{n} DM_i$$

where DM is damage and n is the number of half cyclic in cyclic shear stress time history. The soil failure, or liquefaction in this case, occurs when the value of DM equals to or is more than 1.0. To evaluate the equivalent cyclic stress ratio, accumulated damage up to the number of cycle which triggered liquefaction shaking table (double amplitude shear strain = 1.5%) was computed. It is noted that, this value might not be equal to 1.0. However, it was interpolated back for equivalent number of cycle which give damage to unity. By using the given triaxial strength curve, equivalent stress ratio can be evaluated from equivalent number of cycle.

Figure 4-39 - *Figure 4-42* show the relationship of cyclic stress ratio and number of cycle required to reach 1.5% double amplitude shear strain for shaking table during repeated liquefaction with maximum strain amplitude from test T4 (started at 400 gal), T5 (started at 200 gal), T6 (started at 200 gal), T7 (started at 300 gal). It can be seen that during the initial liquefactions at starting acceleration input, the cyclic stress ratio was relative low. With an increase in acceleration level, the cyclic stress ratio increased up to the value of 3.0-4.5. This might also due to much higher relative density after subjected to several stages of low acceleration. Most of the case, the first 2-3 stages, cyclic stress ratio was observed to be increased with lower number of cycle. However, after reaching some certain value, the cyclic stress ratio started to decrease with higher number of cycle to reach 1.5% strain amplitude.

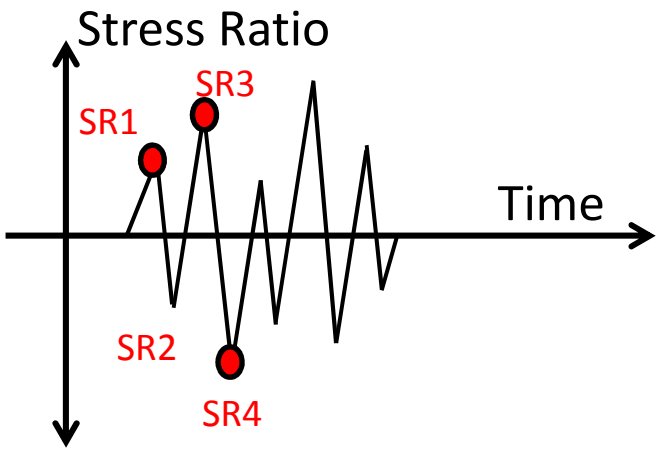

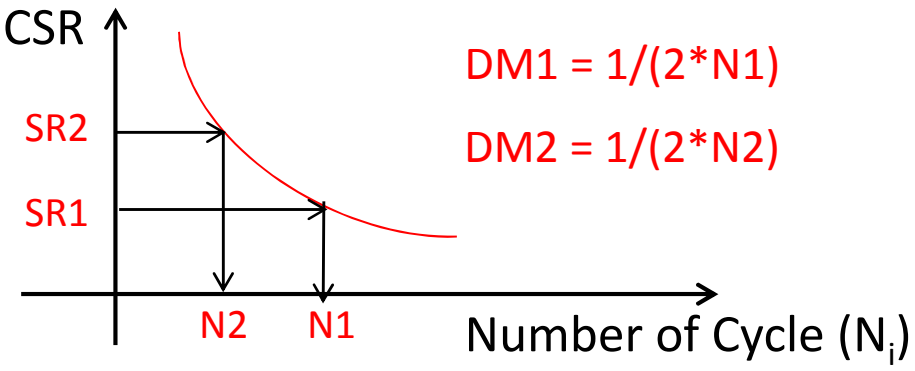

Figure 4-37. Cumulative damage concept process (a) stress ratio of each half pulse (b) damage calculation from given half pulse stress ratios and given triaxial strength curve

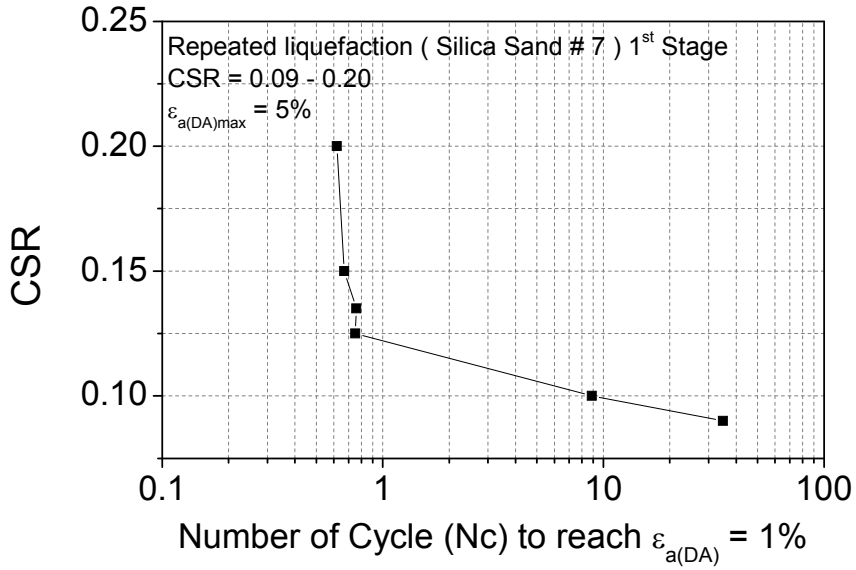

Figure 4-38. Liquefaction curve in the first stage in triaxial

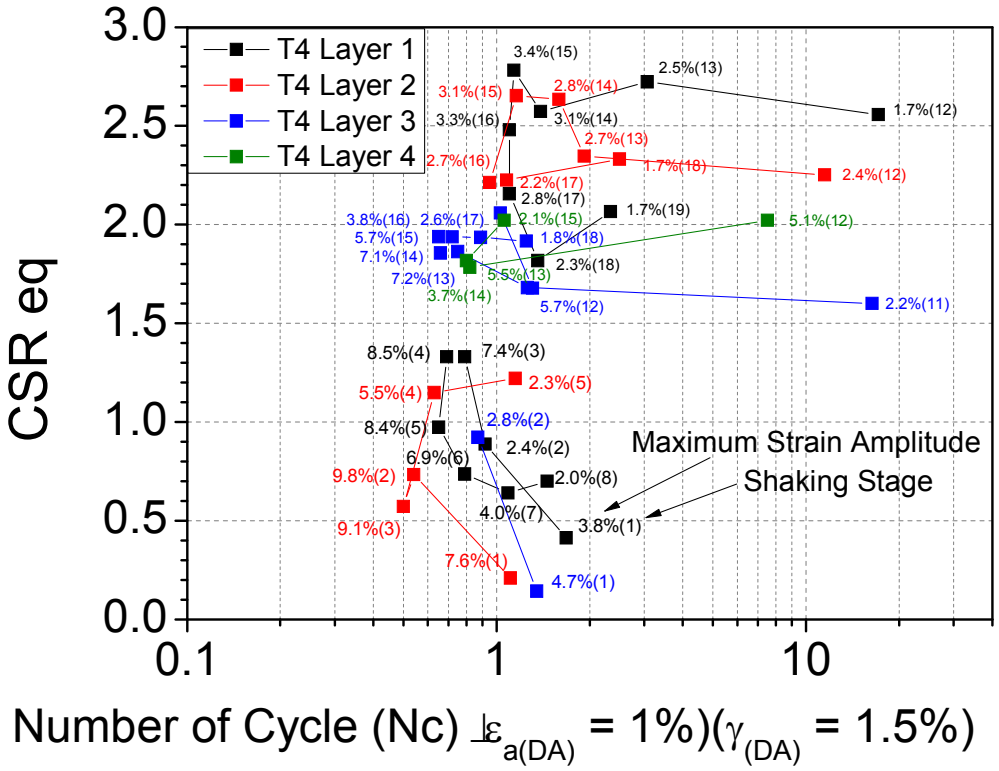

Figure 4-39. Liquefaction curve of shaking table using cumulative damage concept analysis (T4 started at 400 gal)

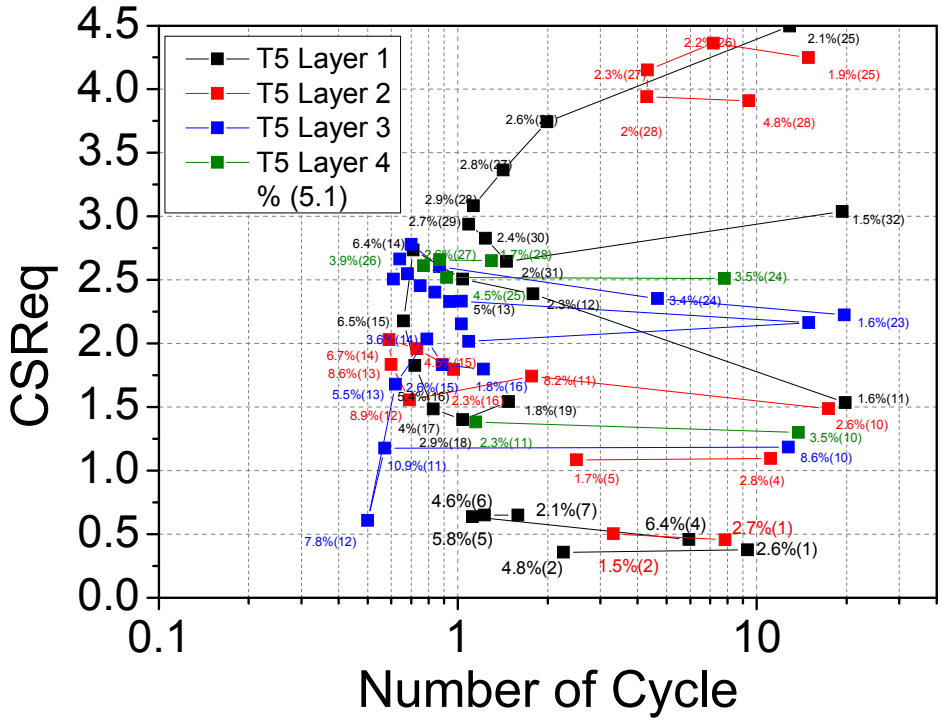

Figure 4-40. Liquefaction curve of shaking table using cumulative damage concept analysis (T5 started at 200 gal)

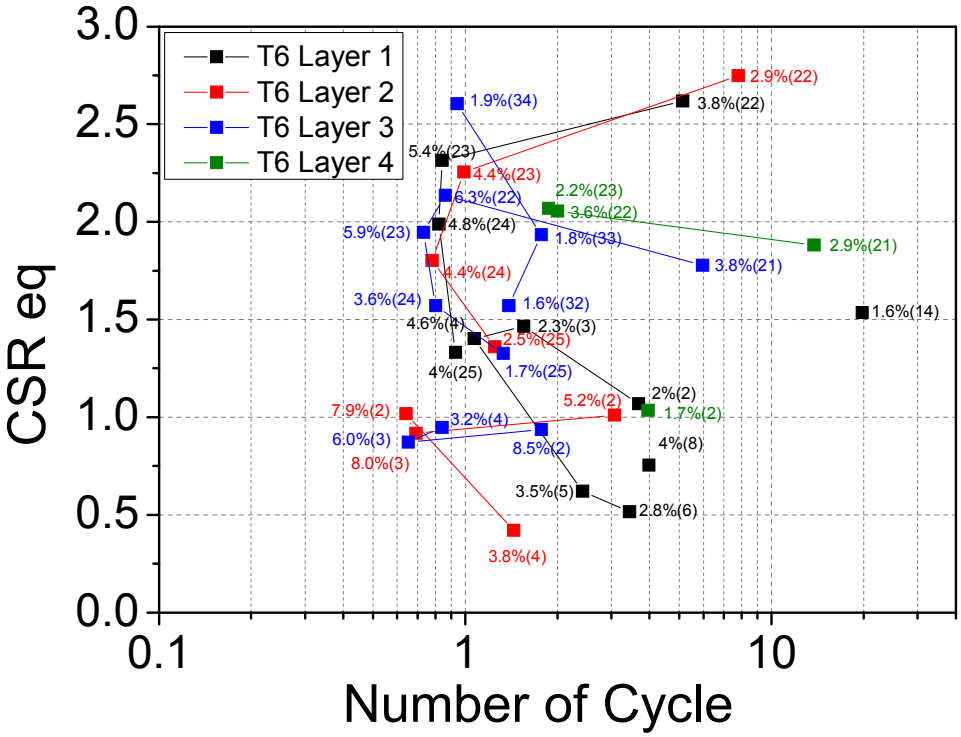

Figure 4-41. Liquefaction curve of shaking table using cumulative damage concept analysis (T6 started at 200 gal)

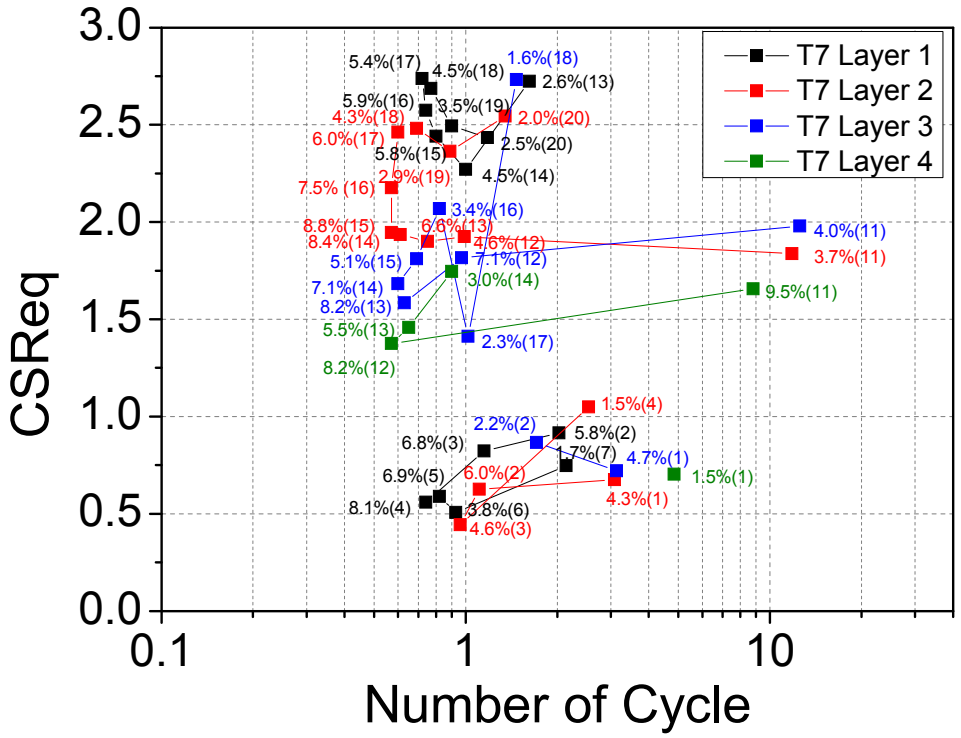

Figure 4-42. Liquefaction curve of shaking table using cumulative damage concept analysis (T7 started at 300 gal)

4.5 Summary

From the analysis of the Silica sand behavior under repeated liquefaction in shaking table test, several observation are drawn as follow;

1. Cyclic resistance in terms of number of cyclic to trigger certain double amplitude shear strain of the first liquefaction stage of any repeated liquefaction was found to relatively high compared to the second. However, the first liquefaction resistance depends on the input acceleration. The higher input acceleration was, the lower cyclic resistance was. In the second stage, cyclic resistance dropped. After several stages of repeated liquefaction, the resistance increased. Repeated liquefaction tends to stop after reaching certain density. In the case of Silica sand, it was observed that when the relative density was approximately 78-83, liquefaction stopped to occur with the largest acceleration of 1000 gal regardless of shaking history.
2. Future liquefaction resistance can be roughly predicted using strain amplitude history of the previous and current liquefaction stage. It was found that when the shear strain amplitude of the previous stage is larger than the current stage, cyclic resistance in the next stage can be expected to be lower. On the other hand, if the previous shear strain amplitude is lower than the current one, liquefaction resistance can be predicted to be higher in the next stage. This prediction is not only applied to the same input acceleration but also lower input acceleration. However, in this experiment, increase in input acceleration during repeated liquefaction was not carried out.
3. By using cumulative damage concept, cyclic stress ratio of the irregular response during liquefaction in model test can be determined. This method seems to be more accurate compared to the conventional method using average of the maximum acceleration since the number of cycle to liquefaction was taken into the account. Consequently, liquefaction curve of the model test can be computed and compare with element test which will be discussed later.

4.6 References

ANNAKAI, M. and LEE, K., 1976. Experimental verification of the equivalent uniform cycle concept for soil, *Symposium on Soil Liquefaction, ASCE National Convention, Philadelphia, Oct* 1976.

ANNAKI, M. and LEE, K., 1977. Equivalent uniform cycle concept for soil dynamics. *Journal of Geotechnical and Geoenvironmental Engineering,* **103**(ASCE 12991 Proceeding),.

DEMIRCI, NURHAN ECEMIS1 HASAN EMRE and KARAMAN, M., EFFECTS OF RELATIVE DENSITY AND COEFFICIENT OF CONSOLIDATION ON RE-LIQUEFACTION POTENTIAL OF SAND.

DONOVAN, N., 1972. *A stochastic approach to the seismic liquefaction problem,* .

ECEMIS, N., DEMIRCI, H.E. and KARAMAN, M., 2015. Influence of consolidation properties on the cyclic re-liquefaction potential of sands. *Bulletin of Earthquake Engineering,* **13**(6), pp. 1655-1673.

EL-SEKELLY, W., DOBRY, R., ABDOUN, T. and STEIDL, J., 2016. Centrifuge modeling of the effect of preshaking on the liquefaction resistance of silty sand deposits. *Journal of Geotechnical and Geoenvironmental Engineering,* **142**(6), pp. 04016012.

GEO NET (2017): http://www.geonet.org.nz

GREEN, R.A. and TERRI, G.A., 2005. Number of equivalent cycles concept for liquefaction evaluations—Revisited. *Journal of Geotechnical and Geoenvironmental Engineering,* **131**(4), pp. 477-488.

HA, I., OLSON, S.M., SEO, M. and KIM, M., 2011. Evaluation of reliquefaction resistance using shaking table tests. *Soil Dynamics and Earthquake Engineering,* **31**(4), pp. 682-691.

IDRISS, I. and BOULANGER, R.W., 2008. *Soil liquefaction during earthquakes.* Earthquake Engineering Research Institute.

KOGA, Y. and MATSUO, O., 1990. Shaking table tests of embankments resting on liquefiable sandy ground. *Soils and Foundations,* **30**(4), pp. 162-174.

LIU, A.H., STEWART, J.P., ABRAHAMSON, N.A. and MORIWAKI, Y., 2001. Equivalent number of uniform stress cycles for soil liquefaction analysis. *Journal of Geotechnical and Geoenvironmental Engineering,* **127**(12), pp. 1017-1026.

PATHAK., R. S., and PATKI, A., Strain Criterion for Initiation of Liquefaction Using Shake Table Test, International Journal of Engineering Research and Technology, Vol. 2 Issue 5, pp.1092-1099

SASAKI, Y., TOWHATA, I., TOKIDA, K., YAMADA, K., MATSUMOTO, H., TAMARI, Y. and SAYA, S., 1992. Mechanism of permanent displacement of ground caused by seismic liquefaction. *Soils and Foundations,* **32**(3), pp. 79-96.

SEED, H.B., MORI, K. and CHAN, C., 1977. Influence of seismic history on liquefaction of sands. *Journal of Geotechnical and Geoenvironmental Engineering,* **103**(Proc. Paper 11318 Proceeding),.

TATSUOKA, F., MAEDA, S., OCHI, K. and FUJII, S., 1986. Prediction of cyclic undrained strength of sand subjected to irregular loadings. *Soils and Foundations,* **26**(2), pp. 73-90.

UENG, T., WU, C., CHENG, H. and CHEN, C., 2010. Settlements of saturated clean sand deposits in shaking table tests. *Soil Dynamics and Earthquake Engineering,* **30**(1), pp. 50-60.

VARGHESE, R.M. and LATHA, G.M., 2014. Shaking Table Studies on the Conditions of Sand Liquefaction, *Geo-Congress 2014: Geo-characterization and Modeling for Sustainability* 2014, pp. 1244-1253.

YE, B., YOKAWA, H., KONDO, T., YASHIMA, A., ZHANG, F. and YAMADA, N., 2006. Investigation on stiffness recovery of liquefied sandy ground after liquefaction using shaking-table tests. *Soil and Rock Behavior and Modeling.* pp. 482-489.

ZEGHAL, M. and ELGAMAL, A., 1994. Analysis of site liquefaction using earthquake records. *Journal of Geotechnical Engineering,* **120**(6), pp. 996-1017.

5. Investigation of Repeated Liquefaction Behavior of Silica Sand using Energy Approach

Contents

Chapter 5 Investigation of Repeated Liquefaction Behavior of Silica Sand using Energy Approach

5.1 Introduction

As discussed earlier in Chapter 3 and 4, liquefaction resistance of silica sand was influenced by many parameters; for example, cyclic stress, relative density and strain history. One of the important keys was strain history (Finn et al. 1970), (Seed et al. 1977), (Ishihara and Okada 1978). In order to analyze further, the method of energy approach was employed. The triaxial and shaking table experiments used for this analysis were the same one that were presented in Chapter 3 and 4.

For the topic of liquefaction, it was firstly pointed out by Nemat-Nasser and Shokooh (1979) that there is a relationship between density change and dissipated energy due to soil particle rearrangement. In drained test, during contractive behavior; i.e. decreasing void ratio, the energy increases while the energy decreases during dilative behavior. The theory of this dissipated energy has also been applied to undrained test as well. After that there have been many studies of dissipated energy together with liquefaction behavior. Most of researches showed that there is a unique relationship between dissipated energy and excess pore water pressure generation for intact specimen regardless of cyclic stress (Towhata and Ishihara,1985). Following the pioneer works, Okada and Nemat-Nasser (1994), Kazama et al. (2000), Jafarian et al. (2012), Kokusho (2013), Azeiteiro et al. (2017) among others, also investigated this behavior. It was suggested that the dissipated energy depends on the type of sand, density and consolidation history. Further studies for liquefaction evaluation by Figueroa et al. (1994) and Kazama et al. (2003) showed that at the initial cycle applied to the specimen, the dissipated energy is relatively higher compared to at high number of cycle.

With suggestions by Ishihara and Okada (1978) and Ishihara and Okada (1982) that there is virtual boundary described as a phase transformation line on the effective stress path which distinguishes specimen behavior from contractive to dilative. When the stress path crossed the boundary, the next liquefaction resistance tends to drop. On the other hand, there is an increase in reliquefaction resistance when the stress path did not cross this boundary. Wahyudi and Koseki (2015) and Aoyagi et al. (2016) used this boundary to separate the dissipated energy

in to positive and negative impact. The positive impact is the total dissipated energy before the stress path touches the phase transformation line while the total dissipated energy after that would be accounted as negative impact. The relationship between positive and negative impact for repeated liquefaction in element test was then pointed out. This study also adopted this approach for both triaxial and shaking table model tests. The Silica sand repeated liquefaction behavior in these two tests was investigated. The detailed analysis, result and discussion are described in this chapter.

5.2 Theory

5.2.1 Dissipated Energy

In general, work is a product of force-displacement and it can be described as equation

$$W = \int F ds$$

where W is work, F is force and s is displacement. In the case of undrained cyclic triaxial test, the dissipated energy can be computed using the area of the hysteretic loop of deviatoric stress and axial strain relationship or shear stress and shear strain relationship for shaking table test as schematically shown in *Figure 5-1*. This area can be calculated by using mathematic integration as expressed in equations for triaxial test conducted under constant lateral stress (in total stress) and shaking table test accordingly.

$$\sum \Delta W = \int q \, d\, \varepsilon_a$$

$$\sum \Delta W = \int \tau \, d\gamma$$

where ΔW is the total dissipated energy per unit volume (J/m^3), q is deviator stress, ε_a is axial strain, τ is shear stress and γ is shear strain. The computation on stress-strain relationship is illustrated in *Figure 5-2* for triaxial test and *Figure 5-3* for shaking table test. The integration was made using sampling rate of the test which was 1 second for triaxial test and 0.002 second for shaking table test.

The energy computation can be described in detail as follows,

In triaxial test,

$$W = \int \sigma_v d\varepsilon_v + 2\sigma_h d\varepsilon_h - p' d\varepsilon_{vol} + p' d\varepsilon_{vol} \text{ (Noted that } \gamma = 0)$$

where W is dissipated energy, σ_v is vertical stress, σ_h is horizontal stress, p' is mean effective stress, q is deviatoric stress, ε_v is vertical strain, ε_h is horizontal strain and ε_{vol} is volumetric strain.

Since,

$$p' d\varepsilon_{vol} = \frac{\sigma_v + 2\sigma_h}{3} \times (d\varepsilon_v + 2d\varepsilon_h)$$

$$p' d\varepsilon_{vol} = \frac{1}{3}\sigma_v d\varepsilon_v + \frac{4}{3}\sigma_h d\varepsilon_h + \frac{2}{3}\sigma_v d\varepsilon_h + \frac{2}{3}\sigma_h d\varepsilon_v$$

Thus, the dissipated energy equation for triaxial can be describe further as,

$$W = \int \sigma_v d\varepsilon_v + 2\sigma_h d\varepsilon_h - p' d\varepsilon_{vol} + p' d\varepsilon_{vol}$$

$$W = \int \sigma_v d\varepsilon_v + 2\sigma_h d\varepsilon_h - \frac{1}{3}\sigma_v d\varepsilon_v - \frac{4}{3}\sigma_h d\varepsilon_h - \frac{2}{3}\sigma_v d\varepsilon_h - \frac{2}{3}\sigma_h d\varepsilon_v + p' d\varepsilon_{vol}$$

$$W = \int \frac{2}{3}\sigma_v d\varepsilon_v + \frac{2}{3}\sigma_h d\varepsilon_h - \frac{2}{3}\sigma_v d\varepsilon_h - \frac{2}{3}\sigma_h d\varepsilon_v + p' d\varepsilon_{vol}$$

$$W = \int \frac{2}{3}(\sigma_v - \sigma_h)(d\varepsilon_v - d\varepsilon_h) + p' d\varepsilon_{vol}$$

$$W = \int \tfrac{2}{3} q(d\varepsilon_v - d\varepsilon_h) + p' d\varepsilon_{vol} \text{ where } d\varepsilon_h = -\tfrac{1}{2} d\varepsilon_v$$

$$W = \int \frac{2}{3} q(d\varepsilon_v + \frac{1}{2} d\varepsilon_v) + p' d\varepsilon_{vol}$$

$$W = \int q d\varepsilon_v + p' d\varepsilon_{vol} \text{ where } d\varepsilon_{vol} = 0$$

$$W = \int q d\varepsilon_v$$

In the shaking table tests, $d\gamma_{vh}$ is predominant, thus

$$W = \int \tau d\gamma_{vh}$$

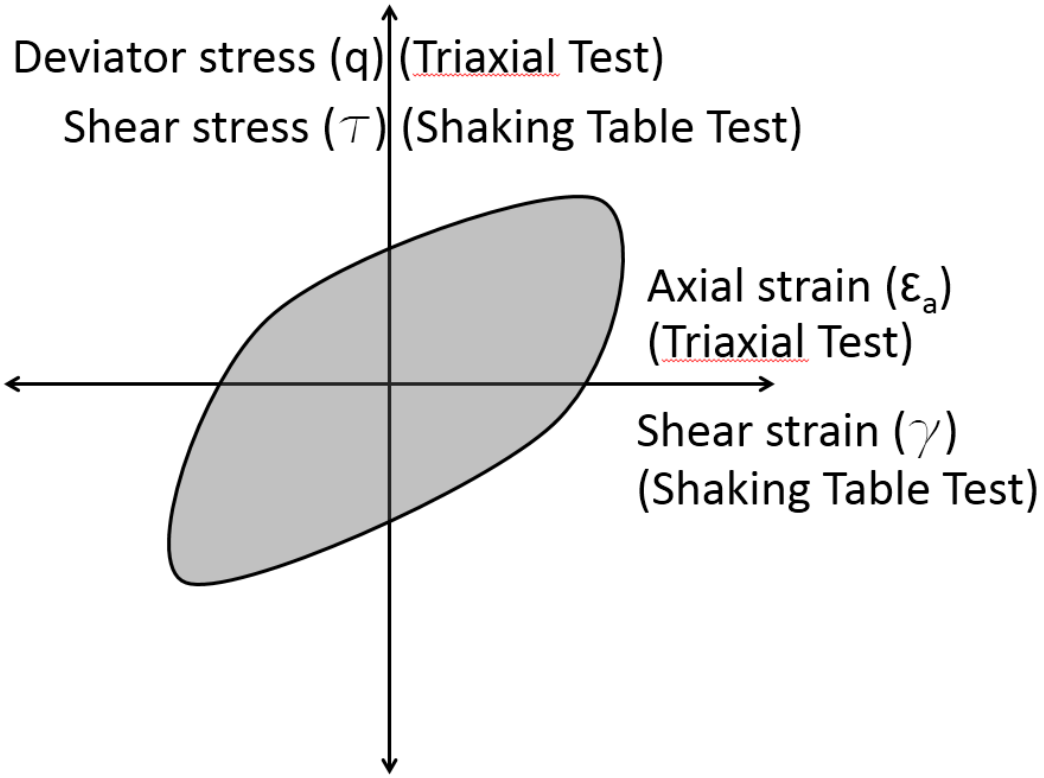

Figure 5-1. Hysteretic loop of deviatoric stress and axial strain relationship for energy computation

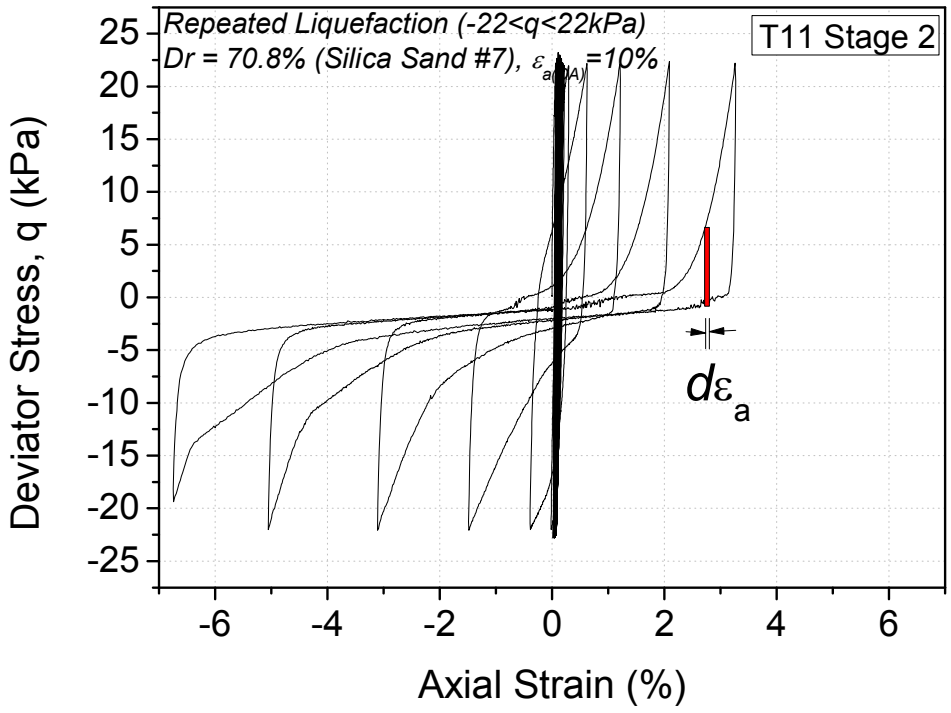

Figure 5-2. Dissipated energy computation for cyclic undrained triaxial test

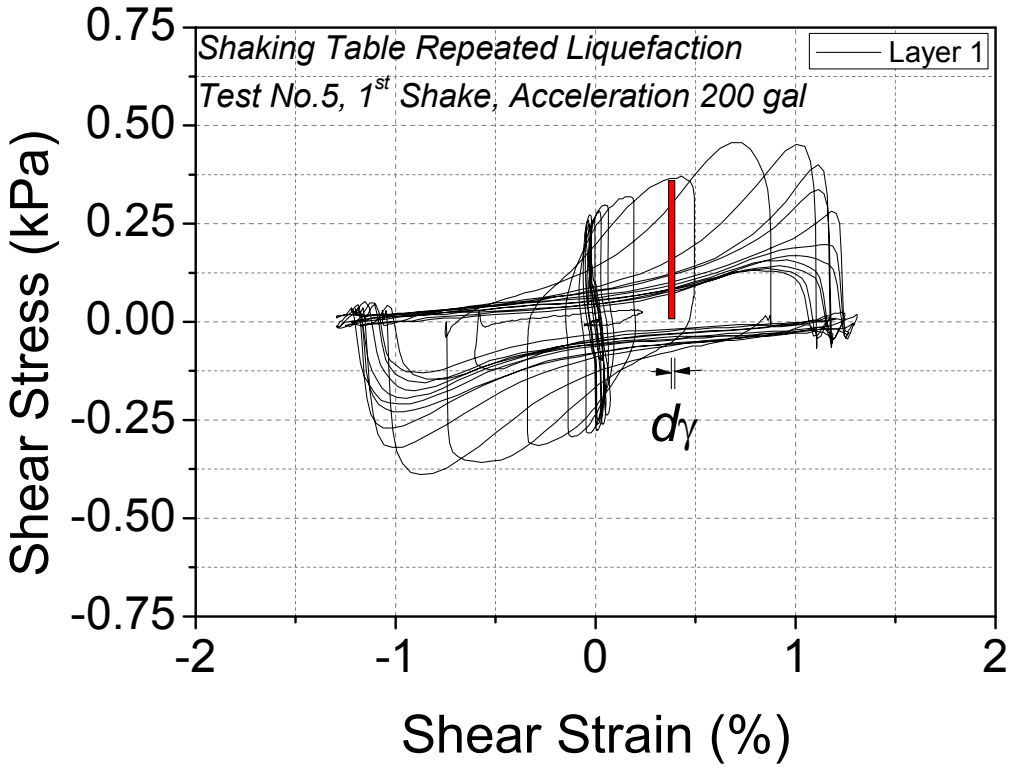

Figure 5-3. Dissipated energy computation for cyclic undrained triaxial test

5.2.2 Modified Dissipated Energy

The modified dissipated energy; i.e. normalized dissipated energy, method was developed to overcome the effect of confining pressure. In this case, the modified dissipated energy can be computed using the area of the hysteretic loop of stress ratio of current deviatoric stress to current mean effective stress and axial strain relationship in the case of triaxial or hysteretic loop of stress ratio of current shear stress to current mean effective stress and shear strain for shaking table as schematically illustrated in Figure 5-4. This area is can be calculated in the same manner as described in normal dissipated energy calculation in previous section using simple integration as present in *Figure 5-5* for triaxial test and *Figure 5-6* for shaking table test by using equation as follow,

$$\sum \Delta W' = \int \frac{q}{p'} \, d\,\varepsilon_a$$

$$\sum \Delta W' = \int \frac{\tau}{p'} \, d\,\varepsilon_a$$

where $\Delta W'$ is the total dissipated energy, q is deviator stress, ε_a is axial strain, τ is shear stress, γ is shear strain and p' is mean effective stress. It is noted that modified dissipated energy is non-unit. In the similar manner as normal dissipated energy, the integration was made using sampling rate of the test which was 1 second for triaxial test 0.002 second for shaking table.

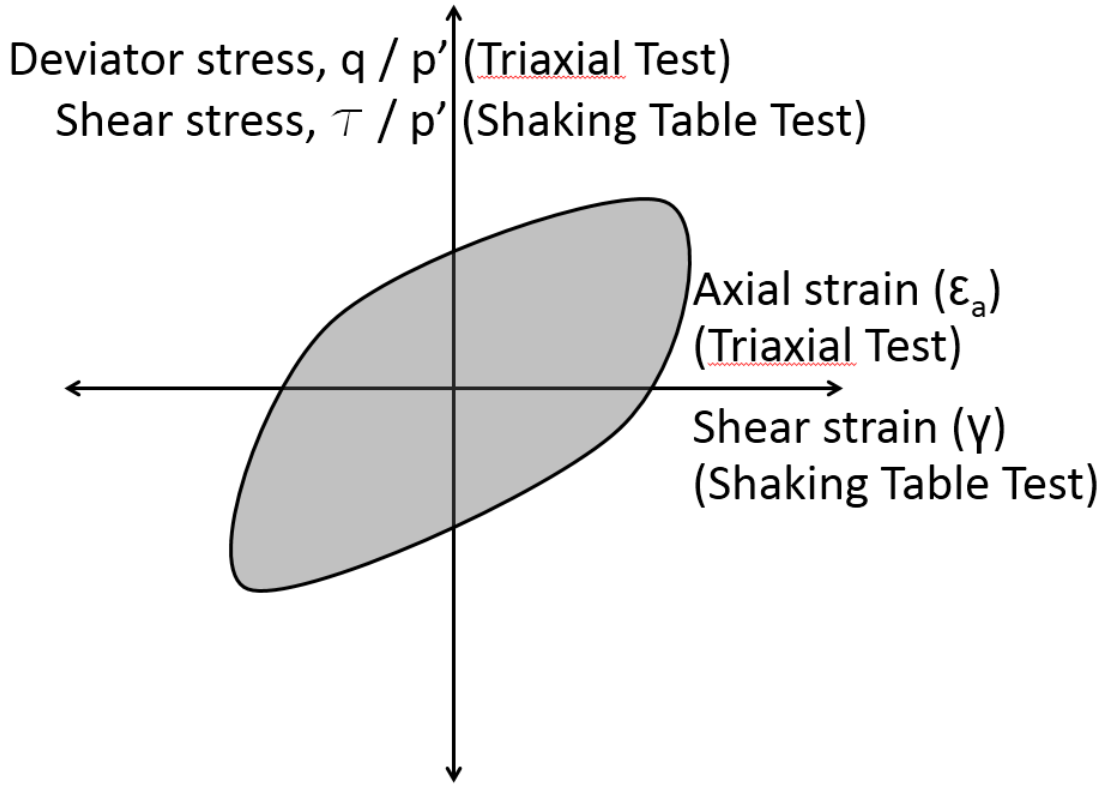

Figure 5-4. Hysteretic loop of deviatoric stress normalized by current mean effective stress and axial strain relationship for energy computation

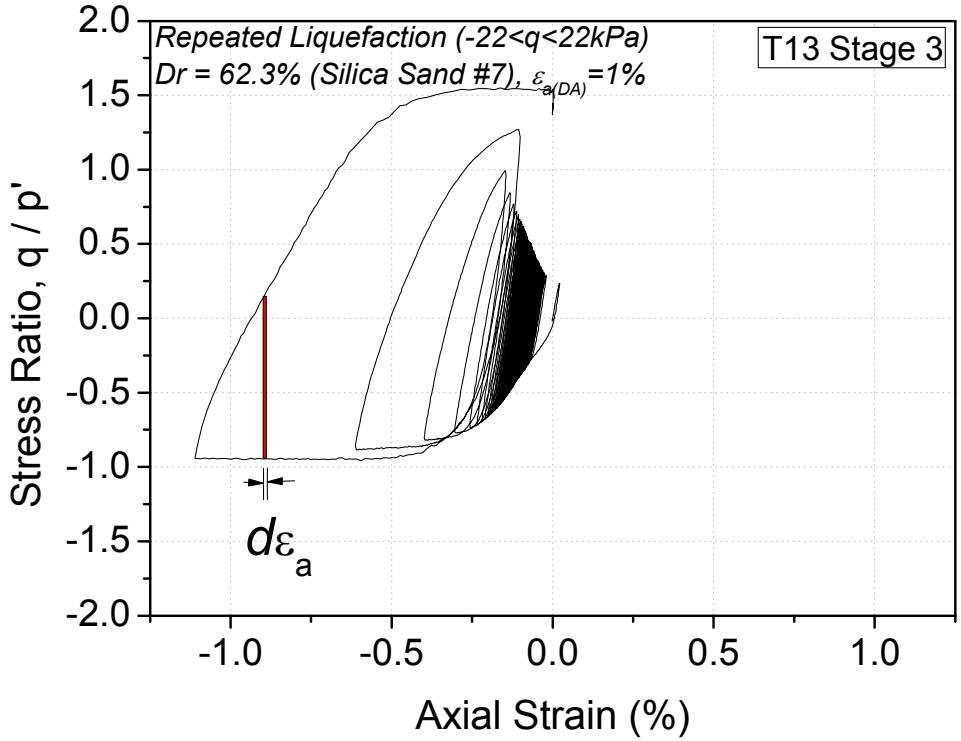

Figure 5-5. Modified dissipated energy computation for cyclic undrained triaxial test

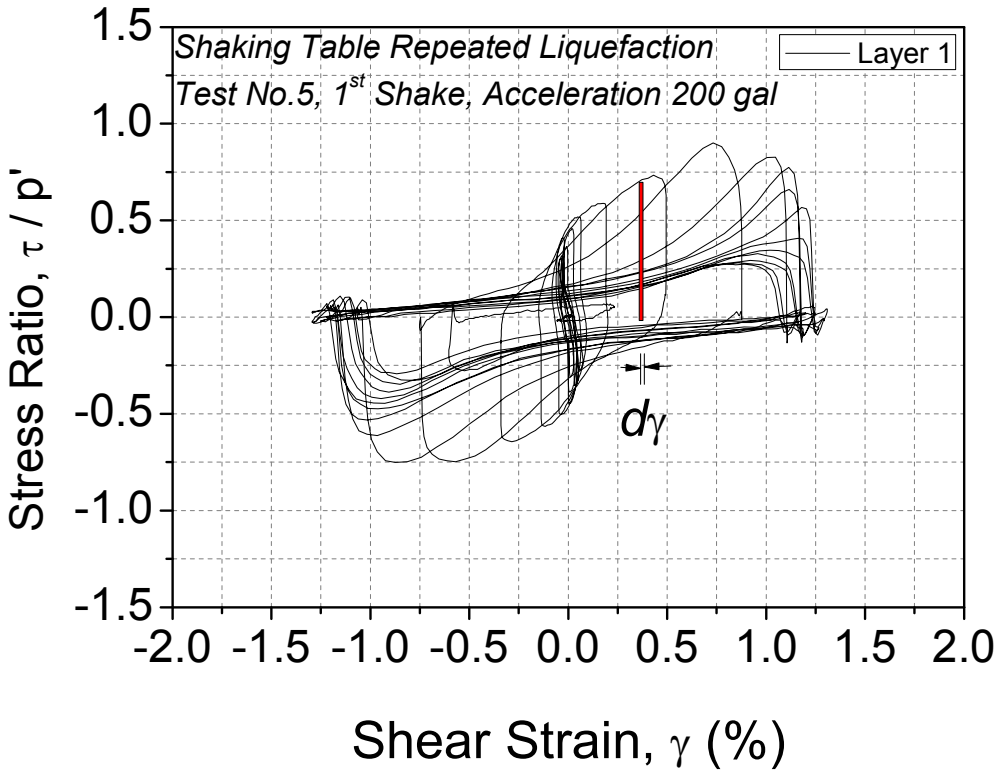

Figure 5-6. Modified dissipated energy computation for shaking table test

5.2.3 Accumulated strain

The accumulated axial strain and shear strain is also vital in dissipated energy analysis. Evaluation of accumulated axial strain or accumulated shear strain can be described as equations below together with *Figure 5-7* and *Figure 5-8* for triaxial test and shaking table test, respectively.

$$\sum \varepsilon_a = \int |\varepsilon_a| \, dt$$

$$\sum \gamma = \int |\gamma| \, dt$$

where ε_a is axial strain, γ is shear strain and t is elapsed time.

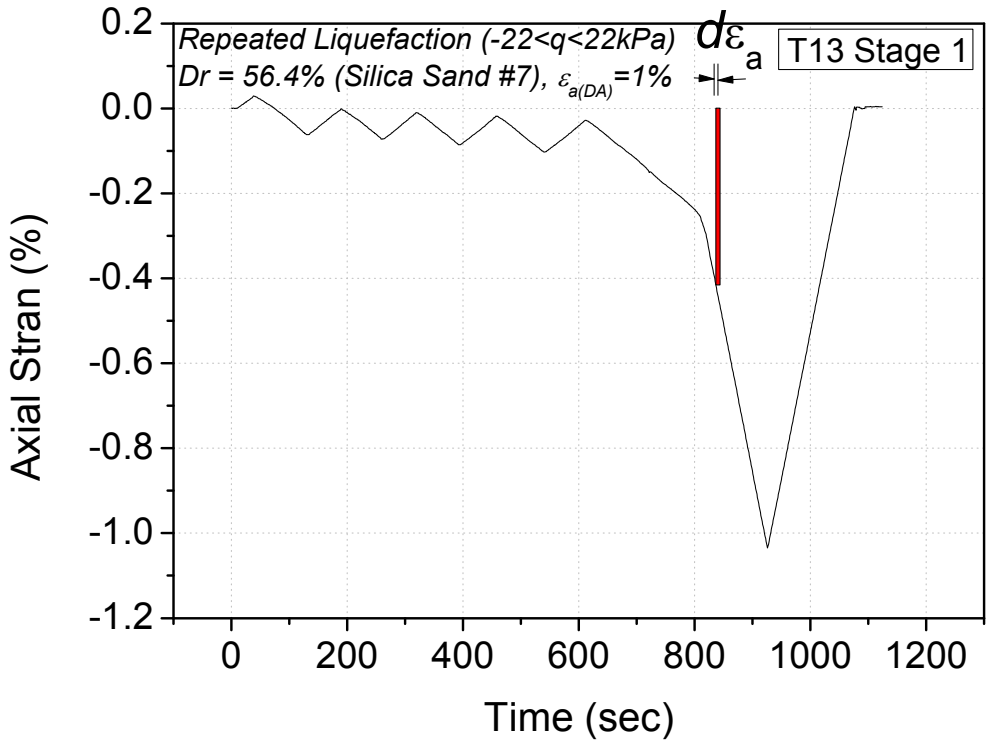

Figure 5-7. Accumulated axial strain computation for cyclic undrained triaxial test

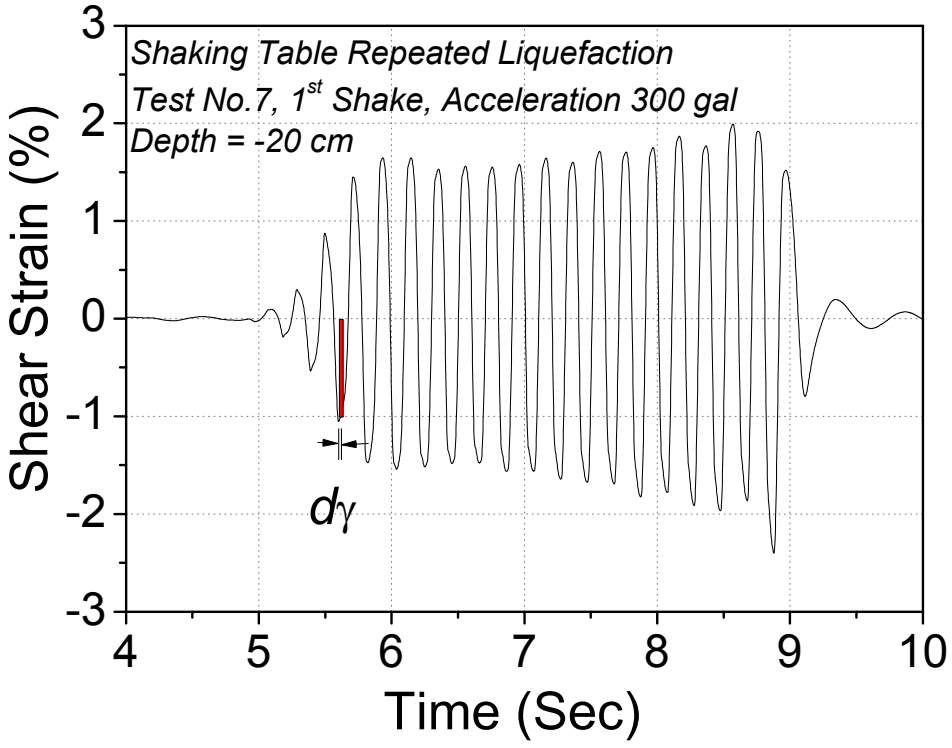

Figure 5-8. Accumulated axial strain computation for shaking table test

5.2.4 Phase transformation line

The phase transformation line is a virtual line through the origin in effective stress space to indicate transition of soil behavior from contractive to dilative for undrained case. In drained case, this virtual line sometimes refers to the characteristic line where contractive (or volume reduction) behavior changes to dilative. An example of phase transformation line in the case of liquefaction test is given in *Figure 5-9*. It can be seen that there are at least two points marked in circles indicating behavior change. Contractive behavior occurs during excess pore water pressure generation; i.e. decrease in effective stress, while dilative behavior occurs when there is a decrease in excess pore water pressure; i.e. increase in effective stress.

However, in the case of loose sand and low strain amplitude, the phase transformation line is sometimes not clear as shown in *Figure 5-10*. As presented, there seems to be no point indicating behavior change in this case. In order to draw phase transformation line correctly in the case where there is a limitation. The angle of phase transformation line was computed in the cases where able to do so. It was found that the angle of phase transformation line is rather

similar regardless of relative density, liquefaction stage and strain history (see *Figure 5-23*). The calculation is presented in *Figure 5-11*. It is noted that in triaxial test, the phase transformation line on compression side and extension side may not be the same. Normally, it is specimen is stronger on the compression side.

The phase transformation line can be used as a virtual boundary to distinguish reliquefaction behavior as firstly purposed by Ishihara and Okada (1978) and Ishihara and Okada (1982). The total dissipated energy before and after the phase transformation line were computed to investigate repeated liquefaction behavior following the work of Wahyudi and Koseki (2015) and Aoyagi et al. (2016).

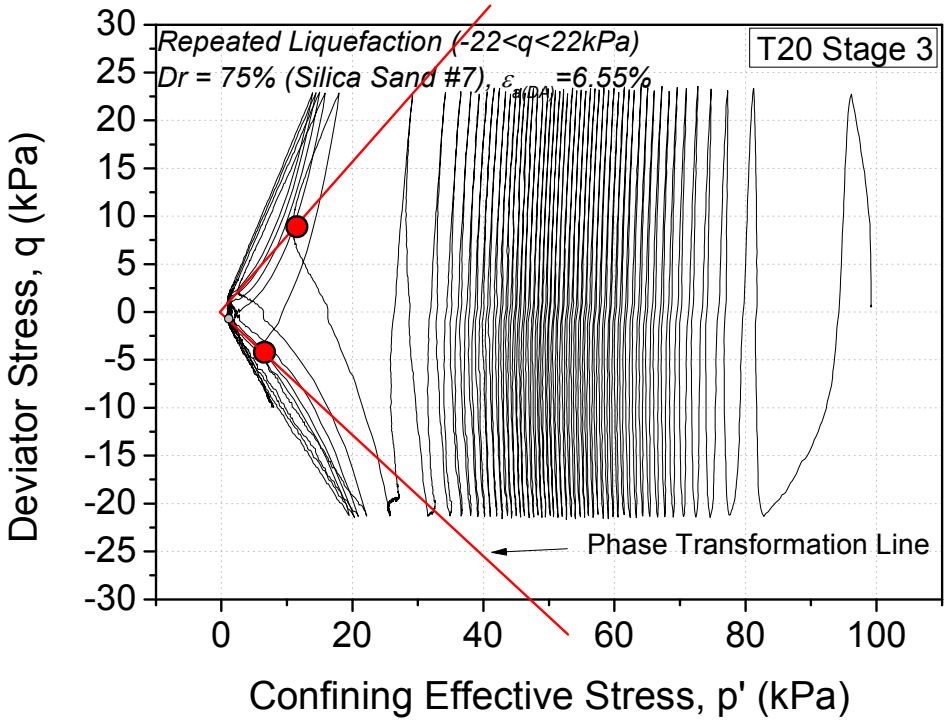

Figure 5-9. Phase transformation line in traxial liquefaction test (T20, $\varepsilon_{a(DA)}$=6.55%, CSR = 0.11, third liquefaction stage)

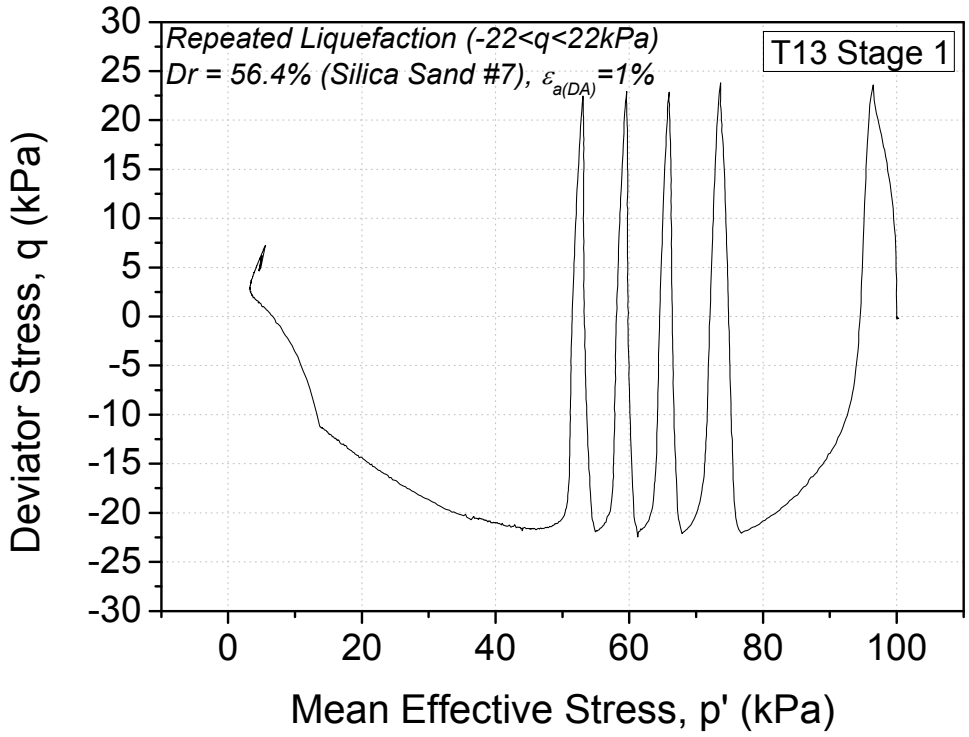

Figure 5-10. Effective Stress path (T13, $\varepsilon_{a(DA)}$=1.0%, CSR = 0.11, first liquefaction stage)

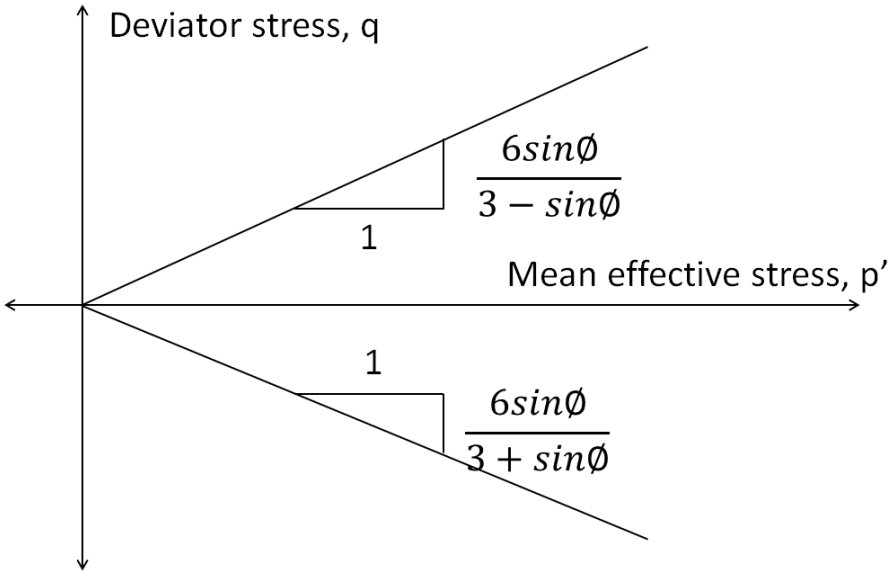

Figure 5-11. Phase transformation line angle calculation

5.3 Results and Discussion

5.3.1 Energy dissipation of the silica sand in a triaxial apparatus

The method of energy dissipation was employed in repeated liquefaction analysis. The results of repeated liquefaction test in traiaxial apparatus described in Chapter 3 were used for dissipated energy calculation. To sum up, in the first liquefaction stage, there were test results of specimens subjected to various double amplitude strain histories. By using described equations, dissipated energy and accumulated axial strain of these results were calculated. Typical relationships between deviator stress and axial strain of liquefaction test from stage 1 to stage 4 are presented in *Figure 5-12*. In addition, corresponding typical dissipated energy and accumulated axial strain are shown in *Figure 5-13*. By using combination of these two types of figures together, relationship between dissipated energy and accumulated axial strain can be drawn as shown in *Figure 5-14*. In general, dissipated energy increased with certain increasing rate to a point at which the increasing rate changed to be higher for some time. After that the increasing rate of dissipated energy slightly dropped.

In order to compare the repeated liquefaction behavior, the dissipated energy and accumulated axial strain relationship at different stages was plotted in *Figure 5-15*. It can be clearly seen that the points where the accumulated rate of dissipated energy were different among different stages. The rate changed relatively early in the first stage at about 0.8% accumulated axial strain. At higher stages, the rate change was also found at larger value of accumulated axial strain at approximately 2.5%, 4.5% and 15.5% for the liquefaction stage 2, 3 and 4 respectively. However, in this case, the second changing rate was not found in the first liquefaction stage as the target double amplitude axial strain might be too low at 2.0% and it did not reach that changing point yet before test termination. The total dissipated energy at different stages was not equal which might due to cyclic history. Another possible reason is relative density (Dief and Figueroa 2007). In the later stages, specimen was subjected to excess pore water pressure dissipation and reconsolidation providing an increase in relative density.

For further investigation, the relationship of dissipated energy and accumulated axial strain of the first liquefaction stage of all specimens was plotted as shown in *Figure 5-16* and the close-up around origin is given in *Figure 5-17*. Each specimen was subjected to different strain

amplitude history but under the same CSR at 0.11. It is noted that all the specimens in this case did not experience any liquefaction or loading history; i.e. intact or virgin specimen. A unique relationship between dissipated energy and accumulated axial strain can be seen. Initially, the dissipated energy increased with a constant rate of about 0.060 J/m3/% up to approximately 1% accumulated axial strain. After that, the increasing rate sharply changed to a about 0.123 J/m3/%. It is quite obvious that this changing point occurs at similar value of accumulated axial strain about 1%. The dissipated energy increased further up to some extent where the second changing rate occurred. However, this second changing rate did not occur at the same value of accumulated axial strain. This is because the test was terminated at different double amplitude strain history. Once the target strain was reached, the test stopped and the left-over strain was adjusted back to 0%. Because of this termination the second rate changing point occurred differently (see *Figure 5-18*). Besides, if the test continued further, it is expected that the second changing point should occur at similar value of accumulated axial strain.

In addition, Towhata and Ishihara (1985) discovered a unique relationship between dissipated energy; i.e. shear work, and excess pore water pressure in an undrained torsional shear test in hollow cylinder device using Toyoura sand. It was suggest that this unique relationship is independent of the stress amplitude where liquefaction resistance is ranging approximately 2-40 cycles. In this thesis with Silica sand with number seven grading in an undrained cyclic triaxial test, it was confirmed that unique relationship also independent of strain amplitude as shown in *Figure 5-19*. However, as each specimen was terminated at different strain amplitude, giving different total dissipated energy. The lowest total dissipated energy was observed in the specimen which was subjected to 1% strain amplitude while specimen with 10% strain amplitude showed the largest dissipated energy. However, in the range of 0-0.2 J/m^3, there is an obvious unique line. It should be noted that this unique trend of dissipated energy might be due to same conditions of the test which were intact specimens, confining pressure and relative density.

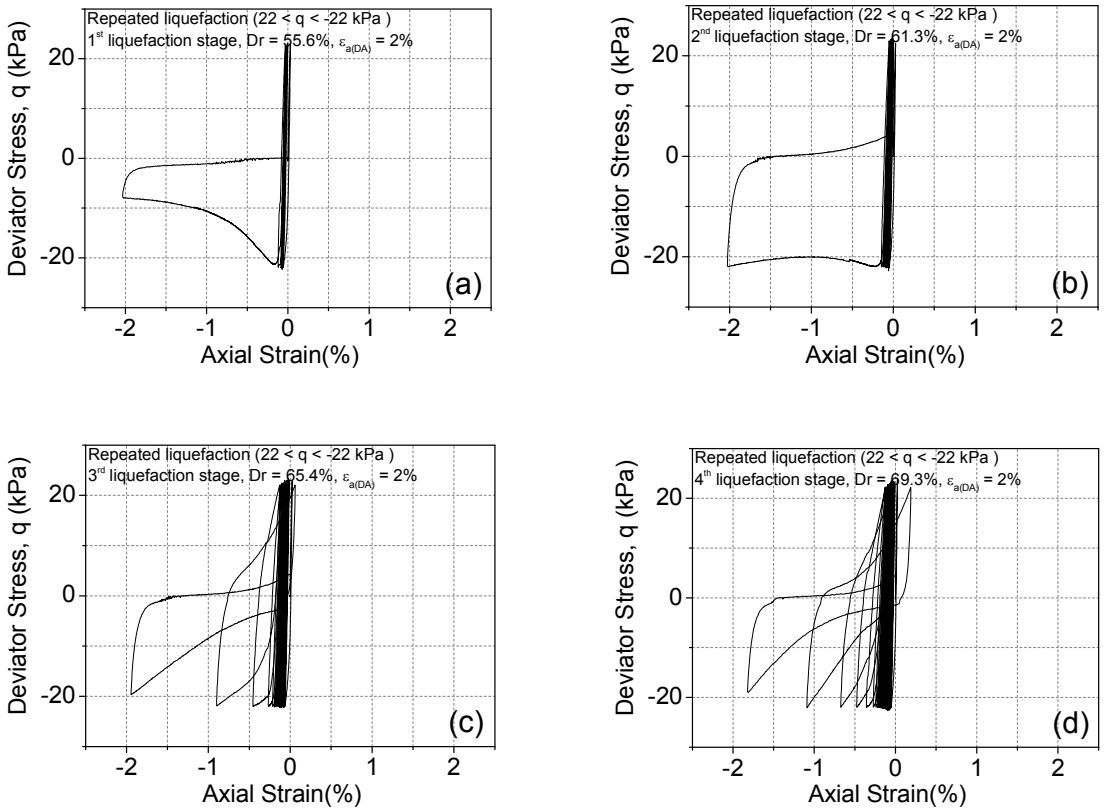

Figure 5-12. Typical deviator stress – axial strain relationships of the repeated liquefaction test stage 1 (a), stage 2 (b), stage 3 (c) and stage 4 (d) (T15 Test) (CSR = 0.11, $\varepsilon_{a(DA)}$ = 2%)

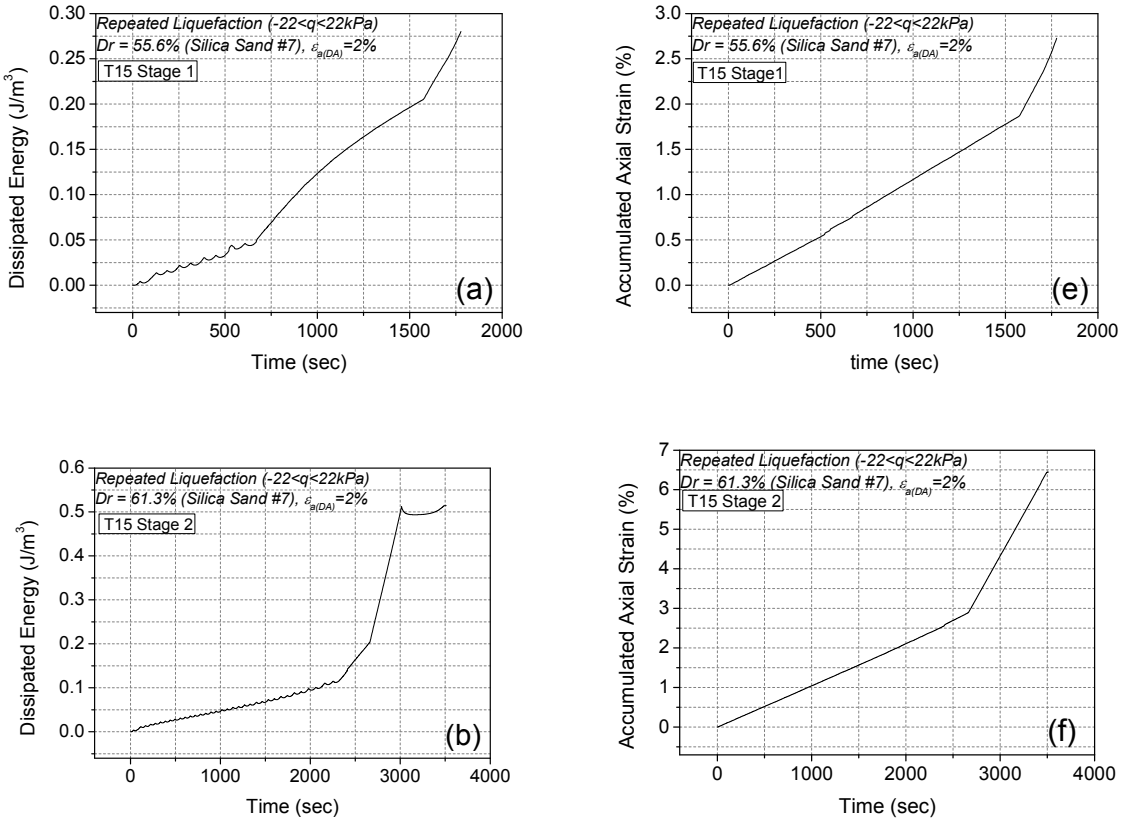

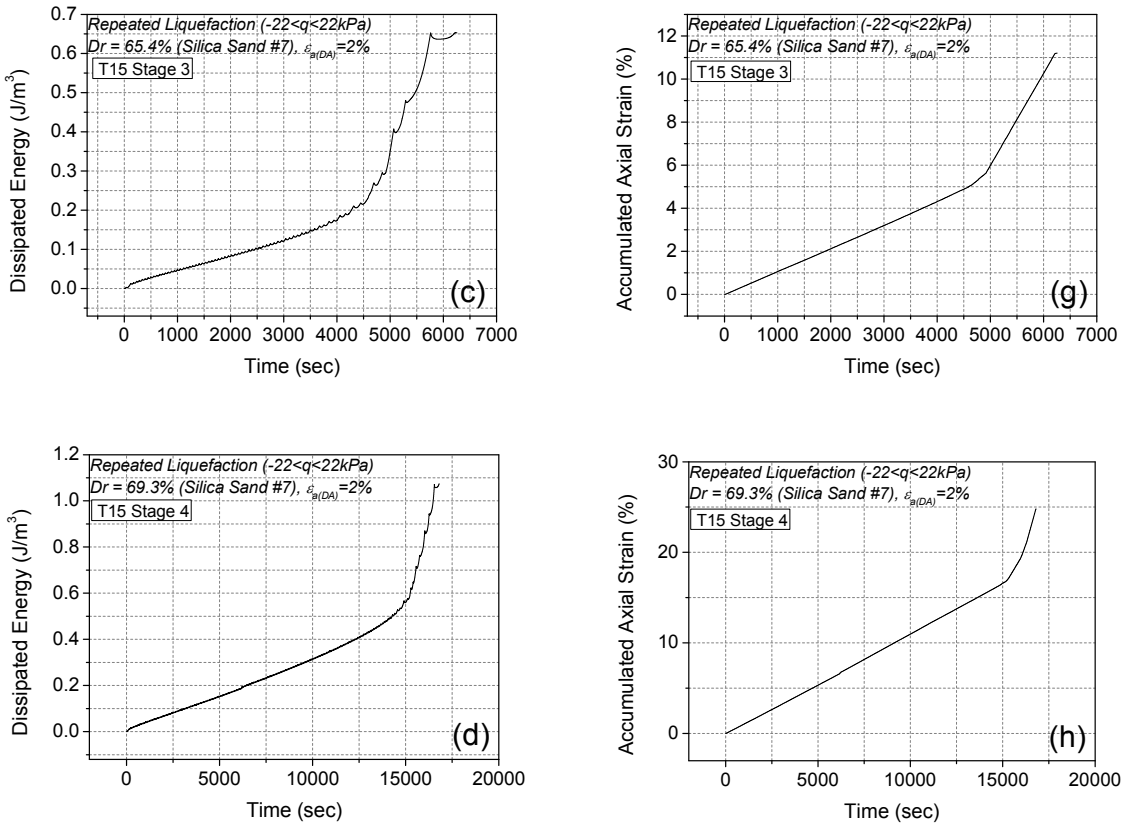

Figure 5-13. Typical dissipated energy and accumulated axial strain time histories of the repeated liquefaction test stage 1 (a, e), stage 2 (b, f), stage 3 (d, g) and stage 4 (d, h) (T15 Test) (CSR = 0.11, $\varepsilon_{a(DA)}$ = 2%)

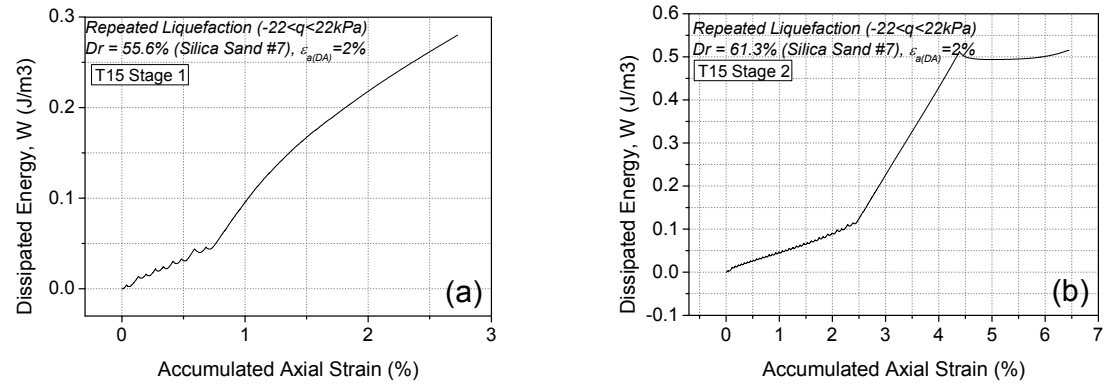

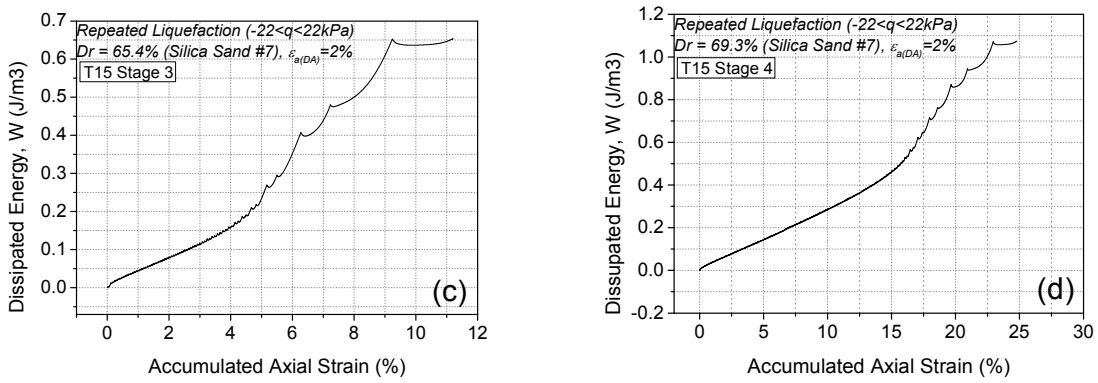

Figure 5-14. Typical dissipated energy and accumulated axial strain relationships of the repeated liquefaction test stage 1 (a), stage 2 (b), stage 3 (d) and stage 4 (d) (T15 Test) (CSR = 0.11, $\varepsilon_{a(DA)}$ = 2%)

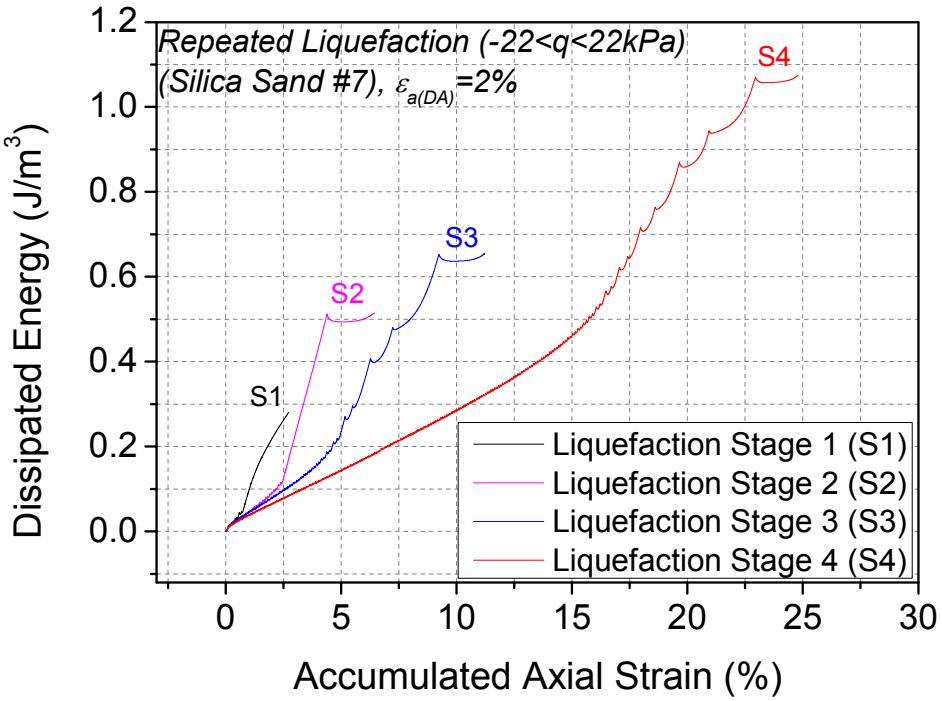

Figure 5-15. Typical dissipated energy and accumulated axial strain relationships of the repeated liquefaction test stage 1-4

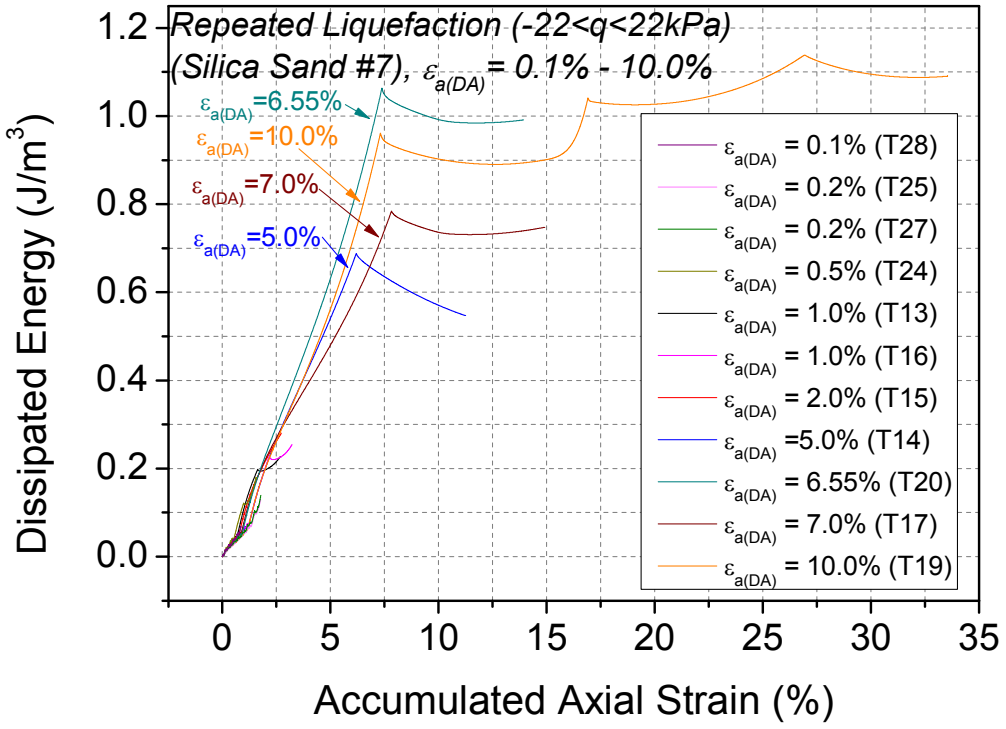

Figure 5-16. Relationship of dissipated energy and accumulated axial strain of silica sand during the first liquefaction stage

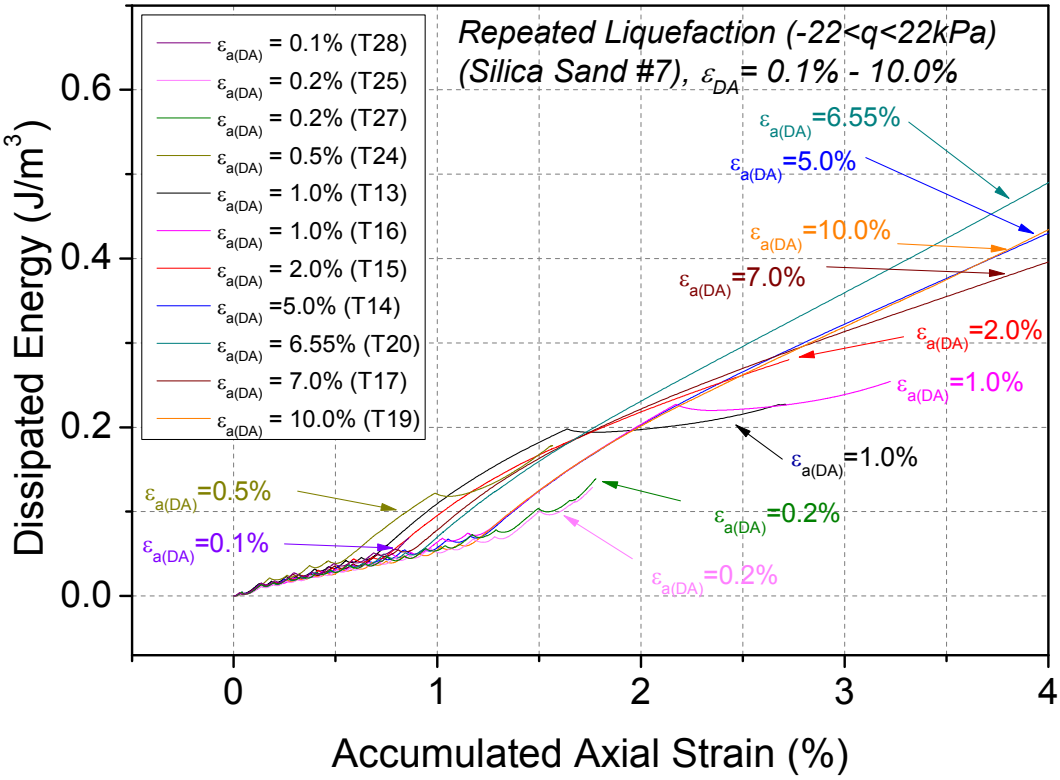

Figure 5-17. Close-up around origin area of Relationship of dissipated energy and accumulated axial strain of silica sand during the first liquefaction stage

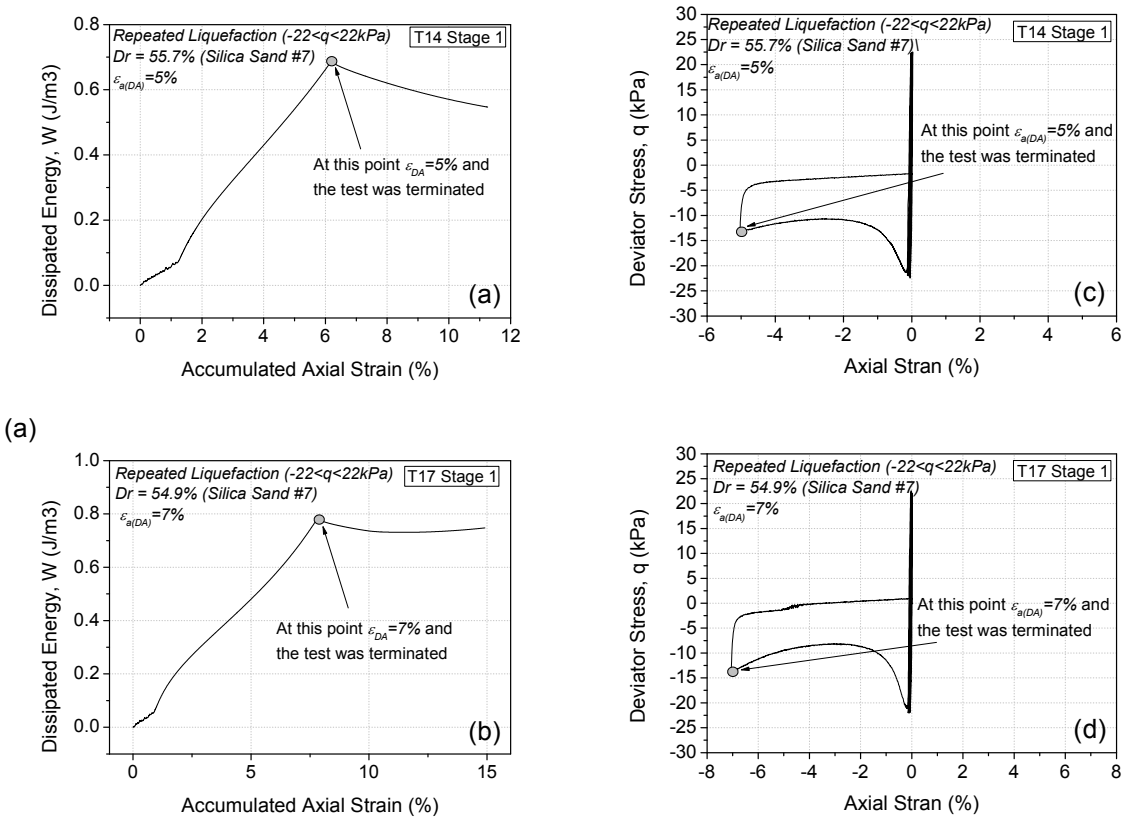

Figure 5-18. The point where the tests were terminated in relationship of dissipated energy and accumulated axial strain (a, b) and corresponding relationship of deviator stress and axial strain (c, d)

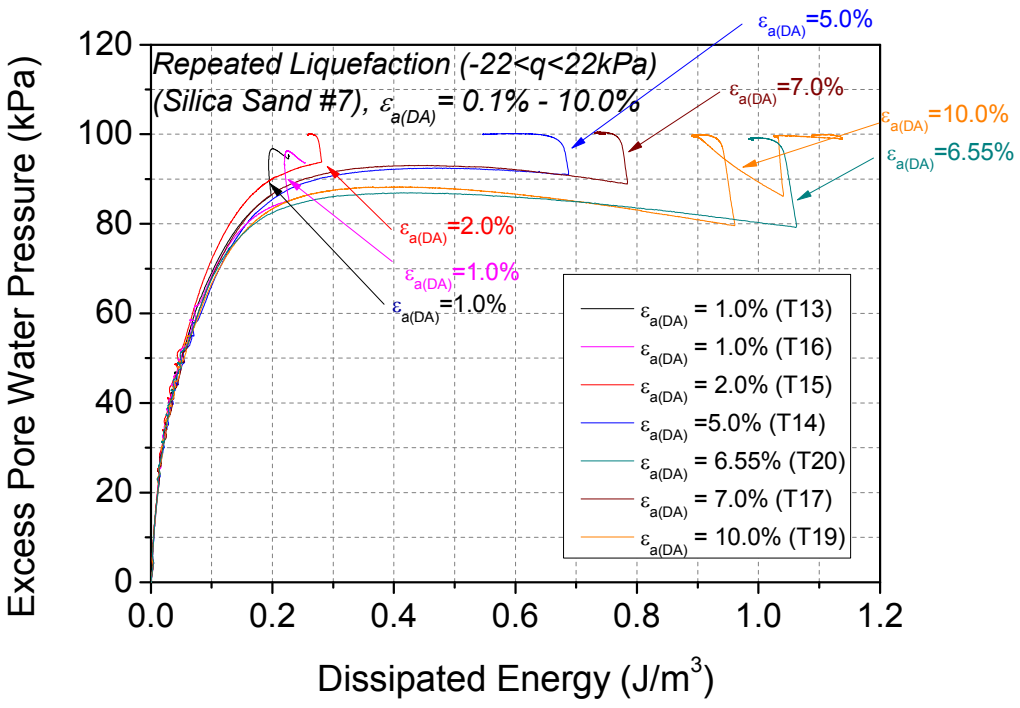

Figure 5-19. Relationship between dissipated energy and excess pore water pressure of specimen subjected to different strain amplitudes during the first stage of liquefaction

5.3.2 Energy dissipation of the silica sand in a triaxial apparatus to investigate the first two stages of repeated liquefaction behavior in triaxial apparatus

Wahyudi and Koseki (2015) and Aoyagi et al. (2016) were two of the pioneer works on energy-based approach in repeated liquefaction for large number of stages. It was suggested that the energy rate changing points are corresponding with phase transformation line in effective stress path. An example is given in *Figure 5-20* in terms of relationship between dissipated energy and accumulated axial strain, stress path and effective stress path. Before reaching point 1; i.e. touching phase transformation line, dissipated energy increased linearly with accumulation of axial strain. After point 1, before reaching point 2, there was a change in accumulation rate of dissipated energy but the effective stress still did not decrease largely. However, after point 2, accumulation rate of dissipated energy increased significantly together with reduction in mean effective stress. At this stage, specimen seems to change from contractive behavior to dilative. When reaching point 3, accumulation rate of dissipated energy changed again becoming lower corresponding with zero effective stress and initial liquefaction. It should be noted that in the initial stage of liquefaction, phase transformation was hardly drawn; thus, it was estimated to be the same as in the later stages.

In order to investigate repeated liquefaction behavior, energy approach was used to determine the future liquefaction resistance by several researcher; for example, Wahyudi and Koseki (2015). It was found that total dissipated energy during the first liquefaction stage; i.e. specimen which have not experienced any liquefaction history, can be used to evaluate liquefaction potential of the second liquefaction stage. For Toyoura sand it was found that the specimen subjected to pre-shearing of 0.5% shear strain showed highest future liquefaction resistance Wahyudi and Koseki (2015). This value of strain is sometime called as “threshold strain”. When specimen subjected to this threshold strain value, it is believed that the cyclic resistance in the next stage becomes highest. However, as pointed out by Suzuki and Toki (1984), the value of threshold strain seems to be depend on the loading condition. Thus, with different loading condition or different testing apparatus, the finding threshold strain of the same material can be different.

By following previous researchers with the triaxial test data of specimens subjected to different strain amplitudes, liquefaction resistance in the second stage was plotted versus total dissipated

energy in the first stage as shown in *Figure 5-21*. It can be seen that when future liquefaction resistance became highest when the total dissipated energy was approximately 0.13 J/m3. After exceeding 0.13 J/m3, which was corresponding to 0.2% axial strain pre-shearing history, cyclic resistance in future liquefaction decreased. Thus, it can be said that the threshold strain of the Silica sand in cyclic triaxial test was found to be about 0.2% double amplitude axial strain. In between 0.2% and 0.5% axial strain history, there was a sharp decrease in second liquefaction stage. For the specimens subjected to larger 1% axial strain history, the second cyclic resistance was rather constant in the range between approximately 10-20 cycles. It is quite obvious that there was a limit of dissipated energy which can be advantageous or detrimental.

Wahyudi and Koseki (2015) also pointed out from the cyclic stacked-ting shear test using Toyoura sand that when the effective stress path crosses the phase transformation line for the first time, the behavior tends to change from contractive to be more dilative. During contractive behavior, total dissipated energy affects the next liquefaction resistance positively. However, after crossing the phase transformation line, dissipated energy in the previous liquefaction stage would cause negative impact which reduce future cyclic resistance. In further discussion, the accumulation of dissipated energy before phase transformation line is called “positive impact” and that after phase transformation line is called “negative impact”

The finding described above was then used in this thesis. The effective stress paths of the specimen with pre-shearing of 0.1%, 0.2% and 0.5% strain amplitude are presented in *Figure 5-22* together with phase transformation line. It can be seen from the figure that stress path of specimen subjected to 0.5% strain amplitude crossed the phase transformation line promoting accumulation of negative impact. However, effective stress path of the specimens with 0.1% and 0.2% pre-sheared did not reach phase transformation line. There was only positive impact accumulated in those specimens. In addition, stress path of the specimen which subjected to only 0.1% strain amplitude, terminated far from phase transformation line resulting in lower positive impact and lower future cyclic resistance compared to specimen with 0.2% pre-sheared. It must be noted that the phase transformation line in the case where the test was terminated at low strain amplitude was duplicated from the later stage where the line can be drawn. This is based on the assumption that phase transformation line is not influenced by liquefaction history. In order to confirm the assumption, the angle of phase transformation line and angle of failure line was calculated where available as shown in *Figure 5-23*. It can be seen that the angle of failure line was in the range of 18-22 degree.

The described energy approach was used in the repeated liquefaction analysis for both triaxial and shaking table test result. However, due to the different confining pressure in those test, modified energy approach in which confining pressure is taken into the account was used instead. The detailed investigation is discussed later on. Before doing so, as there might be an error in mean effective stress measurement, it is better to apply some correction factors before using modified energy approach. The detail of correction factors is described in the next chapter.

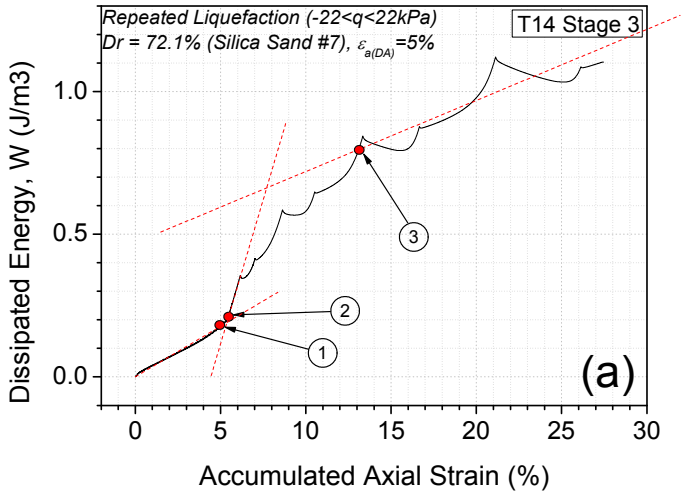

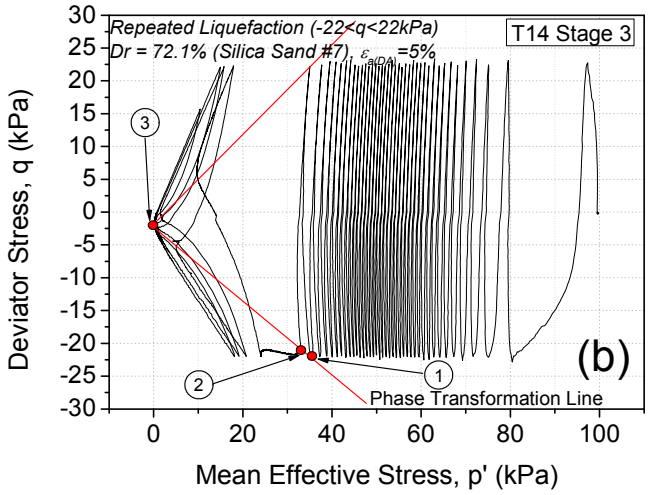

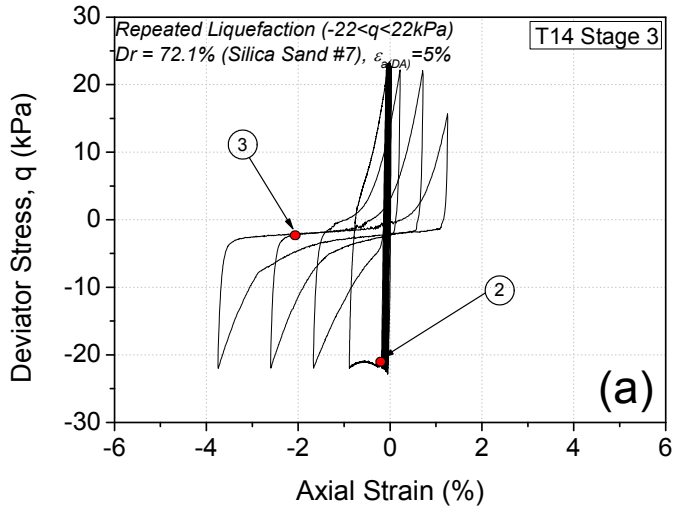

Figure 5-20. . (a) Relationship between dissipated energy and accumulated axial strain, (b) stress path and (c) effective stress path (T14 Test) (CSR = 0.11, $\varepsilon_{a(DA)}$ = 5%)

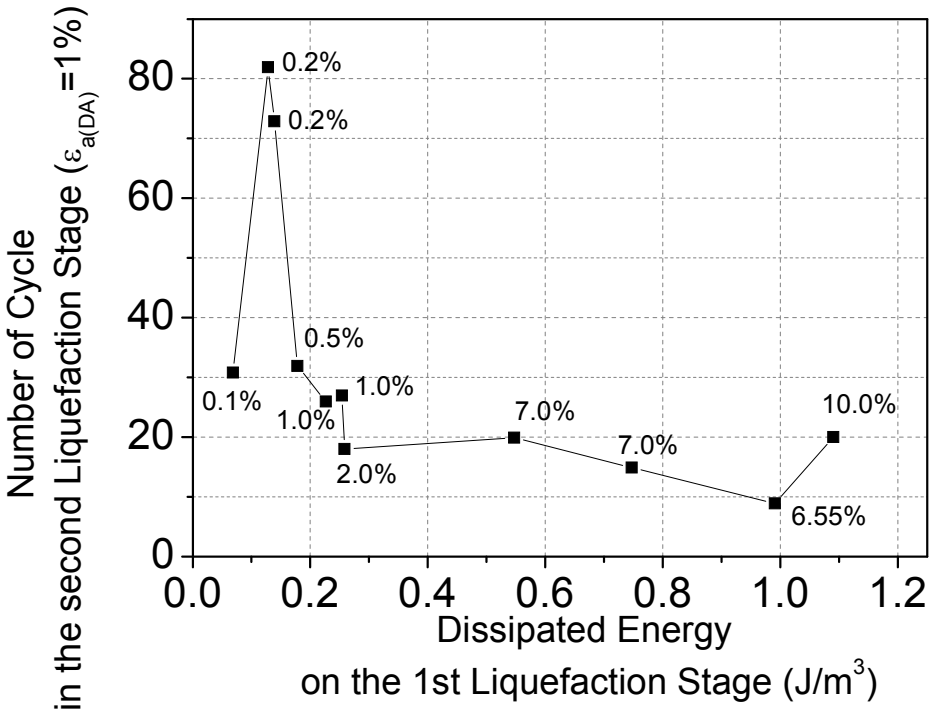

Figure 5-21. The effect of dissipated energy in the first liquefaction stage on the second liquefaction resistance

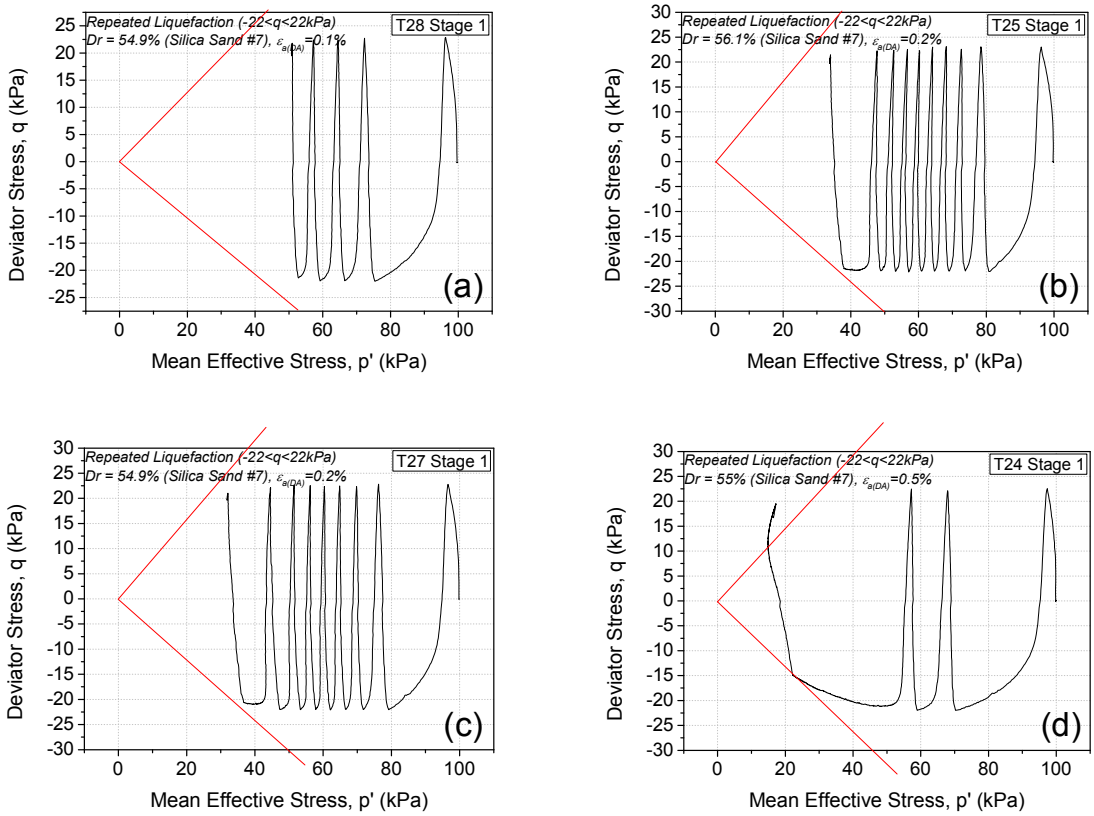

Figure 5-22. Effective stress path of specimens subjected to pre-shearing of (a) 0.1%, (b) 0.2%, (c) 0.2% and (d) 0.5% axial strain amplitude

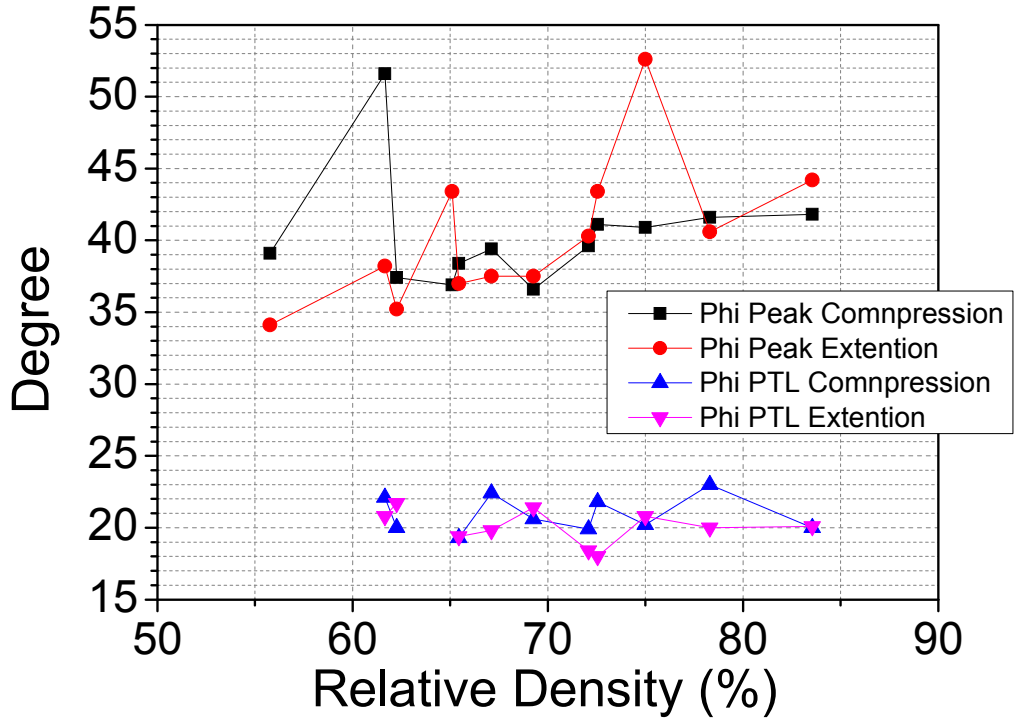

Figure 5-23. Angle of Phase transformation line and failure line at different relative density

5.3.3 Correction factors

In order to compare the result of triaxial tests and shaking table tests of which confining pressures are not equal. Modified energy dissipation in the case of triaxial was computed from hysteretic loop of relationship between ratio of deviator stress and confining pressure and axial strain (see *Figure 5-24*). As can be seen in the figure, the stress path behavior was somehow peculiar; thus, some corrections in stress should be carried out which were stress correction and membrane correction.

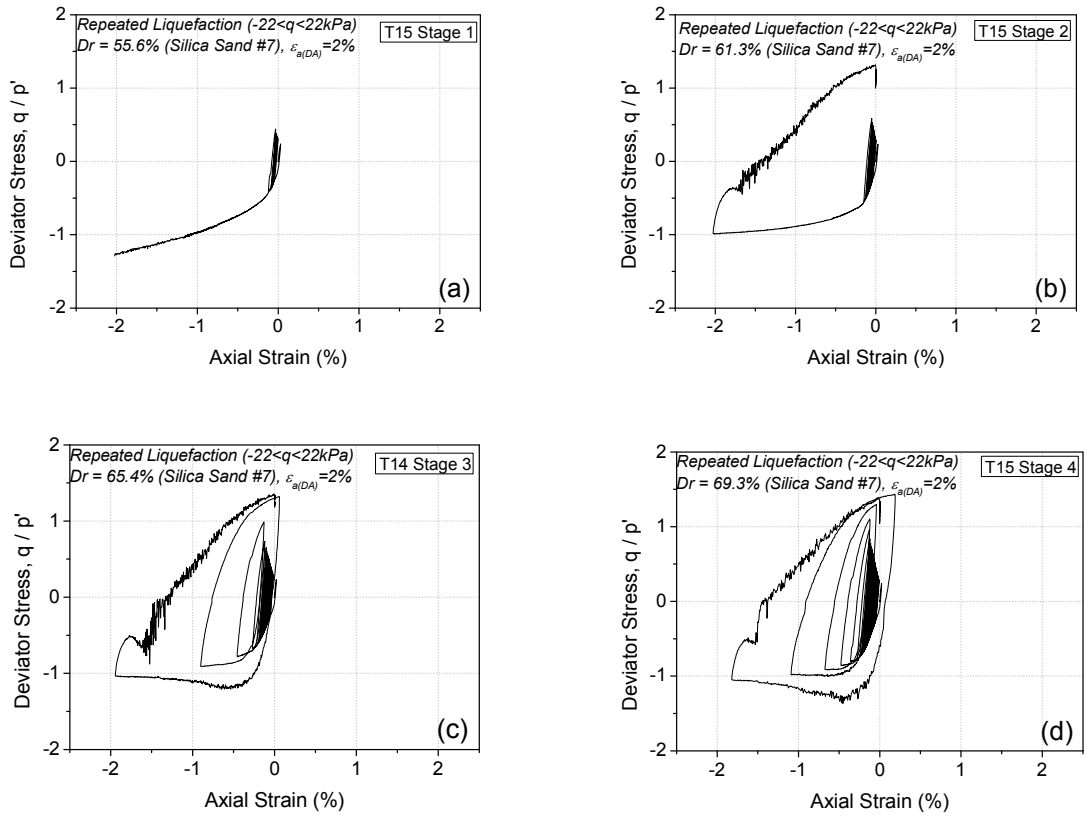

Figure 5-24. Typical deviator stress / mean effective stress – axial strain relationships of the repeated liquefaction test stage 1 (a), stage 2 (b), stage 3 (c) and stage 4 (d) (T15 Test) (CSR = 0.11, $\varepsilon_{a(DA)}$ = 2%)

5.3.2.1 Stress Correction

The corresponding effective stress path of *Figure 5-24* is presented in *Figure 5-25*. It can be seen that, in some cases, the effective stress path did not pass through the origin as indicated as a close-up view in *Figure 5-26*. Koseki et al. (2005) suggested that this behavior might due to some possible reasons such as effect of interlocking and error in stress measuring of the

monitoring system itself. In order to compute ratio of deviator stress to mean effective stress correctly, the stress correction was applied following the equation

$$q_{corr} = q \pm \Delta q$$

$$p'_{corr} = p' \pm \Delta p'$$

Where q_{corr} and p'_{corr} are deviator stress and mean effective stress after correction. q and p' are deviator stress and mean effective stress before correction. Δq and Δp' are correction value for deviator stress and mean effective stress which can be obtained by effective stress path as can be seen from the example of stress path in *Figure 5-26*.

The comparison of relationship of the stress ratio and axial strain with and without correction is presented in *Figure 5-27*. It can be seen that after stress correction of both deviator stress and mean effective stress, peculiar behavior can be eliminated as already confirm by Koseki et al. (2005). In some cases, where error in stress measuring resulting in negative value of mean effective stress, which is of course unrealistic, there was significant difference in relationship between stress ratio (deviator stress to mean effective stress) and axial strain as can be seen in *Figure 5-28* and the corresponding effective stress path before stress correction application is shown in *Figure 5-29*.

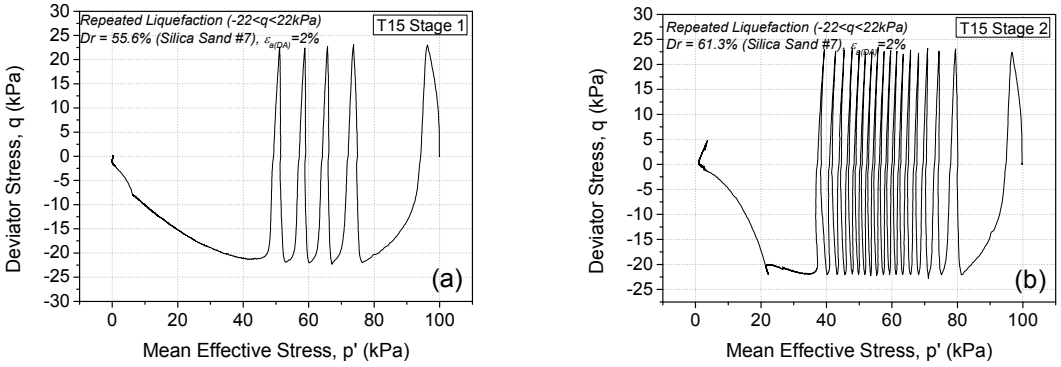

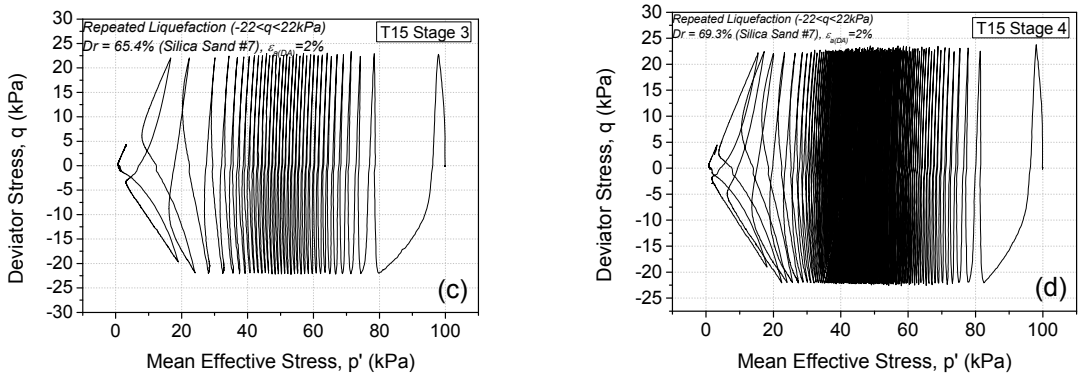

Figure 5-25. Typical effective stress path of the repeated liquefaction test stage 1 (a), stage 2 (b), stage 3 (c) and stage 4 (d) (T15 Test) (CSR = 0.11, $\varepsilon_{a(DA)}$ = 2%)

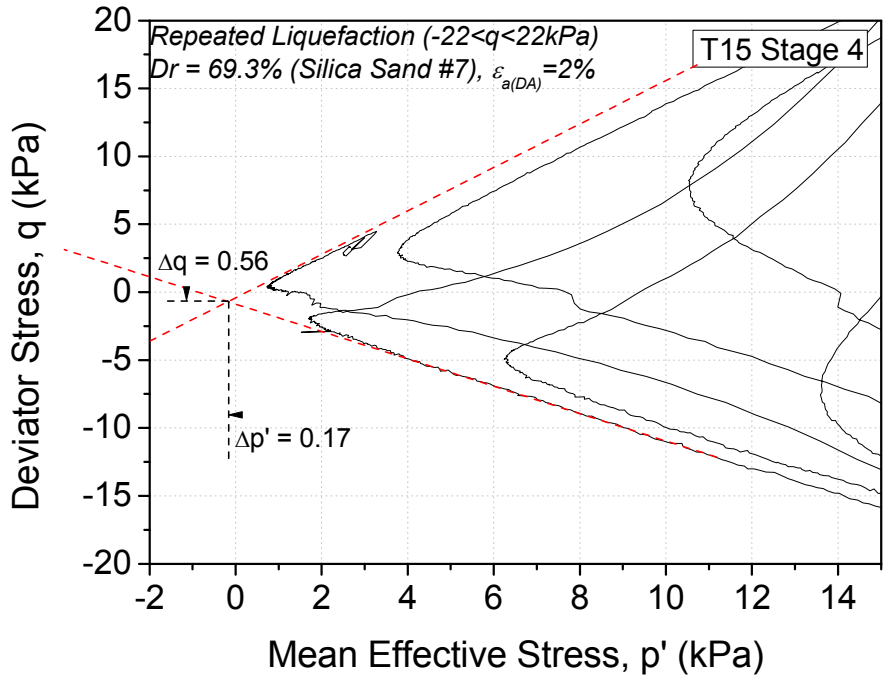

Figure 5-26. Close-up of effective stress path in origin area of Figure 5-25(d) (T15 Test Stage 4) (CSR = 0.11, $\varepsilon_{a(DA)}$ = 2%)

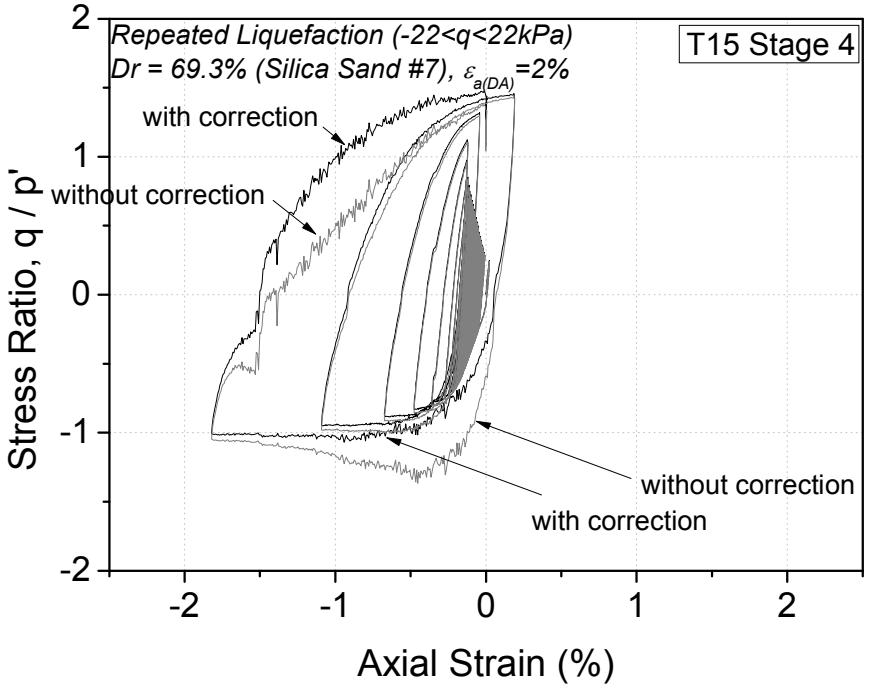

Figure 5-27. Comparison of effective stress path with and without stress correction of the repeated liquefaction test stage 4 (T15 Test) (CSR = 0.11, $\varepsilon_{a(DA)}$ = 2%)

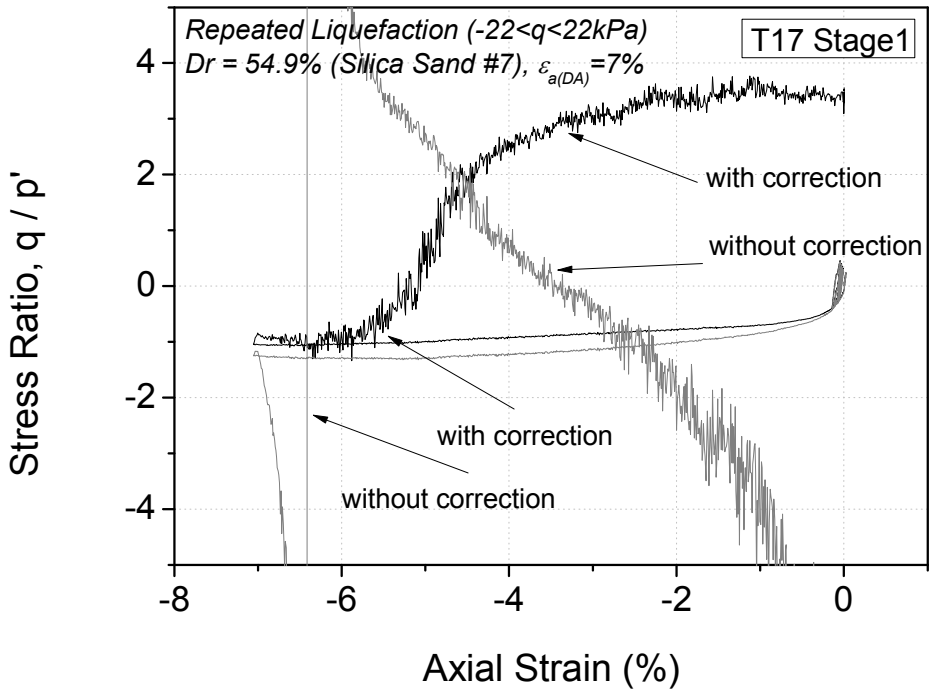

Figure 5-28. Comparison of stress path with and without stress correction of the repeated liquefaction test stage 1 (T17 Test) (CSR = 0.11, $\varepsilon_{a(DA)}$ = 7%)

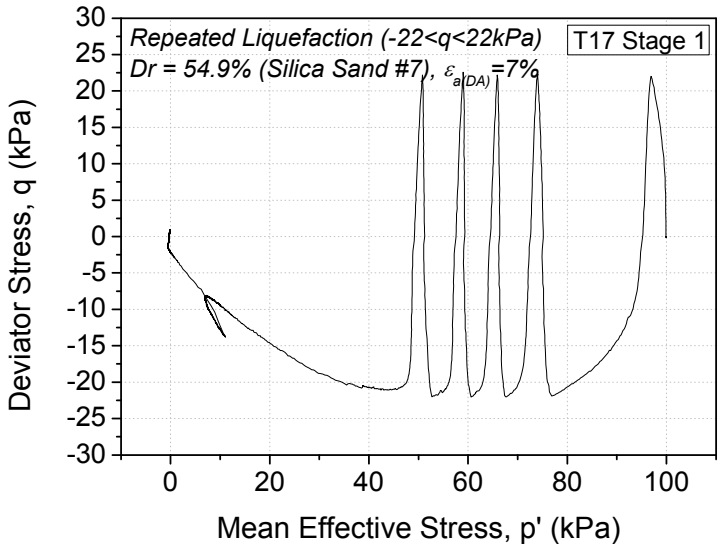

Figure 5-29. Corresponding effective stress path of the Figure 5-28 before stress correction application (T17 Test) (CSR = 0.11, $\varepsilon_{a(DA)}$ = 7%)

2.2.3.2 Membrane Correction

In order to compute modified dissipated energy correctly, the deviator stress was then corrected for membrane force (Henkel and Gilbert, 1952). During extension in cyclic loading, membrane force can be significant. The membrane correction follows equation,

$$\Delta\sigma_{am} = -\frac{\left(\frac{8}{3}\right)\left(E_m t_m(2\varepsilon_a + \varepsilon_r)\right)}{d}$$

$$\Delta\sigma_{rm} = -\frac{\left(\frac{4}{3}\right)\left(E_m t_m(\varepsilon_a + 2\varepsilon_r)\right)}{d}$$

where $\Delta\sigma_{am}$ and $\Delta\sigma_{rm}$ are correction value due to membrane force for axial stress and radial stress, Em is young modulus of membrane (1.4kN/cm^2), tm is membrane thickness (0.3mm in this study), d is specimen diameter, εa and εr are axial strain and radial strain. In the case of undrained triaxial where there is no specimen volume change, radial strain is half negative of axial strain. As a result, membrane force correction in radial stress is zero. Relationship between ratio of deviator stress to mean effective stress and axial strain for comparison of with/without correction is presented in *Figure 5-30*. It can be seen that membrane force slightly affects the relationship, although less comparing with stress correction.

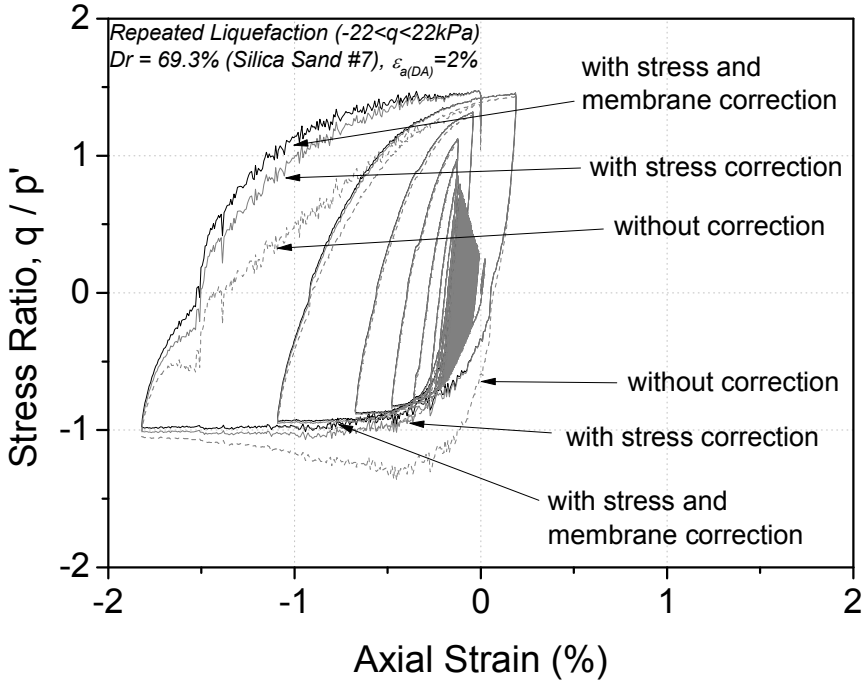

Figure 5-30. Comparison of =stress path with and without stress and membrane correction of the repeated liquefaction test stage 1 (T17 Test) (CSR = 0.11, $\varepsilon_{a(DA)}$ = 7%)

5.3.4 Modified Energy dissipation of the silica sand in a triaxial apparatus

After correcting stress for stress and membrane force, modified dissipated energy; i.e. normalized dissipated energy, was computed from the corrected relationship between ratio of deviator stress to mean effective stress and axial strain. Typical of those relationships at different liquefaction stages are shown in *Figure 5-31*. Besides, the corresponding relationships of modified dissipated energy and accumulated axial strain are given in *Figure 5-32*. It can be seen that unlike the case of normal dissipated energy, the change in accumulation rate of modified dissipated energy tends to occur only once throughout the liquefaction test. With increase in number of liquefaction stages, both modified energy and accumulated axial strain increased.

The modified dissipated energy in every specimen in triaxial test with various strain amplitude during the first stage of liquefaction was computed and plotted versus accumulated axial strain as shown in *Figure 5-33* with close-up around origin in *Figure 5-34*. In similar manner as normal dissipated energy, there is a unique relationship of modified dissipated energy with accumulated axial strain as well.

In order to investigate repeated liquefaction behavior, modified dissipated energy was divided into two categories as positive impact, which is advantageous for the next future cyclic resistance, and negative impact, which promotes lower next liquefaction resistance. The virtual boundary was defined as the point on phase transformation line which first trigger behavior change from contractive in dilative as shown in *Figure 5-35*. *Figure 5-36* presents relationship between positive impact and negative impact which was generated in the previous liquefaction stage together with the liquefaction resistance in the next stage in log scale. Unique trend of weak (Nc = 0-20 cycles), moderate (Nc = 21-50 cycles) and strong (Nc > 50 cycles) can be seen clearly regardless of liquefaction stage and relative density. However, when plotting on linear scale, large different of the strong specimens was observed as presented in *Figure 5-37*. Note that the number of cycle presented in the figure is number of cycle required to reach 1% double amplitude axial strain.

One major advantage of modified dissipated energy or normalized dissipated energy is that the total dissipated energy after initial liquefaction is rather constant as can be seen in *Figure 5-16*. Thus, after reaching the initial liquefaction, total dissipated energy of the specimen is rather similar regardless of strain history. In contrast, the dissipated energy normalized by confining pressure (modified dissipated energy) would increase the dissipated energy after initial liquefaction. It can be seen clearly in the *Figure 5-38* that there seems to be no relationship of weak, moderate or strong specimens.

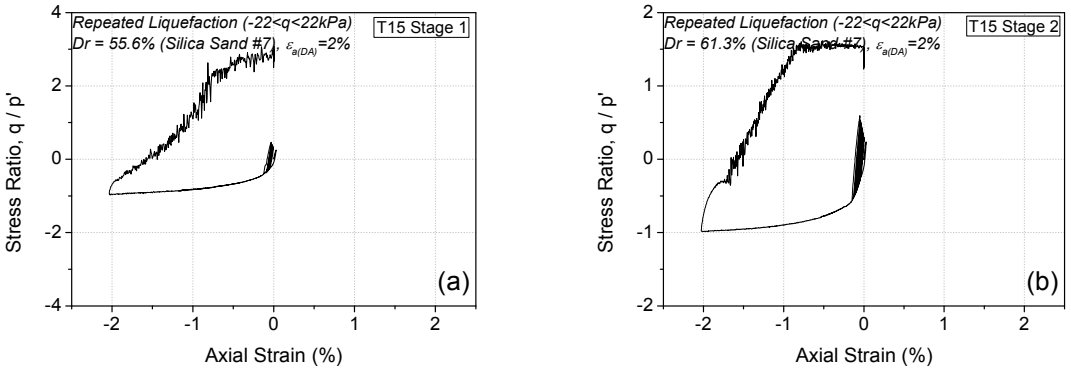

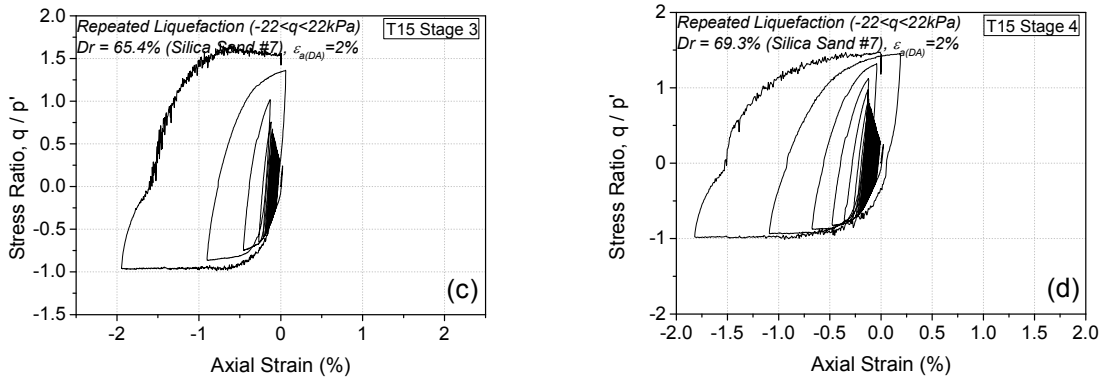

Figure 5-31. Typical corrected relationships deviator stress / mean effective stress – axial strain of the repeated liquefaction test stage 1 (a), stage 2 (b), stage 3 (c) and stage 4 (d) (T15 Test) (CSR = 0.11, $\varepsilon_{a(DA)}$ = 2%)

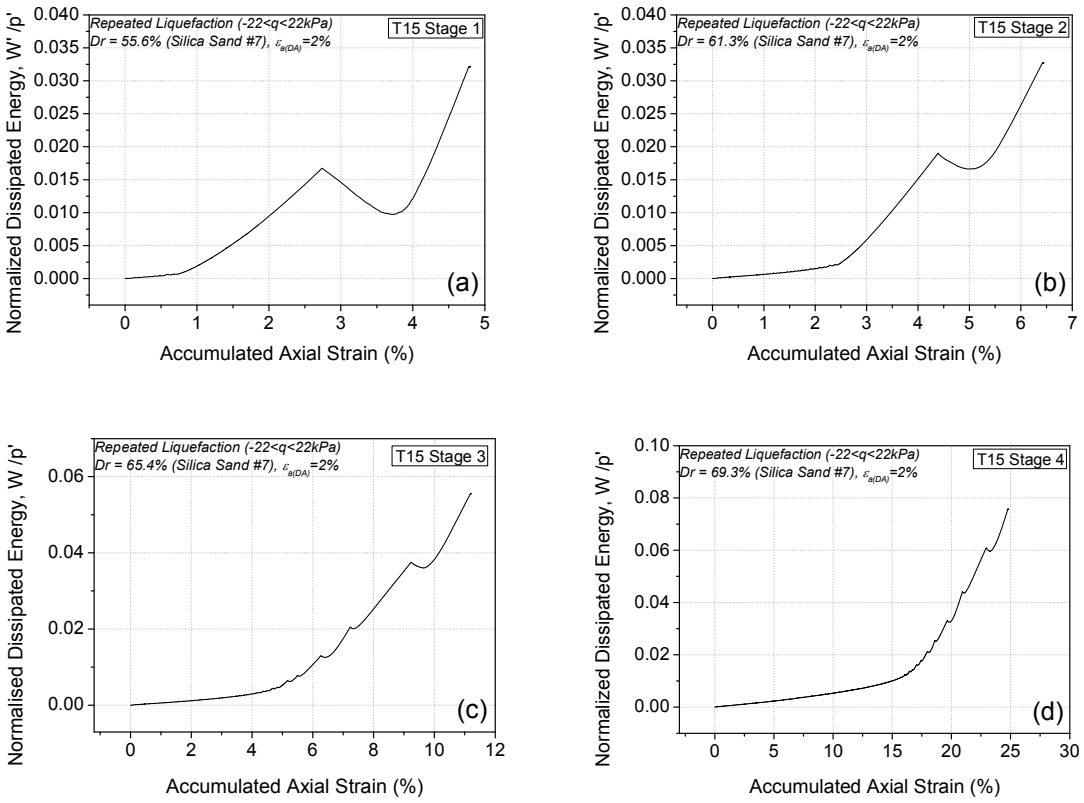

Figure 5-32. Typical modified dissipated energy and accumulated axial strain relationships of the repeated liquefaction test stage 1 (a), stage 2 (b), stage 3 (d) and stage 4 (d) (T15 Test) (CSR = 0.11, $\varepsilon_{a(DA)}$ = 2%)

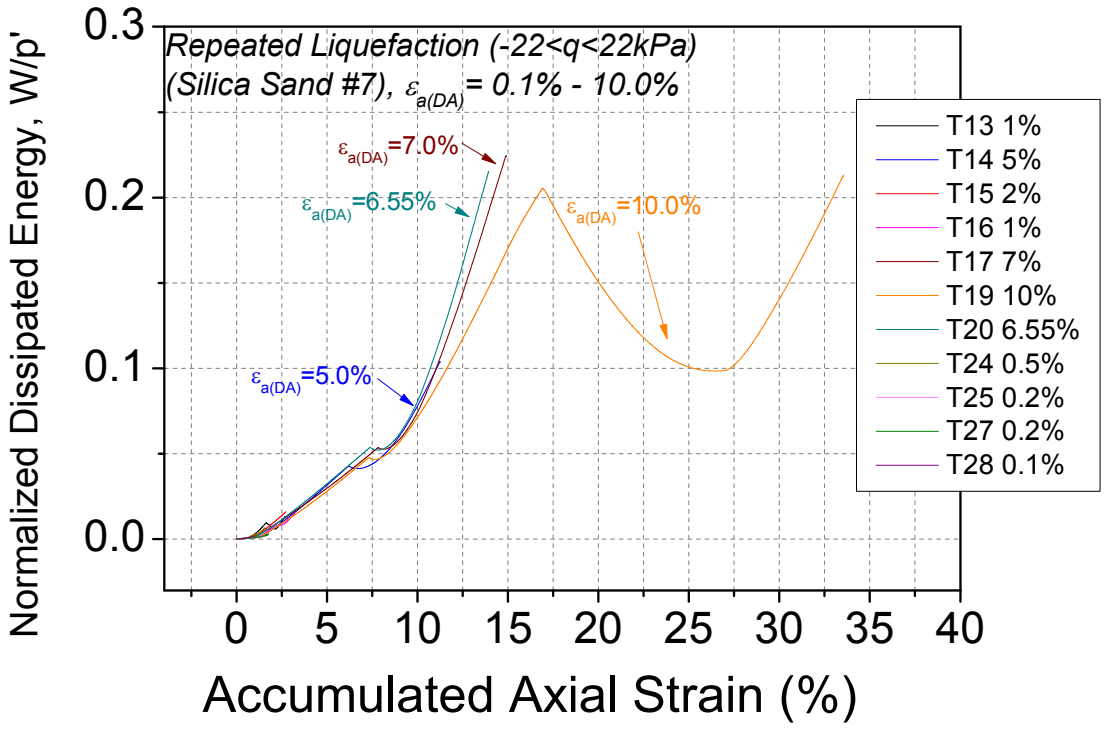

Figure 5-33. Relationship between modified dissipated energy and accumulated axial strain

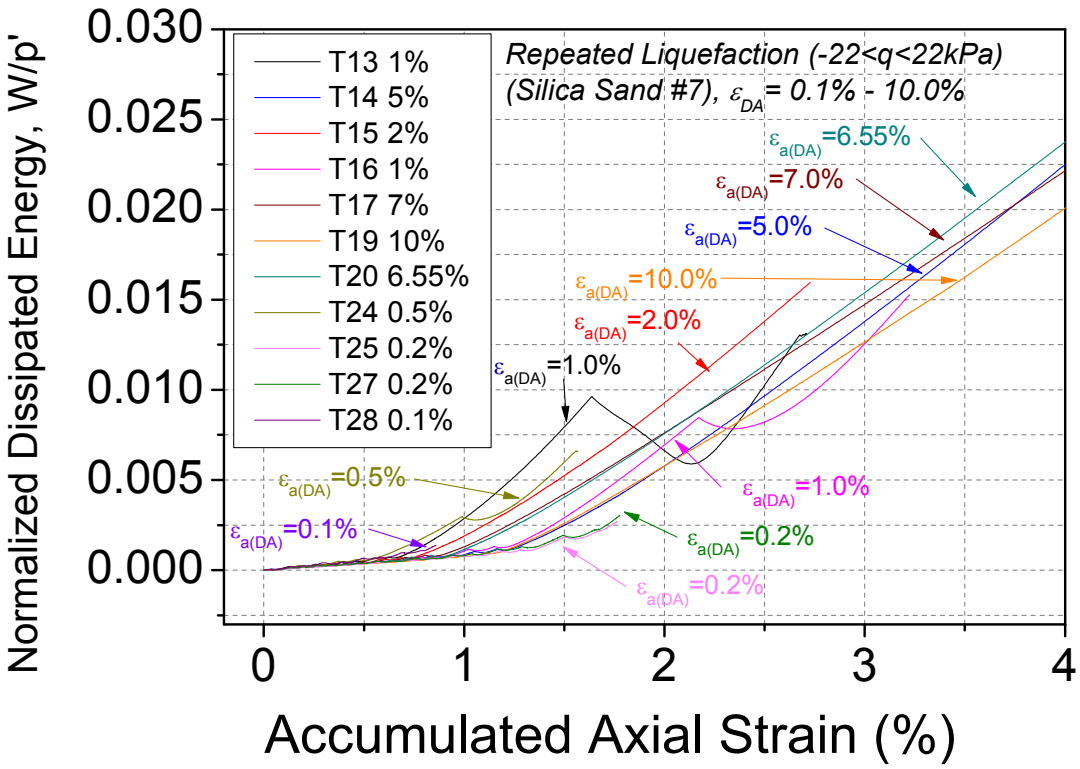

Figure 5-34. Close-up around origin of Relationship between modified dissipated energy and accumulated axial strain

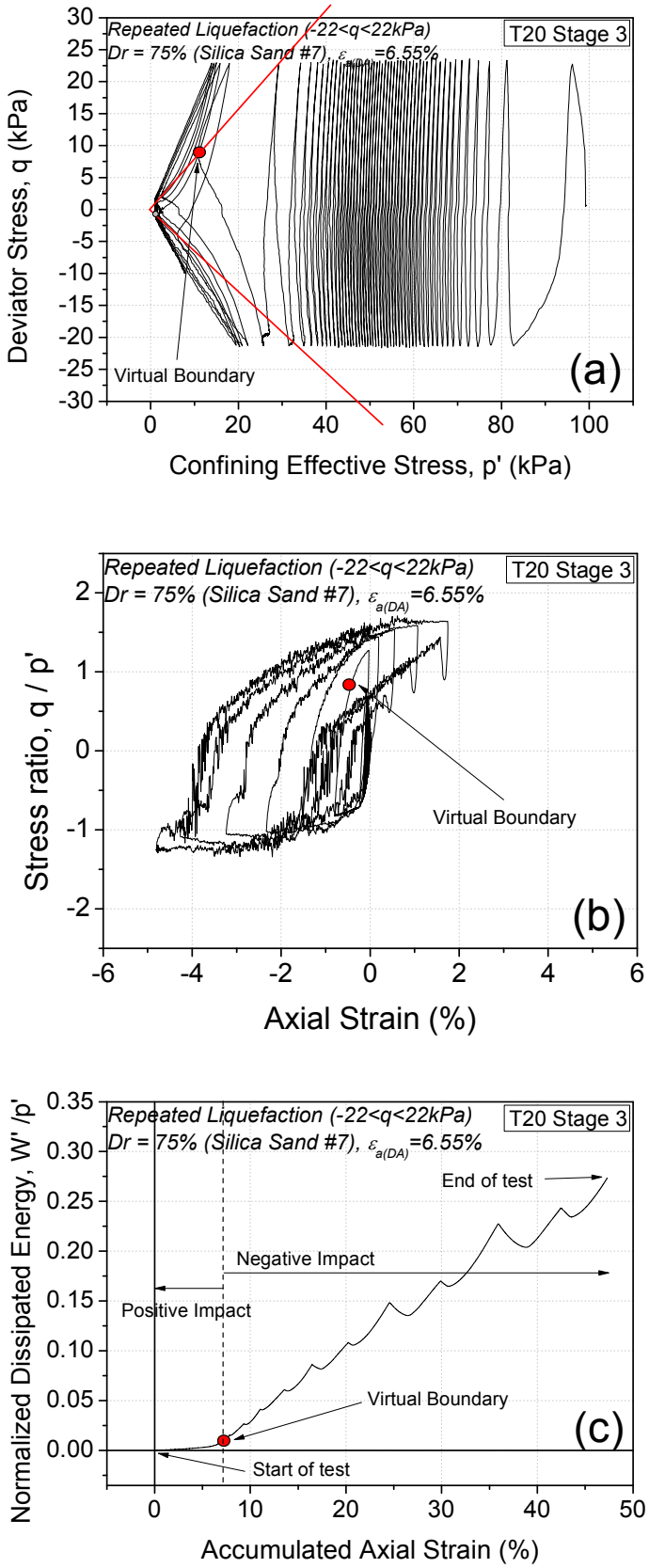

Figure 5-35. Virtual boundary between positive impact and negative impact on (a) effective stress path, (b) relationship of stress ratio and axial strain and (c) relationship of dissipated energy and accumulated axial strain

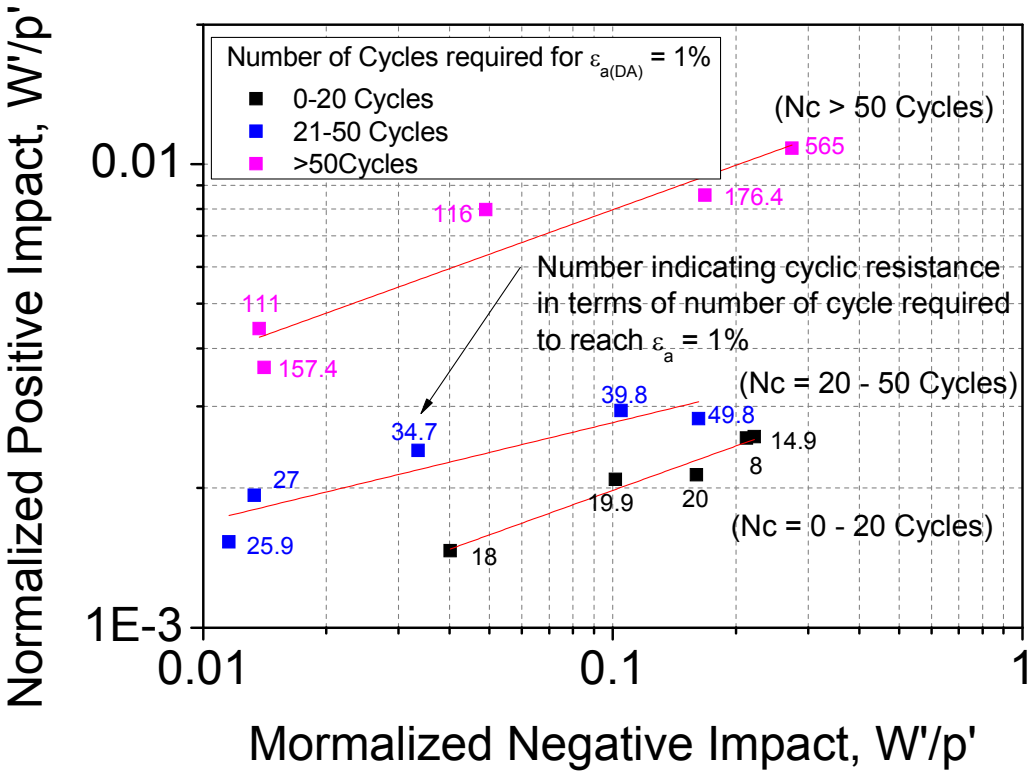

Figure 5-36. Relationship between positive impact and negative impact of the previous liquefaction stage to cyclic resistance of the future liquefaction stage in full logarithmic plot

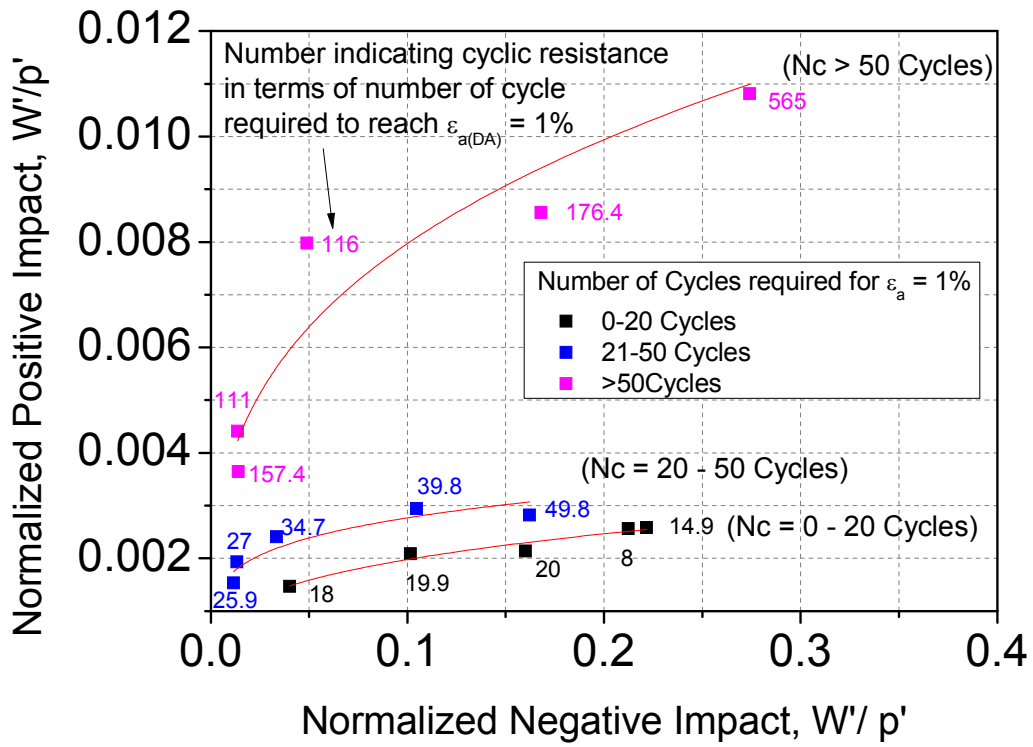

Figure 5-37. Relationship between positive impact and negative impact of the previous liquefaction stage to cyclic resistance of the future liquefaction stage in linear scale

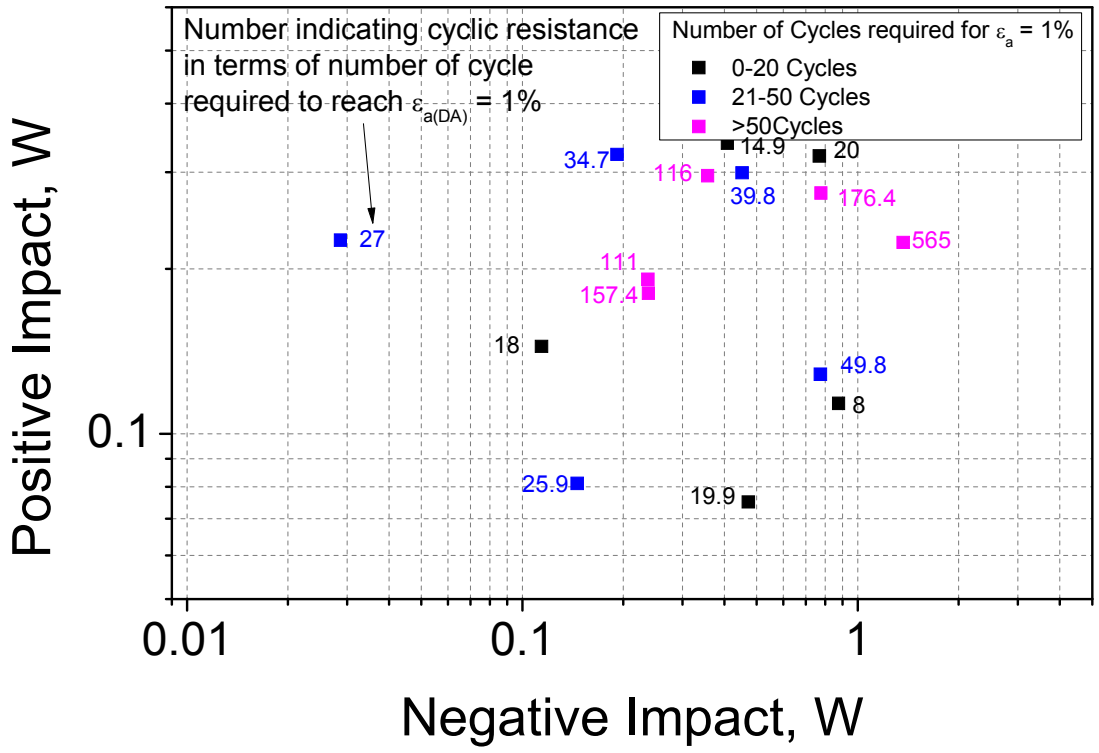

Figure 5-38. Relationship between positive impact and negative impact of the previous liquefaction stage to cyclic resistance of the future liquefaction stage in full logarithmic plot

5.3.5 Modified Energy dissipation of the silica sand in a shaking table to investigate the first two stages of repeated liquefaction behavior

In order to investigate repeated liquefaction in a shaking table apparatus, the method of modified energy approach; i.e. normalized dissipated energy, was employed. As stated previously, there might be an error in measurement of stress; therefore, the stress correction method was also used in shaking table analysis. The calculation was made by means of layers at -10, -20, -30 and -40 cm from the surface by using shear stress and shear strain computed by acceleration data and excess pore water pressure data. An example of stress and effective stress path are shown in *Figure 5-39*. It can be seen clearly that the mean effective stress value was negative during liquefaction giving non-realistic relationship between shear strain and stress ratio which is the ratio of shear stress to current mean effective stress. It must be noted that negative mean effective stress might due to possible sink down of the pore water pressure transducer. Thus, before modified energy calculation, stress was corrected as in triaxial case. The correction factor for example shown in *Figure 5-39* was 0.367 for mean effective stress and -0.033 for shear stress. The corrected stress path was presented in *Figure 5-40* together

with relationship of stress ratio and shear strain. It can be seen that after correction, relationship of stress ratio and shear strain became much more realistic. The examples of corrected typical relationship of each layer are shown in *Figure 5-41* and corresponding effective stress path is given in Figure 5-42. It can be seen that when the ground model did not liquefy, the stress ratio and shear strain was very limited; for example, in the layer 3 and 4. However, in the layer 1 and Layer 2, liquefaction took place resulting in strain softening.

Similar to analysis for triaxial testing, the modified dissipated energy was calculated based on relationship of the stress ratio and shear strain which was divided in to two category; positive impact and negative impact. The total dissipated energy accumulated before the phase transformation line at the point which shown changing behavior from contractive to dilative is defined as positive impact which give advantage to cyclic resistance in the next liquefaction stage. The dissipated energy after that point is accounted as negative impact which promote a decrease in the next liquefaction resistance. *Figure 5-43* shows the virtual boundary between positive impact and negative impact on the mean effective stress path and on the relationship of dissipated energy and accumulated shear strain.

However, in the higher stage of repeated liquefaction in shaking table tests, the shear stresses observed during those tests were not symmetric indicating possible rotation of accelerometers. Examples are given in *Figure 5-44* in terms of effective stress path. It is obvious that positive and negative shear stress were not symmetrical giving difficulty in phase transformation line analysis. It is noted that the reason for unsymmetrical shear stress might due to possible rotation of pre pressure transducers which occurred at high input acceleration resulting in measurement of dynamic water pressure. Thus, only the shaking stages of initial series of repeated liquefaction tests was processed for further analysis.

Further investigation was carried out in the same manner as in analysis of triaxial testing. Relationship of positive impact and negative impact by means of modified dissipated energy generated in previous liquefaction stage to cyclic resistance of the next liquefaction stage as presented in *Figure 5-45*. In the case of shaking table, since the CSR cannot be controlled during shaking, comparing the cyclic resistance in terms of number of cycle to liquefaction may not be appropriate. Thus, the cyclic resistance in the next stage was presented by means of CSR_{eq20} which is CSR_{eq} that causes 1.5% double amplitude shear strain at 20 number of cycles which was calculated based on cumulative damage concept. It can be seen that cyclic

resistance in the next liquefaction stage increased with positive impact regardless of liquefaction stage. With larger negative impact, liquefaction resistance decreased. Virtual lines were drawn on the graph indicating trend line of weak ground model to strong ground model.

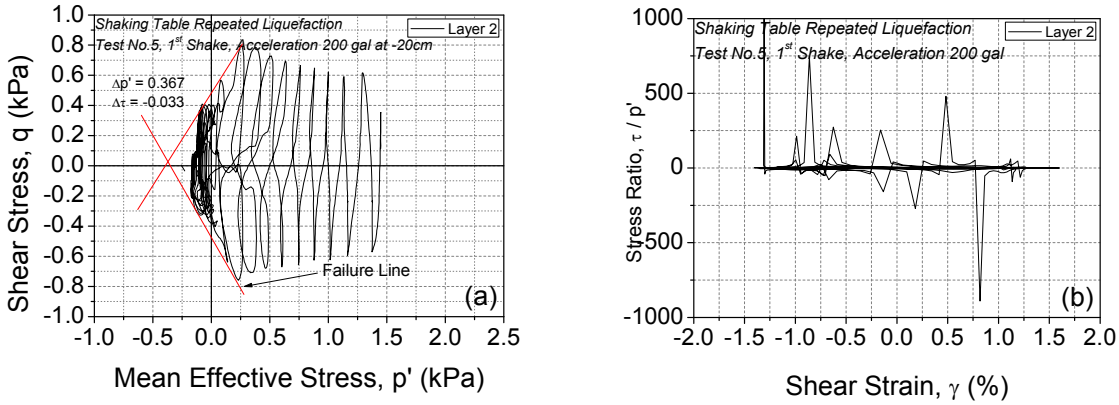

Figure 5-39. (a) effective stress path (b) stress path in term of ratio of shear stress to mean effective stress (T5, Layer2, Shaking stage 1)

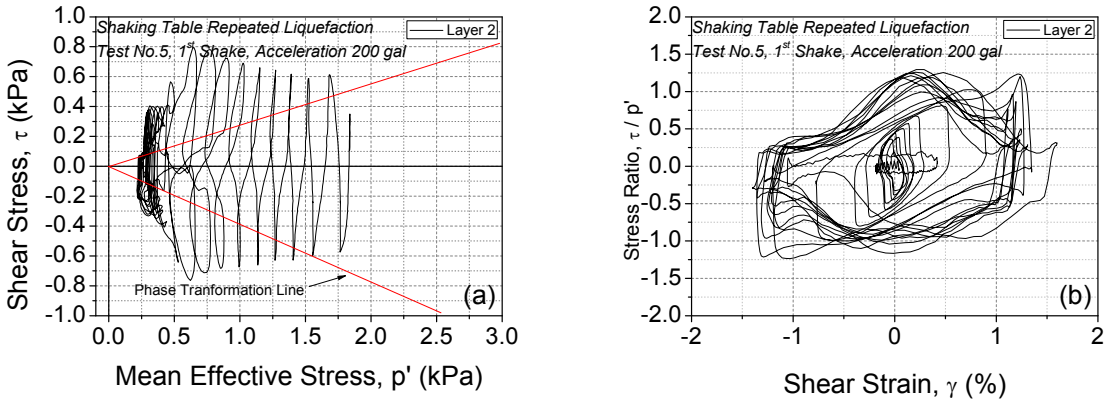

Figure 5-40. (a) Corrected effective stress path (b) corrected stress path in term of ratio of shear stress to mean effective stress (T5, Layer2, Shaking stage 1)

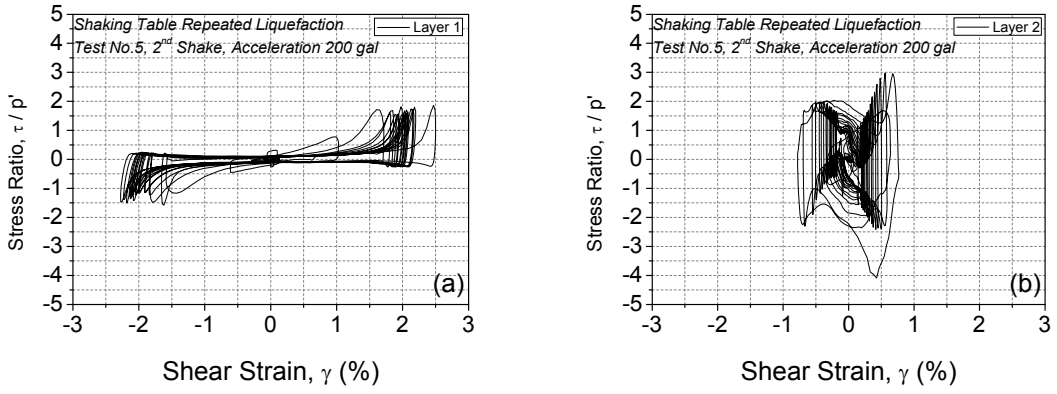

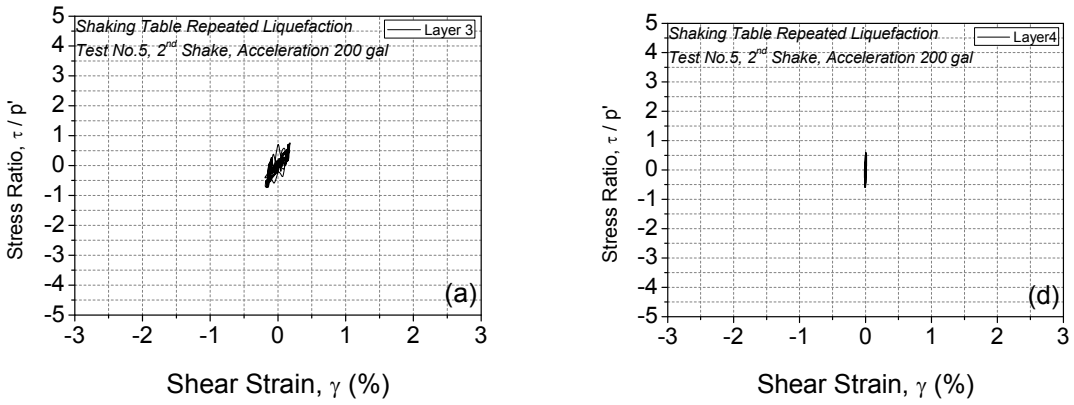

Figure 5-41. Typical relationship between stress ratio of shear stress and mean effective stress to shear strain of (a) Layer 1, (b) Layer 2, (c) Layer 3 and (d) Layer 4 (T5 started at 200 gal stage 2)

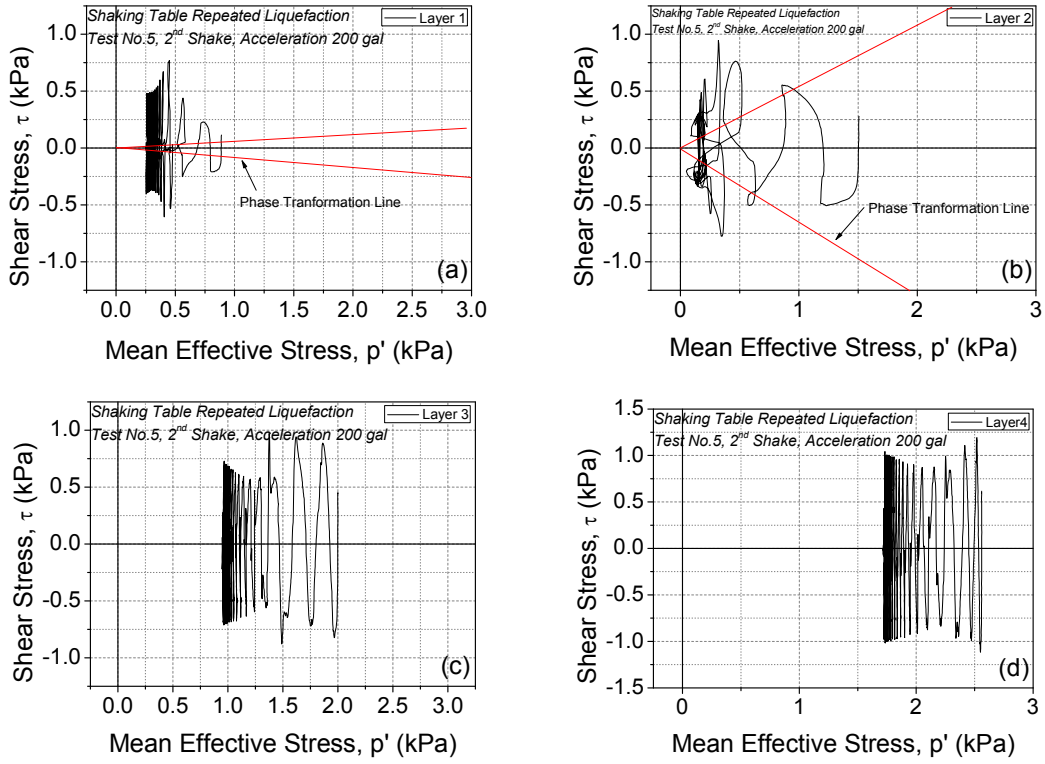

Figure 5-42. Typical mean effective stress path of (a) Layer 1, (b) Layer 2, (c) Layer 3 and (d) Layer 4 (T5 started at 200 gal stage 2)

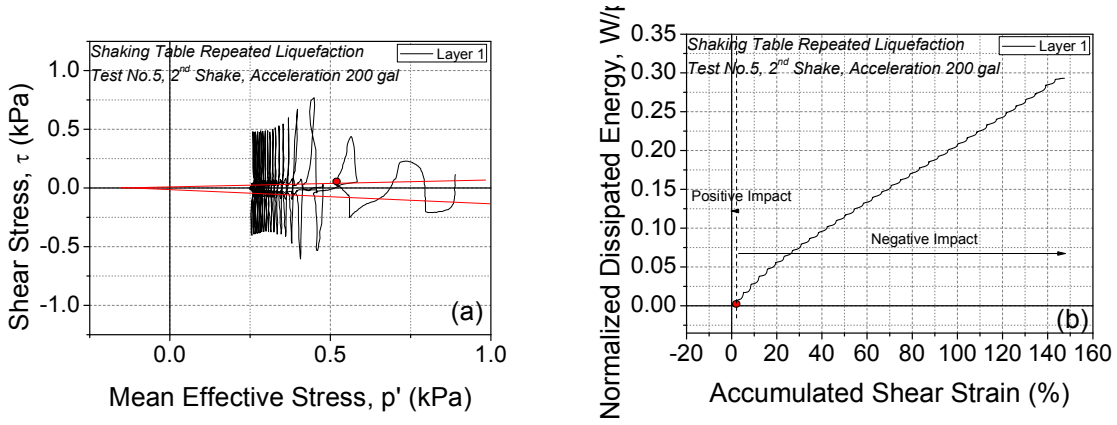

Figure 5-43. Virtual boundary between positive impact and negative impact on (a) the mean effective stress path and (b) on the relationship of dissipated energy and accumulated shear strain

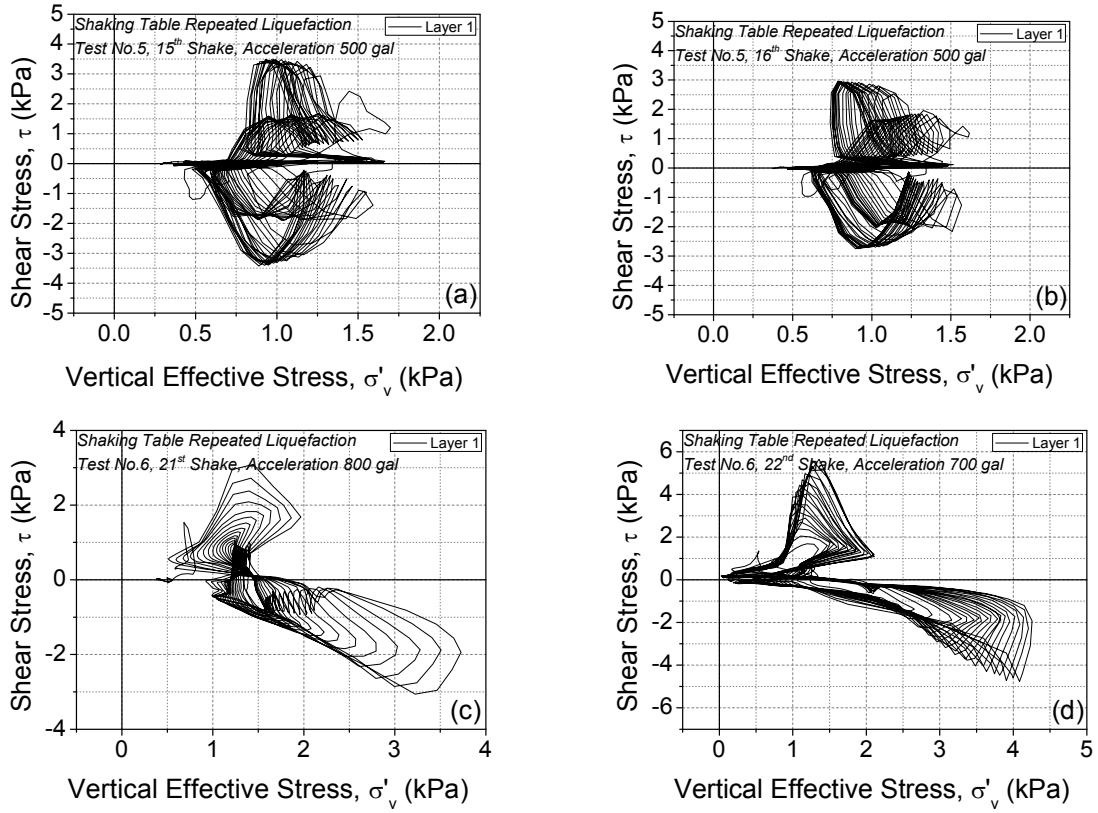

Figure 5-44. Effective stress paths of the shaking table tests at large number of stages (a) T5 Layer1 15th stage @ 500 gal (b) T5 Layer1 16th stage @ 500 gal (c) T6 Layer1 21st stage @ 800 gal and (d) T6 Layer1 22nd stage @ 700 gal

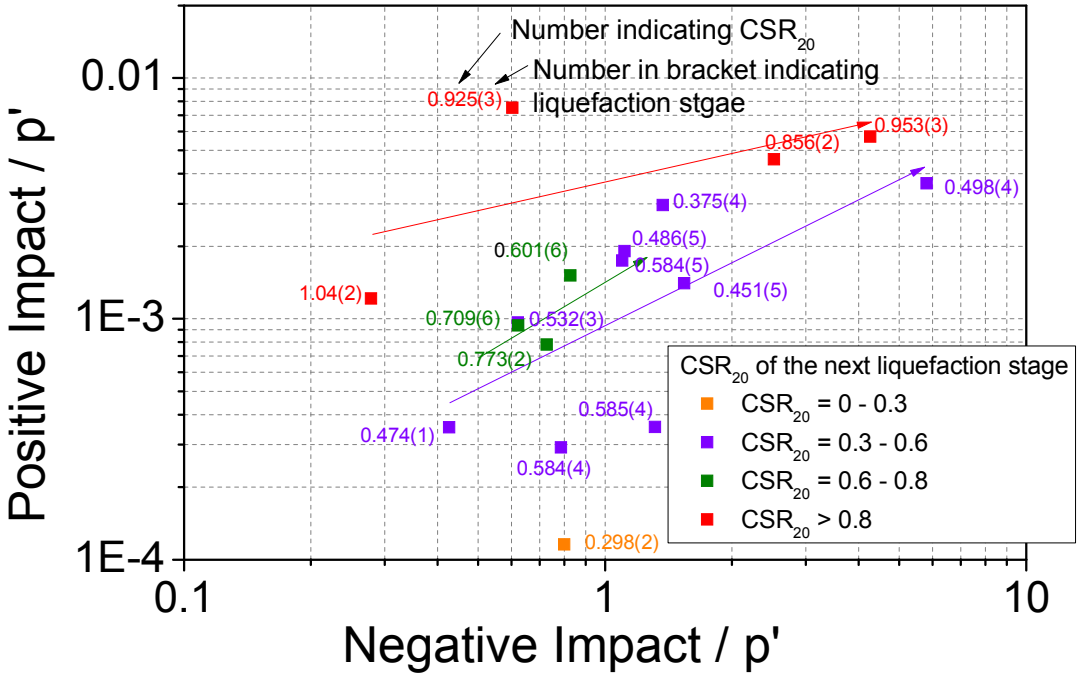

Figure 5-45. Relationship of positive impact and negative impact generated in previous liquefaction stage to cyclic stress ratio at 20 cycles of the next liquefaction stage

5.5 Summary

From the analysis of the Silica sand behavior under repeated liquefaction in triaxial and shaking table apparatus based on energy approach, several conclusion can be made as followed;

1. In the first liquefaction stage, the dissipated energy of specimens subjected to various strain amplitude history is unique in terms of relationship with accumulated strain and excess pore water pressure generation. However, the specimen with lower strain amplitude had smaller total dissipated energy.
2. By using energy analysis during the first two stages liquefaction of specimen with various strain amplitude history, relationship between total dissipated energy of the first liquefaction stage and cyclic resistance of the second liquefaction stage was found. The specimen with 0.2% strain history showed highest cyclic resistance called as threshold strain. This is due to virtual boundary pointed by phase transformation line. The total dissipated energy before the phase transformation line is advantageous to the cyclic resistance in the next stage while the total energy after the phase transformation line causes a decrease in the next liquefaction resistance. The total energy dissipation

specimen with 0.2% strain history was only in positive regime. However, the specimen with 0.1% strain amplitude was also in the positive regime but the total dissipated energy was much lower. Negative impact was produced for the specimens with over 0.5% strain history.

3. With modified dissipated energy method, the correction factors are needed to eliminate errors in monitoring system and also membrane force in triaxial tests. It was found that with correction factors, the stress and strain relationship was much more realistic.
4. Modified dissipated energy was used in this analysis by normalizing by current mean effective stress. By using the modified dissipated energy, relationship between normalized dissipated energy which causes positive impact and negative impact to the next liquefaction resistance was successfully drawn for both triaxial and shaking table tests. It was found that there are unique trend lines for the weak to strong specimen. The weak specimen would have low positive impact with high negative impact. On the other hand, the stronger specimen would have higher positive impact and lower negative impact.

5.6 References

AOYAGI, Y., WAHYUDI, S., KOSEKI, J., SATA, T. and MIYASHITA, Y., 2016 Behavior of Multiple-Liquefaction under Small to Large Strain Levels and Its Analysis Based on Dissipated Energy. JSCE Journal of Earthquake Engineering, 72(4), pp.I_167-I_176

AZEITEIRO, R.J., COELHO, P.A., TABORDA, D.M. and GRAZINA, J.C., 2017. Energy-based evaluation of liquefaction potential under non-uniform cyclic loading. *Soil Dynamics and Earthquake Engineering,* **92**, pp. 650-665.

DIEF, H.M. and FIGUEROA, J.L., 2007. Liquefaction assessment by the unit energy concept through centrifuge and torsional shear tests. *Canadian Geotechnical Journal,* **44**(11), pp. 1286-1297.

FIGUEROA, J.L., SAADA, A.S., LIANG, L. and DAHISARIA, N.M., 1994. Evaluation of soil liquefaction by energy principles. *Journal of Geotechnical Engineering,* **120**(9), pp. 1554-1569.

FINN, W., BRANSBY, P.L. and PICKERING, D.J., 1970. Effect of strain history on liquefaction of sand. *Journal of Soil Mechanics & Foundations Div,* **96**(SM6),.

HENKEL, D. and GILBERT, G., 1952. The effect measured of the rubber membrane on the triaxial compression strength of clay samples. *Geotechnique,* **3**(1), pp. 20-29.

ISHIHARA, K. and OKADA, S., 1982. Effects of large preshearing on cyclic behavior of sand. *Soils and Foundations,* **22**(3), pp. 109-125.

ISHIHARA, K. and OKADA, S., 1978. Effects of stress history on cyclic behavior of sand. *Soils and Foundations,* **18**(4), pp. 31-45.

JAFARIAN, Y., TOWHATA, I., BAZIAR, M., NOORZAD, A. and BAHMANPOUR, A., 2012. Strain energy based evaluation of liquefaction and residual pore water pressure in sands using cyclic torsional shear experiments. *Soil Dynamics and Earthquake Engineering,* **35**, pp. 13-28.

KAZAMA, M., SENTO, N., OMURA, H., TOYOTA, H. and MASAKI, K., 2003. Liquefaction and settlement of reclaimed ground with gravelly decomposed granite soil. *Soils and Foundations,* **43**(3), pp. 57-72.

KAZAMA, M., YAMAGUCHI, A. and YANAGISAWA, E., 2000. Liquefaction resistance from a ductility viewpoint. *Soils and Foundations,* **40**(6), pp. 47-60.

KOKUSHO, T., 2013. Liquefaction potential evaluations: energy-based method versus stress-based method. *Canadian Geotechnical Journal,* **50**(10), pp. 1088-1099.

KOSEKI, J., YOSHIDA, T. and SATO, T., 2005. Liquefaction properties of Toyoura sand in cyclic tortional shear tests under low confining stress. *Soils and Foundations,* **45**(5), pp. 103-113.

NEMAT-NASSER, S. and SHOKOOH, A., 1979. A unified approach to densification and liquefaction of cohesionless sand in cyclic shearing. *Canadian Geotechnical Journal,* **16**(4), pp. 659-678.

OKADA, N. and NEMAT-NASSER, S., 1994. Energy dissipation in inelastic flow of saturated cohesionless granular media. *Geotechnique,* **44**(1), pp. 1-19.

SEED, H.B., MORI, K. and CHAN, C., 1977. Influence of seismic history on liquefaction of sands. *Journal of Geotechnical and Geoenvironmental Engineering,* **103**(Proc. Paper 11318 Proceeding),.

SUZUKI, T. and TOKI, S., 1984. Effects of preshearing on liquefaction characteristics of saturated sand subjected to cyclic loading. *Soils and foundations,* **24**(2), pp. 16-28.

TOWHATA, I. and ISHIHARA, K., 1985. Shear work and pore water pressure in undrained shear. *Soils and foundations,* **25**(3), pp. 73-84.

WAHYUDI, S. and KOSEKI, J., ANALYSIS OF RE-LIQUEFACTION PROPERTIES BASED ON ENERGY APPROACH.

6. Comparison of Triaxial and Shaking Table Tests under Repeated Liquefaction

Contents

Chapter 6 Comparison of Triaxial Test and Shaking Table Test under Repeated Liquefaction

6.1 Introduction

There have been several attempts for comparing the results of shaking table tests with element tests under liquefaction behavior. Ohara and Suzuoka (1972) was one of the pioneer works to compare both test results. The shaking table and triaxial liquefaction tests were conducted with the same relative density of specimens. The comparison was made in terms of relationship cyclic stress ratio (CSR) and number of cycle to cause liquefaction. Higher liquefaction resistance was found in the shaking table apparatus. Another comparisons were also reported by Pathak et al. (2010) and Pathak et al. (2013). They carried out liquefaction tests in shaking table apparatuses and compared the result with element tests results from the literature by the other researchers. The comparison was made together with simple shear tests and torsional shear tests. The observed liquefaction resistance was also highest in shaking table apparatus.

It is generally difficult to compare the liquefaction behavior between element testing and model test. This is because the ground response in model test is normally in irregular pattern whereas uniform pattern in element test and also due to, in some cases, difference in effective stress. Thus, in order to compare, evaluation of equivalent cyclic stress from irregular response is needed. In the past, some researchers directly used uniform input motion (shaking table test) to compute cyclic stress and compare the result. However, the ground response is much different from the input motion as shown in *Figure 6-1*. It can be seen that the input motion is uniform with lower acceleration level. Thus, using input motion for cyclic stress calculation may not be accurate or may be under estimate of cyclic shear stress.

One of the widely used methods for evaluation of equivalent cyclic stress from irregular response was purposed by Seed and Idriss (1971). By using laboratory data, the following equation was purposed.

$$\tau = 0.65 \times \frac{\gamma h}{g} \times a_{max} \times r_d$$

where τ is equivalent cyclic shear stress, γ is soil unit weight, h is depth from ground surface, g is earth gravity acceleration, a_{max} is maximum ground response acceleration and r_d is stress reduction coefficient. Since then, this method has been used by not only many researchers but also practical engineers. This method was further modified for liquefaction potential evaluation (Iwasaki et al., 1981). Some of the comparisons were made based on this method of cyclic stress evaluation.

However, from the equation, it can be seen that the computed equivalent cyclic shear stress is dependent of time, number of cycle, repeated liquefaction conditions and only consider peak acceleration. Some of researches suggested that the method purposed by Seed et al. (1983) has some limitations. Kokusho et al. (2015) reported that by using simplified procedure to evaluate liquefaction potential of the liquefaction site in Hokaaido was found to be underestimate compared to energy-base method. In this case, the maximum ground acceleration was observed to be very low of about 54 gal but long duration which also caused liquefaction. With simplified method, the site was considered safe from liquefaction with the given acceleration history which was not realistic. Another report was done by MLIT (2011) to reinvestigate liquefaction damage of 112 liquefaction sites after 2011 Tohoku Earthquake in Japan using the method based on the one purposed by Seed and Idriss (1971) and Iwasaki et al. (1981). The analysis showed that this method overestimate safety factor. There were 35 site which did not liquefy during the Earthquake but according to the method the safety factor was less than 1.0.

In this thesis, by cumulative damage concept and combining energy approach, the results comparison between triaxial test and shaking table test under repeated liquefaction was carried out. The method of cumulative damage concept might be more accurate in evaluation of equivalent stress ratio. Tatsuoka et al. (1986) showed that by using the cumulative damage concept, the results of stress amplitude and number of cycle relationship agreed well with the measured results during Tokachi-Oki earthquake. Whereas, the energy approach could possibly eliminate the effect of confining pressure.

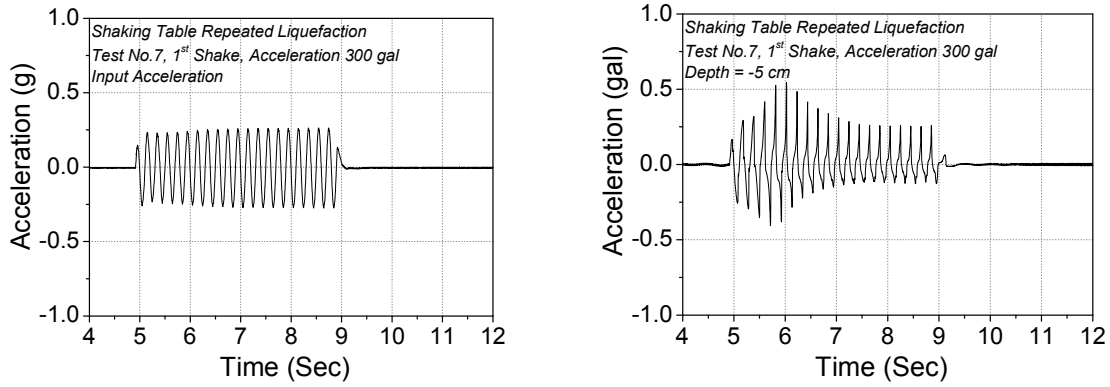

Figure 6-1. (a) Input acceleration (b) ground response acceleration

6.2 Comparison in terms of cyclic stress ratio (CSR)

The comparison between triaxial test and shaking table test was carried out in terms of cyclic stress ratio and number of cycle to reach 1% double amplitude axial strain for triaxial test and 1.5% double amplitude shear strain for shaking table test. It is noted that the CSR of shaking table test was computed using cumulative damage concept marked as CSReq (equivalent CSR). *Figure 6-2* shows comparison liquefaction curve of the first liquefaction stage between shaking table test and triaxial test. It can be seen that cyclic resistance observed in shaking table test was higher than that in triaxial test especially although the result of shaking table test seemed to be scatter as also reported in literature. It is noted that for the case of T6 which was started at input acceleration of 200 gal, the ground model did not liquefy. Thus, the result is excluded since there might be possible effects of pre-shearing.

For the second liquefaction stage, the comparison is given in *Figure 6-3* together with the first liquefaction. It is noticeably that second liquefaction resistance in shaking table test was also larger than that in triaxial test. The different in liquefaction resistance between the two tests seemed to be much more than observed in the first liquefaction stage. However, in some cases, a decrease in CSReq was observed; for example, T5 Layer 1 and T7 Layer 1. This behavior was different from traxial testing where all the tests at various CSR value showed an increase in strength. Apart from those two example, CSReq of all the layers increased in the second stage indicating stronger liquefaction resistance. In addition, the increase in liquefaction resistance observed in shaking table tests was much larger than in triaxial tests. The comparison of liquefaction stage 1 to 4 is given in *Figure 6-4*. It can be seen that the data of shaking table

test was scatter; however, it is still clear that the observed liquefaction resistance for all stages was much higher than in the triaxial test.

Further analysis for the rest of shaking stages of shaking table tests (T4, T5, T6 and T7) are given in *Figure 6-5*, *Figure 6-6*, *Figure 6-7* and *Figure 6-8*. It can be seen from every test that during initial repeated liquefaction test, CSReq are relatively low. At higher input acceleration, CSReq increased sharply indicating much stronger liquefaction resistance.

The possible reasons for higher liquefaction resistance in shaking table test are contributed to several factors;

1. Confining pressure condition

   The confining pressure in triaxial test was 100 kPa for all specimens. However, the confining pressure in shaking table was relatively much lower compared to triaxial tests. The initial mean effective stress was ranging approximately from 0.9 kPa to 2.6 kPa depending on the depth. Koseki et al. (2005) suggested that liquefaction resistance can be higher in the case of lower confining pressure due to interlocking of particles.

2. Degree of saturation

   The specimens in triaxial tests were all saturated using vacuum method. Degree of saturation was checked by confirming B-value to be over 0.95. On the other hand, in shaking table, saturation was done by just letting water in soil container through a pipe attached at the bottom. There was no confirmation of B-value. In such a case, it is believed that the degree of saturation in shaking table was much lower than triaxial. Due to lower degree of saturation, higher liquefaction resistance can be expected.

3. Drainage Condition

   It was fully undrained condition in triaxial test while in shaking table test, it was partially drained through surface of ground model. Due to this partially drainage condition, during shaking, excess pore water pressure which was generated from cyclic loading can be dissipated.

However, this comparison did not take mean effective stress in to the account as there was significant difference in mean effective stress of shaking table and triaxial tests. The mean

effective stress in triaxial was 100 kPa for every test while in shaking table was varies depending on the depth of each layer ranging from approximately 0.9 - 2.6 kPa assuming that the coefficient of earth pressure at rest is 0.5. In order to overcome this difference, modified dissipated energy which was describe in Chapter 5 was employed and discussed in the next section.

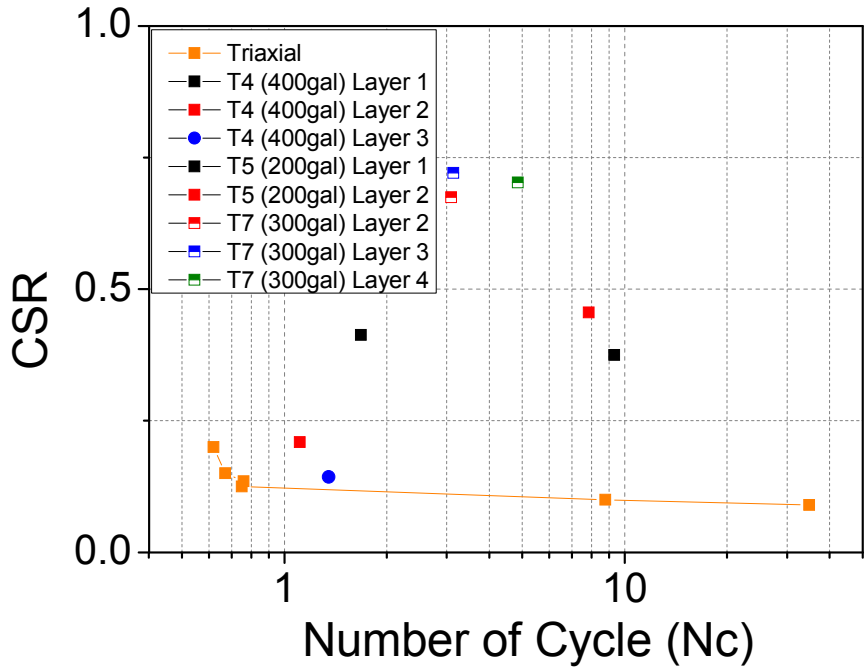

Figure 6-2. Comparison liquefaction curve in the first liquefaction stage between shaking table test and triaxial test

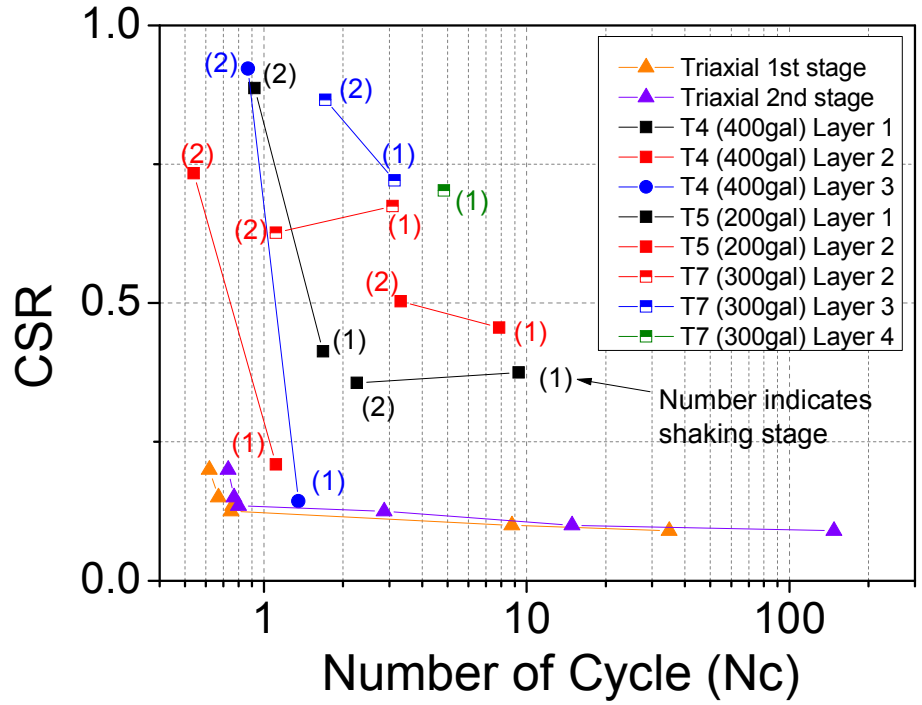

Figure 6-3. Comparison liquefaction curve in the first and second liquefaction stage between shaking table test and triaxial test

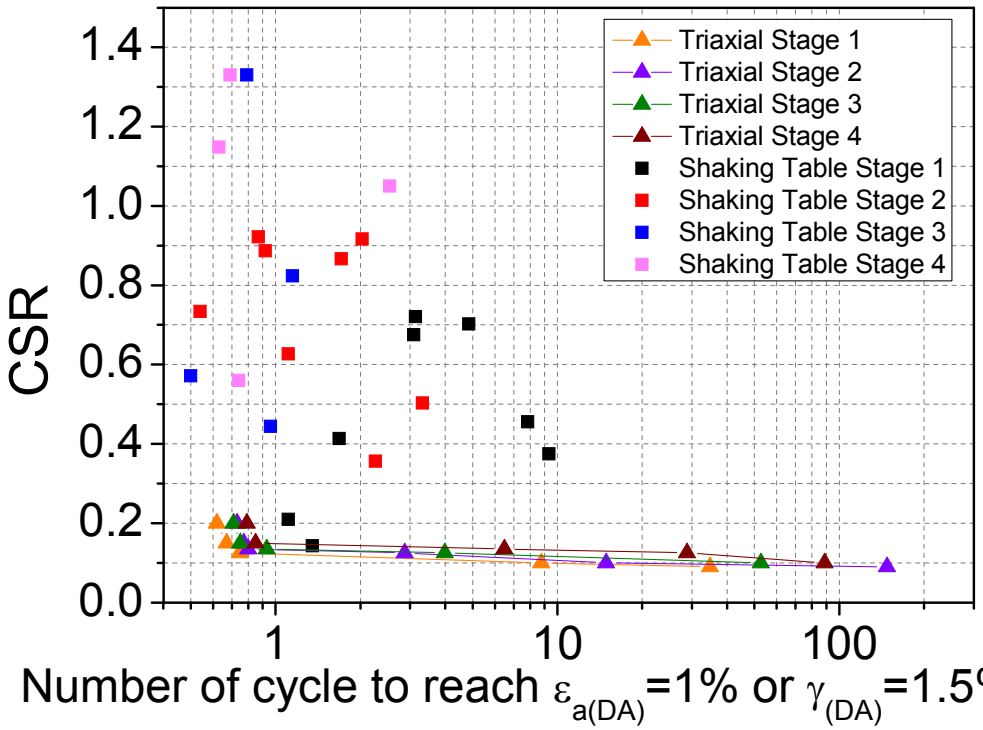

Figure 6-4. Comparison liquefaction resistance from liquefaction stage 1 to stage4 between shaking table test and triaxial test

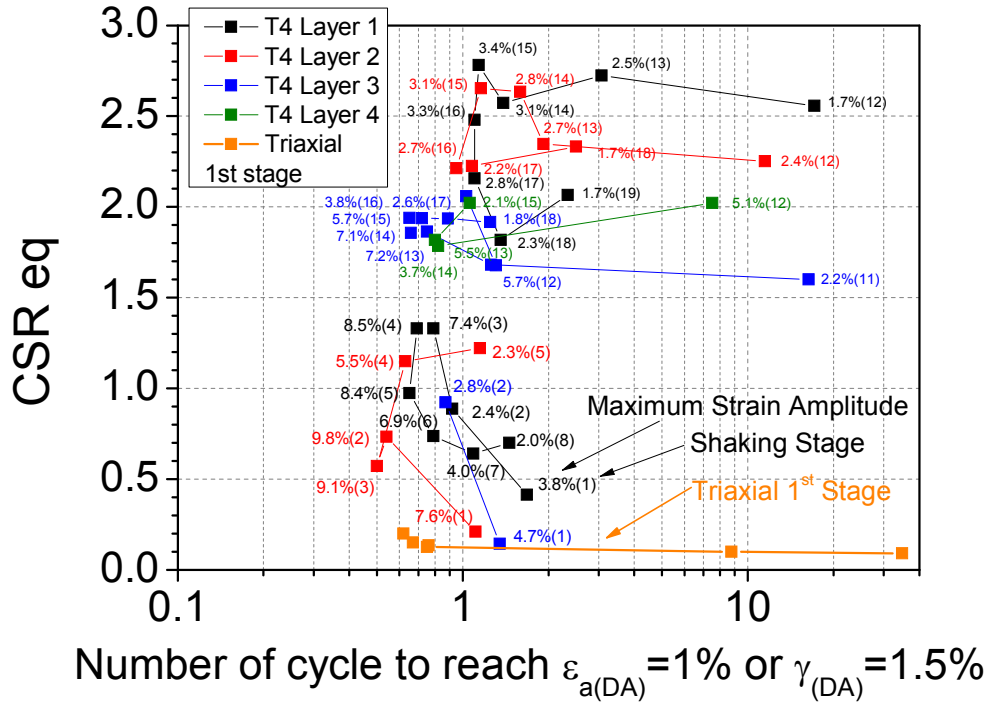

Figure 6-5. Comparison liquefaction curve between shaking table test (T4 started from 400 gal) and the first triaxial liquefaction test

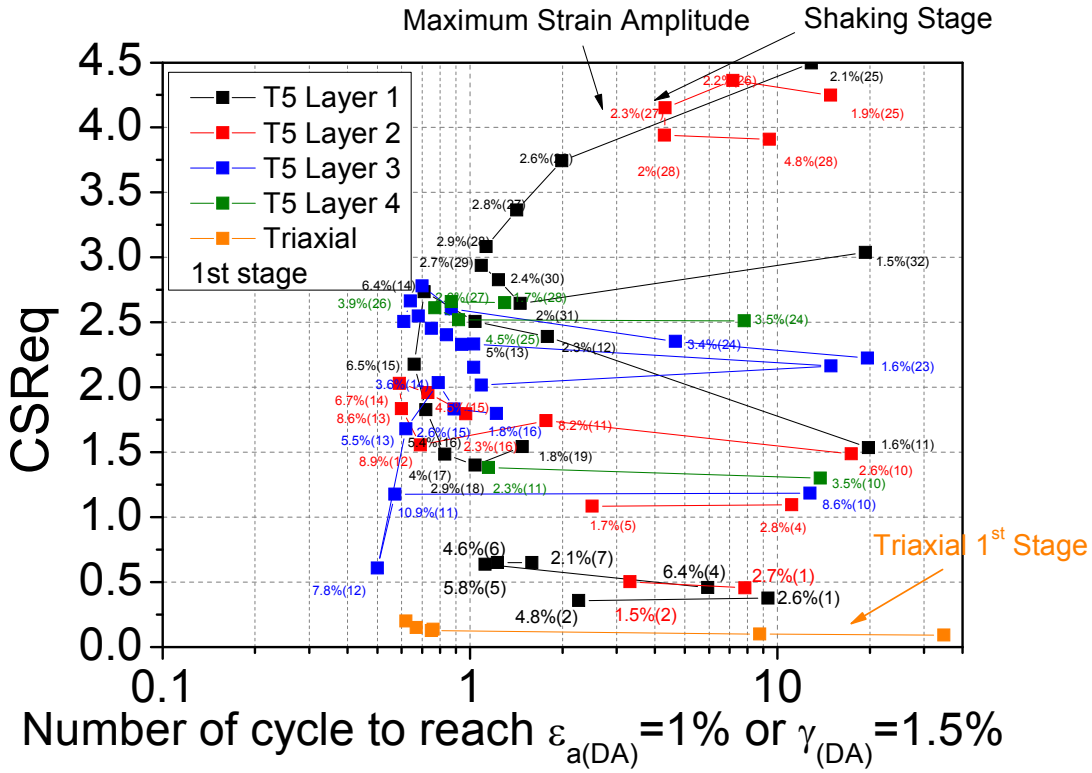

Figure 6-6. Comparison liquefaction curve between shaking table test (T5 started from 200 gal) and the first triaxial liquefaction test

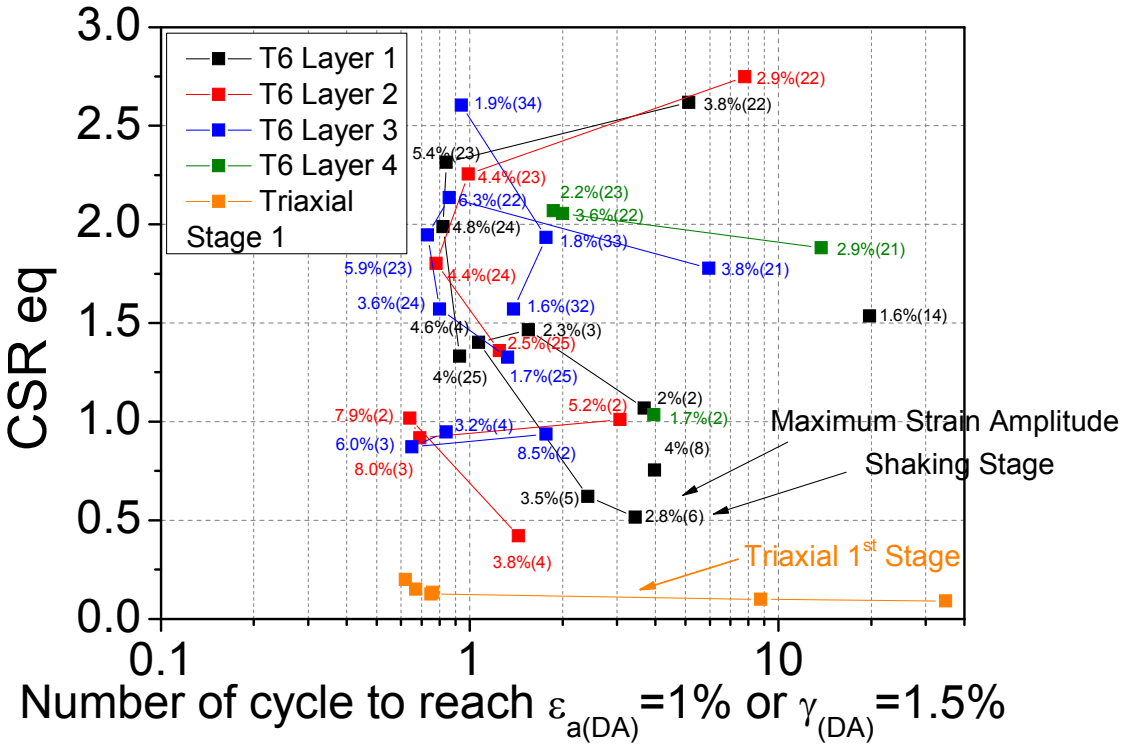

Figure 6-7. Comparison liquefaction curve between shaking table test (T6 started from 200 gal) and the first triaxial liquefaction test

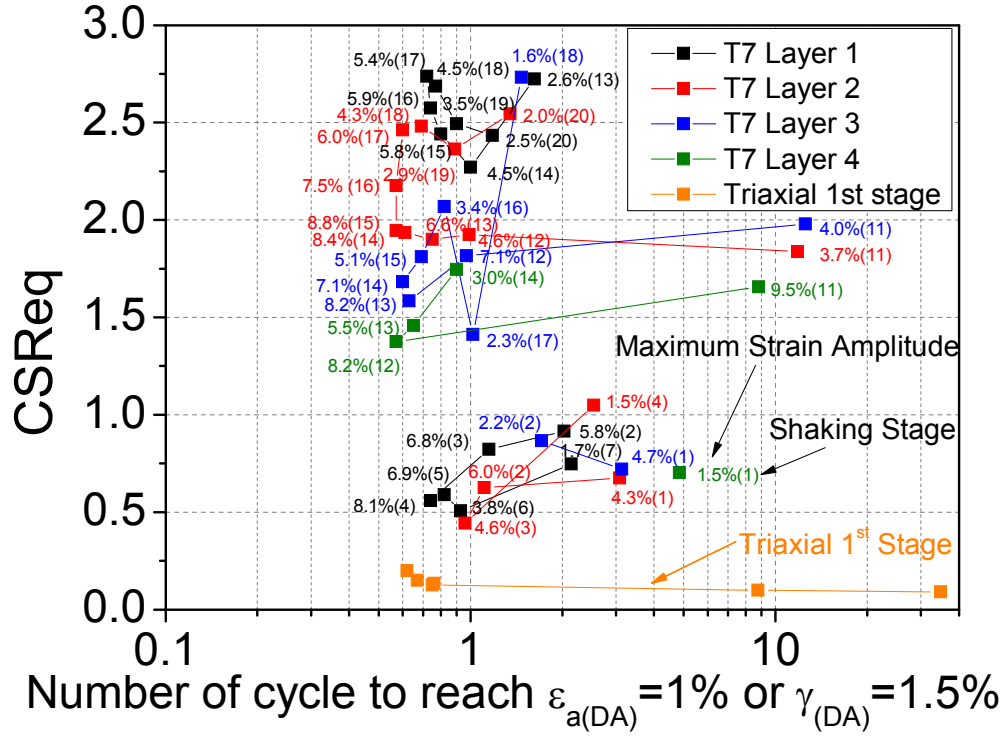

Figure 6-8. Comparison liquefaction curve between shaking table test (T7 started from 300 gal) and the first triaxial liquefaction test

6.3 Comparison in terms of dissipated energy

As there was a difference in confining pressure between two types of test. The comparison between triaxial test and shaking table test was carried out in terms of modified dissipated energy which causes positive impact and negative impact in the previous liquefaction stage with the next stage liquefaction resistance. In chapter 5, the relationship of dissipated energy and the future liquefaction resistance was well established for both tests and the method of calculation for the impacts using energy approach was already detailed described.

By combining the results together, relationship of positive impact, negative impact generated during previous liquefaction stage and cyclic resistance of the next liquefaction stage (in terms of number of cycle to reach 1% double amplitude axial strain or 1.5% double amplitude shear strain) is presented in *Figure 6-9*. It can be seen that the result of shaking table seems to be corresponding with the result of triaxial tests. With much lower number of cycle to reach target strain, most of the results of shaking table tests lied below the triaxial test results. However, the CSR used in triaxial was 0.11 for all cases, but the CSR in shaking table was different between each test and each layer. Thus, CSR between these two tests was not the same. The comparison was then made in terms of CSR which caused liquefaction at 20 cycles marked as CSR_{20}.

The relationship of the modified dissipated energy which causes negative and positive impact in the previous liquefaction stage and the next stage liquefaction resistance in terms of CSR_{20} is given in *Figure 6-10*. As discussed previously, in general, under the same negative impact, the weak specimen should show lower positive impact. On the other hand, the strong specimen should show larger positive impact. The independent results of both tests seemed to be corresponding with the statement above. However, after combing the results together, the results of triaxial tests lied above that of shaking table tests although the liquefaction resistance in terms of CSR_{20} observed in triaxial tests was much lower as discussed in the previous section. This indicates inconsistence of the results from two types of test using the energy approach.

There are several possible reasons for inconsistence of dissipated energy between triaxial and shaking table test. The first one is the boundary between the positive impact and negative

impact. In this thesis, the phase transformation line was used as a virtual boundary as it can distinguish the change in soil behavior. The total dissipated energy before the stress path crosses the phase transformation line (contractive behavior) was accounted as positive impact where the total dissipated energy after that (dilative behavior) was accounted as negative impact. This is because the behavior before touching the phase transformation line is contractive behavior and after the boundary, the soil behaves in dilative manner. However, since in cyclic loading test, the stress path, after first touches the phase transformation line, crosses the line again and again as can be seen in the *Figure 6-11* and *Figure 6-12* for both triaxial and shaking table test respectively. This indicates that there is still a change in soil behavior after passing the phase transformation line. Thus, it might be more accurate to also distinguish the contractive behavior out of dilative behavior after passing the boundary marked as shadow in both figures. The stress path of shaking table test touches the phase the boundary much faster than the triaxial stress path. This may causes overestimation of negative impact together with underestimation of positive impact in shaking table test. It may also overestimate and underestimate impacts of triaxial test results; however, the proportion is largely different. Second possible reason is the difference in confining pressure. It had been proven that the lower confining pressure results in lower dissipated energy (Figueroa et al., 1994). In this study, the dissipated energy was normalized by current mean effective stress. However, there might still be possible effect of different confining pressure.

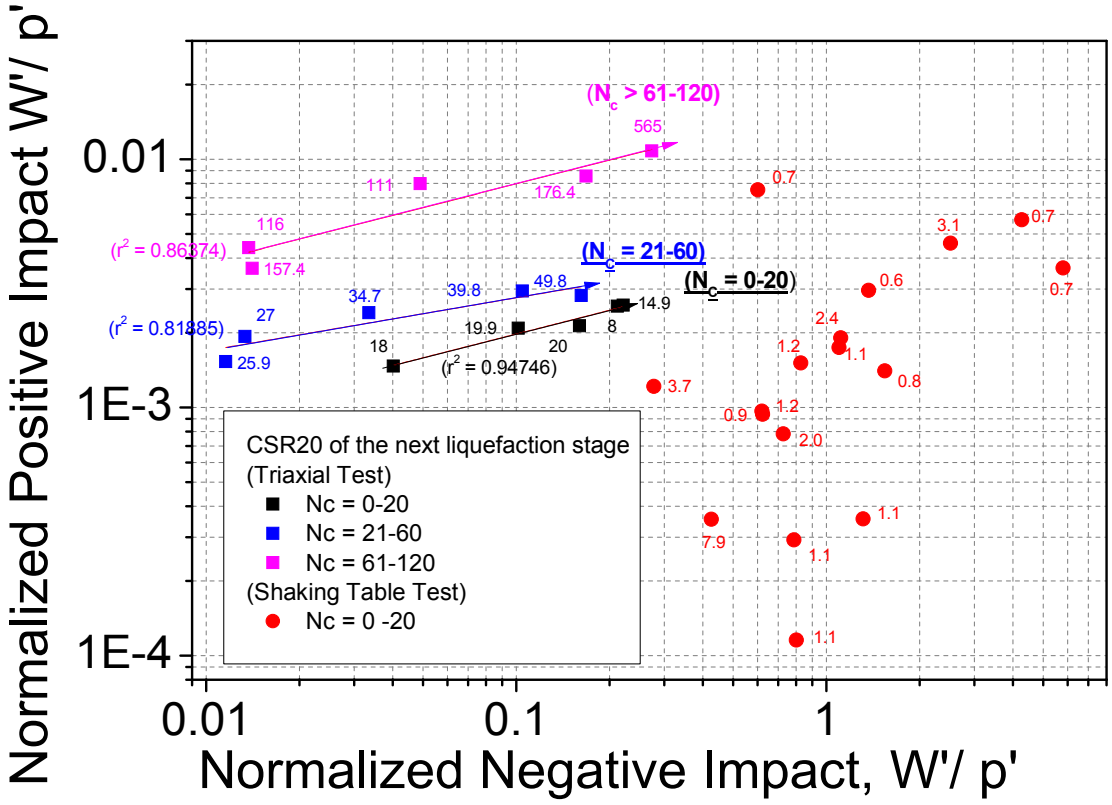

Figure 6-9. Relationship between positive impact and negative impact to the next liquefaction resistance in term of number of cycle

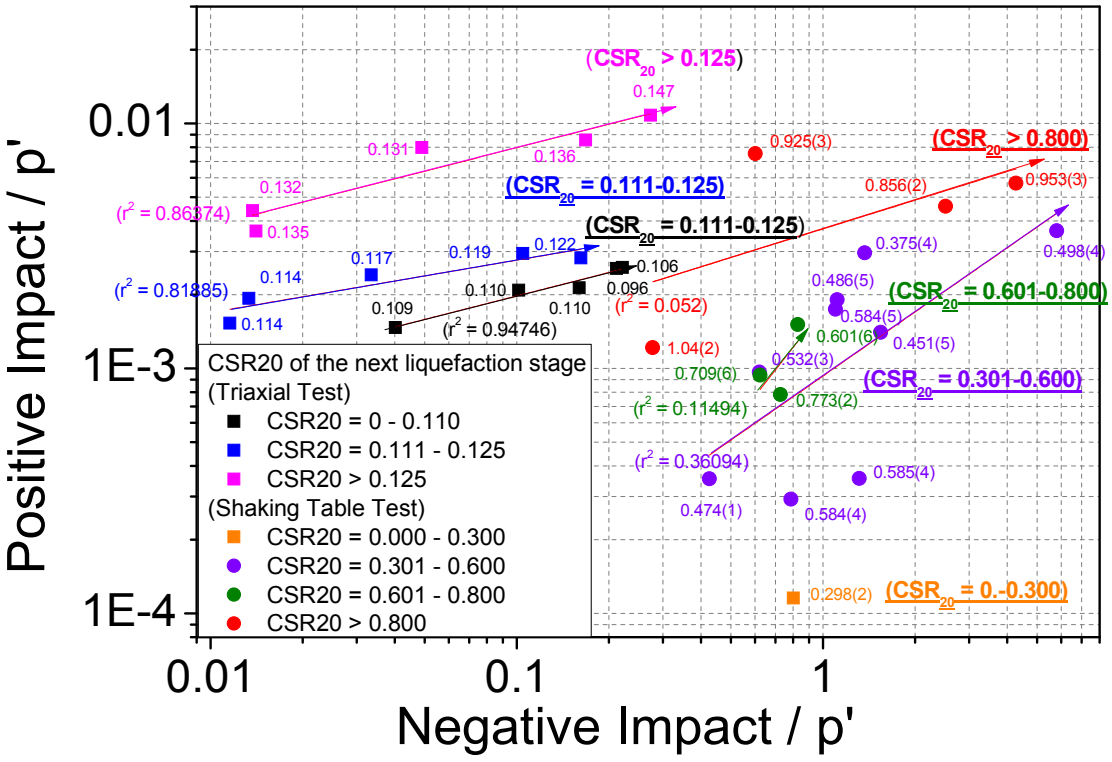

Figure 6-10. Relationship between positive impact and negative impact to the next liquefaction resistance in term of CSR which caused liquefaction at 20 cycles

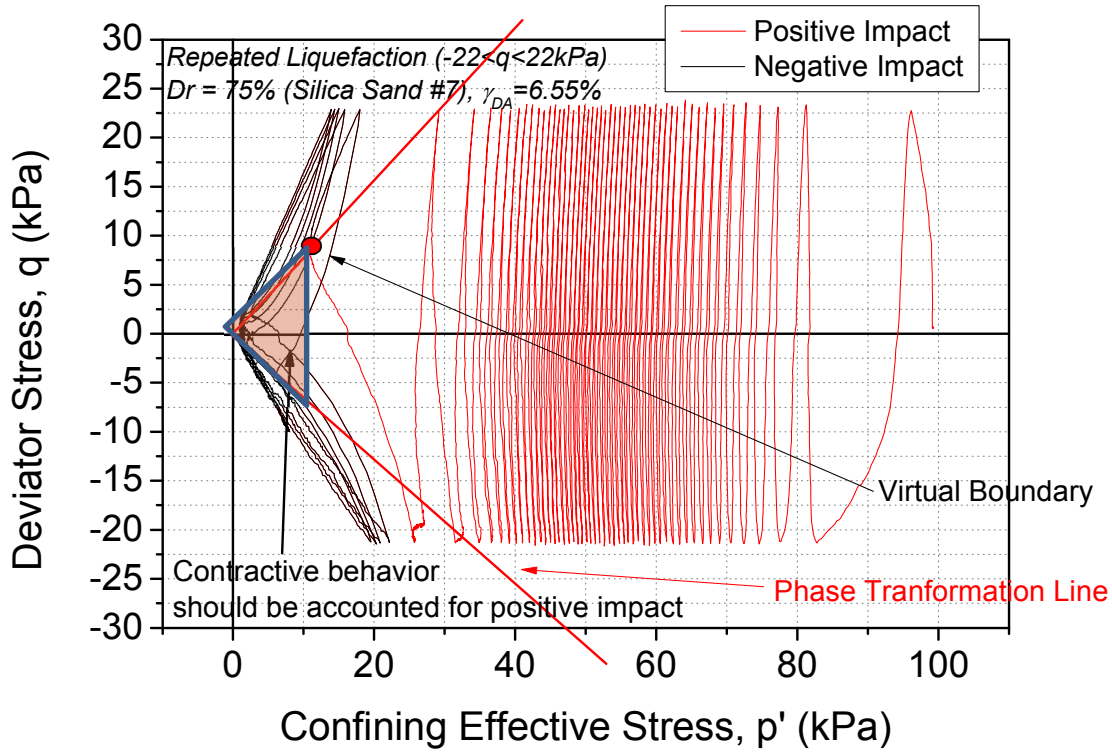

Figure 6-11. Effective stress path of specimen in triaxial test

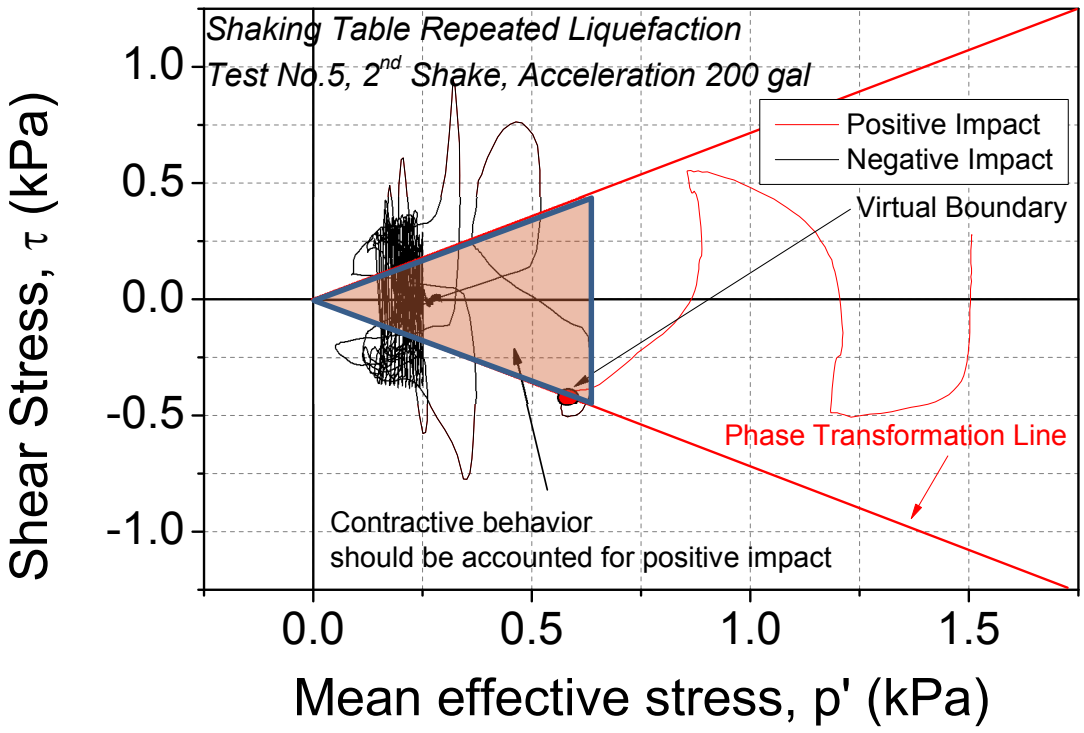

Figure 6-12. Effective stress path of ground model in shaking table test

6.4 Summary

The repeated liquefaction tests were carried out in triaxial and shaking table apparatus. The results of both test were then compared using the method of cumulative damage concept and energy approach. The several conclusions can be drawn as follow;

1. By converting irregular stress ratio into equivalent stress ratio, relationship between cyclic stress ratio and number of cycle to reach 1% double amplitude axial strain and 1.5% double amplitude shear strain for shaking table and triaxial test results can be drawn. It was found that the liquefaction resistance in shaking table test in the first to forth liquefaction stage was higher than that in the triaxial test. Also, the larger increase in liquefaction resistance was found in shaking table test.
2. The possible reasons for higher liquefaction resistance in shaking table test are low degree of saturation, partially drainage condition through ground model surface and lower confining pressure.
3. The further comparison was made using energy approach. The relationship of the modified dissipated energy which causes negative and positive impact in the previous liquefaction stage and the next stage liquefaction resistance in terms of CSR_{20} was drawn for both triaxial and shaking table test. In general, under the same negative impact, the weak specimen should show lower positive impact. On the other hand, the strong specimen should show larger positive impact. However, the comparison showed lower positive and higher negative impact in shake table test result indicating inconsistent of both test since the higher liquefaction resistance was found in shaking table. Possible reason may due to overestimation of negative impact and underestimation of positive impact.

6.5 References

FIGUEROA, J.L., SAADA, A.S., LIANG, L. and DAHISARIA, N.M., 1994. Evaluation of soil liquefaction by energy principles. *Journal of Geotechnical Engineering,* **120**(9), pp. 1554-1569.

IWASAKI, T., TOKIDA, K. and TATSUOKA, F., 1981. Soil liquefaction potential evaluation with use of the simplified procedure.

KOKUSHO, T., MIMORI, Y. and KANEKO, Y., 2015. Energy-Based Liquefaction Potential Evaluation and its Application to a Case History, *Proc. 6th International Conference on Earthquake Geotechnical Engineering, Christchurch, NZ, Paper* 2015, pp. 24.

KOSEKI, J., YOSHIDA, T. and SATO, T., 2005. Liquefaction properties of Toyoura sand in cyclic tortional shear tests under low confining stress. *Soils and Foundations,* **45**(5), pp. 103-113.

MILT (2011) 「液状化対策技術検討会議」検討成果 (In Japanese)

OHARA, S., and SUZUOKA, N., 1972. The Results of Experiment on the Liquefaction of Saturated Sands with a Shaking Box: Comparison with Other Methods. *Soils and Foundations*. 12(4). PP.85-94. (In Japanese)

PATHAK, S., DALVI, R. and KATDARE, A., 2010. Earthquake Induced Liquefaction using Shake Table Test.

PATHAK, S., KSHIRSAGAR, M. and JOSHI, M., 2013. Liquefaction triggering criterion using shake table test. *Int.J.Eng.Tech,* **5**, pp. 4439-4449.

SEED, H.B., IDRISS, I. and ARANGO, I., 1983. Evaluation of liquefaction potential using field performance data. *Journal of Geotechnical Engineering,* **109**(3), pp. 458-482.

SEED, H.B. and IDRISS, I.M., 1971. Simplified procedure for evaluating soil liquefaction potential. *Journal of Soil Mechanics & Foundations Div,* .

TATSUOKA, F., MAEDA, S., OCHI, K. and FUJII, S., 1986. Prediction of cyclic undrained strength of sand subjected to irregular loadings. *Soils and Foundations,* **26**(2), pp. 73-90.

7. Conclusions and Recommendations

Contents

Chapter 7 Conclusions and Recommendation

7.1 Conclusion

There are three main objectives of this study which consists of investigation of the Silica sand repeated liquefaction behavior in triaxial and shaking table apparatuses and comparison of the results of both tests using two methods which were cumulative damage concept and energy approach.

7.1.1 Repeated liquefaction behavior of the Silica sand in triaxial apparatus

There were in total three test series conducted in the triaxial apparatus to investigate the effect of cyclic stress ratio, the effect of strain amplitude and the effect of small strain amplitude. The first test series was done by using different cyclic stress ratio and constant strain amplitude while the other two test series were carried out using constant cyclic stress ratio but various strain amplitude. It must be noted that the repeated liquefaction test in triaxial apparatus was limited up to about 4 stages due to membrane wrinkle. Based on the outcomes the following conclusions can be made.

7.1.1.1 The effect of cyclic stress ratio

1. Regarding relative density during repeated liquefaction test, the cyclic stress ratio applied to the specimens did not affect the change in relative density during excess pore water dissipation and reconsolidation. The change in relative density of specimens with various cyclic stress ratio but same strain amplitude was found to be similar.
2. Soil resistance against repeated liquefaction increased with liquefaction stages for all cyclic stress ratios ranging from 0.90 – 0.20. Similar trend of relationship between cyclic stress ratio and liquefaction resistance in terms of number of cycle to reach 5% double amplitude axial strain was found to be similar among liquefaction stages.

7.1.1.2 The effect of strain amplitude

1. Strain amplitude history greatly affected the relative density change during excess pore water pressure dissipation and reconsolidation in each stage of liquefaction. The specimen subjected to larger axial strain showed larger increase in relative density.
2. Strain amplitude history did not only affect relative density change but also reliquefaction resistance. It was found that the specimens subjected to low axial strain amplitude (<2%) showed high repeated liquefaction resistance although their relative density were lower than the specimens which were subjected to high axial strain amplitude. However, random increasing trend of repeated liquefaction resistance was found among the specimens with higher 5% axial strain amplitude history.

7.1.1.3 The effect of cyclic stress ratio

1. Among the specimens subjected to 0.1%, 0.2% and 0.5% axial strain amplitude, it was pointed out that the specimens subjected to 0.2% axial strain history showed the highest reliquefaction resistance. It can be said that 0.2% axial strain amplitude is the threshold strain for silica sand in the triaxial apparatus. This behavior can be describe using energy approach.

7.1.2 Repeated liquefaction behavior of the Silica sand in shaking table apparatus

Repeated liquefaction tests were carried out on the silica sand in shaking table apparatus. There were in total 2 types of testing program which were the test with increase in acceleration and test with decrease acceleration. Unlike the triaxial test, there is no limitation of number of liquefaction in shaking table test. Thus, the repeated liquefaction test can be carried out up to the capacity of shaking table. From the results of the tests, the following conclusions can be drawn.

1. Liquefaction resistance in terms of number of cycle to reach target strain amplitude was found to be higher than the second liquefaction stage. Besides, it was also discovered that during further repeated liquefaction series at higher input acceleration, this behavior was also discovered.

2. The effect of strain amplitude on the relative density change during excess pore water pressure dissipation and reconsolidation was also observed. With the larger input acceleration which generally causes larger strain amplitude, there was also larger change in relative density. However, when the repeated liquefaction at the same input acceleration tended to stop, relative density change was limited. Besides, the final relative density was found to be approximately 80% where the ground model stopped to liquefy regardless of strain history of liquefaction history.
3. Based on repeated liquefaction test results, a brief method of future liquefaction based on current and previous maximum strain amplitude was purposed. It was found that when the shear strain amplitude of the previous stage is larger than the current stage, cyclic resistance in the next stage can be expected to be lower. On the other hand, if the previous shear strain amplitude is lower than the current one, liquefaction resistance can be predicted to be higher in the next stage.
4. By using acceleration data during liquefaction, relationship of stress and strain can be drawn. Together with cumulative damage concept, it was possible to calculate equivalent cyclic stress ratio. With this method, the relationship of cyclic stress ratio and number of cycle to reach target strain amplitude can also be made.

7.1.3 Investigation of repeated liquefaction behavior using energy approach

Both triaxial and shaking table test results were analyzed using energy approach. Several conclusions can be made as follow.

1. Dissipated energy of the specimen with the same relative density is unique in terms of relationship with accumulated strain and excess pore water pressure generation.
2. The dissipated energy can be divided into two types using a virtual boundary (phase transformation line). The total dissipated energy before reaching phase transformation line in the effective stress path is called positive impact. This positive impact is benefitcial to the next liquefaction resistance. The total dissipated energy after the stress path crosses the phase transformation line is, on the other hand, disadvantageous to the future liquefaction resistance. However, the dissipated energy after initial liquefaction; i.e. zero effective stress, is rather constant; thus the dissipated energy normalized by the current mean effective stress, called as modified dissipated energy was employed. By using the modified dissipated energy, the

relationship between normalized dissipated energy which causes positive impact and negative impact to the next liquefaction resistance was successfully drawn for both triaxial and shaking table tests.

7.1.4 Comparison of repeated liquefaction behavior of the Silica sand in triaxial and shaking table tests

Both triaxial and shaking table tests were conducted to investigate repeated liquefaction behavior of the Silica sand and their results were compared using cumulative damage concept and energy approach. The following conclusions were drawn.

1. With cumulative damage concept, equivalent cyclic stress ratio can be computed from irregular stress response in shaking table tests. The results of the shaking table tests were then able to compare with the results of triaxial tests. It was found that the liquefaction and reliquefaction resistance in the shaking table apparatus was higher than that in the triaxial apparatus.
2. Further investigation on comparison was made using energy approach after finding the trend of normalized dissipated energy which causes positive impact and negative impact to the future liquefaction resistance. It was found that by using the energy approach, the results of shaking table and triaxial tests were not consistent which might due to the different in confining pressure.
3. The possible reasons of higher liquefaction resistance in shaking table apparatus were pointed out. Firstly, the degree of saturation of the shaking table specimen was lowered. Secondly, the ground model in shaking table apparatus was exposed to the atmosphere. This can be the route of excess pore water pressure dissipation during shaking whereas the drainage condition in triaxial apparatus was fully undrained. Finally, the lower coning pressure in shaking table can result in higher liquefaction resistance.

7.2 Recommendations

The recommendations for future researches and studies can be divided in to three parts which are remaining investigation of repeated liquefaction behavior of the silica sand in both triaxial and shaking table apparatus and comparison.

7.2.1 Future researches and studies on the repeated liquefaction behavior of the Silica sand in triaxial apparatus

Several testing programs was not carried out in this thesis due time limit. Thus, the additional triaxial tests are purposed.

1. In the effect of strain amplitude study, all the specimens in triaxial tests were prepared to achieve initial relative density of 50-55% and subjected to various axial strain amplitude. The relative density of the specimens since the first to the final liquefaction was in the range of 55-80%. It is also better to compare all these liquefaction resistance results of specimens with various strain histories and the virgin liquefaction specimen. Thus, the single liquefaction stage tests for the specimen with relative density ranging from 55% to 80% are purposed to compare the behavior between intact specimen and post liquefaction specimen under the same relative density.
2. In the effect of small strain history, only 0.1%, 0.2% and 0.5% double amplitudes were applied to the specimens in the first liquefaction stage. It was found that specimen with 0.2% axial strain pre-shearing showed the highest reliquefaction resistance and 0.2% was concluded as threshold strain. However, the gap between 0.2% and 0.5% strain amplitude might be too high. Thus another two tests with the pre-shear axial strain of 0.3% and 0.4% are purposed to address the true threshold strain.

7.2.2 Future researches and studies on the repeated liquefaction behavior of the Silica sand in shaking table apparatus

1. Since the effect of small strain was studied in the triaxial apparatus, it is also purpose shaking tables test with small pre-shearing strains to verify the effect of small strain in the model test. This can be done by input low acceleration to the ground model
2. There are two testing programs conducted in the shaking table test which were the test with repeat acceleration and decrease acceleration when the ground model showed shear strain more than 1.5%. From these two testing program this study point out a brief method to predict future liquefaction resistance using current and previous maximum strain amplitude. This method was also verified with several earthquake records. However, the method can only cover two cases which are the earthquakes

with the same magnitude and the earthquakes with lower magnitude. Thus, there is one missing scenario which is where higher magnitude in the second earthquake. Therefore, the test series where the input acceleration is increased when the shear strain is larger than 1.5% are purposed.

3. At large number of liquefaction stage, there might be possible movement of the sensors inside ground model resulting in error in monitoring data. Some possible modifications of the apparatus are purposed. Firstly, the pore water pressure transducer can be installed attached with the soil container wall at desired depth on the side perpendicular to the shaking direction. In this case, location of the pore water pressure transduce is fixed from sinking and rotating but it would rise difficulty in variation of measuring position.

7.2.3 Future researches and studies on comparison of repeated liquefaction behavior in triaxial and shaking table tests.

Both triaxial and shaking table tests by means of repeated liquefaction were conducted and the results were compared using cumulative damage concept and energy approach. By using the cumulative damage concept, the equivalent cyclic stress ratio in shaking table tests can be computed and compared with the results of triaxial tests. It was found that the liquefaction resistance in shaking table apparatus was higher than that in triaxial apparatus. However, together with the energy approach, the both results were not consistent. This might due to overestimation and underestimation of both positive impact and negative impact. In this study, the total dissipated energy before stress path touches the phase transformation line (during contractive behavior) was accounted for positive impact and after the phase transformation line (during dilative behavior) was accounted for negative impact. However, after touches the phase transformation line, the specimens still exhibited contractive behavior promoting overestimation of negative impact and underestimation of positive impact. Thus, the new analysis is purposed to extract the dissipated energy during contractive behavior after passing phase transformation line and to take those dissipated energy into positive impact. For the different in confining pressure, the lower confining pressure in triaxial test and higher ground model depth in shaking table test can be employed.

Appendix A

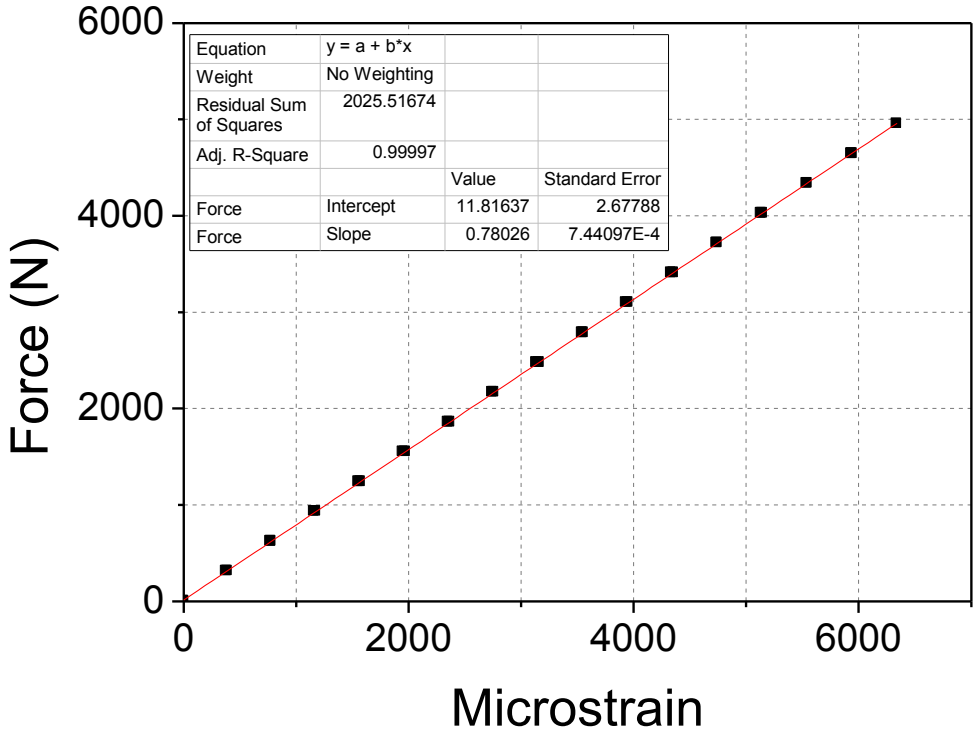

Figure 1. Load cell calibration

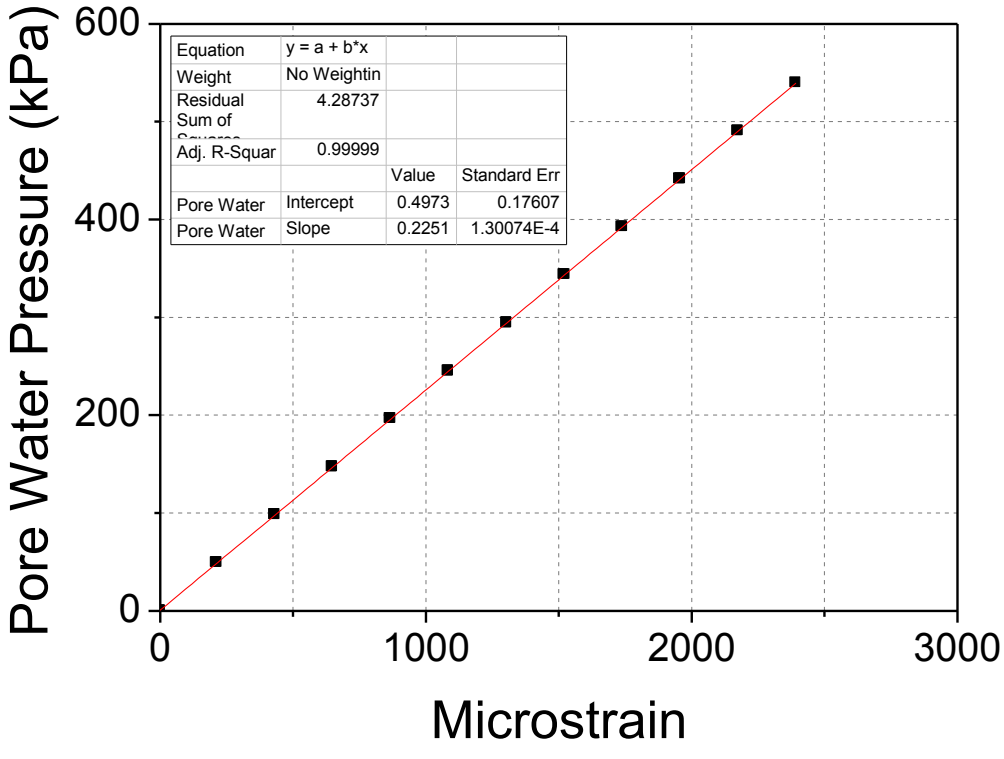

Figure 2. Pore water pressure transducer calibration

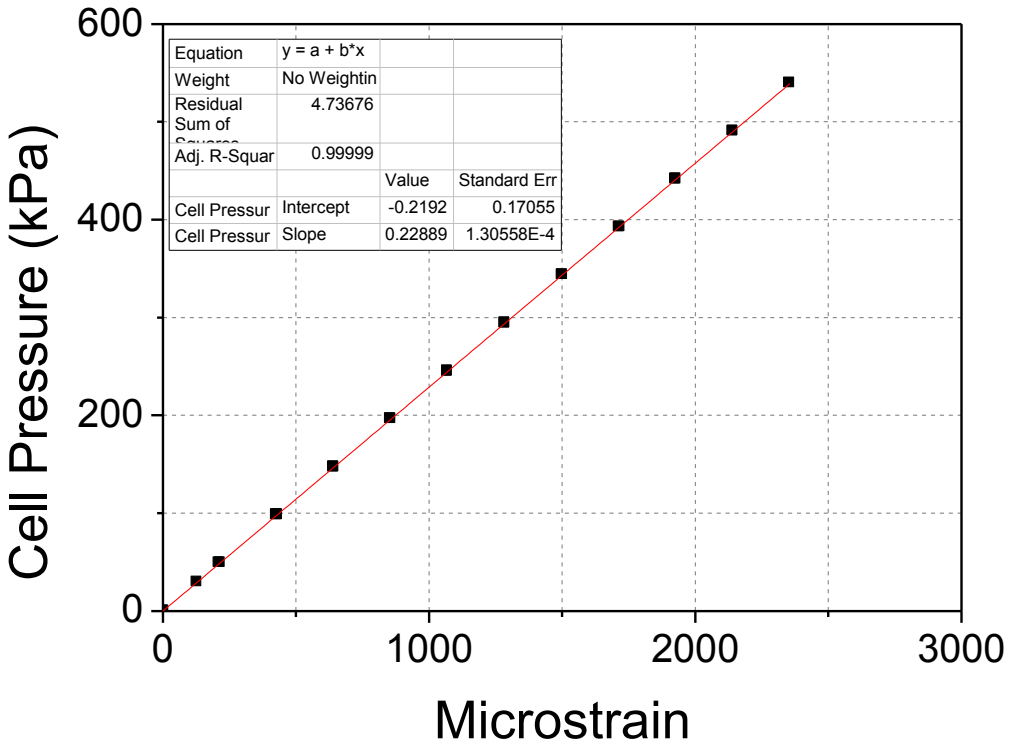

Figure 3. Cell pressure calibration

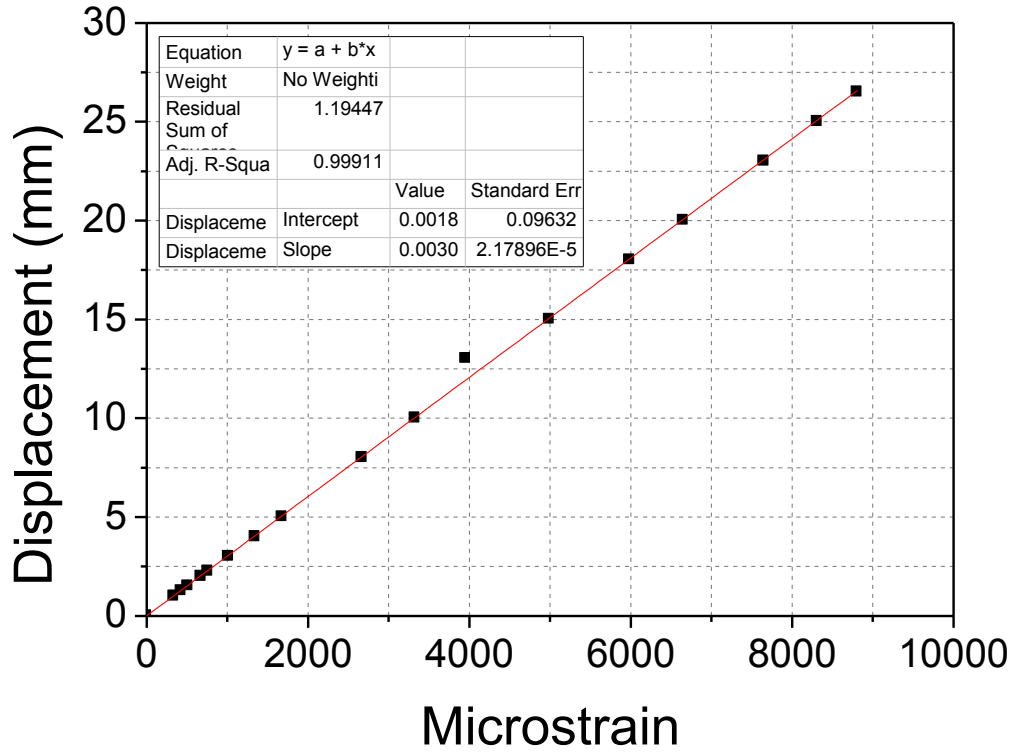

Figure 4. External displacement transducer

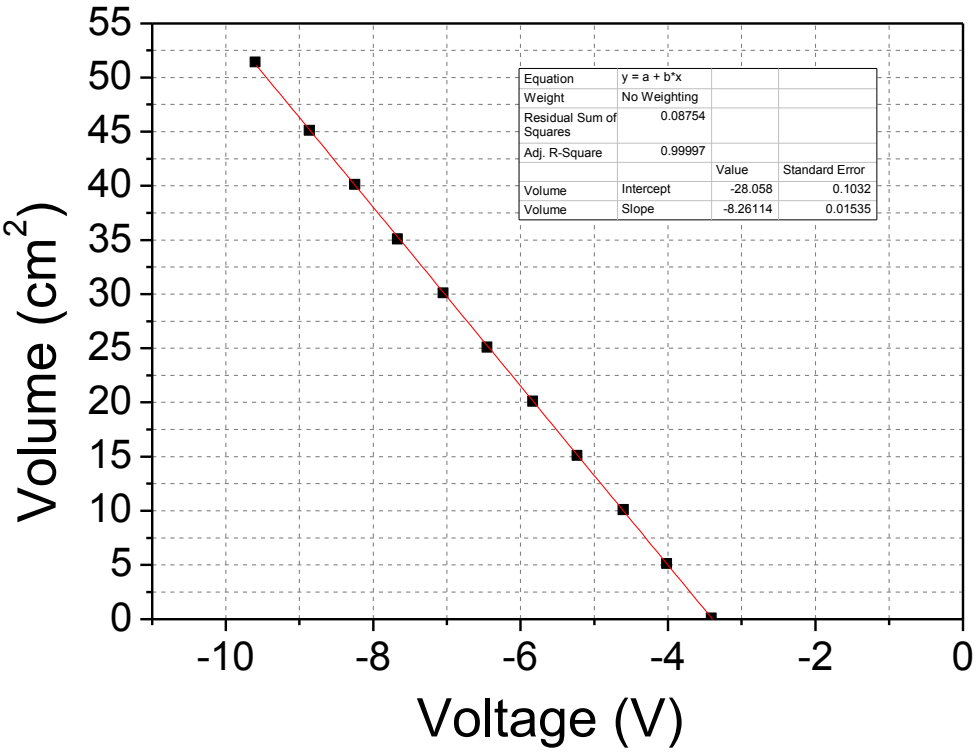

Figure 5. Low capacity differential pressure transducer

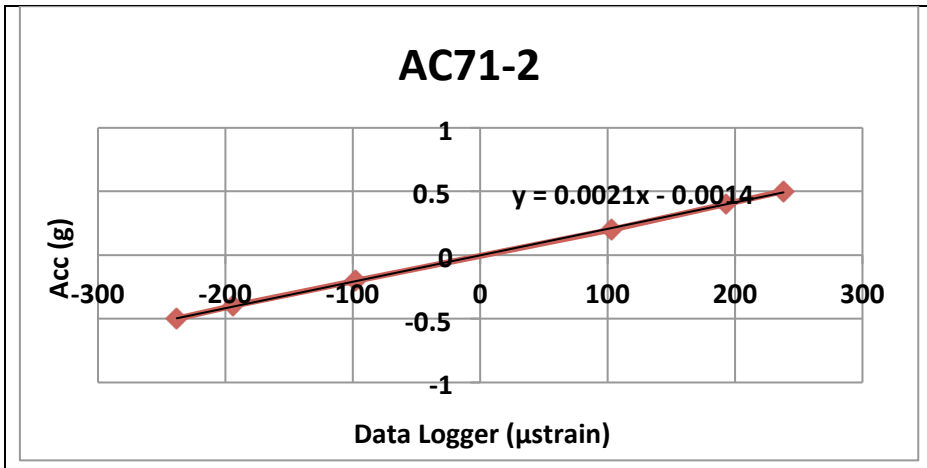
AC71-2
y = 0.0021x - 0.0014
Acc (g)
Data Logger (µstrain)
1
0.5
0
-0.5
-1
-300
-200
-100
0
100
200
300

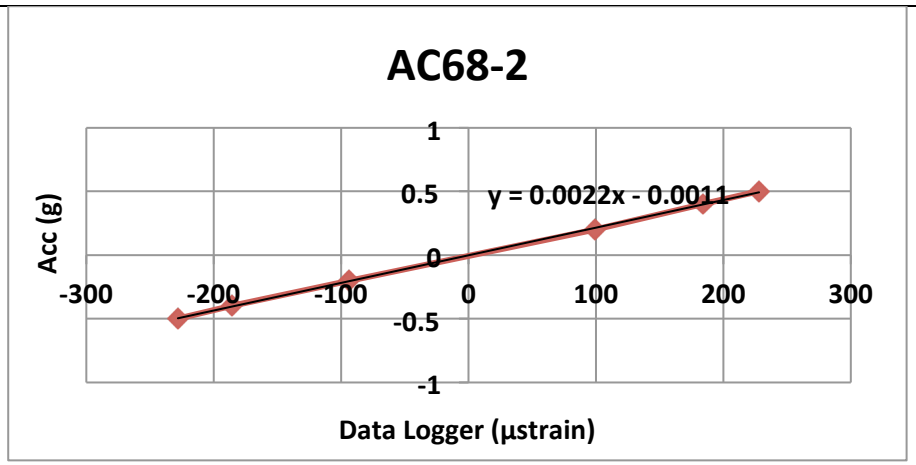
AC68-2
y = 0.0022x - 0.0011
Acc (g)
Data Logger (µstrain)
1
0.5
0
-0.5
-1
-300
-200
-100
0
100
200
300

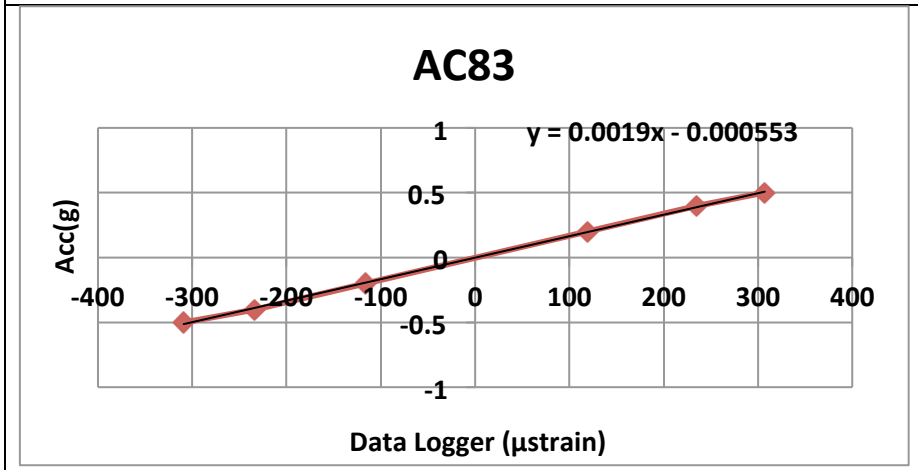
AC83
y = 0.0019x - 0.000553
Acc(g)
Data Logger (µstrain)
1
0.5
0
-0.5
-1
-400
-300
-200
-100
0
100
200
300
400

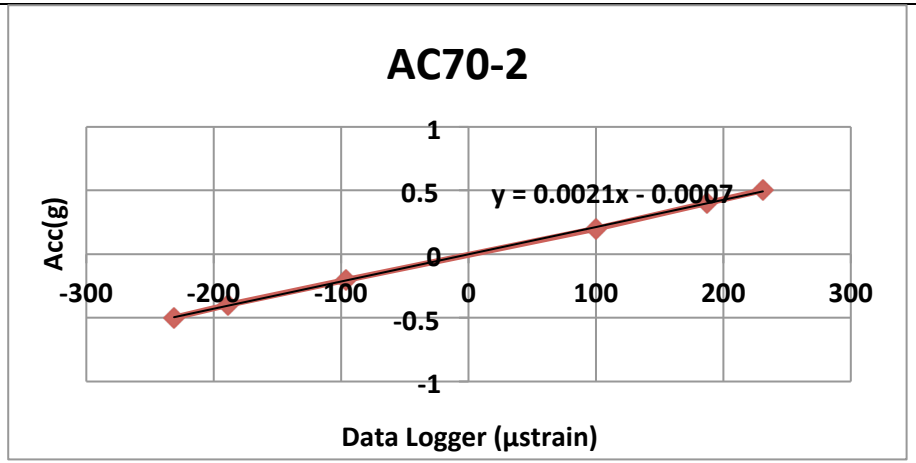
AC70-2
y = 0.0021x - 0.0007
Acc(g)
Data Logger (µstrain)
1
0.5
0
-0.5
-1
-300
-200
-100
0
100
200
300

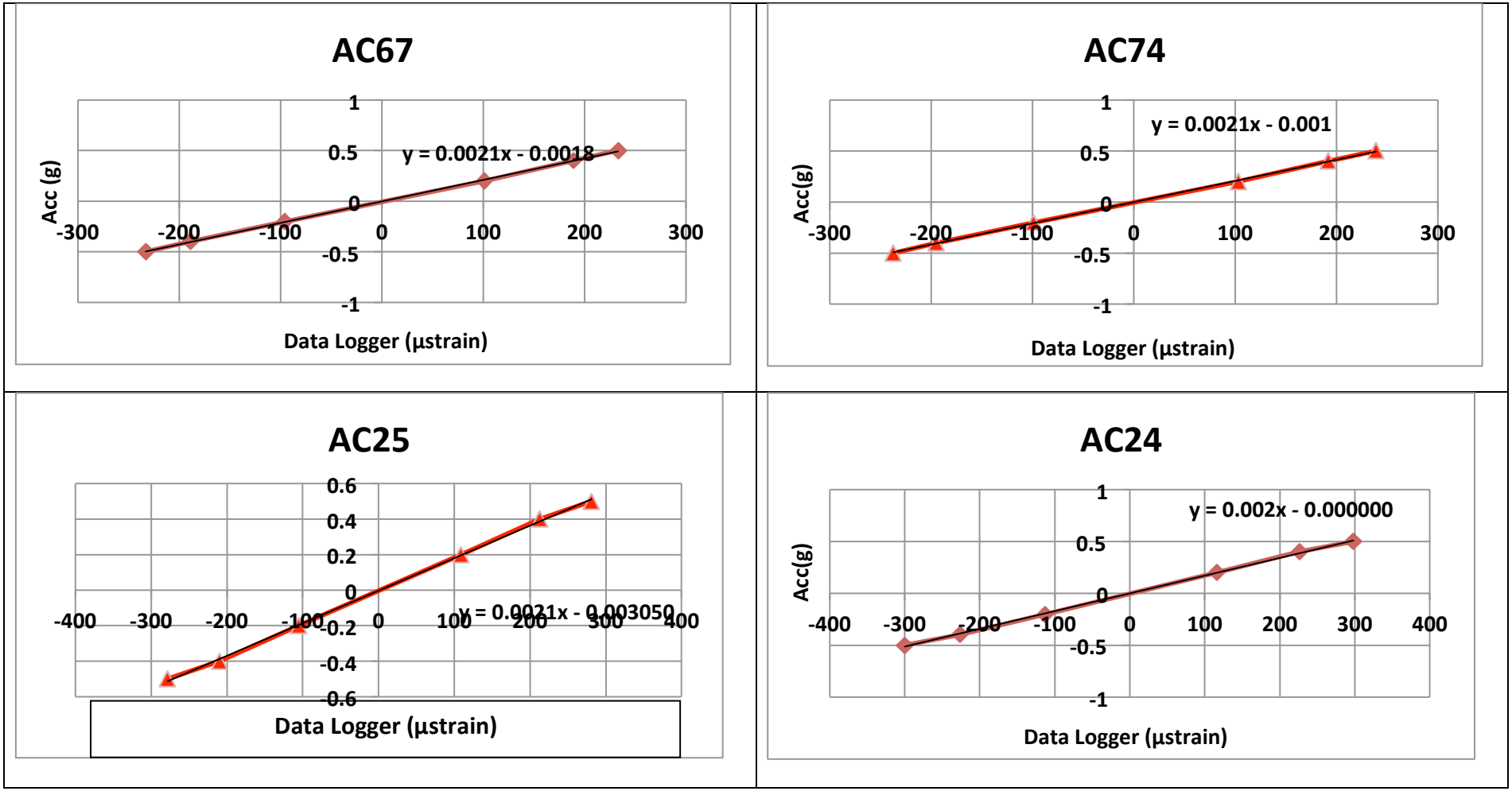
AC67
y = 0.0021x - 0.0018
Acc (g)
Data Logger (µstrain)
AC74
y = 0.0021x - 0.001
Acc(g)
Data Logger (µstrain)
AC25
y = 0.0021x - 0.003050
Data Logger (µstrain)
AC24
y = 0.002x - 0.000000
Acc(g)
Data Logger (µstrain)

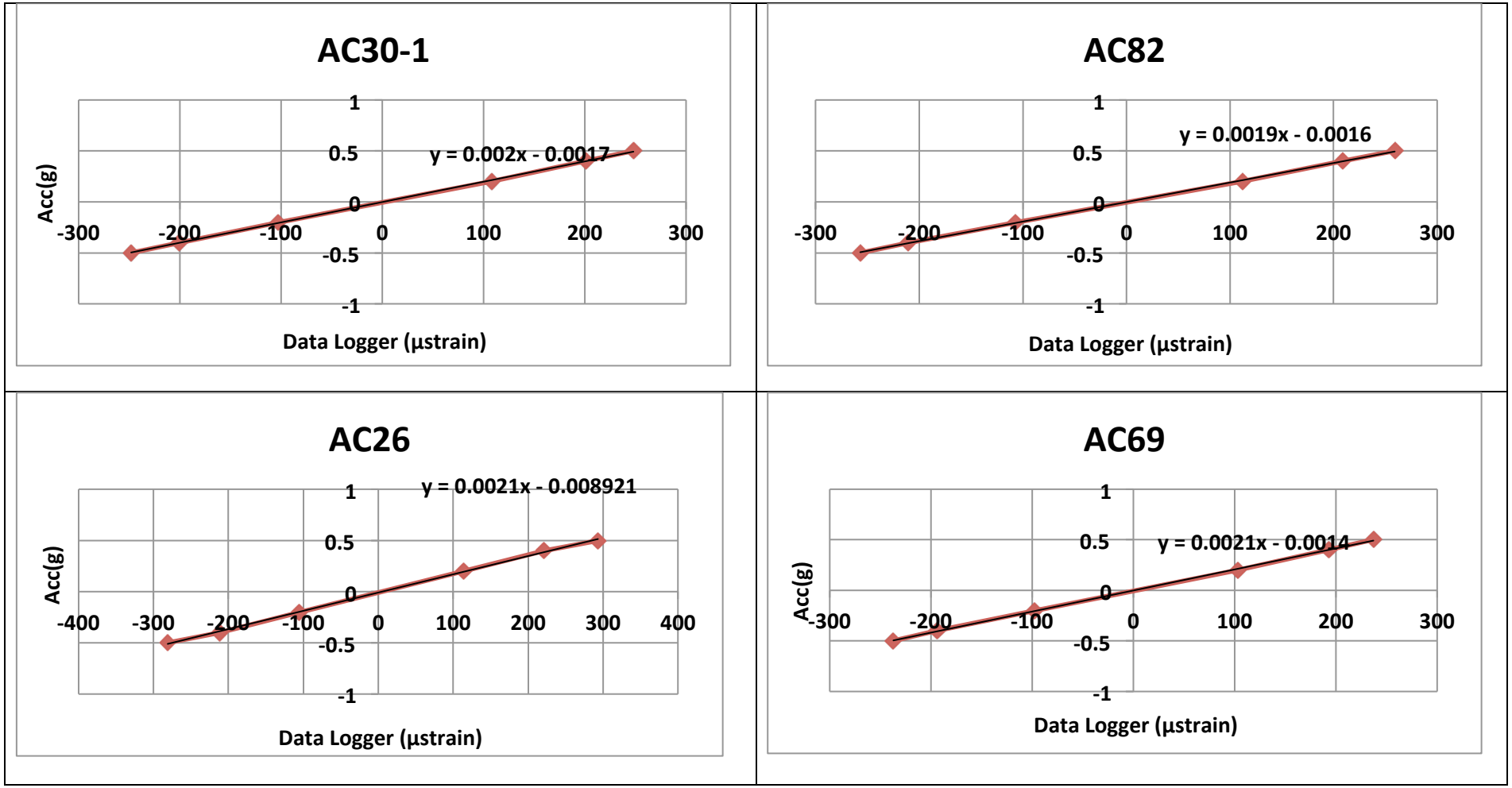
AC30-1
y = 0.002x - 0.0017
Acc(g)
Data Logger (µstrain)
AC82
y = 0.0019x - 0.0016
Data Logger (µstrain)
AC26
y = 0.0021x - 0.008921
Acc(g)
Data Logger (µstrain)
AC69
y = 0.0021x - 0.0014
Acc(g)
Data Logger (µstrain)

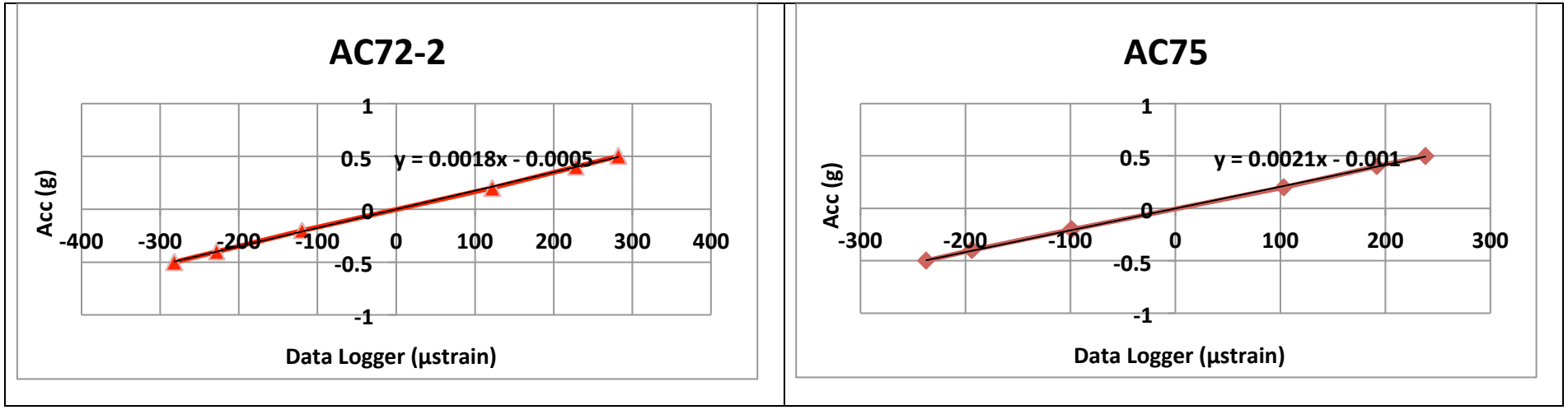

Figure 6. Accelerometer Calibration

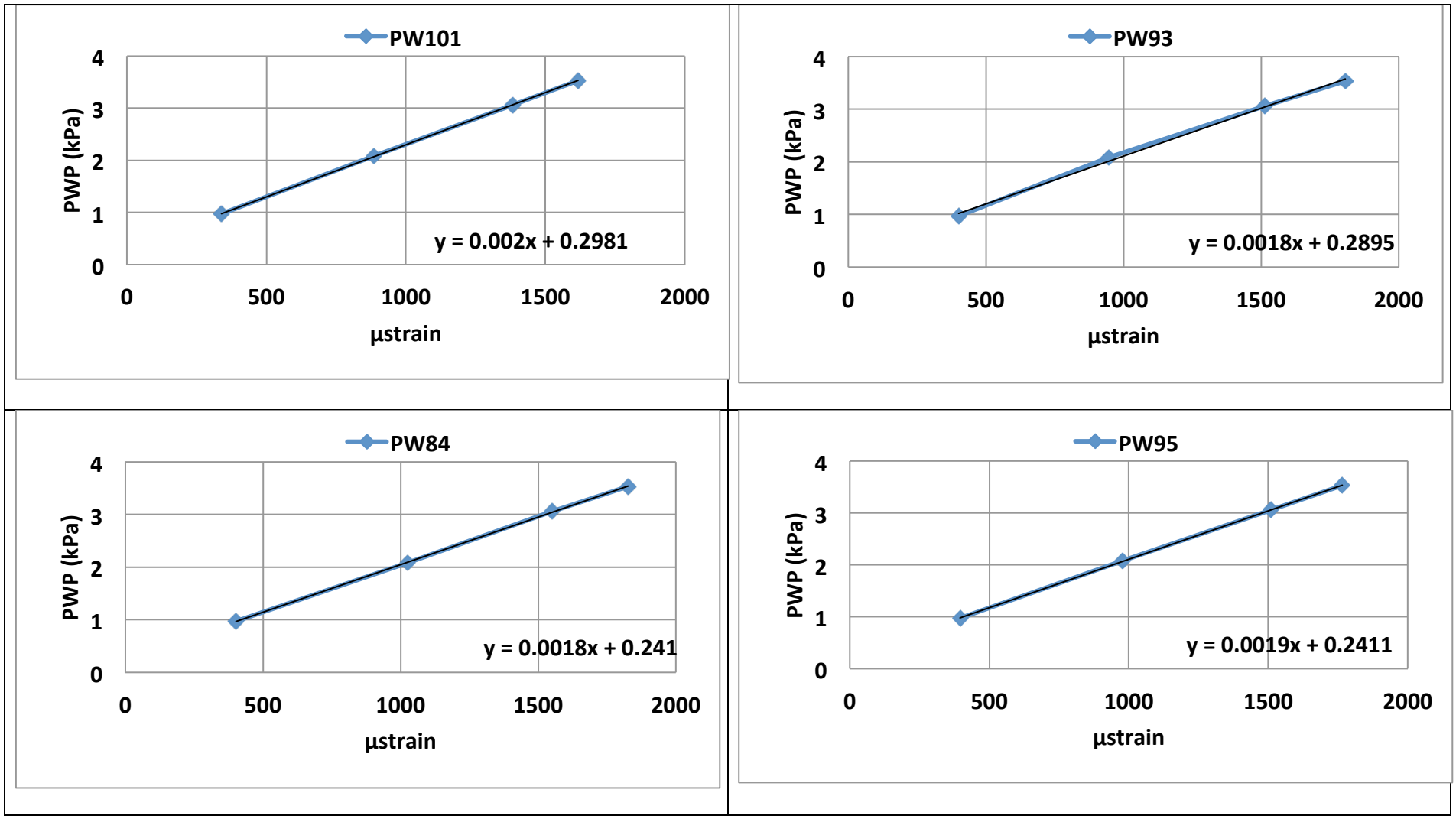
PW101
PWP (kPa)
µstrain
y = 0.002x + 0.2981
PW93
PWP (kPa)
µstrain
y = 0.0018x + 0.2895
PW84
PWP (kPa)
µstrain
y = 0.0018x + 0.241
PW95
PWP (kPa)
µstrain
y = 0.0019x + 0.2411

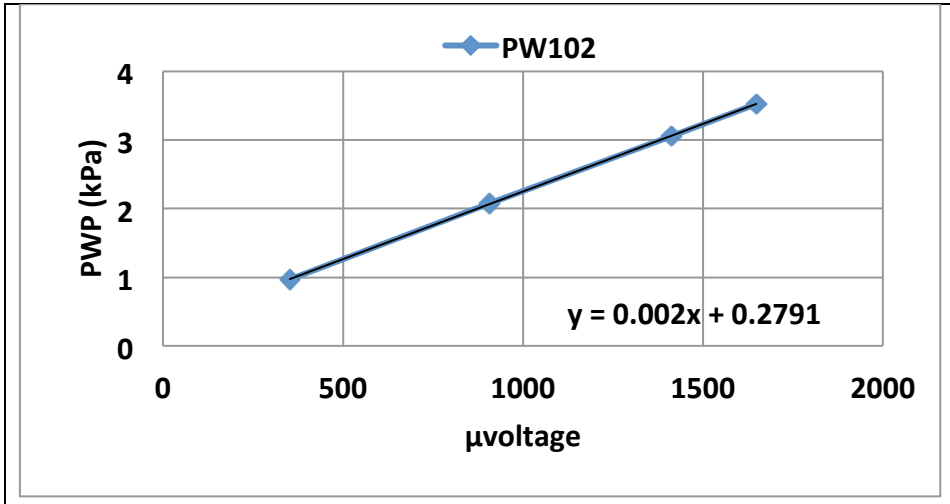
PW102
PWP (kPa)
0
1
2
3
4
0
500
1000
1500
2000
µvoltage
y = 0.002x + 0.2791

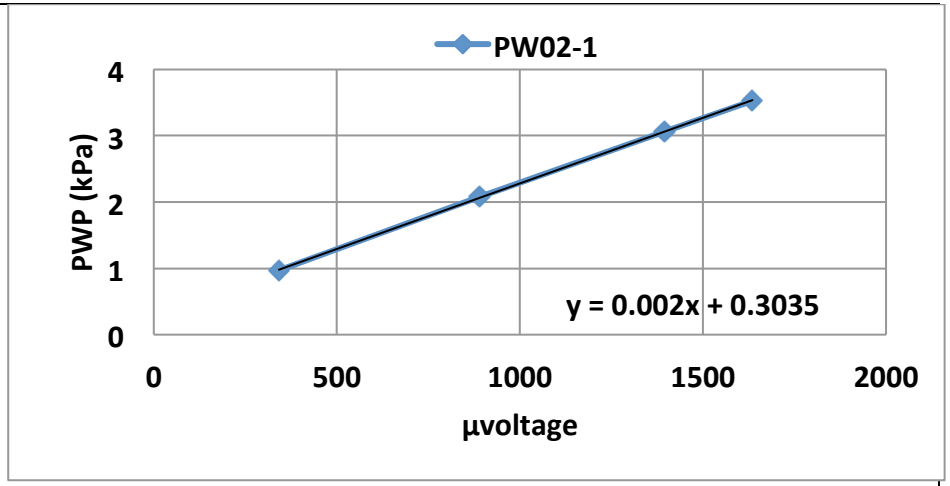
PW02-1
PWP (kPa)
0
1
2
3
4
0
500
1000
1500
2000
µvoltage
y = 0.002x + 0.3035

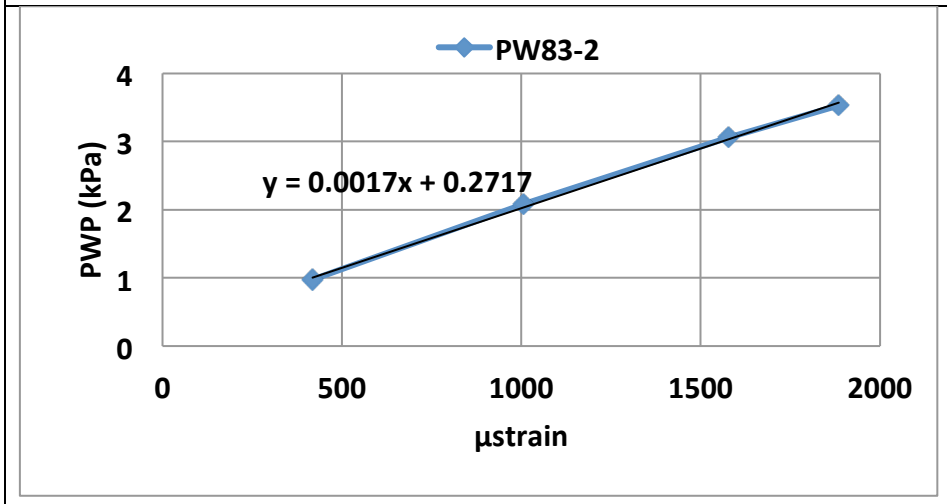
PW83-2
PWP (kPa)
0
1
2
3
4
0
500
1000
1500
2000
µstrain
y = 0.0017x + 0.2717

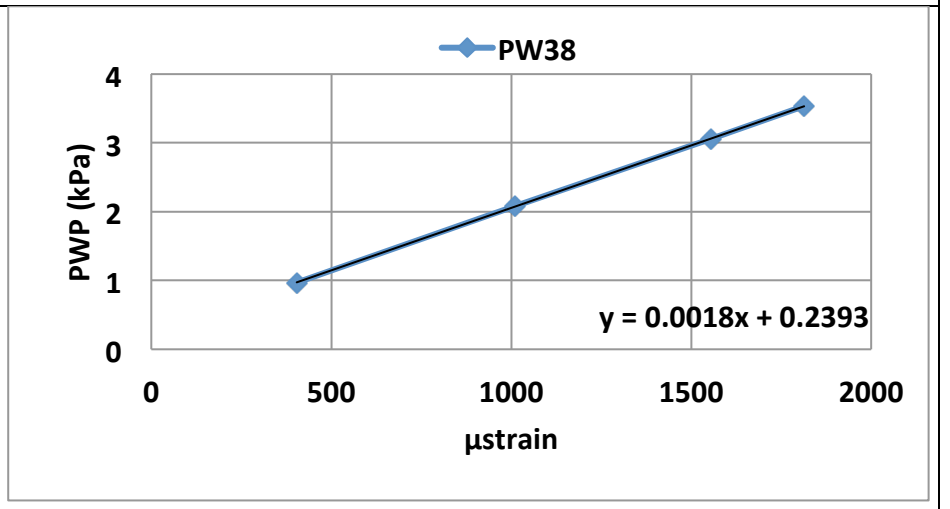
PW38
PWP (kPa)
0
1
2
3
4
0
500
1000
1500
2000
µstrain
y = 0.0018x + 0.2393

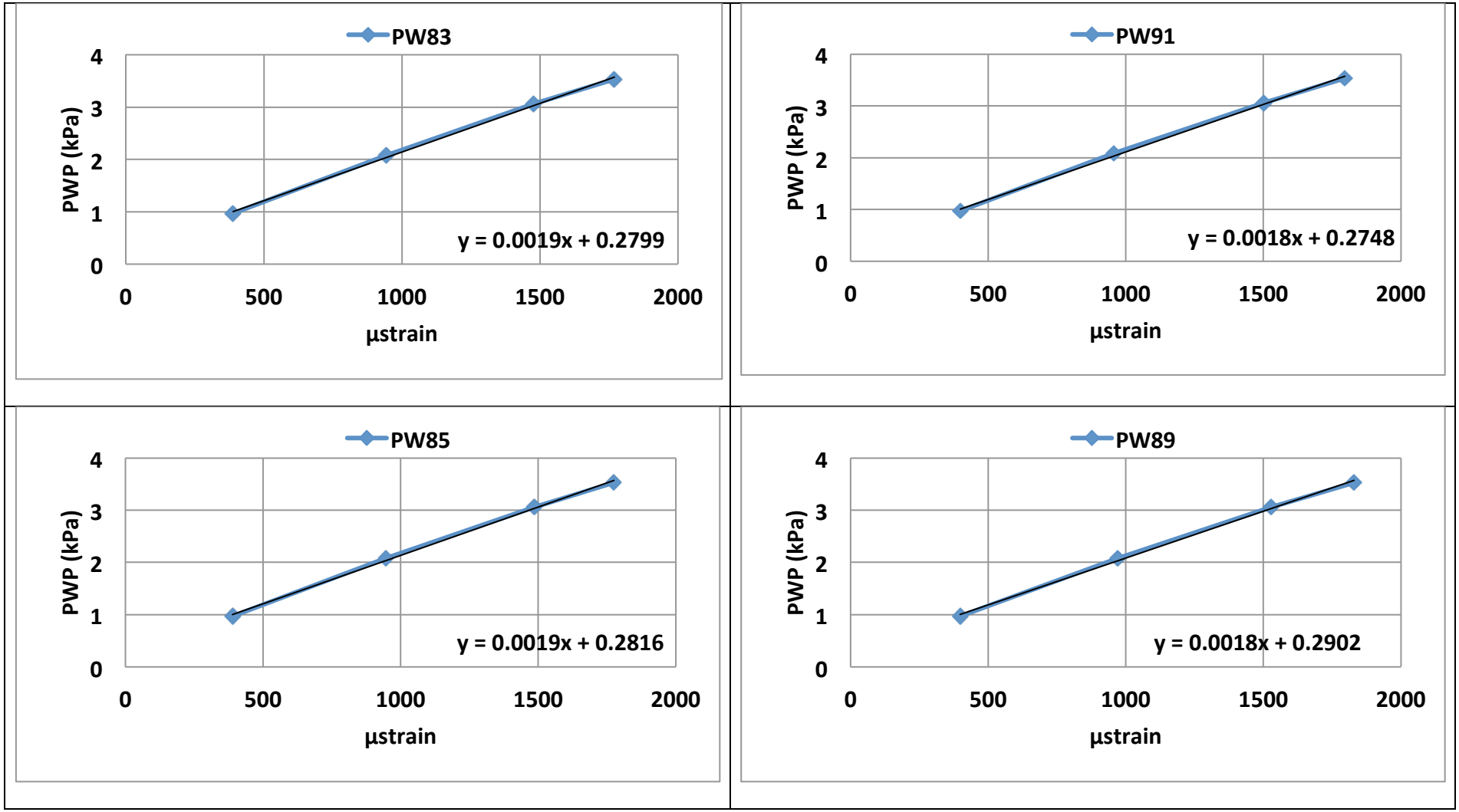
PW83
PWP (kPa)
µstrain
y = 0.0019x + 0.2799
PW91
PWP (kPa)
µstrain
y = 0.0018x + 0.2748
PW85
PWP (kPa)
µstrain
y = 0.0019x + 0.2816
PW89
PWP (kPa)
µstrain
y = 0.0018x + 0.2902

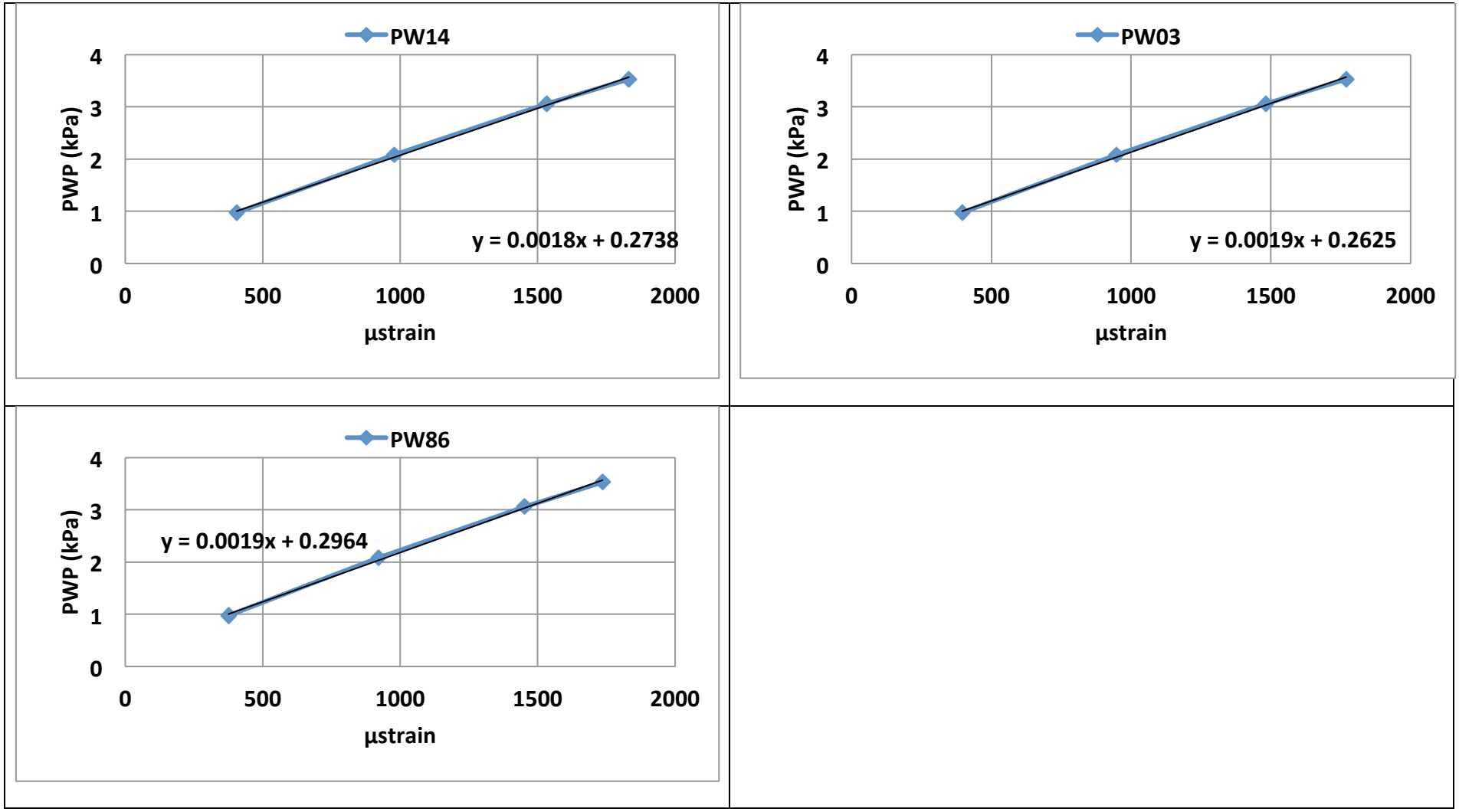

Figure 7 Pore water pressure calibration

Appendix B

Examples of primary wave (p-wave) record of shaking table test in each input acceleration.

Type / Acceleration	Source	Receiver
Pure Water / 0 gal	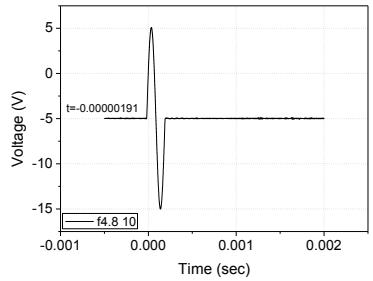	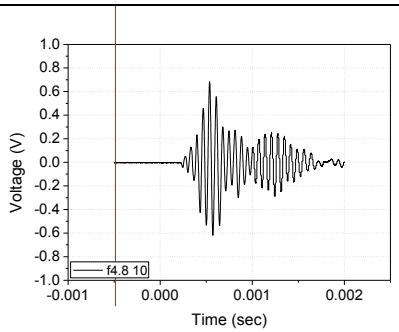
Ground Model / 300 gal	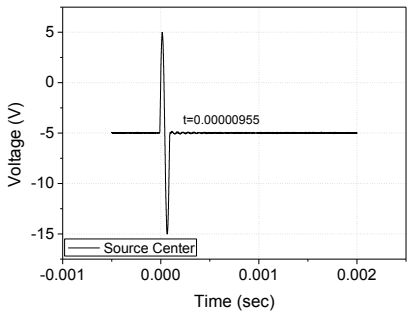	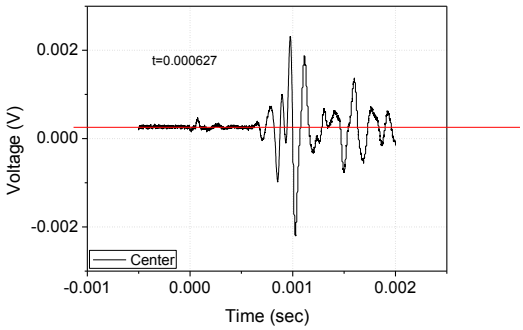
Ground Model / 400 gal	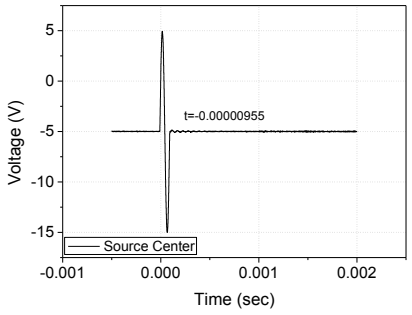	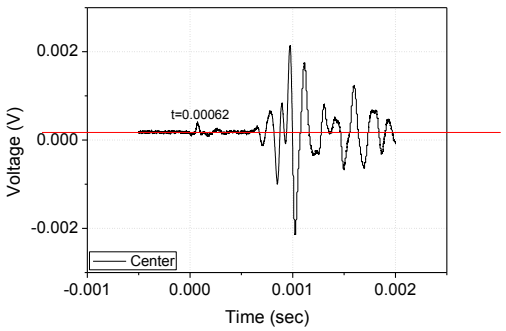
Ground Model / 500 gal	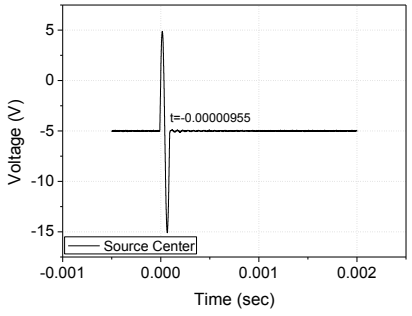	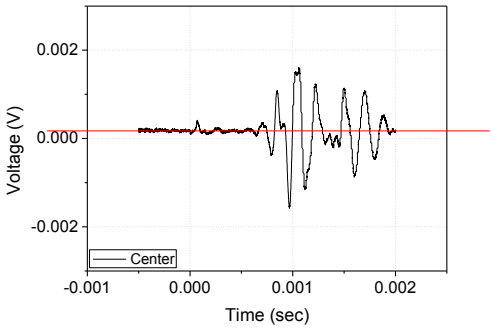

Ground Model / 600 gal	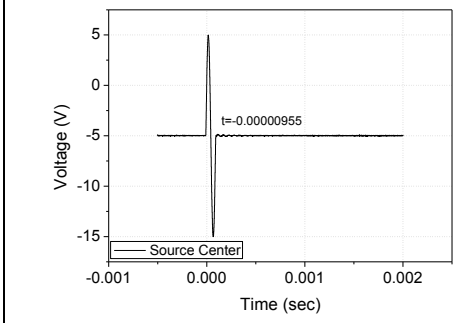	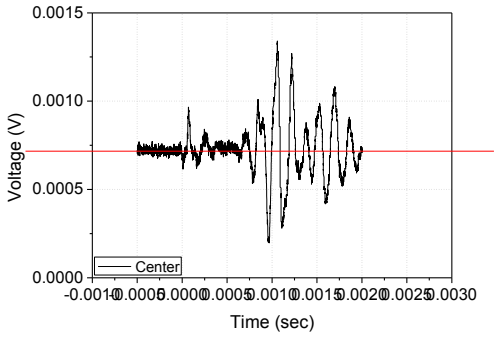
Ground Model / 700 gal	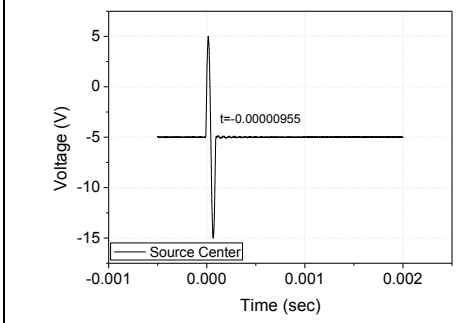	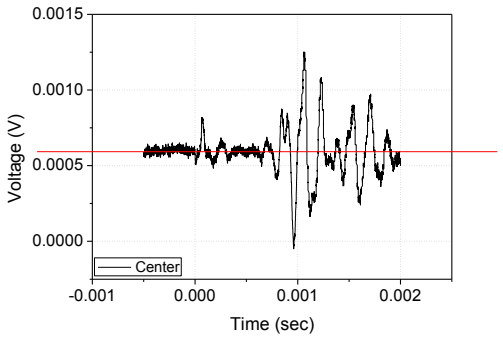
Ground Model / 800 gal	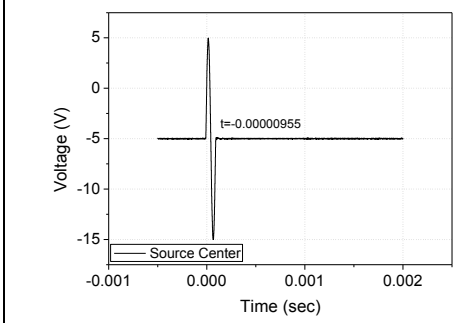	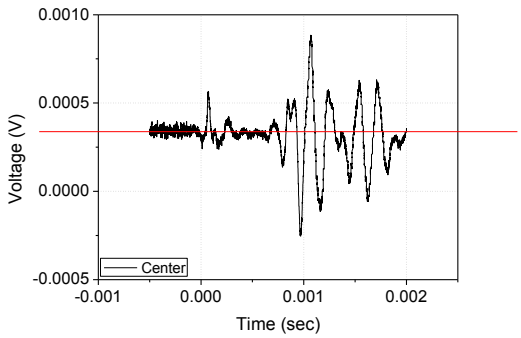
Ground Model / 900 gal	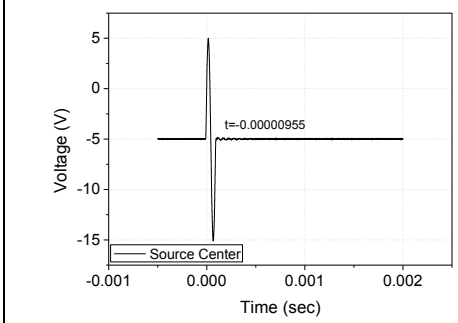	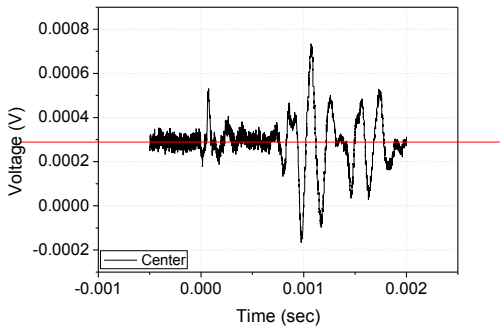
Ground Model / 1000 gal